

Self-Similar Solutions to Compressible Flow Problems

THESIS

Submitted in partial fulfilment
of the requirements for the degree of

DOCTOR OF PHILOSOPHY

by

NARSIMHULU DUNNA

ID. No. 2011PHXF0015H

Under the Supervision of
Prof. ADDEPALLI RAMU

&

Under the Co-supervision of
Prof. DIPAK KUMAR SATPATHI



BITS Pilani
Pilani | Dubai | Goa | Hyderabad

BIRLA INSTITUTE OF TECHNOLOGY AND SCIENCE, PILANI

2018

BIRLA INSTITUTE OF TECHNOLOGY AND SCIENCE, PILANI

CERTIFICATE

This is to certify that the thesis entitled “**Self-Similar Solutions to Compressible Flow Problems**” and submitted by **NARSIMHULU DUNNA, ID No. 2011PHXF0015H** for award of Ph.D. of the Institute embodies original work done by him under my supervision.

Signature of the Supervisor

Name: Dr. ADDEPALLI RAMU

Designation: Professor

Department of Mathematics

BITS-Pilani, Hyderabad Campus

Jawahar Nagar, Shameerpet (Mandal)

Hyderabad-500 078, Telangana, India.

Date:

Signature of the Co-supervisor

Name: Dr. DIPAK KUMAR SATPATHI

Designation: Professor

Department of Mathematics

BITS-Pilani, Hyderabad Campus

Jawahar Nagar, Shameerpet (Mandal)

Hyderabad-500 078, Telangana, India.

Date:

ACKNOWLEDGEMENTS

I would like to thank my supervisor, Prof. Addepalli Ramu, for the patient guidance, encouragement and advice he has provided throughout my time as his student. I have been extremely lucky to have a supervisor who cared so much about my work, and who responded to my questions and queries so promptly.

I would also like to thank Co-supervisor Prof. Dipak Kumar Satpathi for his valuable suggestions during my doctoral research endeavor. Completing this work would have been all the more difficult were it not for the support and friendship provided by the other members of the Department of Mathematics in BITS-Pilani Hyderabad campus.

I am thankful to BITS-Pilani Hyderabad campus, the Institute and the Department of Mathematics for providing with all required facilities.

I acknowledge with thanks the financial and technical support provided by Department of Science and Technology, New Delhi, through Inspire fellowships (IF110071).

Nobody has been more important to me in the pursuit of this doctoral degree than the members of my family. I would like to thank my parents, whose love, blessings and guidance are with me in whatever I pursue. They are the ultimate role models. I dedicate this thesis to my Parents.

TABLE OF CONTENTS

Abstract	i
List of Figures	vii
List of Tables	xviii
List of Symbols	xx
CHAPTER 1. Introduction	1
CHAPTER 2. Literature Review	13
CHAPTER 3. Similarity Solutions to Shock Waves in Non-ideal Magnetogasdynamics	22
3.1 Introduction	22
3.2 Governing Equations	29
3.3 Numerical Solution	35
3.4 Results and Discussion	37
CHAPTER 4. Numerical Solution to Strong Cylindrical Shock Wave in the Presence of Magnetic Field	50
4.1 Introduction	50
4.2 Basic Equations	52
4.2.1 Boundary conditions	53
4.3 Solution Procedure	54
4.3.1 The numerical solution	57
4.4 Results and Discussion	59
CHAPTER 5. Magnetogasdynamics Shock Waves a Numerical Study	82
5.1 Introduction	82
5.2 Basic Equations and Boundary Conditions	84

5.2.1 Boundary conditions	85
5.2.2 Conservation equations and boundary conditions	86
5.3 Solution Procedure	90
5.3.1 Evaluation of $\beta(\rho/\rho_0)$ the measure of shock strength	90
5.3.2 Numerical integration solution procedure	92
5.4 Results and Discussion	92
CHAPTER 6. Similarity Solution of Spherical Shock	
Waves – Effect of Viscosity	125
6.1 Introduction	125
6.2 Formulation of the Problem	128
6.2.1 Boundary conditions	129
6.2.2 Transformation of basic equations	130
6.3 Solution Procedure	134
6.3.1 Evaluation of β	134
6.3.2 Solutions of the transformed equations	136
6.3.3 Numerical solution without viscosity ($K = 0$)	136
6.3.4 Numerical solution with viscosity ($K \neq 0$)	137
6.4. Results and Discussion	138
CHAPTER 7. Self-Similar Motion of Strong Converging	
Cylindrical and Spherical Shock Waves in Non-ideal	
Stellar Medium	171
7.1 Introduction	171
7.2 Formulation of the Problem	174
7.2.1 Rankine-Hugoniot relations	176
7.2.2 One-dimensional self-similar motion	177
7.3 Numerical Solution	179
7.3.1 Finite difference formulation	179

7.3.2 Evaluation of $\beta(\rho/\rho_0)$ the measure of shock strength	181
7.3.3 Numerical solution of flow parameters	183
7.4. Results and Discussion	183
CHAPTER 8. Self-Similar Solution of One-dimensional	
Strong Converging Cylindrical and Spherical Shock	
Waves in Non-ideal Gas	211
8.1 Introduction	211
8.2 Mathematical Formulation of Problem	216
8.2.1 Governing equations	216
8.2.2 Condensed matter EOS of Mie-Gruneisen model	218
8.2.3 Boundary conditions	220
8.3 Similarity Analysis by Invariance Groups	222
8.4 Self-Similar Solutions	229
8.5 Numerical Solution to Converging Shock Wave	234
8.5.1 Replacing derivatives by finite differences	235
8.6 Analysis for System of Equations (8.48-8.50) without	
Viscosity	237
8.7 Results and Discussion	241
Conclusions	263
Future Scope of Work	272
References	273
List of Publications and Presentations	291
Biography of the Candidate	294
Biography of the Supervisor	295

ABSTRACT

An attempt has been made in this thesis to investigate the self-similar solutions for some compressible flow problems behind the strong shock waves propagating into a non-ideal gas of Mie-Gruneisen equation of state (EOS). With the aid of similarity method, group invariance method, Chester-Chisnell-Whitham (CCW) method, finite difference method etc., the approximate analytical and numerical solutions for the self-similar flows behind strong shock waves are obtained. The effect of non-idealness of the equation of state, magnetic pressure, effect of viscosity etc., on the flow variables and the similarity exponent α are investigated. The thesis consists of eight chapters. The first chapter is devoted to literature survey on the subject and a brief account of the problems investigated. Chapter two consists of brief account of the literature reviewed, the gap areas, the concept of model generation and the solution procedure.

In the third chapter, similarity solutions to shock waves in non-ideal magnetogasdynamics is presented. We consider system of partial differential equations describing the one dimensional unsteady cylindrical flow of an inviscid non-ideal gas with dust particles and study various aspects of non-linear wave propagation. The medium generated due to implosion is assumed to be of Mie-Gruneisen type with magnetic or non-magnetic in nature. Impulsive motion of the piston may produce instantaneous unsteady shock which may grow or decay with time, depending on the condition of the undisturbed gas and the behaviour

of the piston. The forms of these waves are altered by convection which distorts the wave form by causing the compression phase to move forward faster than the expansion phase. Thus it is assumed that plasma is generated with an infinite electrical conductivity and permeated by an axial magnetic field orthogonal to the trajectories of gas particles. Similarity solution to this problem is attempted. Analytical solution to the assumed model is difficult and numerical solution is presented. The numerical solution presented provides a global solution to the implosion problem which is valid for a range of physically meaningful parameters which represent the EOS of Mie-Gruneisen type. In this work we presented the EOS generated by considering the material property. This process defines both dusty gas and condensed matter EOS. This concept is different from the existing models of the definition of dusty gas and condensed matter and is more realistic than mere assumption of perfect gas. It is assumed that the motion of the piston obeys exponential law. Numerical computations are performed to obtain the similarity exponent for the CCW rule using MATLAB. The computed values of the similarity exponent are in good agreement with those obtained using CCW method and are presented in tabular form. This approximation provides a quick and relatively accurate determination of the similarity exponent and stability of shocks in non-ideal gas. Also the numerical description of the flow field behind the wave front in a non-ideal magnetogasdynamics regime is presented. An attempt is made as to show the magnetic field strength effect on the flow

parameters in a non-ideal medium. The effects are presented in the form of graphs pictorially.

In chapter four, numerical solution to strong cylindrical shock wave in the presence of magnetic field is studied. The medium generated due to implosion is assumed to be of Mie-Gruneisen type with or without magnetic material. In the implosion process (by impulse method) plasma is assumed to be generated. It is assumed that this plasma has an infinite electrical conductivity and permeated by an axial magnetic field orthogonal to the trajectories of gas particles. Numerical solution presented here provides a global solution to the implosion problem which is valid for a range of physically meaningful parameters which represent the EOS of Mie-Gruneisen type. Numerical computations are performed to obtain the similarity exponent iteratively using MATLAB. This problem was investigated with an aim to understand the mechanical properties of shock waves in the presence of strong magnetic field; to study the behavior of shock characteristics such as shock strength, shock density, shock speed, shock over pressure, and impulse.

In chapter five, a model to determine the similarity solutions to the problem of gas dynamic flow under the influence of strong magnetic field is presented. The problem treated here involves distinct features: the global behavior of the physical parameter has been studied; the initial pressure ratio is confined to a moderate value. The path of the piston is imposed as boundary condition. Thus an

accelerated, a decelerated or a constant velocity piston can be specified. Self-similarity requires the velocity of shock and the velocity of piston to be proportional to some power law $R(t) \propto (t)^\alpha$ where $R(t)$ is the position of the shock wave front from the center at time t and α is the similarity exponent. The numerical values of similarity exponents and profiles of flow variables are obtained. These are presented through the illustrative graphs and tables. The magnetic field effects on the flow variables through a medium and total energy under the influence of strong magnetic field are also presented.

The chapter six describe similarity solution of spherical shock waves and effect of viscosity. This problem is investigated to understand complete mechanism of shock wave which include, viscous terms and study the dissipation effects on the propagation of shock waves including viscosity under the effect of magnetic field. Also to study and confirm the effect of (i) the non-idealness parameter and the viscosity parameters on the shock strength and the flow variables respectively, (ii) effect of discontinuities of the physical parameters due to viscosity and (iii) complete flow field depending on the magnitude of the viscosity. To define this type of shock process spherically symmetric conservation equations are considered. The viscosity term suggested by Von Neumann and Richtmyer is included into the hydrodynamic equations for spherically symmetric flow. The main advantage of artificial viscosity approach is its simplicity thereby high

computational efficiency and oscillations in the flow profiles dampen and the smoothness in the profiles increases.

In chapter seven, a model to determine the self-similar solutions for converging spherical and cylindrical strong shock waves in stellar atmosphere under the action of monochromatic radiation in non-uniform stellar interiors with constant intensity on a unit area with the assumption that the medium of propagation to be non-ideal gas is studied. Shock is assumed to be strong and obeys a power law. It is assumed that the radiation flux moves through the gas with constant intensity on a unit area of the shock wave propagation in a direction opposite to the radiation flux. The medium of flow is assumed to be obeying the EOS of Mie-Gruneisen type i.e., Royce EOS. The perfect gas EOS results too are obtained from Royce EOS, and were found to match very closely with the literature.

In chapter eight, self-similar solution of shock wave in condensed matter generated by impulsive load with the medium described by the EOS of Mie-Gruneisen type has been studied. The similarity exponent depends on the EOS parameters. In this work we employed the method of Lie group invariance under infinitesimal point transformations to study the problem of the self-similar solution of converging spherical and cylindrical imploding shock waves near the centre of implosion. The flow assumes a self-similar character in a non-ideal gas satisfying the EOS of Mie-Gruneisen type. Finite difference method is employed for the numerical solution of the governing equations with a check on error

tolerance of 8 significant digits. The similarity solution remains valid as long as the strong shock approximation is applicable across the shock wave. The one-parameter infinitesimal group of transformations were used with great accuracy to predict the physical behavior of the strong converging spherical and cylindrical shock wave which is normally generated by the rapid release of energy from a centered source and the properties of the ambient gas into which the shock wave is expanding. It is assumed that the limiting motion will be self-similar as the wave converges to the center. The numerical technique employed to study the nature of shock dynamics through a non-ideal medium described by the EOS of Mie-Gruneisen type. We obtained a self-similar solution of converging shock wave near the centre (axis) of implosion and investigated the behavior of flow parameters immediately behind the shock front in condensed matter EOS for a physically meaningful range of Gruneisen parameters.

LIST OF FIGURES

Figure 3.1: Collapsing cylindrical shock waves in non-ideal medium; (a) an imploding strong shock, (b) converges on the center, and (c) rebounds, reshocking previously shocked material	24
Figure 3.2(a): Density profiles for dusty gas	42
Figure 3.2(b): Velocity profiles for dusty gas	43
Figure 3.2(c): Pressure profiles for dusty gas	44
Figure 3.2(d): Magnetic pressure profiles for dusty gas	45
Figure 3.3(a): Density profiles for condensed matter	46
Figure 3.3(b): Velocity profiles for condensed matter	47
Figure 3.3(c): Pressure profiles for condensed matter	48
Figure 3.3(d): Magnetic pressure profiles for condensed matter	49
Figure 4.1: Graphical approach of ϕ , ψ and π when $C_0 > 0.1$; (a) dusty gas for $M = 1.4$, (b) dusty gas for $M = 1.5$, (c) Royce EOS for $a = 1.0$, $\Gamma_0 = 1.78$, and (d) perfect gas for $\gamma = 1.4$	65
Figure 4.2(a): Density profiles for dusty gas when $M = 1.4$	66
Figure 4.2(b): Velocity profiles for dusty gas when $M = 1.4$	67
Figure 4.2(c): Pressure profiles for dusty gas when $M = 1.4$	68
Figure 4.2(d): Magnetic pressure profiles for dusty gas when $M = 1.4$	69
Figure 4.3(a): Density profiles for Royce EOS when $\Gamma_0 = 1.78$, $C_0 = 0.02$	70
Figure 4.3(b): Density profiles for Royce EOS when $\Gamma_0 = 1.78$, $C_0 = 0.05$	71
Figure 4.4(a): Velocity profiles for Royce EOS when $\Gamma_0 = 1.78$, $C_0 = 0.02$	72

Figure 4.4(b): Velocity profiles for Royce EOS when $\Gamma_0 = 1.78, C_0 = 0.05$	73
Figure 4.5(a): Pressure profiles for Royce EOS when $\Gamma_0 = 1.78, C_0 = 0.02$	74
Figure 4.5(b): Pressure profiles for Royce EOS when $\Gamma_0 = 1.78, C_0 = 0.05$	75
Figure 4.6(a): Magnetic pressure profiles for Royce EOS when $\Gamma_0 = 1.78, C_0 = 0.02$	76
Figure 4.6(b): Magnetic pressure profiles for Royce EOS when $\Gamma_0 = 1.78, C_0 = 0.05$	77
Figure 4.7(a): Density profiles for perfect gas when $\gamma = 1.4$	78
Figure 4.7(b): Velocity profiles for perfect gas when $\gamma = 1.4$	79
Figure 4.7(c): Pressure profiles for perfect gas when $\gamma = 1.4$	80
Figure 4.7(d): Magnetic pressure profiles for perfect gas when $\gamma = 1.4$	81
Figure 5.1: Graphical approach to estimate positive roots of equation $\phi(C_0, \Gamma_0, \beta) = 0$ in the case of McQueen EOS; when (a) $C_0 = 0.02$ and (b) $C_0 = 0.05$	95
Figure 5.2: Graphical approach to estimate positive roots of equation $\psi(b, C_0, \Gamma_0, \beta) = 0$ in the case of Royce EOS; when (a) $C_0 = 0.02$ and (b) $C_0 = 0.05$	95
Figure 5.3(a): Velocity profiles for Mc Queen EOS for $\Gamma_0 = 2.25$ and different values of C_0	96
Figure 5.3(b): Pressure profiles for Mc Queen EOS for $\Gamma_0 = 2.25$ and different values of C_0	97
Figure 5.3(c): Magnetic pressure profiles for Mc Queen EOS for $\Gamma_0 = 2.25$ and different values of C_0	98

Figure 5.3(d): Energy profiles for Mc Queen EOS for $\Gamma_0 = 2.25$ and different values of C_0	99
Figure 5.3(e): Velocity profiles of Royce EOS for $b = 1.0$, $\Gamma_0 = 2.25$, and different values of C_0	100
Figure 5.3(f): Pressure profiles of Royce EOS for $b = 1.0$, $\Gamma_0 = 2.25$, and different values of C_0	101
Figure 5.3(g): Magnetic pressure profiles of Royce EOS for $b = 1.0$, $\Gamma_0 = 2.25$, and different values of C_0	102
Figure 5.3(h): Energy profiles of Royce EOS for $b = 1.0$, $\Gamma_0 = 2.25$, and different values of C_0	103
Figure 5.3(i): Velocity profiles of Royce EOS for $b = 1.2$, $\Gamma_0 = 2.25$, and different values of C_0	104
Figure 5.3(j): Pressure profiles of Royce EOS for $b = 1.2$, $\Gamma_0 = 2.25$, and different values of C_0	105
Figure 5.3(k): Magnetic pressure profiles of Royce EOS for $b = 1.2$, $\Gamma_0 = 2.25$, and different values of C_0	106
Figure 5.3(l): Energy pressure profiles of Royce EOS for $b = 1.2$, $\Gamma_0 = 2.25$, and different values of C_0	107
Figure 5.4(a): Velocity profiles of Mc Queen EOS for $\Gamma_0 = 2.25$, magnetic effect $C_0 = 0$, and $m = 2, 3$	108
Figure 5.4(b): Pressure profiles of Mc Queen EOS for $\Gamma_0 = 2.25$, magnetic effect $C_0 = 0$, and $m = 2, 3$	109
Figure 5.4(c): Energy profiles of Mc Queen EOS for $\Gamma_0 = 2.25$, magnetic effect $C_0 = 0$, and $m = 2, 3$	110
Figure 5.5(a): Velocity profiles of Royce EOS for $\Gamma_0 = 2.25$, $m = 2$, magnetic effect $C_0 = 0$, and different values of b	111
Figure 5.5(b): Velocity profiles of Royce EOS for $\Gamma_0 = 2.25$, $m = 3$, magnetic effect $C_0 = 0$, and different values of b	112

Figure 5.5(c): Pressure profiles of Royce EOS for $\Gamma_0 = 2.25$, $m = 2$, magnetic effect $C_0 = 0$, and different values of b	113
Figure 5.5(d): Pressure profiles of Royce EOS for $\Gamma_0 = 2.25$, $m = 3$, magnetic effect $C_0 = 0$, and different values of b	114
Figure 5.5(e): Energy profiles of Royce EOS for $\Gamma_0 = 2.25$, $m = 2$, magnetic effect $C_0 = 0$, and different values of b	115
Figure 5.5(f): Energy profiles of Royce EOS for $\Gamma_0 = 2.25$, $m = 3$, magnetic effect $C_0 = 0$, and different values of b	116
Figure 5.6(a): Velocity profiles of perfect gas EOS for $\gamma = 1.4$, $m = 2$, and different values of C_0	117
Figure 5.6(b): Velocity profiles of perfect gas EOS for $\gamma = 1.4$, $m = 3$, and different values of C_0	118
Figure 5.6(c): Pressure profiles of perfect gas EOS for $\gamma = 1.4$, $m = 2$, and different values of C_0	119
Figure 5.6(d): Pressure profiles of perfect gas EOS for $\gamma = 1.4$, $m = 3$, and different values of C_0	120
Figure 5.6(e): Magnetic pressure profiles of perfect gas EOS for $\gamma = 1.4$, $m = 2$, and different values of C_0	121
Figure 5.6(f): Magnetic pressure profiles of perfect gas EOS for $\gamma = 1.4$, $m = 3$, and different values of C_0	122
Figure 5.6(g): Energy profiles of perfect gas EOS for $\gamma = 1.4$, $m = 2$, and different values of C_0	123
Figure 5.6(h): Energy profiles of perfect gas EOS for $\gamma = 1.4$, $m = 3$, and different values of C_0	124
Figure 6.1: Schematic diagram of spherical shock wave propagation	128
Figure 6.2: Flow with shock wave	132
Figure 6.3: Graphical approach of $M(\beta)$ for Royce EOS when $\Gamma_0 = 1.78$ and various values of d	146

Figure 6.4: Graphical approach of $N(\beta)$ for van der Waals EOS	
when $\gamma = 1.4$ and various values of b	146
Figure 6.5(a): Density profiles for Royce EOS when $\Gamma_0 = 1.78$,	
$K = 0$	147
Figure 6.5(b): Velocity profiles for Royce EOS when $\Gamma_0 = 1.78$,	
$K = 0$	147
Figure 6.5(c): Pressure profiles for Royce EOS when	
$\Gamma_0 = 1.78, K = 0$	148
Figure 6.5(d): Magnetic pressure profiles for Royce EOS when	
$\Gamma_0 = 1.78, K = 0$	148
Figure 6.6(a): Density profiles for Royce EOS when $\Gamma_0 = 1.78$,	
$K = 0.00349$	149
Figure 6.6(b): Velocity profiles for Royce EOS when $\Gamma_0 = 1.78$,	
$K = 0.00349$	149
Figure 6.6(c): Pressure profiles for Royce EOS when $\Gamma_0 = 1.78$,	
$K = 0.00349$	150
Figure 6.6(d): Magnetic pressure profiles for Royce EOS when	
$\Gamma_0 = 1.78, K = 0.00349$	150
Figure 6.7(a): Density profiles for Royce EOS when $\Gamma_0 = 1.78$,	
$K = 0.0349$	151
Figure 6.7(b): Velocity profiles for Royce EOS when $\Gamma_0 = 1.78$,	
$K = 0.0349$	151
Figure 6.7(c): Pressure profiles for Royce EOS when $\Gamma_0 = 1.78$,	
$K = 0.0349$	152
Figure 6.7(d): Magnetic pressure profiles for Royce EOS when	
$\Gamma_0 = 1.78, K = 0.0349$	152
Figure 6.8(a): Density profiles for Royce EOS when $\Gamma_0 = 1.78$,	
$K = 0.349$	153

Figure 6.8(b): Velocity profiles for Royce EOS when $\Gamma_0 = 1.78$, $K = 0.349$	153
Figure 6.8(c): Pressure profiles for Royce EOS when $\Gamma_0 = 1.78$, $K = 0.349$	154
Figure 6.8(d): Magnetic pressure profiles for Royce EOS when $\Gamma_0 = 1.78, K = 0.349$	154
Figure 6.9(a): Density profiles for van der Waals EOS when $\gamma = 1.4, K = 0$, and $a = 0.0025$	155
Figure 6.9(b): Velocity profiles for van der Waals EOS when $\gamma = 1.4, K = 0$, and $a = 0.0025$	155
Figure 6.9(c): Pressure profiles for van der Waals EOS when $\gamma = 1.4, K = 0$, and $a = 0.0025$	156
Figure 6.9(d): Magnetic pressure profiles for van der Waals EOS when $\gamma = 1.4, K = 0$, and $a = 0.0025$	156
Figure 6.10(a): Density profiles for van der Waals EOS when $\gamma = 1.4, K = 0.00349$, and $a = 0.0025$	157
Figure 6.10(b): Velocity profiles for van der Waals EOS when $\gamma = 1.4, K = 0.00349$, and $a = 0.0025$	157
Figure 6.10(c): Pressure profiles for van der Waals EOS when $\gamma = 1.4, K = 0.00349$, and $a = 0.0025$	158
Figure 6.10(d): Magnetic pressure profiles for van der Waals EOS when $\gamma = 1.4, K = 0.00349$, and $a = 0.0025$	158
Figure 6.11(a): Density profiles for van der Waals EOS when $\gamma = 1.4, K = 0.0349$, and $a = 0.0025$	159
Figure 6.11(b): Velocity profiles for van der Waals EOS when $\gamma = 1.4, K = 0.0349$, and $a = 0.0025$	159
Figure 6.11(c): Pressure profiles for van der Waals EOS when $\gamma = 1.4, K = 0.0349$, and $a = 0.0025$	160

Figure 6.11(d): Magnetic pressure profiles for van der Waals EOS	
when $\gamma = 1.4$, $K = 0.0349$, and $a = 0.0025$	160
Figure 6.12(a): Density profiles for van der Waals EOS when	
$\gamma = 1.4$, $K = 0.349$, and $a = 0.0025$	161
Figure 6.12(b): Velocity profiles for van der Waals EOS when	
$\gamma = 1.4$, $K = 0.349$, and $a = 0.0025$	161
Figure 6.12(c): Pressure profiles for van der Waals EOS when	
$\gamma = 1.4$, $K = 0.349$, and $a = 0.0025$	162
Figure 6.12(d): Magnetic pressure profiles for van der Waals EOS	
when $\gamma = 1.4$, $K = 0.349$, and $a = 0.0025$	162
Figure 6.13(a): Density profiles for van der Waals EOS when	
$\gamma = 1.4$, $K = 0$, and $a = 0.0075$	163
Figure 6.13(b): Velocity profiles for van der Waals EOS when	
$\gamma = 1.4$, $K = 0$, and $a = 0.0075$	163
Figure 6.13(c): Pressure profiles for van der Waals EOS when	
$\gamma = 1.4$, $K = 0$, and $a = 0.0075$	164
Figure 6.13(d): Magnetic pressure profiles for van der Waals EOS	
when $\gamma = 1.4$, $K = 0$, and $a = 0.0075$	164
Figure 6.14(a): Density profiles for van der Waals EOS when	
$\gamma = 1.4$, $K = 0.00349$, and $a = 0.0075$	165
Figure 6.14(b): Velocity profiles for van der Waals EOS when	
$\gamma = 1.4$, $K = 0.00349$, and $a = 0.0075$	165
Figure 6.14(c): Pressure profiles for van der Waals EOS when	
$\gamma = 1.4$, $K = 0.00349$, and $a = 0.0075$	166
Figure 6.14(d): Magnetic pressure profiles for van der Waals EOS	
when $\gamma = 1.4$, $K = 0.00349$, and $a = 0.0075$	166
Figure 6.15(a): Density profiles for van der Waals EOS when	
$\gamma = 1.4$, $K = 0.0349$, and $a = 0.0075$	167

Figure 6.15(b): Velocity profiles for van der Waals EOS when $\gamma = 1.4, K = 0.0349, \text{ and } a = 0.0075$	167
Figure 6.15(c): Pressure profiles for van der Waals EOS when $\gamma = 1.4, K = 0.0349, \text{ and } a = 0.0075$	168
Figure 6.15(d): Magnetic pressure profiles for van der Waals EOS when $\gamma = 1.4, K = 0.0349, \text{ and } a = 0.0075$	168
Figure 6.16(a): Density profiles for van der Waals EOS when $\gamma = 1.4, K = 0.349, \text{ and } a = 0.0075$	169
Figure 6.16(b): Velocity profiles for van der Waals EOS when $\gamma = 1.4, K = 0.349, \text{ and } a = 0.0075$	169
Figure 6.16(c): Pressure profiles for van der Waals EOS when $\gamma = 1.4, K = 0.349, \text{ and } a = 0.0075$	170
Figure 6.16(d): Magnetic pressure profiles for van der Waals EOS when $\gamma = 1.4, K = 0.349, \text{ and } a = 0.0075$	170
Figure 7.1: Solution domain $D(\lambda)$ and discrete finite difference grid	179
Figure 7.2: Graphical approach of $Z(\beta)$ in the case of Royce EOS; (a) $\Gamma_0 = 1.4$ and (b) $\Gamma_0 = 2.0$	186
Figure 7.3(a): Density profiles for Royce EOS when $\Gamma_0 = 1.4,$ $\sigma = 1.42, \text{ and } \Omega = 2$	187
Figure 7.3(b): Density profiles for Royce EOS when $\Gamma_0 = 1.4,$ $\sigma = 1.42, \text{ and } \Omega = 3$	188
Figure 7.4(a): Density profiles for Royce EOS when $\Gamma_0 = 2.0,$ $\sigma = 1.42, \text{ and } \Omega = 2$	189
Figure 7.4(b): Density profiles for Royce EOS when $\Gamma_0 = 2.0,$ $\sigma = 1.42, \text{ and } \Omega = 3$	190
Figure 7.5(a): Velocity profiles for Royce EOS when $\Gamma_0 = 1.4,$ $\sigma = 1.42, \text{ and } \Omega = 2$	191

Figure 7.5(b): Velocity profiles for Royce EOS when $\Gamma_0 = 1.4$, $\sigma = 1.42$, and $\Omega = 3$	192
Figure 7.6(a): Velocity profiles for Royce EOS when $\Gamma_0 = 2.0$, $\sigma = 1.42$, and $\Omega = 2$	193
Figure 7.6(b): Velocity profiles for Royce EOS when $\Gamma_0 = 2.0$, $\sigma = 1.42$, and $\Omega = 3$	194
Figure 7.7(a): Pressure profiles for Royce EOS when $\Gamma_0 = 1.4$, $\sigma = 1.42$, and $\Omega = 2$	195
Figure 7.7(b): Pressure profiles for Royce EOS when $\Gamma_0 = 1.4$, $\sigma = 1.42$, and $\Omega = 3$	196
Figure 7.8(a): Pressure profiles for Royce EOS when $\Gamma_0 = 2.0$, $\sigma = 1.42$, and $\Omega = 2$	197
Figure 7.8(b): Pressure profiles for Royce EOS when $\Gamma_0 = 2.0$, $\sigma = 1.42$, and $\Omega = 3$	198
Figure 7.9(a): Radiation profiles for Royce EOS when $\Gamma_0 = 1.4$, $\sigma = 1.42$, $\Omega = 2$	199
Figure 7.9(b): Radiation profiles for Royce EOS when $\Gamma_0 = 1.4$, $\sigma = 1.42$, $\Omega = 3$	200
Figure 7.10(a): Radiation profiles for Royce EOS when $\Gamma_0 = 2.0$, $\sigma = 1.42$, $\Omega = 2$	201
Figure 7.10(b): Radiation profiles for Royce EOS when $\Gamma_0 = 2.0$, $\sigma = 1.42$, $\Omega = 3$	202
Figure 7.11(a): Density profiles for perfect gas when $\sigma = \gamma$ and $\Omega = 2$	203
Figure 7.11(b): Density profiles for perfect gas when $\sigma = \gamma$ and $\Omega = 3$	204
Figure 7.12(a): Velocity profiles for perfect gas when $\sigma = \gamma$ and $\Omega = 2$	205

Figure 7.12(b): Velocity profiles for perfect gas when $\sigma = \gamma$ and $\Omega = 3$	206
Figure 7.13(a): Pressure profiles for perfect gas when $\sigma = \gamma$ and $\Omega = 2$	207
Figure 7.13(b): Pressure profiles for perfect gas when $\sigma = \gamma$ and $\Omega = 3$	208
Figure 7.14(a): Radiation profiles for perfect gas when $\sigma = \gamma$ and $\Omega = 2$	209
Figure 7.14(b): Radiation profiles for perfect gas when $\sigma = \gamma$ and $\Omega = 3$	210
Figure 8.1(a): Velocity profiles for condensed matter EOS when $\Gamma_0 = 1.017, K = 0$	247
Figure 8.1(b): Pressure profiles for condensed matter EOS when $\Gamma_0 = 1.017, K = 0$	248
Figure 8.2(a): Velocity profiles for condensed matter EOS when $\Gamma_0 = 2.12, K = 0$	249
Figure 8.2(b): Pressure profiles for condensed matter EOS when $\Gamma_0 = 2.12, K = 0$	250
Figure 8.3(a): Velocity profiles for different values of Γ_0 when $m = 2, K = 0$	251
Figure 8.3(b): Velocity profiles for different values of Γ_0 when $m = 3, K = 0$	252
Figure 8.4(a): Pressure profiles for different values of Γ_0 when $m = 2, K = 0$	253
Figure 8.4(b): Pressure profiles for different values of Γ_0 when $m = 3, K = 0$	254
Figure 8.5(a): Velocity profiles for condensed matter when $\Gamma_0 = 1.017, m = 2, K \neq 0$	255

Figure 8.5(b): Velocity profiles for condensed matter	
when $\Gamma_0 = 1.017, m = 3, K \neq 0$	256
Figure 8.6(a): Pressure profiles for condensed matter	
when $\Gamma_0 = 1.017, m = 2, K \neq 0$	257
Figure 8.6(b): Pressure profiles for condensed matter	
when $\Gamma_0 = 1.017, m = 3, K \neq 0$	258
Figure 8.7(a): Velocity profiles for condensed matter	
when $\Gamma_0 = 2.12, m = 2, K \neq 0$	259
Figure 8.7(b): Pressure profiles for condensed matter	
when $\Gamma_0 = 2.12, m = 2, K \neq 0$	260
Figure 8.8(a): Velocity profiles for condensed matter	
when $\Gamma_0 = 2.12, m = 3, K \neq 0$	261
Figure 8.8(b): Pressure profiles for condensed matter	
when $\Gamma_0 = 2.12, m = 3, K \neq 0$	262

LIST OF TABLES

Table 3.1: The values of similarity exponent for dusty gas flow when $C_0 = 0.02$, α_n - Runge-Kutta method, α_c - CCW method	39
Table 3.2: The values of similarity exponent for condensed matter when $C_0 = 0.02$, α_n - Runge-Kutta method, α_c - CCW method	40
Table 4.1: The values of similarity exponent α for dusty gas flow	60
Table 4.2: The values of similarity exponent α for Royce EOS when $\Gamma_0 = 1.78$	60
Table 4.3: The values of similarity exponent α for Royce EOS when $\Gamma_0 = 2.02$	60
Table 4.4: The values of similarity exponent α for perfect gas EOS	60
Table 4.5: Maximum values of flow parameters G, V, Z, B for different values of C_0	63
Table 5.1: Selected values of β and α for McQueen EOS for different values of C_0	91
Table 5.2: Selected values of β and α for Royce EOS for different values of C_0 and an arbitrary constant b	91
Table 6.1: Similarity exponent α for Royce EOS when $\Gamma_0 = 1.78$ and 2.12	145
Table 6.2: Similarity exponent α for van der Waals EOS when $\gamma = 1.4$ and 1.6	145
Table 7.1: Selected values of similarity exponent α	182

for Royce EOS	
Table 7.2: Selected values of similarity exponent α	
for perfect gas	183
Table 8.1: Selected results of the similarity exponent α for perfect	
gas and the condensed matter EOS in the case of	
cylindrical geometry	241
Table 8.2: Selected results of the similarity exponent α for perfect	
gas and the condensed matter EOS in the case of	
spherical geometry	242

LIST OF SYMBOLS

A	Coefficient matrix of order 4 x 4 for derivative of state function F_v ; van der Waals gas constant for molecular cohesive forces
A^0	Proportionality constant
\tilde{A}	Dimensional constant
a	Arbitrary constant
a_0	Initial equilibrium speed of sound
a^2	Equilibrium speed of sound
B	New dimensionless magnetic pressure; van der Waals gas constant for finite size of molecules
B_{max}	Maximum value of reduced magnetic pressure
b	Arbitrary constant; non-idealness parameter
C	Matrix of order 4 x 1
C_0	Cowling number
c_1	Alfven speed of sound
c_p	Specific heat of the gas at constant pressure
c_v	Specific heat of the gas at constant volume
c_{pm}	Specific heat of the mixture at constant pressure
c_{sc}	Specific heat of the materials in condensed matter
c_{vm}	Specific heat of the mixture at constant volume
D	Speed of the shock wave or shock velocity; column vector
d	An arbitrary constant; non-idealness parameter
E	Total energy inside a blast wave
E_0	Initial energy input of explosion
e	Specific internal energy or internal energy per unit mass of volume

F	New dimensionless pressure; constant parameter; material property of the dusty gas particles; column vector
F_t, F_r	Partial derivatives with respect to time t and spacial coordinate r
F_v	Column vector of order 4×1
f	Dimensionless pressure
G	New dimensionless density; new dimensionless viscosity term; column vector
g	Dimensionless viscosity; non-dimensional density
G_m	Material property
G_{max}	Maximum value of reduced density
H	Magnetic field strength or transverse magnetic field
h	Magnetic pressure; step size
i (<i>subscript</i>)	Number of grid points
J	New dimensionless radiation flux
j	Flux of monochromatic radiation per unit area
j_0	Dimensional constant
K	Viscosity coefficient; absorption coefficient
k_0	Dimensional constant
k_c	Condensed parameter
L	New dimensionless magnetic pressure; lower triangular matrix
l	Dimensionless magnetic pressure
$l_{ij} (i \geq j)$	Diagonal elements of lower triangular matrix L
M	Material property of the dusty gas particles
$m = 1, 2, 3$	Planer, cylindrical, and spherical geometries of shock wave

P	New dimensionless pressure
\hat{P}	Dimensionless pressure
P^*	New dimensionless pressure
p	Pressure of the gas particles
p_0	Dimensional constant
q	Artificial viscosity
r	Single spatial coordinate or space coordinate
$R(t), R_s(t)$	Shock position at a time t
t	Time coordinate
t_c	Collapse time
U	New dimensionless pressure; upper triangular matrix
\hat{U}	Dimensionless velocity
U^*	New dimensionless velocity
$u_{ij} (i < j)$	Diagonal elements of upper triangular matrix U
$U_s(t)$	Shock speed
u	Fluid velocity; velocity of gas particles
V	New dimensionless velocity
\hat{V}	Dimensionless density
V^*	New dimensionless density
V_{max}	Maximum value of reduced velocity
v	Velocity of gas particles; non-dimensional velocity
$\nu = 1, 2, 3$	Planer, cylindrical, and spherical geometries of shock wave
W	The scale of velocity
X	Solution matrix of order 4 x 1
\dot{X}_1	Shock velocity
x	Space coordinate

$\Delta x, \Delta \lambda$	Spatial interval for space and similarity variable respectively
Y	Matrix of order 4 x 1
Z	New dimensionless pressure; volume fraction of the condensed matter
Z_0	The loss of compressibility of the condensed matter
Z_{max}	Maximum value of reduced pressure
ρ	Density of the gas particles
ρ_0	Density of unperturbed medium; dimensional constant
μ	Magnetic permeability
ε	Group parameter
$[\cdot]_{r, t}$	Partial differentiation with respect to time t and radial coordinate r
$[\dots]_1^2$	It represents the difference between the values of ahead upstream and behind downstream regions across shock wave respectively
$\Gamma(\rho/\rho_0)$	Mie-Gruneisen coefficient
Γ, Π	Functions to be determined according to EOS under consideration
π	Non-dimensional pressure
Γ_0	Non-ideal parameter; specific heat of the solid particles; Gruneisen parameter
α	Similarity exponent
α_0	Initial guess of α
α_n	Obtained values of similarity exponent for RK method
α_c	Obtained values of similarity exponent for CCW method
β	Measure of the shock strength
γ	Specific heat ratio of perfect gas

ξ	Similarity variable or self-similar coordinate
ξ_{min}	Minimum value of similarity variable ξ
ξ_{max}	Maximum value of similarity variable ξ
λ	Similarity variable
ψ	Dimensionless density; non-dimensional radiation flux
Ψ	New dimensionless density
ϕ	Dimensionless velocity
Φ	New dimensionless velocity
σ	Material property
\mathcal{L}	Lie derivative in the direction of the extended vector field
$\Omega = 2, 3$	It denotes the geometrical index for cylindrical and spherical cases of the shock waves respectively
1 and 0	Subscripts 1 and 0 denote the values immediately in front of the shock, behind the shock respectively
/	Differentiation with respect to ξ

Abbreviations

CCW	Chisnell-Chester-Whitham Method
DIA	Dust-Ion-Acoustic
DA	Dust-Acoustic
EOS	Equation of State
MATLAB	MATrix LABoratory
ODE	Ordinary Differential Equation
PDE	Partial Differential Equation
RK	Runge-Kutta Method
SIE	Specific Internal Energy

Chapter-1

Introduction

Fluids are a subcategory of the matter which includes gases and liquids. Gases and liquids called fluids because of their ability to flow, ability to deform when a force is applied, and high fluidity. At the atomic level, fluids are composed of atoms or molecules which flow easily; they are not tightly packed and fluid obtains the shape of the container which it occupies. The main difference between compressible and incompressible fluid is that a force applied to a compressible fluid changes the density of a fluid whereas a force applied to an incompressible fluid does not change the density to a considerable degree. Although almost all fluids are compressible, liquids are known as incompressible fluids and gases are called compressible fluids.

In general, gases (and plasma = ionized gas) are called compressible fluid. In normal temperature and pressure conditions, the volume or the density of a fluid does not change. But gases show variation in volume (hence in density) in the presence of even small variations in temperature or pressure. To name a particular fluid compressible, it should show a considerable change of density when a pressure or a force is applied. At the molecular level, when a pressure is applied on a gas, the pressure affects the gas in all directions, causing the molecules of the gas to result in a high degree of collisions. These collisions give more time

for the gas molecules to interact with each other and more attraction forces between molecules may occur. These attraction forces reduce the motion of gas molecules. This results in the compression of the gas.

In a compressible fluid, the imposition of a force at one end of a system does not result in an immediate flow throughout the system. Instead, the fluid compresses near where the force was applied; that is, its density increases locally in response to the force. The compressed fluid expands against neighboring fluid particles causing the neighboring fluid itself to compress and setting in motion a wave pulse that travels throughout the system. The pulse of higher density fluid takes some time to travel from the source of the disturbance down through the pipe to the far end of the system.

In more advanced fluid dynamic terms, the ratio between the velocity of flow and the velocity of sound in the fluid is greater than 0.3 for compressible fluids. This ratio is also called Mach number.

Compressibility becomes important for high speed flows where $M > 0.3$

$M < 0.3$ – subsonic & incompressible

$0.3 < 0.8$ – subsonic & compressible

$0.8 < 1.2$ – transonic flow – shock waves appear mixed subsonic and sonic flow regime

$M > 3.0$ – hypersonic flow, shock waves and other flow changes are very strong.

The study of compressible flow is relevant to high-speed vehicles i.e., aircraft, jet engines, rocket motors, high-speed entry into a planetary atmosphere, gas pipelines, commercial applications such as abrasive blasting, and many other fields. The study of gas dynamics is often associated with the flight of modern high-speed aircraft and atmospheric reentry of space-exploration vehicles. The resistance from the surroundings on its body should be minimum. In order to maintain such minimum resistance the concept of aerofoil is useful. An aerofoil is the term used to describe the cross-sectional shape of an object that, when moved through a fluid such as air, creates an aerodynamic force. Aerofoils are employed on aircraft as wings to produce lift or as propeller blades to produce thrust. Aerodynamics is the way air moves around things. The rules of aerodynamics explain how an airplane is able to fly. Anything that moves through air reacts to aerodynamics. Thus the motion of the air around the wings or around the body of the vehicle produces shock waves.

Shock wave (also spelled shockwave), or shock, is a type of propagating disturbance. When a wave moves faster than the local speed of sound in a fluid, it is a shock wave. Like an ordinary wave, a shock wave carries energy and can propagate through a medium; however, it is characterized by an abrupt, nearly discontinuous change in pressure, temperature and density of the medium.

The abruptness of change in the features of the medium, characterize shock waves and the study of unsteady flow of compressible fluid behind the strong shock

propagation associated with the phenomena like explosion, implosion etc., is of importance in many fields of science and engineering such as aerodynamics, astrophysics, nuclear science, and plasma physics. These flows are governed by nonlinear partial differential equations of hyperbolic type. To study such flows one has to solve the nonlinear partial differential equations for which there are no analytical solutions. Immense progress in the study of shock waves has been made by Taylor [1, 2], Sedov [3] and Stanyukovich [4] by making use of similarity method. The similarity method simplifies the problem without losing the nonlinear nature of the governing equations. The solution of the self-similar problem depends in determining the numerical value of similarity exponent α that characterizes the space-time path of the infinite strength incoming (converging) and finite-strength reflected (diverging) shock waves in the proximity to the location of collapse. The applications of similarity methods are detailed in the texts [4-9]. It is because of this reason valuable contributions were made in various shock wave problems such as laser induced shock waves [10], underground nuclear explosion [11, 12], and double detonation supernovae [13, 14]. Theoretical investigation of shock wave behaviour near the centre of convergence was first studied by Guderley [15]. Guderley's observation is that certain physical assumptions alone lead to a self-similar problem formulation. The self-similar problems were investigated independently by Chester [16], Chisnell [17] and Whitham [18]. In recent developments of the shock wave theory many new mathematical models and approximate analytical methods were found

to be useful to solve a variety of shock wave problems. Among these some of the well known methods are Von Neuman method [19], Quasi-steady method due to Oshima [20], Phase plane analysis [5, 7, 8], late stage equivalence principle [21], operator splitting methods [22], Multi-scale finite element approximation [23], etc.

In this thesis an attempt has been made to investigate the approximate analytical and numerical solutions for some shock wave problems with applications in aerodynamics and many engineering and scientific applications. There are eight chapters following the present one dealing with different problems. The summaries of these chapters are presented briefly.

The study of similarity solutions to shock waves in non-ideal magnetogas-dynamics is carried out by many authors [24-28] because of their applications in aerodynamics, astrophysics, nuclear science and plasma physics. These authors concluded that the similarity solution to their model is valid under constant axial current and valid for small times, for some arbitrary constants obeying some power law relating the shock radius R_s , time t and the similarity exponent α . In general it is written as $R_s \propto (-t)^\alpha$. They assumed that the shock is propagating into a medium satisfying the EOS of perfect gas. Such a simple equation of state may not be true in reality for these type of problems.

In chapter three, the self-similar solution for imploding cylindrical shock waves generated due to impulsive motion of piston in non-ideal medium is presented.

The flow is assumed to be one dimensional unsteady cylindrical flow of an inviscid non-ideal gas with dust particles. The investigation involves study of various aspects of nonlinear wave propagation. The medium generated due to such implosion is assumed to be of Mie-Gruneisen type with magnetic or non-magnetic in nature. Impulsive motion of the piston is assumed to produce an instantaneous unsteady shock which may grow or decay with time, depending on the condition of the undisturbed gas and the behaviour of the piston. The form of these waves are altered by convection which distorts the wave form by causing the compression phase to move forward faster than the expansion phase. Thus it is assumed that plasma is generated and has an infinite electrical conductivity and permeated by an axial magnetic field orthogonal to the trajectories of gas particles. The equations of motion governing such motion are system of non-linear partial differential equations. Analytical solution to the assumed model is difficult and numerical solution is presented. The numerical solution discussed in this chapter gives global solution to the implosion problem. This is valid for a range of physically meaningful parameters which represent the EOS of Mie-Gruneisen type. In this chapter apart from considering the non-ideal models of Pai, Anisimov and Spinner [29, 30], we considered the EOS which depend on material property. By this both dusty gas and condensed matter EOS are defined exclusively. This was found to be more realistic than mere assumption of perfect gas. We assume that the motion of the piston obeys a power law [31]. Computations are performed to obtain the similarity exponent using Runge-Kutta

4th order (RK) method and CCW method. The computed values of the similarity exponent are in good agreement with those obtained using CCW method and are presented in tabular form. The assumed approximation provides a quick and relatively accurate method of determination of the similarity exponent and stability of shocks in non-ideal gas. Also the numerical description of the flow field behind the wave front in a non-ideal magnetogasdynamics regime is presented. An attempt is made to develop the magnetic field strength effect on the flow parameters in a non-ideal medium. All numerical computations are made using MATLAB.

In this chapter, we studied the numerical solution to strong cylindrical shock waves in the presence of magnetic field satisfying the EOS of Mie-Gruneisen type. Similarity solutions to such problems are carried out by authors Ponchaut et al. [32], Genot [33], Bazalitski et al. [34], Viswakarma and Srivastava [35], Pullin et al. [36], and Mostert et al. [37]. They assumed the problem to be an implosion problem of converging cylindrical shock wave in ideal gas.

In chapter four, we studied the numerical solution to a strong cylindrical shock wave in the presence of magnetic field. The medium generated due to implosion is assumed to be of Mie-Gruneisen type with or without magnetic material. In the implosion process (by impulse method) plasma is assumed to be generated. It is assumed that this plasma has an infinite electrical conductivity and permeated by an axial magnetic field orthogonal to the trajectories of gas particles. Numerical

solution presented is a very general solution to the implosion problem and is valid for a very large range of physically meaningful parameters which represent the EOS of Mie-Gruneisen type. Numerical computations are performed to obtain the similarity exponent iteratively using MATLAB. The aim of the present work is to understand the mechanical properties of shock waves in the presence of strong magnetic field; to study the behavior of shock characteristics such as shock strength, shock density, shock speed, shock over pressure, and impulse. In this chapter, we studied effect of magnetic field on flow variables in the presence of dusty gas particles. The behavior of approximate reduced density, velocity, pressure, and magnetic pressure behind the shock front in Royce EOS, and in perfect gas is investigated. The effect of measure of shock strength β , along with the similarity exponent α on converging geometry or area of contraction of the shock wave is studied.

In chapter five, a model to determine the similarity solutions to the problem of gas dynamic flow under the influence of strong magnetic field is presented. The model involves distinct features: the global behavior of the physical parameter has been studied; the initial pressure ratio is confined to a moderate value. The path of the piston is imposed as boundary condition. Thus an accelerated, a decelerated or a constant velocity piston can be specified. Self-similarity requires the velocity of shock and the velocity of piston to be proportional to some power law $R(t) \propto (t)^\alpha$ where $R(t)$ is the position of the shock wave front from the

center at time t and α is the similarity exponent. The numerical values of similarity exponents and profiles of flow variables are obtained. These are presented through the illustrative graphs and tables. The magnetic field effects on the flow variables through a medium and total energy under the influence of strong magnetic field are presented.

With an aim to investigate the effect of viscosity and to confirm the effect of (i) the non-idealness parameter and the viscosity parameters on the shock strength and the flow variables respectively, (ii) effect of discontinuities of the physical parameters due to viscosity and (iii) complete flow field depending on the magnitude of the viscosity the problem of similarity solutions of spherical shock waves and effect of viscosity is presented in chapter six. The effect of viscosity in physics and mathematical investigation shows that the presence of viscosity means the existence of a continuous, differentiable solution. The actual formulation of artificial viscosity introduced by von Neumann and Richtmyer [40] involved adding a viscosity term to the momentum equation, that augments the pressure in the instance there is shock compression and is independent of shock strength. Thus the system generated by artificial viscosity term will satisfy the Rankine-Hugoniot jump conditions [41] in the shock region and has little effect outside the shock layer. It is also observed the removal of inhomogeneities in velocities, is due to distribution of cohesive forces in the fluids [42]. This viscosity effect was found to be one of the most important effects in the equations

of motion. The shock heating of solar corona discussed by Orta et al. [43] have shown that the shock thickness and profile depend on viscosity and resistivity and as a consequence heating ultimately occurs. Ballai et al. [44] in the study of dispersive shock waves concluded that the effect of dispersion will alter the amplitude and propagation speed of a shock wave and also discussed in detail the viscosity effect. The supersonic flows exhibit an important property i.e., the coexistence of shock waves with viscous effects for many fluid dynamic systems [45]. In our study an attempt is made to understand the evolution of disturbances in viscous flow and its mechanisms in MHD for the development of efficient methods for controlling different types of flows.

A theoretical model for strong converging cylindrical and spherical shock waves in non-ideal gas characterized by the EOS of the Mie-Gruneisen type in stellar medium is investigated in chapter seven. Several authors Gail et al. [46], Fleck and Schmitz [47], Barnwal and Srivastava [48], Nicastro [49], etc., have investigated the shock wave problems in stellar atmosphere of the motion of a gas under the action of monochromatic radiation assuming the medium to be an ideal gas which may not be true in reality. The governing equations of unsteady one dimensional compressible flow including monochromatic radiation in Eulerian hydrodynamics are considered. The non-ideal medium of the gas is included in the governing equations by the presence of the type of EOS considered. Shock is assumed to be strong and propagating into a medium

according to a power law. In the present work, two different equations of state (EOS) of Mie-Gruneisen type have been considered and the cylindrical and spherical cases are worked out in detail. The complete set of governing equations is formulated as finite difference problem and solved numerically using MATLAB. The numerical technique applied in this chapter provides a complete solution to the problem for the flow variables, the similarity exponent α for different Gruneisen parameters. It is observed that increase in measure of shock strength β has effect on the shock front i.e., the velocity and pressure behind the shock front increases quickly in the presence of the monochromatic radiation and decreases gradually. A comparison between the results obtained for non-ideal and perfect gas in the presence of monochromatic radiation has been illustrated graphically.

In chapter eight, self-similar solution of one-dimensional strong converging cylindrical and spherical shock waves in non-ideal gas is investigated. Several solution techniques exist for the self-similarity problem. One such method is based on group theoretical approach, such approach is Lie group. Advantages of Lie group method is that it (i) reduces the order of an ordinary differential equation, (ii) leads to the superposition of solutions in terms of transforms for a linear partial differential equation and (iii) transforms nonlinear partial differential equation to linear partial differential equation, called determining equations. In recent times several investigators applied this theory in the field of

similarity analysis viz., [123-127] etc. In this chapter one-parameter infinitesimal group of transformations are used. The strong converging spherical and cylindrical shock wave is assumed to be generated by the rapid release of energy from a centered source. It is assumed that the limiting motion will be self-similar as the wave converges to the center. The numerical technique employed to study the nature of shock dynamics through a non-ideal medium described by the EOS of Mie-Gruneisen type. The study of the problem is to obtain a self-similar solution of converging shock wave near the centre (axis) of implosion and to investigate the behavior of flow parameters immediately behind the shock front in condensed matter EOS for a physically meaningful range of Gruneisen parameters.

Chapter-2

Literature Review

Compressible flow or gas dynamics is the branch of fluid mechanics that deals with flows having significant changes in fluid density. Gases mostly display such behavior. The study of compressible flow is relevant to high-speed vehicles i.e., aircraft, jet engines, rocket motors, high-speed entry into a planetary atmosphere, gas pipelines, commercial applications such as abrasive blasting, and many other fields. The study of gas dynamics is often associated with the flight of modern high-speed aircraft and atmospheric reentry of space-exploration vehicles. At the beginning of the 19th century, investigation into the behavior of fired bullets led to improvement in the accuracy and capabilities of guns and artillery. As the time progressed inventors and researchers sought to understand the physical phenomena involved through experimentation. At the beginning of the 20th century, the study of gas dynamics research shifted to understanding the process involving mathematical and experimental concepts. Korobeinikov [70] and other researchers proposed important concepts ranging from the boundary layer to supersonic shock waves, supersonic wind tunnels, and supersonic nozzle design. Later, Landau and Lifshitz [91] improved the understanding of these flows. Several other notable researchers contributed significantly to the principles considered fundamental to the study of modern gas dynamics.

A related assumption is the no-slip condition where the flow velocity at a solid surface is presumed equal to the velocity of the surface itself, which is a direct consequence of assuming continuum flow. The no-slip condition implies that the flow is viscous, and as a result a boundary layer forms on bodies traveling through the air at high speeds, much as it does in low-speed flow.

Compressible flow problems require more equations: an EOS for the gas and a conservation of energy equation, for solution process. For the majority of gas-dynamic problems, the simple ideal gas law is the appropriate state equation.

Fluid dynamics problems have two overall types of reference frames, called Lagrangian and Eulerian [91]. The Lagrangian approach follows a fluid mass of fixed identity as it moves through a flow field. The Eulerian reference frame, in contrast, does not move with the fluid. Rather it is a fixed frame or control volume that fluid flows through. The Eulerian frame is most useful in a majority of compressible flow problems, but requires that the equations of motion be written in a compatible format along with EOS.

Compressible flows are recognized by the property, the Mach number. The Mach number (M) is defined as the ratio of the speed of an object (or of a flow) to the speed of sound. For instance, in air at room temperature, the speed of sound is about 340 m/s (1,100 ft/s). M can range from 0 to ∞ , but this broad range falls naturally into several flow regimes. These regimes are subsonic, transonic, supersonic, hypersonic and hypervelocity flow. The flow regimes are not chosen

arbitrarily, but rather arise naturally from the strong mathematical background that underlies compressible flow [91]. At very slow flow speeds the speed of sound is so much faster that it is mathematically ignored, and the Mach number is irrelevant. Once the speed of the flow approaches the speed of sound, however, the Mach number becomes all-important, and shock waves begin to appear. Thus the transonic regime is described by a different (and much more difficult) mathematical treatment. In the supersonic regime the flow is dominated by wave motion at oblique angles similar to the Mach angle. Above about Mach 5, these wave angles grow so small that a different mathematical approach is required, defining the hypersonic speed regime. Finally, at speeds comparable to that of planetary atmospheric entry from orbit, in the range of several km/s, the speed of sound is now comparatively so slow that it is once again mathematically ignored in the hypervelocity regime.

Another very important concept frequently used is self-similarity that results when the symmetry of a physical problem leads to a reduction in the number of the independent variables. In this way a considerable simplification is achieved, that frequently allows the analytical treatment of the problem. Very elegant solutions can thus be derived. Usually the self-similar behavior appears in the intermediate asymptotics of phenomena, when certain details of the initial or boundary conditions are no longer relevant, so that the corresponding parameters can be ignored. The peculiarities of the passage to the limit that leads to the

intermediate asymptotics of a given problem allows to classify the similarity solutions as self-similarities of the first and second kind. Self-similarity of the first kind can be established by dimensional analysis (eventually supplemented by other symmetry considerations). The self-similarities of the second kind cannot be derived in this way: it is necessary to follow the evolution of the solution either experimentally or numerically until it passes into its self-similar asymptotics, or they can be obtained by direct construction. In the second case this process leads to a nonlinear eigenvalue problem.

The major objective of the study of compressible fluid flow lies in the study of shock waves. Shock waves are a physical phenomenon which occur in a medium subjected to high speed movement in the transonic and supersonic range. Historically it took some time to get the correct understanding of the mechanical and thermodynamic interaction of the related physical quantities which takes place when material passes through a shock front. The shock layer is the region where the change of state takes place. It is geometrically small with respect to all other quantities at a typical technical application. A shock wave is a type of propagating disturbance. Like an ordinary wave, it carries energy and can propagate through a medium (solid, liquid, gas or plasma) or in some cases in the absence of a material medium, through a field such as the electromagnetic field. Shock waves are characterized by an abrupt, nearly discontinuous change in the characteristics of the medium. Across a shock there is always an extremely rapid

rise in pressure, temperature and density of the flow. A shock wave travels through most media at a higher speed than an ordinary wave. A shock wave will collide with “normal” stationary air, and give some of the energy to it. As the energy spreads to larger and larger volumes of air, the shock wave decays into a "normal" sound wave pulse. But before that, the wall of highly compressed air will travel at supersonic speed. The shocks can be categorized as moving shocks, bow shocks, attached shocks, recompression shocks etc. The phenomenon of shock has been first mathematically described by Hugoniot [91] in the case of the one dimensional flow of a perfect gas. The EOS has a decisive effect on the shock phenomena that can exist in the material such as weak shock or strong shock. There are five laws or theorems and the most important of them is the Rankine-Hugoniot (R-H) equations. These are derived from the conservation laws of mass, momentum, and energy. These equations include terms containing the velocities of the material on both sides of the shock wave. If the equations are manipulated to eliminate these terms, then a single equation containing only thermodynamic variables of state is obtained. This is the Hugoniot equation, and it is the starting point for many investigations. The medium into which the shock propagates and decays and the behavior of flow variables is the study of many researchers because theory of shock waves has several applications in science and engineering. The major applications are in the area of astrophysics, nuclear science, geophysics, plasma physics etc. This has motivated us to study in an investigative way and research the area of shock waves. The research problems

pertains to some self-similar solutions to shock wave problems in non-ideal medium. The introduction chapter of my thesis gives more details. The medium considered is of Mie-Gruneisen type considering different EOS. In this work not only self-similar solutions but also lie-group approach, classical numerical methods, CCW method and finite difference methods are attempted. Some of the many research articles referred are as follows.

A theoretical study of the imploding shock wave near the center of convergence, in an ideal gas was first investigated by Guderley [15]. Several authors contributed to this investigation and we mention the contributions of Hafner [54], Manganaro and Oliveri [26], Sharma and Radha [96], Ali and Hunter [24], Sharma and Arora [97], Stanyukovich [6], Chisnell [17, 84], Lazarus and Richtmyer [50], Ramu and Ranga Rao [57], Madhumita and Sharma [38], Sen [98]. The similarity solutions of converging spherical and cylindrical shock wave problems with different equation of states (EOS) were investigated by several authors [1, 6, 7, 9, 12, 15, 19, 22, 24]. The existence and effects of the viscous forces for the similarity solutions to shock wave problems were studied by several researchers [101-104]. Landau and Lifshitz [91] and Zeldovich and Raizer [7] have studied the entropy production in a viscous medium and developed an analytical model for the shock process based on Hugoniot curves considering the effects of viscosity and heat conduction.

The role of viscosity in physics and mathematical investigation of model problems suggest that the presence of viscosity implies the existence of a continuous, differentiable solution. This mathematical theory does not guarantee this in general. The actual formulation of artificial viscosity introduced by von Neumann and Richtmyer [40] involved adding a viscosity term to the momentum equation, that augments the pressure in the instance there is shock compression and is independent of shock strength. The new system will satisfy the Rankine-Hugoniot jump conditions [41] in the shock region and has little effect outside the shock layer. The resistance to variations in distribution of cohesive forces in fluids experienced result in removing the inhomogeneities in velocities. These types of resistances result in the phenomenon of viscosity in fluid motions [42]. This viscosity effect was found to be one of the most important effects in the equations of motion. The shock heating of solar corona discussed by Orta et al. [43] have shown that the shock thickness and profile depend on viscosity and resistivity and as a consequence heating ultimately occurs. Ballai et al. [44] in the study of dispersive shock waves concluded that the effect of dispersion will alter the amplitude and propagation speed of a shock wave and also discussed in detail the viscosity effect. The supersonic flows exhibit an important property i.e., the coexistence of shock waves with viscous effects for many fluid dynamic systems [45]. Also the viscous interactions of solar wind stream were studied by Korzhov et al. [45]. The study of interplanetary shock waves are produced due to coronal mass ejection and solar winds and study of these is very important for space

weather purposes. The shock waves occur where the solar wind changes from being supersonic to being subsonic. In the supersonic regime of compressible gas flow the interaction of shock waves with viscosity is a very important problem. Mathematically this can be approximated to a hydrodynamic case.

It is observed from most of the literature reviewed the researchers have developed shock wave problems with the assumption that the medium into which the shock propagates to be an ideal gas. The gap areas have been identified and the following assumptions have been implemented in our work viz.,

- (i) the assumption of ideal gas medium may not be true in reality hence non-ideal medium is considered,
- (ii) EOS of the medium is to be of Mie-Gruneisen type,
- (iii) use of Cowling number,
- (iv) introducing artificial viscosity, etc.

The main objective in the study is to implement the above assumptions and develop alternative solution methods and obtain high accuracy general solution.

The error tolerance is taken to be 10^{-6} .

The methodology involves in the developing a feasible mathematical model along with suitable boundary conditions. The mathematical model governing equations are highly non-linear partial differential equation of hyperbolic type with moving boundary conditions. The closed form analytical solutions to the developed

models will be difficult as can be seen from reviewed literature. In each of the mathematical model developed the solution methodology involves use of group theoretical approach, non-dimensionalisation of the governing equations along with numerical solution and validation of the results.

Chapter-3

Similarity Solutions to Shock Waves in Non-ideal

Magnetogasdynamics

3.1 Introduction

Shock waves are common phenomena and the study of shock waves has several applications in the areas of aerodynamics, astrophysics, nuclear science, and plasma physics. The strong shock wave problem in converging cylindrically or spherically in a gas is well known in hydrodynamics and is considered important in converging compressible flow to the laser induced shock waves [10], underground nuclear explosion [11, 12] and in astrophysical applications to double detonation supernovae [13, 14]. Converging shock waves have been a field of interest since second world war from both mathematical and physical point of view. Theoretical investigation of shock wave behaviour near the centre of convergence was first studied by Guderley [15]. Guderley observed that certain physical assumptions alone lead to a self-similar problem formulation. The solution of the self-similar problem depended on determining the numerical value of similarity exponent α . Converging and diverging shock wave are investigated independently by Chester [16], Chisnell [17] and Whitham [18] with approximate methods, specifically to geometrical shock dynamics. In their solutions, the

similarity exponent in the expression for Mach number as a function of shock radius for the spherical case is exactly twice that for the cylindrical case.

The study of shock waves for peaceful applications is another area of interest for assessment and prediction of disasters, underground explorations, etc. Shock waves are produced due to the sudden release of an enormous amount of energy from sources such as a nuclear explosion, detonation, or rupture of a pressurized vessel. Shock waves are common phenomena in the interstellar medium in the presence of supersonic motions, supernova explosions, central part of star burst galaxies, etc. Imploding shock waves have been a field of continuing research interest over the years as possible methods for generating high-pressure, high-temperature plasmas at the center of convergence, as well as to understand the basic fluid dynamics involved in the process. Shock waves are generated by point explosions (nuclear explosions and detonation of solid explosives), high pressure gas containers (chemical explosions) and laser beam focusing. Shock wave phenomena also arises in astrophysics, hypersonic aerodynamics and hypervelocity impact, etc. Understanding the properties of the shock waves both in the near-field and the far-field is useful with regard to the characteristics such as shock strength, shock overpressure, shock speed, and impulse. The motion of the converging/diverging shock is assumed to be radially symmetric. Pre-shocked gas is assumed to be uniform and at rest. The incoming shock is reflected at the center of symmetry, such that the symmetry condition, i.e., zero particle velocity

at the center, is maintained at all times. The outgoing reflected shock is propagated into a non-uniform flow field which has been produced by the incoming shock (Figure 3.1). The shock waves propagate into the medium and effect on the flow field. Thus, the shock propagation should be determined together with the flow field from the governing equations and the shock-jump relations. However, even in a uniform medium, the problem of the shock propagation in general cannot be solved analytically. We also note the works of Lazarus and Richtmyer [50], Lazarus [51, 52], Van Dyke and Guttman [53], Hafner [54], Wu and Roberts [55], Madhumita and Sharma [56], Ramu and Rangarao [57], Patel and Rangarao [58] as contributions towards the investigation of the implosion problem. These authors calculated the numerical value of the similarity exponent (a function of the adiabatic exponent and geometry) with high accuracy using various techniques.

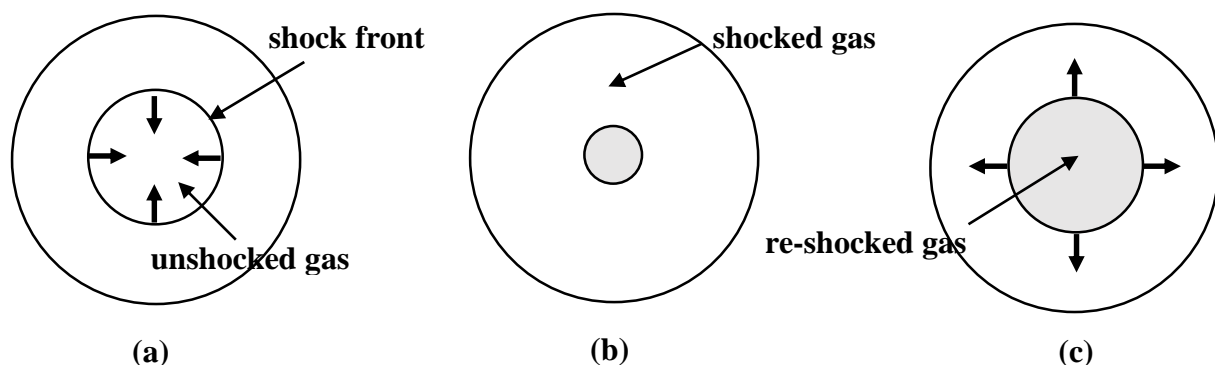


Figure 3.1. Collapsing cylindrical shock waves in non-ideal medium; (a) an imploding strong shock, (b) converges on the center and (c) rebounds, reshocking previously shocked material.

The ‘classic’ Guderley problem, reviewed by Meyer-ter-Vehn and Schalk [59], Zeldovich and Raizer [7] has variations that have been explored in detail. Axford and Holm [60] used group theoretic techniques to determine a more general EOS (represented through the adiabatic bulk modulus) that admits self-similar solutions for a Guderley-type problem. Wu and Roberts [55] investigated the special case of a strong shock wave converging into a van der Waals gas. Several authors investigated similarity solutions for strong shock waves converging into dusty gases [61, 62], variable-density gases [56, 63, 64], radiating gases [49, 65]. The self-similar solution of the classical Guderley implosion problem in a dust-laden gas has been studied by Hirschler and Steiner [66]. This self-similar solution covers the collapse as well as the expansion of the reflected shock. Ponchaut et al. [32, 67] and Hornung et al. [39] considered the universality of imploding shock solutions from examination of approximate solutions for the Guderley problem and computed solutions of converging shocked flows.

The study of shock wave in dusty gas and in condensed matter is of great importance due to its application to nozzle flow, fluidized beds, centrifugal separation of particular matter from fluids, rocket-fuel combustion products, underground or underwater explosions, etc. Sedov [5], Miura and Glass [68, 69], and Korobeinikov [70] investigated the generalized the well known solution of a strong explosion due to an instantaneous release of energy in a gas, considering the case of two phase flow of a mixture of perfect gas and small solid particles.

The flow resulting from the passage of a shock wave through a dusty-gas layer studied theoretically by Miura and Glass [68] have developed a criteria for the wave reflection at the contact surface separating the pure gas from the dusty-gas layer in terms of the properties. Again, Miura and Glass [69] obtained an analytical solution for planar dusty gas flow with constant velocities of the shock and the piston moving behind it. Investigations into dusty plasmas include aspects of fundamental problems in the physics of plasmas, hydrodynamics, kinetics of phase transitions, nonlinear physics, etc. Similarity solutions for strong shock waves converging into a dusty gas EOS of Mie-Gruneisen type has attracted the interest of many researchers. Narasimhulu Naidu et al. [71] obtained an approximate analytical solution for a self-similar flow behind a strong shock wave propagating outward in a particle laden gas with variable total energy release by employing integral method. Suzuki et al. [72] obtained similarity solutions for plane or line source explosions in a dusty gas. Higashino and Suzuki [73], extended the analysis by expanding the self-similar flow variables to a series of inverse squares of shock Mach numbers to a first order of approximation. Employing the method of characteristics, the unsteady propagation of shock waves in a dusty gas in order to clarify the effects of the inter particle and particle gas interactions during the relaxation process has been studied by Higashino [74]. Jena and Sharma [61] used the similar method to study the problem of shock wave propagation through a dusty gas mixture obeying the EOS of Mie-Gruneisen type. They found that the problem admits a self-similar solution only when the ambient

medium ahead of the shock is of uniform density. Rai [62] studied the problem of converging spherical and cylindrical detonation waves in dusty medium with constant density and releasing a constant amount of energy per unit mass to dusty gas. He developed an expression for similarity exponent and studied the effects of constant density and dust particles on the front velocity and flow parameters analytically. Steiner and Hirschler [75] have considered analytic solutions for the unsteady one-dimensional self-similar flow field between a strong shock and a moving piston behind it in a dusty gas. They have shown that the flow field is mainly affected by the dust's impact on the speed of sound. A similarity solution has been obtained by Gretler and Regenfelder [76, 77] for a laser-driven strong shock wave propagating into a mixture of gas and small solid particles. Mamun and Shukla [78] have been investigated non-planer (viz. cylindrical and spherical) electro-acoustic (DIA and DA) shock waves by employing the reductive perturbation method. They examined the effects of cylindrical and spherical geometries on the time evolution of dust-ion-acoustic and dust-acoustic shock structures.

In this chapter, the self-similar solution for imploding cylindrical shock waves in non-ideal medium is presented. We consider system of partial differential equations describing the one dimensional unsteady cylindrical flow of an inviscid non-ideal gas with dust particles and study various aspects of non-linear wave propagation. The medium generated due to implosion is assumed to be of Mie-

Gruneisen type with magnetic or non-magnetic in nature. Impulsive motion of the piston may produce instantaneous unsteady shock which may grow or decay with time, depending on the condition of the undisturbed gas and the motion of the piston. The forms of these waves are altered by convection which distorts the wave form by causing the compression phase to move forward faster than the expansion phase. Thus it is assumed that plasma is generated with an infinite electrical conductivity and permeated by an axial magnetic field orthogonal to the trajectories of gas particles. Similarity solution to this problem is attempted. Analytical solution to the assumed model is difficult and numerical solution is presented. The numerical solution presented provides a global solution to the implosion problem and is valid for a range of physically meaningful parameters which represent the EOS of Mie-Gruneisen type. In the present work apart from considering the non-ideal models described by Pai, Anisimov and Spinner [29, 30], we presented the EOS generated by including the material property. This process defines both dusty gas and condensed matter EOS. This concept is different from the existing models of the definition of dusty gas and condensed matter and is more realistic than mere assumption of perfect gas. It is assumed that the motion of the piston obeys exponential law [31] and computations are performed to obtain the similarity exponent using MATLAB and CCW rule. The computed values of the similarity exponent are in good agreement with those obtained using CCW method and are presented in tabular form. This approximation provides a quick and relatively accurate determination of the

similarity exponent and stability of shocks in non-ideal gas. The numerical description of the flow field behind the wave front in a non-ideal magnetogasdynamics regime is also presented. An attempt is made as to study the magnetic field strength effect on the flow parameters in a non-ideal medium. These effects are presented in the form of graphs.

3.2 Governing Equations

Neglecting the viscous stress, body forces, thermal radiation and heat-conduction of the medium the equations governing the motion of one-dimensional unsteady compressible flow of strong converging cylindrical shock waves into a non-ideal gas can be expressed into the following form Korobeinikov, Anisimov and Kravchenko [70, 79]

$$\rho_t + v\rho_r + \rho v_r + \rho v r^{-1} = 0 \quad (3.1)$$

$$v_t + vv_r + \rho^{-1}(p_r + h_r) = 0 \quad (3.2)$$

$$e_t + ve_r - \rho^{-1}p \left(\frac{\partial}{\partial t} + v \frac{\partial}{\partial r} \right) \log \left(\frac{\rho}{\rho_0} \right) = 0 \quad (3.3)$$

$$h_t + vh_r - \rho^{-1}2h(\rho_t + v\rho_r) = 0 \quad (3.4)$$

where ρ is the density, ρ_0 is the density of unperturbed medium, p is the pressure, v is the velocity of gas particles, e is the specific internal energy (SIE), $h = \frac{\mu H^2}{2}$ is the magnetic pressure, H and μ being the magnetic field strength and the magnetic permeability respectively. The subscripts denote partial differentiation.

The independent variables are the single spatial coordinate r , and time t . The shock position is given by $R_s(t)$ and its speed is $U_s(t) = \frac{dR_s}{dt}$.

The system of equations (3.1-3.4) is supplemented with an EOS of Mie-Gruneisen type [57].

$$p = \rho e \Gamma(\rho/\rho_0) \quad (3.5)$$

here $\Gamma(\rho/\rho_0)$ is the Mie-Gruneisen coefficient. In order to obtain the similarity solutions of the problem the density of the undisturbed medium, ρ_0 is assumed to be constant. The shock jump conditions connect the pre-shock and post-shock fields. Shock is assumed to be strong and propagating into a medium at rest whose EOS is of Mie-Gruneisen type, according to the power law $R_s(t) \propto (1 - t/t_c)^\alpha$, where t_c is the collapse time, α is similarity exponent. After the collapse at $t = t_c$, the reflected shock wave begins to propagate through the medium away from the axis, whilst the medium continues to converge on the axis. Shock trajectory (i.e., shock position) $R_s(t)$ does not depend on the initial pressure pulse and approaches the similarity exponent α of the self-similar problem for time $t \rightarrow \infty$. Anisimov and Kravchenko [79] obtained a similarity solution describing the flow generated by an impulsive load, and the dependence of the similarity exponent upon EOS parameters which is true for a certain class of the equations of state [7, 80].

The converging shock wave problem is investigated by adopting an approximation on the Gruneisen coefficient to reduce the governing system of equations to first order ordinary differential equations of Poincare type. At the shock front, $r = R_s(t)$ the Rankine-Hugoniot jump conditions are

$$v_1 = \left(1 - \frac{\rho_0}{\rho_1}\right) U_s(t) \quad (3.6)$$

$$p_1 - p_0 + h_1 - h_0 = \rho_0 U_s(t) v_1 \quad (3.7)$$

$$e_1 - e_0 = \frac{v_1^2}{2} - \left[\frac{p_0}{\rho_1} + \frac{h_0}{\rho_1} \left(1 - \frac{\rho_1}{\rho_0}\right) \right] \left(1 - \frac{\rho_1}{\rho_0}\right) \quad (3.8)$$

$$h_1 = h_0 \left(\frac{\rho_1}{\rho_0}\right)^2 \quad (3.9)$$

The strong shock limit ($p_1 \geq p_0$ and $h_1 \geq h_0$) of the Rankine-Hugoniot jump conditions may be used to connect the flow just behind the shock to that just ahead of the shock front:

$$\left. \begin{aligned} \frac{\rho_1}{\rho_0} = \beta, \quad v_1 = \left(1 - \frac{1}{\beta}\right) U_s(t), \\ \frac{p_1}{\rho_0} = \left(1 - \frac{1}{\beta} - \frac{C_0 \beta^2}{2}\right) U_s^2(t), \quad \frac{h_1}{\rho_0} = \frac{C_0 \beta^2}{2} U_s^2(t) \end{aligned} \right\} (3.10)$$

where $C_0 = \frac{2h_0}{\rho_0 U_s^2(t)}$ is the Cowling number associated with magnetic property. If

$C_0 = 0$, the propagation of shock waves is without magnetic field and β is the measure of the shock strength. The subscripts 1 and 0 refers to the values immediately in front of the shock and behind the shock respectively.

With the above relations (3.10), the equation (3.5) can be written as

$$\left(2 - \frac{c_0 \beta^3}{(\beta-1)}\right) = (\beta - 1)\Gamma(\beta) \quad (3.11)$$

We seek self-similar solutions of governing equations (3.1-3.4) for which all the variables can be written in the form of products of a function of time t and a function of the dimensionless self-similar coordinate. Considering a new independent variable, $\xi = \frac{r}{R_s(t)}$ the flow pattern can be written in terms of the dimensionless functions of ξ as [7]

$$\rho = \rho_0 G(\xi), \quad v = U_s(t)V(\xi), \quad p = \rho_0 U_s^2(t)Z(\xi), \quad h = \rho_0 U_s^2(t)B(\xi) \quad (3.12)$$

where new dimensionless variables G , V , Z and B as functions of similarity variable ξ , which are to be determined in such a way that the partial differential equations (3.1-3.4), together with conditions (3.10), are invariant with respect to the transformations (3.12). The existence of such a group of transformations allows the number of independent variables in the problem to be reduced by one, and thereby allowing the system (3.1-3.4) to be replaced by a system of ordinary differential equations.

With the help of transformations (3.12) and using the simple mathematics we obtain the following form on the governing equations

$$\frac{\partial \rho}{\partial t} = \frac{d\rho_0}{dt} G - \rho_0 \frac{dG}{d\xi} \frac{r}{R_s^2(t)} \frac{dR_s}{dt} = \dot{\rho}_0 G - \rho_0 \xi \frac{dG}{d\xi} \frac{U_s(t)}{R_s(t)} \quad (3.13)$$

$$\frac{d\rho}{dr} = \frac{\rho_0}{R_s(t)} \frac{dG}{d\xi} \quad (3.14)$$

where dot denotes differentiation with respect to time.

The governing equations (3.1-3.4) may be transformed to a system of ODEs in the dimensionless variables ξ , $G(\xi)$, $V(\xi)$, $Z(\xi)$, and $B(\xi)$.

$$(\xi - V) \frac{1}{G} \frac{dG}{d\xi} - \frac{dV}{d\xi} = \frac{V}{\xi} \quad (3.15)$$

$$(\xi - V) \frac{dV}{d\xi} - \frac{1}{G} \left(\frac{dZ}{d\xi} + \frac{dB}{d\xi} \right) = \lambda V \quad (3.16)$$

$$\frac{1}{Z} \frac{dZ}{d\xi} - \phi(G) \frac{1}{G} \frac{dG}{d\xi} = \frac{2\lambda}{(\xi - V)} \quad (3.17)$$

$$\frac{1}{B} \frac{dB}{d\xi} - \frac{2}{G} \frac{dG}{d\xi} = \frac{2\lambda}{(\xi - V)} \quad (3.18)$$

where

$$\phi(G) = 1 + \Gamma(G) + \frac{G}{\Gamma(G)} \frac{d\Gamma(G)}{dG} \quad (3.19)$$

$$\lambda = 1 - \frac{1}{\alpha} \quad (3.20)$$

The function $\phi(G)$ involves EOS with material property, which defines non-ideal medium.

The system of equations (3.15-3.18) can be written into the following matrix form,

$$\begin{bmatrix} (\xi - V)/G & -1 & 0 & 0 \\ 0 & (\xi - V) & -1/G & -1/G \\ -\Phi(G)/G & 0 & 1/Z & 0 \\ -2/G & 0 & 0 & 1/B \end{bmatrix} \begin{bmatrix} \frac{dG}{d\xi} \\ \frac{dV}{d\xi} \\ \frac{dZ}{d\xi} \\ \frac{dB}{d\xi} \end{bmatrix} = \begin{bmatrix} V/\xi \\ \lambda V \\ \frac{2\lambda}{(\xi - V)} \\ \frac{2\lambda}{(\xi - V)} \end{bmatrix} \quad (3.21)$$

Also, the boundary conditions at the strong shock ($\xi = 1$) may be written as

$$G(1) = \beta, \quad V(1) = 1 - \frac{1}{\beta}, \quad Z(1) = 1 - \frac{1}{\beta} - \frac{c_0\beta^2}{2}, \quad B(1) = \frac{c_0\beta^2}{2} \quad (3.22)$$

The system of equations (3.15-3.18) can be solved for the derivatives $\frac{dG}{d\xi}$, $\frac{dV}{d\xi}$, $\frac{dZ}{d\xi}$,

and $\frac{dB}{d\xi}$ which are of the following form

$$\frac{dG}{d\xi} = \frac{\Delta_1}{\Delta}, \quad \frac{dV}{d\xi} = \frac{\Delta_2}{\Delta}, \quad \frac{dZ}{d\xi} = \frac{\Delta_3}{\Delta}, \quad \frac{dB}{d\xi} = \frac{\Delta_4}{\Delta} \quad (3.23)$$

where

$$\Delta = \frac{1}{G^2Z} [G(\xi - V)^2 - \phi(G)Z - 2B] \quad (3.24)$$

$$\Delta_1 = \frac{1}{Z} \left[\lambda V + \frac{V(\xi - V)}{\xi} + \frac{2\lambda Z}{(\xi - V)G} + \frac{2\lambda B}{(\xi - V)G} \right] \quad (3.25)$$

$$\Delta_2 = \frac{1}{G} \left[\frac{V\phi(G)}{\xi G} + \frac{\lambda V(\xi - V)}{Z} + \frac{2\lambda}{G} + \left(\lambda + \frac{V}{\xi G} \right) \frac{2B}{Z} \right] \quad (3.26)$$

$$\Delta_3 = \frac{1}{G} \left[\lambda V\phi(G) + 2\lambda(\xi - V) + \frac{V(\xi - V)\phi(G)}{\xi} + (\phi(G) - 2) \frac{2\lambda B}{G(\xi - V)} \right] \quad (3.27)$$

$$\Delta_4 = \frac{B}{G} \left[\frac{2V(\xi - V)}{\xi Z} + \frac{2\lambda V}{Z} + \frac{4\lambda}{G(\xi - V)} + \frac{2\lambda}{(\xi - V)} \left(\frac{(\xi - V)^2}{Z} - \frac{\phi(G)}{G} \right) \right] \quad (3.28)$$

Since the system (3.1-3.4) is a set of quasilinear hyperbolic partial differential equations, it is difficult to determine a solution without approximations. Here, we assume that there exists a solution of (3.1-3.4) subject to (3.10) along a family of curves, called similarity curves, for which the set of partial differential equations reduce to a set of ordinary differential equations, and also assume that the shock trajectory is embedded in the family of similarity curves. This type of solution is called a similarity solution.

3.3 Numerical Solution

The system of transformed equations are solved using 4th order RK-method and CCW methods using MATLAB.

a) The numerical solution involves solving system of equations (3.23) along with boundary conditions (3.22) using the explicit fourth order Runge-Kutta method. In order to compute similarity exponent α , we integrate equations (3.23) in the domain of interest $1 \leq \xi < \infty$ such that for a chosen value of α all the Δ_i 's become simultaneously zero at the same value of ξ , which is the singular point of the system. Finally we determine the values of α for different values of Mie-Gruneisen coefficient in non-ideal medium.

b) Chester-Chisnell-Whitham method: The case of shock propagating into a uniform quiescent gas, individually obtained a similar relation, using different methods, to relate the shock Mach number and the cross-sectional area of tube.

The relation derived is commonly referred to as the Chester-Chisnell-Whitham (CCW) relation or method. It provides a quasi-one-dimensional analysis. This method was proposed by Whitham [81], which is valid along a positive characteristic to the flow quantities immediately behind the shock. The CCW rule is based on Chester's result for the motion of a shock wave in a channel with a small change in area. The motion of shock waves can be analysed simply by applying the CCW approximation without solving the characteristic equations for the flow behind the shock wave front. Chester [16] considered the motion of a shock wave through a channel consisting of a section of slowly varying area separating two uniform ducts. Chisnell [17] integrated Chester's linearized formula with respect to the area difference between the uniform sections. Whitham [18, 81] showed that the motion of a shock wave can be analysed without solving the whole flow-field behind the shock wave and obtained the differential relation that satisfies the flow quantities along a positive characteristic line pertinent to the flow quantities behind the shock wave. Final formulation of Whitham's rule was very consistent with the results obtained by Chester and Chisnell. This approximate treatment for shock wave motion is generally extended to geometrical shock wave dynamics or ray shock wave theory and is often applied to analyses of shock focus on reflected shock waves from the reflectors.

The basic equations governing the flow (3.1-3.4) may be combined to get the following characteristic equation in terms of shock location $R_s(t)$ as [82]

$$\frac{dp_1}{dR_s(t)} + \frac{dh_1}{dR_s(t)} + \rho_1 c_1 \frac{dv_1}{dR_s(t)} + \frac{1}{R_s(t)} \left(\frac{\rho_1 c_1^2 v_1}{v_1 + c_1} - \frac{2h_1(v_1 - c_1)}{v_1 + c_1} \right) = 0 \quad (3.29)$$

where c_1 is the Alfvén speed in non-ideal medium, defined as

$$c_1 = \left[\left(1 + \Gamma \left(\frac{\rho_1}{\rho_0} \right) \right) \frac{p_1}{\rho_1} + \frac{2h_1}{\rho_1} \right]^{\frac{1}{2}} \quad (3.30)$$

With the help of strong shock conditions (3.10), equation (3.29) reduces to the following form

$$\frac{R_s \dot{U}_s}{U_s^2} + \frac{1}{D} = 0 \quad (3.31)$$

where

$$D = \frac{(1-1/\beta+E)(1-1/\beta)(2+\beta E)}{\beta(E^2(1-1/\beta)-C_0\beta(1-1/\beta-E))}, \quad E = \left[\frac{1}{\beta} \left(\phi(\beta) \left(1 - \frac{1}{\beta} - \frac{C_0\beta^2}{2} \right) + C_0\beta^2 \right) \right]^{1/2}$$

Solving equation (3.31) yields

$$\alpha = \frac{D}{D+1} \quad (3.32)$$

This can be evaluated for different values of Mie-Grüneisen coefficient in non-ideal medium.

3.4 Results and Discussion

Numerical calculations are performed to determine the value of the similarity exponent and to study the behavior of the flow variables behind the shock front.

The similarity exponent is also computed using CCW method for comparison.

Phenomena of interactions between shock waves and dusty gas, condensed matter EOSs are simulated. Dusty plasmas constitute ionized gases containing charged particles of condensed matter. Dust not only modifies the wave spectrum in comparison with dust-free plasma, but can also lead to the appearance of new modes and new mechanisms of damping and instability. Effects of physical parameters such as density, velocity, pressure, and magnetic pressure in both EOSs on the behavior of shock wave propagation are discussed. Numerical results are in good agreement with literature observations. Considering two physically meaningful Mie-Gruneisen coefficients and corresponding values of similarity exponent, flow profiles in both media are presented.

a) An EOS of a medium is obtained by solving the differential equation (3.19), which is given as,

$$\Gamma(G) = \frac{M}{(1-G^{-M})} \quad (3.33)$$

where M is the material property.

Using equation (3.33) and equation (3.11), we obtain a polynomial for β

$$C_0\beta^{M+3} + M\beta^{M+2} - 2(M+1)\beta^{M+1} + (M+2)\beta^M - C_0\beta^3 + 2\beta - 2 = 0 \quad (3.34)$$

which is solved numerically using MATLAB to obtain all roots of the equation and only physically meaningful values of β are considered for investigation.

b) The Mie-Gruneisen coefficient for condensed matter $\Gamma(G)$ as [80]

$$\Gamma(G) = \frac{2}{3} + \left(\Gamma_0 - \frac{2}{3}\right) \frac{(G_m^2 + 1)G}{(G_m^2 + G^2)} \quad (3.35)$$

where G_m and Γ_0 are material properties.

Substituting equation (3.35) in equation (3.11) we obtain a 5th degree polynomial in terms of measure of shock strength as

$$3C_0\beta^5 + 2\beta^4 + A_1\beta^3 + A_2\beta^2 - A_3\beta + 8G_m^2 = 0 \quad (3.36)$$

where

$$A_1 = 3C_0G_m^2 + 3(G_m^2 + 1)\left(\Gamma_0 - \frac{2}{3}\right) - 10,$$

$$A_2 = 2\left\{(4 + G_m^2) - 3(G_m^2 + 1)\left(\Gamma_0 - \frac{2}{3}\right)\right\},$$

$$A_3 = 10G_m^2 - 3(G_m^2 + 1)\left(\Gamma_0 - \frac{2}{3}\right)$$

The equation (3.36) is solved numerically using MATLAB to get all roots of the equation and only physically meaningful roots are taken for computation.

Table 3.1: The values of similarity exponent for dusty gas flow when $C_0 = 0.02$,

α_n - Runge-Kutta method, α_c - CCW method

M	β	α_n	α_c
0.03	1.0137889	0.677064	0.606602
0.05	1.0137898	0.676872	0.607107
0.07	1.0138897	0.676391	0.607961
0.09	1.0140012	0.675090	0.608097
1.78	1.0203	0.565763	0.674709

Table 3.2: The values of similarity exponent for condensed matter when $C_0 = 0.02$, α_n - Runge-Kutta method, α_c - CCW method

Γ_0	G_m	β	α_n	α_c
0.03	0.65	1.0102987	0.782900	0.534364
0.05	0.65	1.0102998	0.781498	0.534692
0.07	0.65	1.0103582	0.778576	0.534891
0.09	0.65	1.0103976	0.777492	0.535609
1.78	0.65	1.0104012	0.779200	0.536582

From the Table 3.1, it is observed that the similarity exponents α_n and α_c values for various M for dusty gas produced good approximation and from Table 3.2, condensed matter did not show good approximation for both R-K and CCW methods which may be due to the contribution of G_m . The behaviour of flow profiles is presented in Figures 3.2 and 3.3 are compared with values obtained from numerical integration of the similarity variable, which is a function of distance and shock position. Figures 3.2 and 3.3 shows that the absolute values of velocity, pressure, and magnetic pressure decreases with an increase in magnetic field strength in dusty gas and condensed matter. The increase in the value of M and decrease in similarity exponent has just the reverse effect in a way that it effectively changes the compression of gas particles, which can be seen from Figures 3.2(c) and 3.3(c). The decay of velocity of gas particles is very fast in a dusty gas whereas in condensed matter it is sufficiently slow. It is observed that the magnetic pressure profiles have a smooth decreasing profile for different α . Again with the increase in the value of α , the shock propagation is observed

to reduce as seen from Figures 3.2(d) and 3.3(d). It is interesting to note that the transient behaviour of $R_s(t)$ does not depend on the amplitude of the initial pressure pulse.

In this problem, we obtained a numerical solution of the system of non-linear ordinary differential equations to determine the similarity exponent. Obtained low distribution of parameters such as density, velocity, pressure and magnetic pressure for two different physically meaningful non-ideal medium such as dusty gas and condensed matter. We employed two numerical techniques Runge-Kutta and CCW methods in the evaluation of similarity exponent in both medium. It is observed that both RK and CCW methods produced a very good approximation for similarity exponents for dusty gas case and were different for condensed matter case as expected. We provided a description of flow pattern and numerical method employed to ensure the solution when integrating the system of equations passing through the singular points in the solution. It is observed that the effect of increasing values of magnetic field strength causes to decrease the values of velocity, pressure and magnetic pressure in dusty gas and condensed matter. It is observed that the density decreases with an increase in magnetic field strength for dusty gas flow, whereas in the case of condensed matter density increases with the effect of an increasing values of magnetic field strength. Also, we observed that the values of similarity exponent decreases with increasing values of magnetic field strength. Moreover, we conclude that the law of shock wave

propagation is rather sensitive to the particular form of the EOS, and the measurement of shock velocities can provide useful information about the EOS.

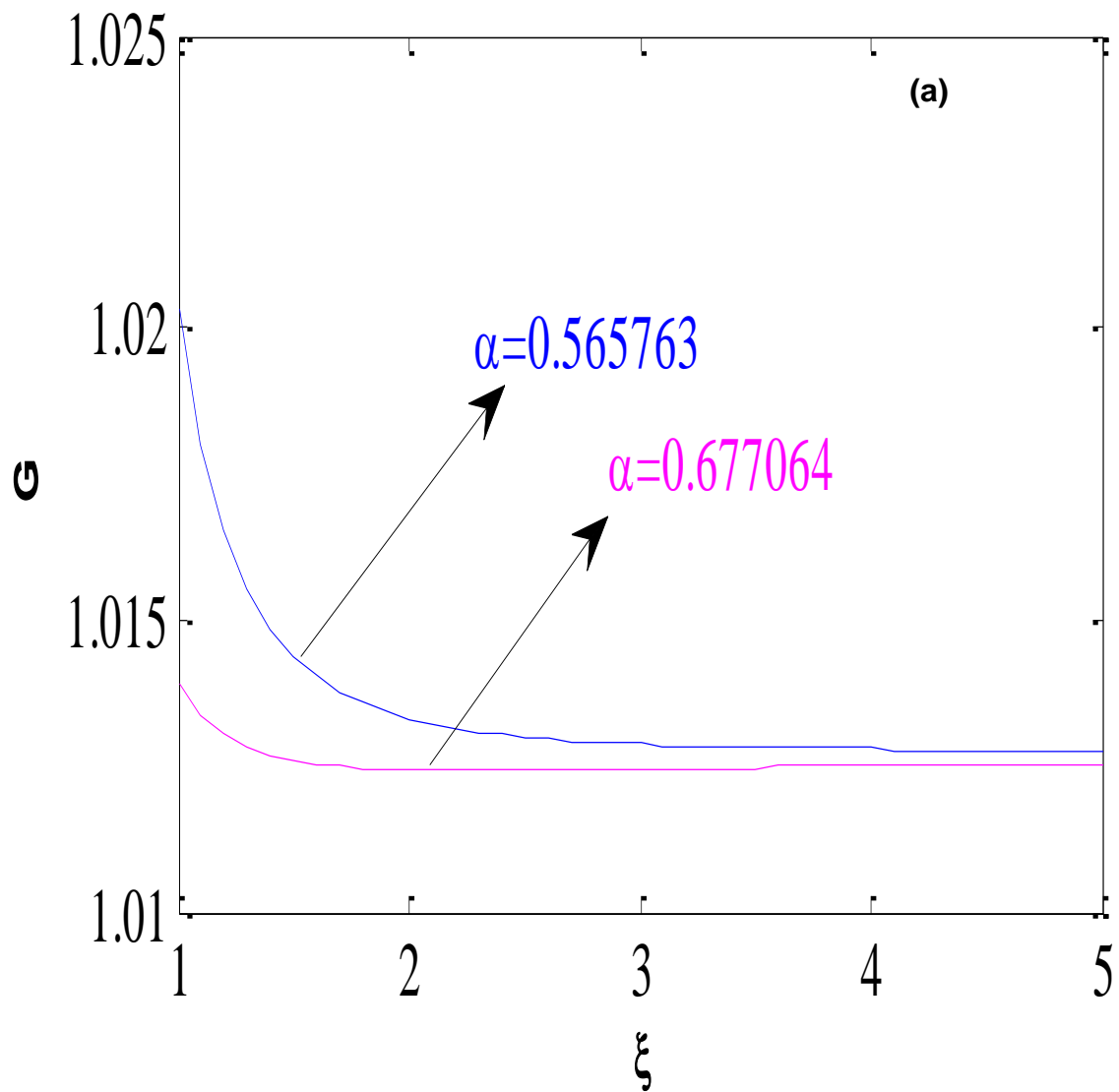


Figure 3.2(a). Density profiles for dusty gas

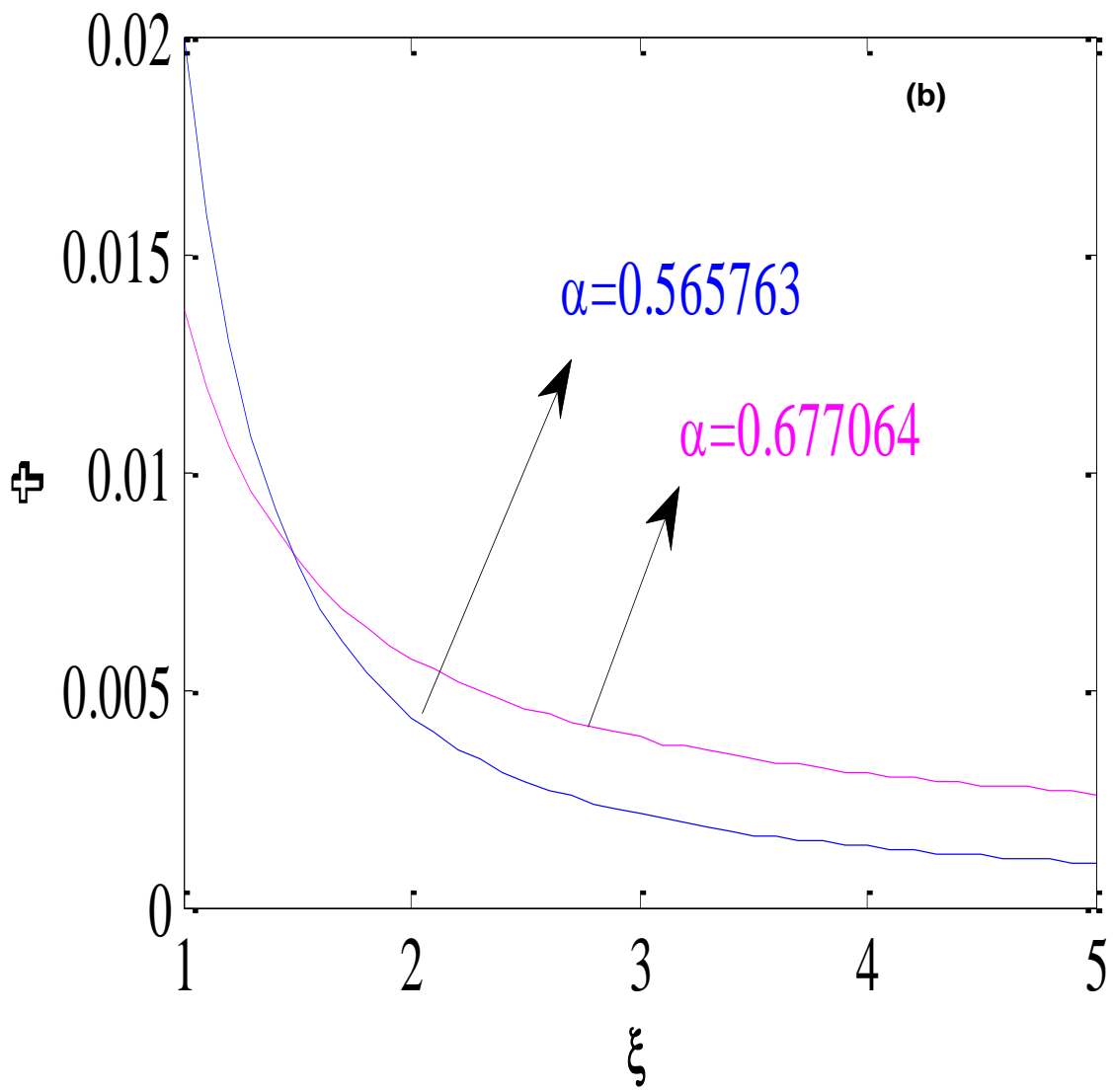


Figure 3.2(b). Velocity profiles for dusty gas

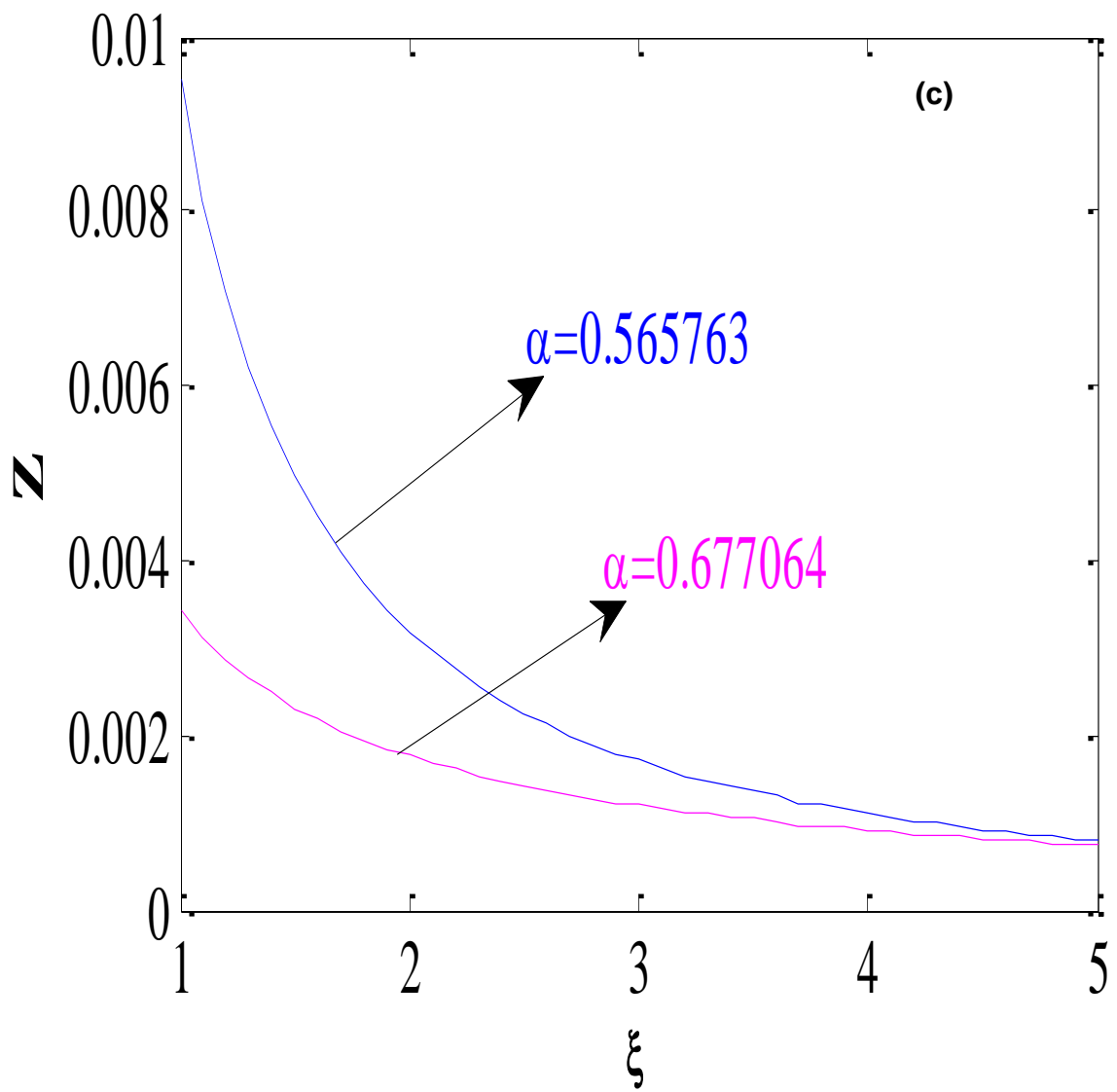


Figure 3.2(c). Pressure profiles for dusty gas

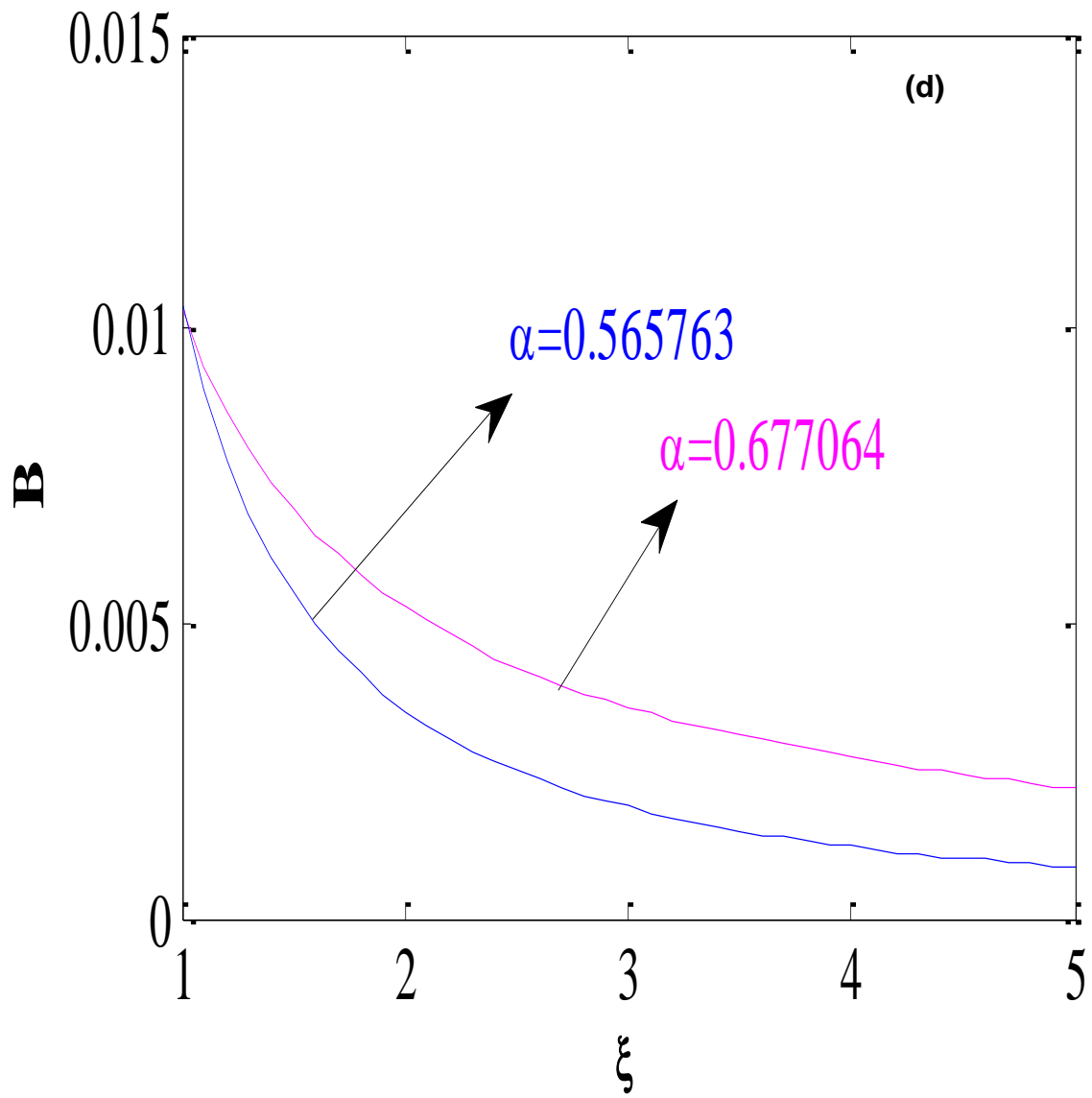


Figure 3.2(d). Magnetic pressure profiles for dusty gas

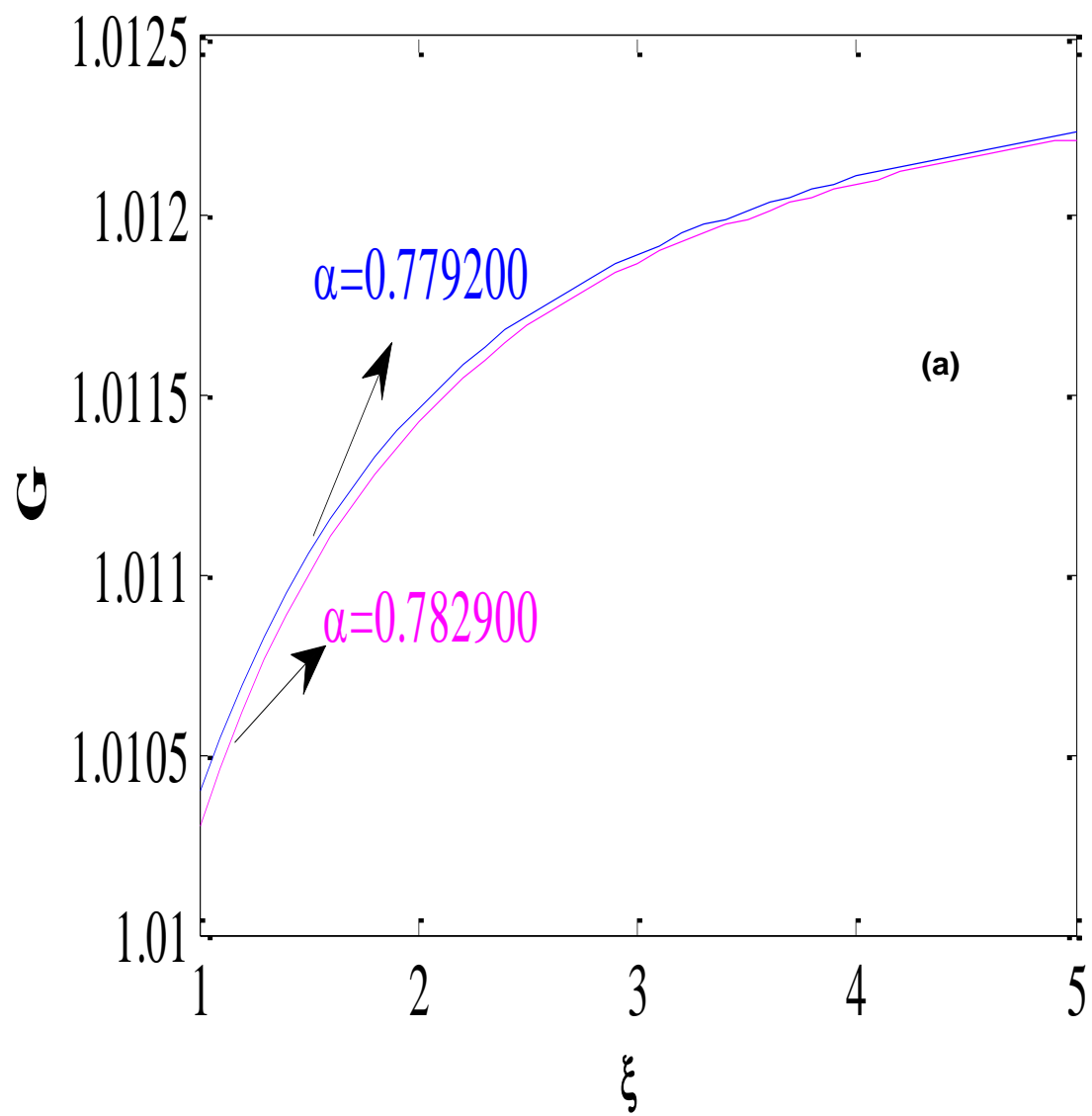


Figure 3.3(a). Density profiles for condensed matter

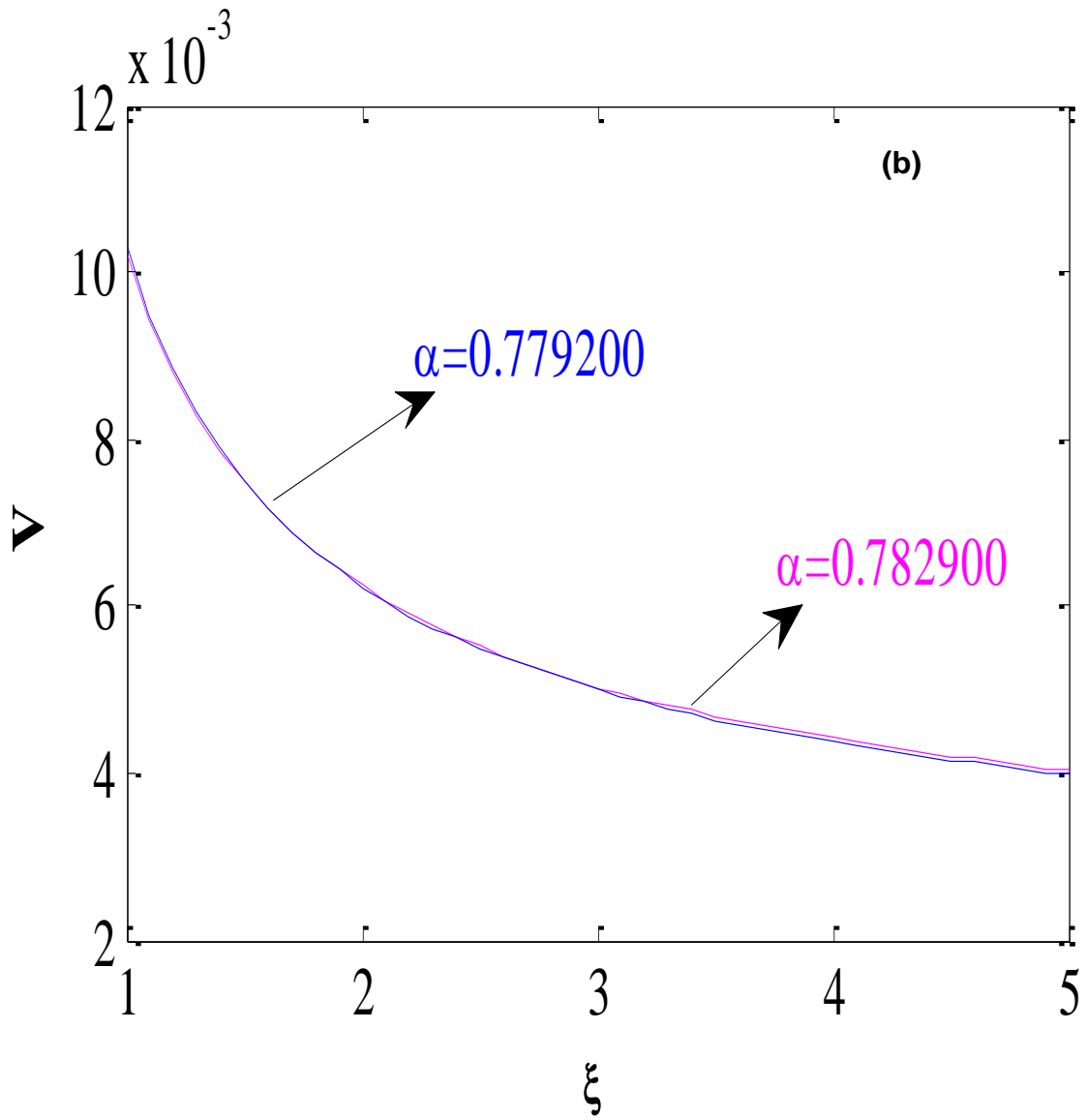


Figure 3.3(b). Velocity profiles for condensed matter

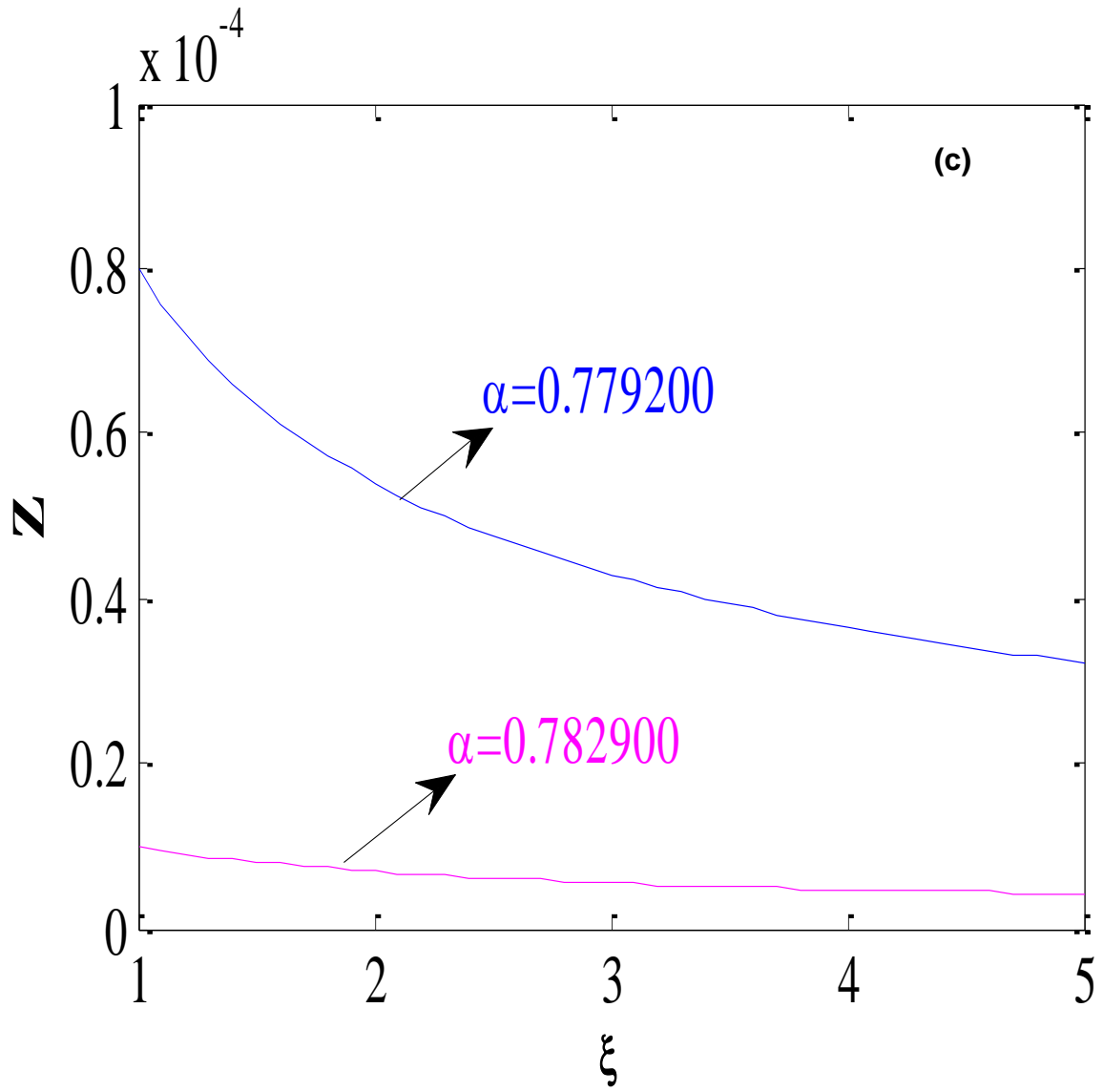


Figure 3.3(c). Pressure profiles for condensed matter

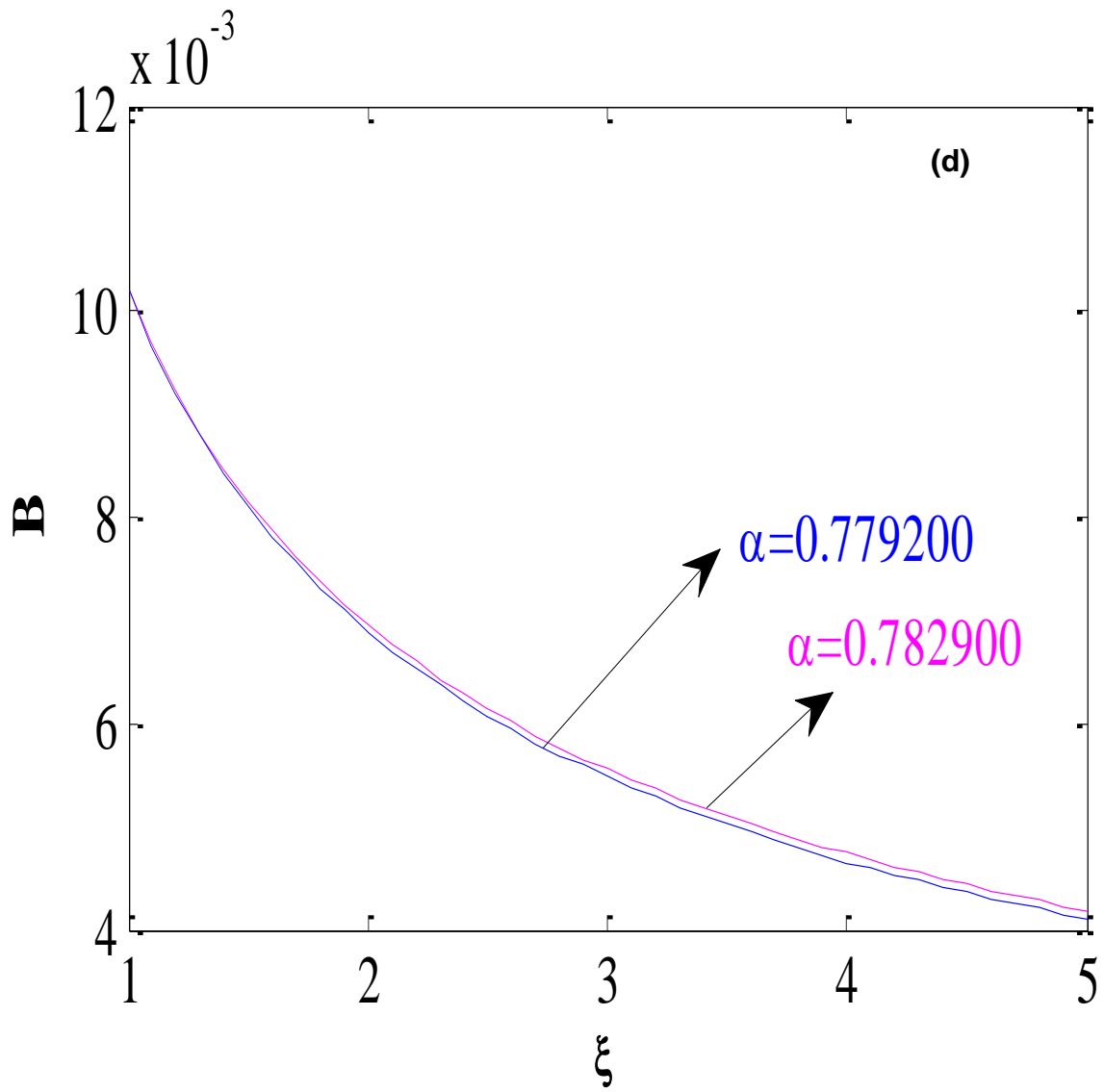


Figure 3.3(d). Magnetic pressure profiles for condensed matter

Chapter-4

Numerical Solution to Strong Cylindrical Shock Wave in the Presence of Magnetic Field

4.1 Introduction

The study of magneto hydrodynamic waves (MHD) in non-ideal medium is of great scientific interest to many areas of astrophysics, geophysics, underground explosions, hypersonic aerodynamics, hypervelocity impact, plasma physics, oceanography, atmospheric sciences, nuclear sciences, etc. Converging shock waves have been a field of growing interest since the early 1940's from both mathematical and physical point of view. The first experimentally produced converging shock waves were presented by Perry and Kantrowitz [83]. The study of shock waves produced due to the explosion or implosion in the presence of magnetic field has received much attention in recent times. Many researchers studied the problem of planar, cylindrical, and spherical MHD shock waves, mathematical [24] as well as experimental point of view. Analytic description of the flow variables at all points behind the converging shocks and approximate analytical determination of the similarity exponent α is detailed by Genot, Chisnell [33, 84]. Analytical solution of spherically imploding shock waves in a perfect gas was studied by Fujimoto and Mishkin [85]. The authors [16-18] have developed independently approximate methods to solve shock wave problems.

Such methods are often referred to as the CCW-method and their results agree well with similarity solution of Guderley [15]. These methods ignore the influence of the flow behind the shock. The solution to the strong spherical and cylindrical piston problem using perturbation technique is discussed in [53]. Several approaches such as the self-similarity method [5-7, 50], power series solution and method of characteristics [32, 54, 86-88] have been used for the theoretical investigations of MHD shock waves in homogeneous and non-homogeneous media.

In recent times study of shock waves in gaseous non-ideal medium has attracted the interest of many researchers due to its extensive applications in the areas of supernova explosions, photo ionized gas, stellar winds, monochromatic radiation, dynamo effect in stars, gamma-ray bursts, etc. A theoretical study of the imploding shock wave in non-ideal medium was investigated by several authors [56, 89, 90] to obtain accurate results.

In this chapter, the self-similar solution of imploding cylindrical shock waves in non-ideal medium is presented. The medium generated due to implosion is assumed to be of Mie-Gruneisen type with or without magnetic material. In the implosion process (by impulse method) plasma is assumed to be generated. It is assumed that this plasma has an infinite electrical conductivity and permeated by an axial magnetic field orthogonal to the trajectories of gas particles. Numerical solution presented here provides a global solution to the implosion problem which

is valid for a range of physically meaningful parameters which represent the EOS of Mie-Gruneisen type. Numerical computations are performed to obtain the similarity exponent iteratively using MATLAB. The aim of the present work is to understand the mechanical properties of shock waves in the presence of strong magnetic field; to study the behaviour of shock characteristics such as shock strength, shock density, shock speed, shock over pressure, and impulse.

4.2 Basic Equations

The governing equations of compressible one-dimensional Euler equations for the motion of a non-ideal gas in the magnetogasdynamics regime with the medium containing no heat conduction, or sinks, viscosity and radiation in non-conservative form can be written as [7, 70, 76, 81, 91, 92]

$$\frac{\partial F_v}{\partial t} + A \frac{\partial F_v}{\partial r} + D = 0, \quad \text{or} \quad F_{vt} + AF_{vr} + D = 0 \quad (4.1)$$

where F_v , D are column vectors of order 4×1 and A is the coefficient matrix of order 4×4 for derivative of state function F_v given as follows

$$F_v = \begin{bmatrix} \rho \\ v \\ e \\ h \end{bmatrix}, \quad A = \begin{bmatrix} v & \rho & 0 & 0 \\ 0 & v & 1/\rho & 1/\rho \\ 0 & p/\rho & v & 0 \\ 0 & 2h & 0 & v \end{bmatrix}, \quad \text{and} \quad D = \begin{bmatrix} \frac{(v-1)\rho v}{r} \\ 0 \\ \frac{(v-1)pv}{\rho r} \\ \frac{2(v-1)hv}{r} \end{bmatrix} \quad (4.2)$$

The equations governing the flow are in general form with $v = 1, 2$ and 3 denoting planar, cylindrical, spherical geometry respectively. t and r are independent variables representing time and space coordinates, ρ is the density, ρ_0 is the

density of unperturbed medium, p is the pressure, v is the velocity of gas particles, e is the specific internal energy, $h = \frac{\mu H^2}{2}$ is the magnetic pressure. H and μ being the magnetic field strength and the magnetic permeability, respectively. The shock position is given by $R_s(t)$ and its speed is $U_s(t) = \frac{dR_s}{dt}$. In this work, the magnetic permeability is assumed to be unity and the electrical conductivity to be infinite. The EOS under equilibrium condition is of Mie-Gruneisen type [57],

$$p = \rho e \Gamma(\rho/\rho_0) \quad (4.3)$$

where $\Gamma(\rho/\rho_0)$ is the Mie-Gruneisen coefficient. Shock is assumed to be strong and propagating into a medium according to the power law $R_s(t) \propto (1 - t/t_c)^\alpha$, where t_c is the collapse time, α is similarity exponent to be determined by the condition that the similarity variable $\xi = \frac{r}{R_s(t)}$ is 1 at the shock front.

4.2.1 Boundary conditions

The strong shock limit of the Rankine-Hugoniot jump conditions may be used to connect the flow just behind the shock to that just ahead of the shock front [7, 76]

$$\left. \begin{aligned} \frac{\rho_1}{\rho_0} &= \beta, & v_1 &= \left(1 - \frac{1}{\beta}\right) U_s(t), \\ \frac{p_1}{\rho_0} &= \left(1 - \frac{1}{\beta} - \frac{c_0 \beta^2}{2}\right) U_s^2(t), & \frac{h_1}{\rho_0} &= \frac{c_0 \beta^2}{2} U_s^2(t) \end{aligned} \right\} (4.4)$$

where $C_0 = \frac{2h_0}{\rho_0 U_s^2(t)}$ is the Cowling number and β is the measure of the shock strength. The suffices '1' and '0' refer to conditions just behind and ahead of the shock respectively.

With the above relations (4.4), the equation (4.3) can be written as

$$\left(2 - \frac{C_0 \beta^3}{(\beta-1)}\right) = (\beta - 1)\Gamma(\beta) \quad (4.5)$$

Equation (4.5) is used to determine the measure of shock strength β for various models of EOS, which are provided in this chapter.

Also, the boundary conditions for the strong shock at ($\xi = 1$) can be written as

$$G(1) = \beta, \quad V(1) = 1 - \frac{1}{\beta}, \quad Z(1) = 1 - \frac{1}{\beta} - \frac{C_0 \beta^2}{2}, \quad B(1) = \frac{C_0 \beta^2}{2} \quad (4.6)$$

4.3 Solution Procedure

The flow field is bounded by the piston and the shock respectively. In the framework of self-similarity shock is assumed to be strong and propagating into a medium according to the power law $R_s(t) \propto (1 - t/t_c)^\alpha$. The counter pressure ahead of the shock can be neglected and t_c is the collapse time. The basic equations are non-dimensionalised using the following transformations [7],

$$\rho = \rho_0 G(\xi), \quad v = U_s(t) V(\xi), \quad p = \rho_0 U_s^2(t) Z(\xi), \quad h = \rho_0 U_s^2(t) B(\xi) \quad (4.7)$$

where the similarity variable $\xi = \frac{r}{R_s(t)}$, G , V , Z , and B are the functions (known as reduced functions) of the non-dimensional variable ξ only. The quantities $U_s(t)$, $\rho_0 U_s^2(t)$ are the velocity scale and pressure scale respectively. Applying transformations (4.7) on the system of equations (4.1) ($v = 2$ for cylindrical geometry) we obtain reduced system of ordinary differential equations in the dimensionless variables ξ , $G(\xi)$, $V(\xi)$, $Z(\xi)$, and $B(\xi)$.

$$\frac{1}{G} \frac{dG}{d\xi} - \frac{1}{(\xi-V)} \frac{dV}{d\xi} = \frac{V}{\xi(\xi-V)} \quad (4.8)$$

$$\frac{dV}{d\xi} - \frac{1}{G(\xi-V)} \left(\frac{dZ}{d\xi} + \frac{dB}{d\xi} \right) = \frac{\lambda V}{(\xi-V)} \quad (4.9)$$

$$\frac{1}{Z} \frac{dZ}{d\xi} - \Phi(G) \frac{1}{G} \frac{dG}{d\xi} = \frac{2\lambda}{(\xi-V)} \quad (4.10)$$

$$\frac{1}{B} \frac{dB}{d\xi} - \frac{2}{G} \frac{dG}{d\xi} = \frac{2\lambda}{(\xi-V)} \quad (4.11)$$

where

$$\lambda = 1 - \frac{1}{\alpha}, \quad \text{and} \quad \Phi(G) = 1 + \Gamma(G) + \frac{G}{\Gamma(G)} \frac{d\Gamma}{dG}$$

Finite difference approximations of the derivatives for the above system of equations (4.8-4.11) are

$$\frac{dG}{d\xi} = \frac{G_{i+1} - G_i}{h}, \quad \frac{dV}{d\xi} = \frac{V_{i+1} - V_i}{h}, \quad \frac{dZ}{d\xi} = \frac{Z_{i+1} - Z_i}{h}, \quad \frac{dB}{d\xi} = \frac{B_{i+1} - B_i}{h} \quad (4.12)$$

the subscripts i represent the grid points. We substitute these derivatives in equations (4.8-4.11) and simplifying result in a system of algebraic equations:

$$(\xi_i - V_i)G_{i+1} - G_i V_{i+1} = (\xi_i - V_i)G_i - \left(1 - \frac{h}{\xi_i}\right) G_i V_i \quad (4.13)$$

$$(\xi_i - V_i)V_{i+1} - \left(\frac{1}{G_i}\right)Z_{i+1} - \left(\frac{1}{G_i}\right)B_{i+1} = (\lambda h + \xi_i - V_i)V_i - \frac{1}{G_i}(Z_i + B_i) \quad (4.14)$$

$$Z_{i+1} - \left(\frac{Z_i \phi(G_i)}{G_i}\right) G_{i+1} = (1 - \phi(G_i))Z_i + \frac{2\lambda h Z_i}{(\xi_i - V_i)} \quad (4.15)$$

$$B_{i+1} - \left(\frac{2B_i}{G_i}\right) G_{i+1} = \left(\frac{2\lambda h}{(\xi_i - V_i)} - 1\right) B_i \quad (4.16)$$

These can be written in the matrix form as

$$\begin{pmatrix} (\xi_i - V_i) & -G_i & 0 & 0 \\ 0 & (\xi_i - V_i) & -1/G_i & -1/G_i \\ -Z_i \phi(G_i)/G_i & 0 & 1 & 0 \\ -2B_i/G_i & 0 & 0 & 1 \end{pmatrix} \begin{pmatrix} G_{i+1} \\ V_{i+1} \\ Z_{i+1} \\ B_{i+1} \end{pmatrix} = \begin{pmatrix} (\xi_i - V_i)G_i + \left(\frac{h}{\xi_i} - 1\right) G_i V_i \\ (\lambda h + \xi_i - V_i)V_i - \frac{1}{G_i}(Z_i + B_i) \\ (1 - \phi(G_i))Z_i + \frac{2\lambda h Z_i}{(\xi_i - V_i)} \\ \left(\frac{2\lambda h}{(\xi_i - V_i)} - 1\right) B_i \end{pmatrix} \quad (4.17)$$

Using Crout's reduction method [93] the system of equations (4.17) are solved for density (G_{i+1}), velocity (V_{i+1}), pressure (Z_{i+1}), and magnetic pressure (B_{i+1}) functions respectively,

where

$$G_{i+1} = P_i + \frac{G_i}{(\xi_i - V_i)} Q_i + \frac{1}{(\xi_i - V_i)^2} R_i + \frac{G_i}{[G_i(\xi_i - V_i)^2 - Z_i \phi(G_i)]} S_i \quad (4.18)$$

$$V_{i+1} = Q_i + \frac{1}{(\xi_i - V_i)G_i} R_i + \frac{(\xi_i - V_i)}{[G_i(\xi_i - V_i)^2 - Z_i \phi(G_i)]} S_i \quad (4.19)$$

$$Z_{i+1} = R_i + \frac{Z_i \phi(G_i)}{[G_i(\xi_i - V_i)^2 - Z_i \phi(G_i)]} S_i \quad (4.20)$$

$$B_{i+1} = S_i \quad (4.21)$$

where

$$P_i = \frac{\left[G_i(\xi_i - V_i) + G_i V_i \left(\frac{h}{\xi_i} - 1 \right) \right]}{(\xi_i - V_i)},$$

$$Q_i = \frac{\left[V_i(\lambda h + \xi_i - V_i) - \frac{1}{G_i}(Z_i + B_i) \right]}{(\xi_i - V_i)},$$

$$S_i = \frac{\left[2B_i G_i (\xi_i - V_i) M_i + \frac{2B_i Z_i \phi(G_i)}{\xi_i} N_i + K_i \right]}{G_i (\xi_i - V_i)^2 [G_i (\xi_i - V_i)^2 - Z_i \phi(G_i) - 2B_i]},$$

$$R_i = \frac{\left[Z_i G_i (\xi_i - V_i) (2\lambda h + \xi_i - V_i) + \frac{Z_i \phi(G_i)}{\xi_i} \{ h G_i V_i (\lambda h + \xi_i - V_i) - (Z_i + B_i) \xi_i \} \right]}{\{ G_i (\xi_i - V_i)^2 - Z_i \phi(G_i) \}},$$

$$M_i = \{ G_i V_i (\lambda h + \xi_i - V_i) - B_i \} (\xi_i - V_i) + 2\lambda h Z_i,$$

$$N_i = (\xi_i - 1)(Z_i + B_i) + (h - \xi_i)(\lambda h + \xi_i - V_i),$$

$$K_i = \left\{ (2\lambda h + \xi_i - 3V_i) + \frac{2h}{\xi_i} V_i \right\} [B_i G_i^2 (\xi_i - V_i)^3 - G_i Z_i B_i \phi(G_i) (\xi_i - V_i)].$$

4.3.1 The numerical solution

The solution to equations (4.18-4.21) involves evaluation of $\beta \left(\frac{\rho}{\rho_0} \right)$ and α considering the EOS of Mie-Gruneisen type [94]

$$\text{a.} \quad \Gamma(G) = \frac{M}{(1 - G^{-M})} \quad (4.22)$$

where M is constant parameter and represents material property of the dusty gas particles.

$$\text{b.} \quad \text{Royce EOS [95]}$$

$$\Gamma(G) = \Gamma_0 - a \left(1 - \frac{1}{G}\right) \quad (4.23)$$

where Γ_0 represents specific heat of the solid particles and ‘ a ’ is an arbitrary constant. Along with equation (4.5), equations (4.22) and (4.23) we obtain the equation in β as

$$\phi(\beta) = C_0\beta^{M+3} + M\beta^{M+2} - 2(M+1)\beta^{M+1} + (M+2)\beta^M - C_0\beta^3 + 2\beta - 2 = 0 \quad (4.24)$$

$$\psi(\beta) = C_0\beta^4 + (\Gamma_0 - a)\beta^3 + (3a - 2 - 2\Gamma_0)\beta^2 + (2 - 3a + \Gamma_0)\beta + a = 0 \quad (4.25)$$

The equation (4.25) reduces to perfect gas EOS when $\Gamma_0 = (\gamma - 1)$, $a = 0$ and along with equation (4.3) the EOS for perfect gas becomes

$$p(\rho, e) = \rho e(\gamma - 1) \quad (4.26)$$

where e is the SIE, $\gamma = \frac{c_p}{c_v}$ denotes the specific heat ratio of perfect gas and ρ , p represent density and pressure respectively. Thus along with $\Gamma_0 = (\gamma - 1)$, and $a = 0$ and equation (4.26) on substituting in equation (4.25) the equation for measure of shock strength β for perfect gas can be written as

$$\pi(\beta) = C_0\beta^3 + (\gamma - 1)\beta^2 - 2\gamma\beta + (\gamma + 1) = 0 \quad (4.27)$$

and the expression for α as

$$\frac{[1 - (\beta - 1)\varphi(\beta)]}{\beta^2} + \frac{1}{2} C_0 \frac{\alpha_0^2}{\alpha^2} [\varphi(\beta) - 2] \beta = 0, \quad \text{where } 0 < \alpha_0 < 1 \quad (4.28)$$

where $\varphi(\beta) = 1 + M$, $\varphi(\beta) = 1 + \Gamma(\beta) - \frac{a}{\beta\Gamma(\beta)}$,

for dusty gas and Royce EOS respectively and β is the root of equations (4.24, 4.25 and 4.27). Starting with a guess values of α , α is evaluated from equation (4.28) using a bracketing method for various values of C_0 , a , M , α_0 , and β . The equations (4.18-4.21) are solved with boundary conditions (4.6) in the region of $1 \leq \xi < \infty$ using MATLAB. The numerical evaluation is carried out from the shock front ($\xi = 1$) and proceed inwards until it reaches $\xi = \infty$, indicating $\xi_{min} = 1$ and $\xi_{max} = 5$, where ξ_{max} corresponds to $\xi = \infty$, $h = \Delta\xi$ and $\xi_i = 1 + (i - 1)h$, $i \geq 1$ is a positive integer, where step size is $h = 0.001$ and the number of grid points were approximately 4000 for the solution procedure. The error tolerance is 8 significant digits.

4.4 Results and Discussion

In this chapter, the entire computational work has been carried out using MATLAB. The computed values of similarity exponent α for various values of measure of shock strength β for the dusty gas, Royce and perfect gas EOS are presented in Tables 4.1-4.4. The unsteady nature of flow variables with the effect of magnetic field for the EOS under consideration are illustrated through Figures 4.2-4.7 for cylindrical converging shock waves. Equations (4.24, 4.25 and 4.27) are solved numerically for all roots of β (Figure 4.1(a)-(d) for graphical solution) which depend on the parameters $C_0 = 0.02, 0.05$; $a = 1.0, 1.2, 1.5$ and $\Gamma_0 = 1.78$ (for Royce EOS) with $(0 < C_0 \leq 0.1)$; and $M = 1.4, 1.5, 1.6, 1.8$ and 2.0 (for dusty gas); and $\gamma = 1.2, 1.4$ and 1.6 (for perfect gas) respectively.

Table 4.1: The values of similarity exponent α for dusty gas EOS flow

M	$C_0 = 0.02$		$C_0 = 0.05$	
	β	α	β	α
1.4	1.01841	0.71357	1.05085	0.71152
1.5	1.01887	0.70525	1.05240	0.70247
1.6	1.01935	0.69694	1.05405	0.69330
1.8	1.02040	0.67982	1.05776	0.67421
2.0	1.02157	0.66226	1.06213	0.65409

Table 4.2: The values of similarity exponent α for Royce EOS when $\Gamma_0 = 1.78$

a	$C_0 = 0.02$		$C_0 = 0.05$	
	β	α	β	α
1.0	2.52063	0.30570	2.26132	0.45097
1.2	2.73109	0.32313	2.39457	0.46735
1.5	3.29655	0.37204	2.70082	0.50691

Table 4.3: The values of similarity exponent α for Royce EOS when $\Gamma_0 = 2.02$

a	$C_0 = 0.02$		$C_0 = 0.05$	
	β	α	β	α
1.0	2.24026	0.28362	2.05447	0.42712
1.2	2.35998	0.29285	2.13702	0.43636
1.5	2.62946	0.31465	2.30779	0.45661

Table 4.4: The values of similarity exponent α for perfect gas EOS

γ	$C_0 = 0.02$		$C_0 = 0.05$	
	β	α	β	α
1.2	6.29241	0.64632	4.49743	0.75963
1.4	4.63191	0.49275	3.67781	0.64173
1.6	3.70626	0.40856	3.13229	0.56545

From the Table 4.1, we observed that with the change in the values of M and C_0 , measure of shock strength β increases, whereas similarity exponent α decreases. It is observed from Table 4.2 and Table 4.3 that the increase in the similarity exponent α , corresponds to the increase in the values of measure of shock strength β and arbitrary constant a for Royce EOS. It is notable from Table 4.4, that the specific heats ratio γ has direct impact on the similarity exponent α and the measure of shock strength β i.e., with increase in the value of γ , the similarity exponent α and β decreases. Also, we may note that the change in similarity exponent α is more prominent and faster in the perfect gas, as compared to that of dusty gas, because of considerable change in the initial strength of shock. The variations of non-dimensional shock velocity, pressure, magnetic pressure and density with ξ for dusty gas, Royce and perfect gas EOS are shown in Figures 4.2-4.7. From Figure 4.2(a-d), it is observed that the flow variables: density, velocity, pressure and magnetic pressure are high at the shock front (for the dusty gas EOS) and increases with the increase in the non-idealness parameter C_0 and reduce gradually as ξ increases. In particular, it is observed that the shock wave travels very slowly i.e., a low value of similarity exponent α in the dusty gas medium for various values of C_0 which is due to increase in strength of shock density. Figures 4.3-4.6 depicts the density, velocity, pressure, and magnetic pressure distributions as functions of dimensionless variable (i.e., reduced distance) over a subset of the computational domain for Royce EOS. Again from

Figures 4.3(a-b), 4.5(a-b), and 4.6(a-b) we note a sharp rise in density, pressure and magnetic pressure distributions behind the shock front, located between $\xi = 1$ and $\xi = 2.0$ and then decrease monotonically along the axis. It may be observed that variation in these peaks is reducing with an increase in the values of the parameter a , which is higher in the case of Cowling number $C_0 = 0.02$, whereas in the case of Cowling number $C_0 = 0.05$ not much variation is observed. It can be seen from Figure 4.4(a) for the case $C_0 = 0.02$ almost sharp rise the velocity profiles in the region $1 \leq \xi < 5$ and thereby rise monotonically as ξ increases. The other case (i.e., $C_0 = 0.05$) we observe a sharp rise in velocity behind the shock front, located between $\xi = 1$ and $\xi = 1.5$ and then decrease in velocity monotonically towards the axis (see Figure 4.4(b)). In particular, with change in the value of a it is observed from Figure 4.4(a-b) that velocity slowly decreases beyond the region $1 \leq \xi < 1.5$ in both cases. Figure 4.7(a-d) depict the density, velocity, pressure, and magnetic pressure as functions of reduced distance over the entire computational domain for perfect gas EOS. The nature of these EOS are similar to those described for other EOS shown in Figures 4.2, 4.3, 4.5, and 4.6. The maximum values of reduced density, velocity, pressure, and magnetic pressure peaks for various values of C_0 in case of Royce EOS, as well as perfect gas for ($a = 0$ and $\Gamma_0 = (\gamma - 1)$) are summarized in the following Table 4.5.

Table 4.5: Maximum values of flow parameters G , V , Z , and B for different values of C_0

	$C_0 = 0.02$				$C_0 = 0.05$			
α	G_{max}	V_{max}	Z_{max}	B_{max}	G_{max}	V_{max}	Z_{max}	B_{max}
0	104.9987	1.2803	20.2175	13.1118	104.8192	1.4161	18.3795	6.0606
1.0	1986.3420	6.2157	606.9698	585.0309	208.1239	1.1365	90.9678	93.8749
1.2	298.2817	5.0537	159.0359	143.4323	203.9085	1.1247	104.5146	105.9147

The problem involving a cylindrical converging strong shock wave has been formulated with a gas of varying density obeying a power law and shock propagates through a medium characterized by a Mie-Gruneisen EOS. The governing equations are non-dimensionalized using suitable similarity transformations. A finite difference scheme is employed to solve the system of non-linear differential equations. Crout's reduction technique is used to solve the system of algebraic equations. The nature of flow variables with the effect of magnetic field in the respective models of EOS is investigated.

From the present study, we notice that the similarity exponent α decreases with an increase in the values of M and fixed C_0 causes an increase in β for dusty gas medium. In perfect gas, similarity exponent α decreases with decrease in β with increasing values of γ and fixed C_0 . In case of Royce EOS the similarity exponent α decreases with an increasing values of Γ_0 and fixed α and C_0 due to decrease in β . The decay of shock wave is more prominent and slower in the dusty gas EOS.

The effect of magnetic field on flow variables is less pronounced for dusty gas particles, because of lower compression between the gas particles. We conclude that the less compressible medium has higher wave propagation speed. As shown in Figures 4.3-4.7, the approximate reduced density, velocity, pressure, and magnetic pressure shows largest peaks to the right behind the shock front in Royce EOS, whereas in perfect gas flow variables have small peaks. This is due to fact that the effect of measure of shock strength β , which causes the change in α and also effect of converging geometry or area of contraction of the shock wave.

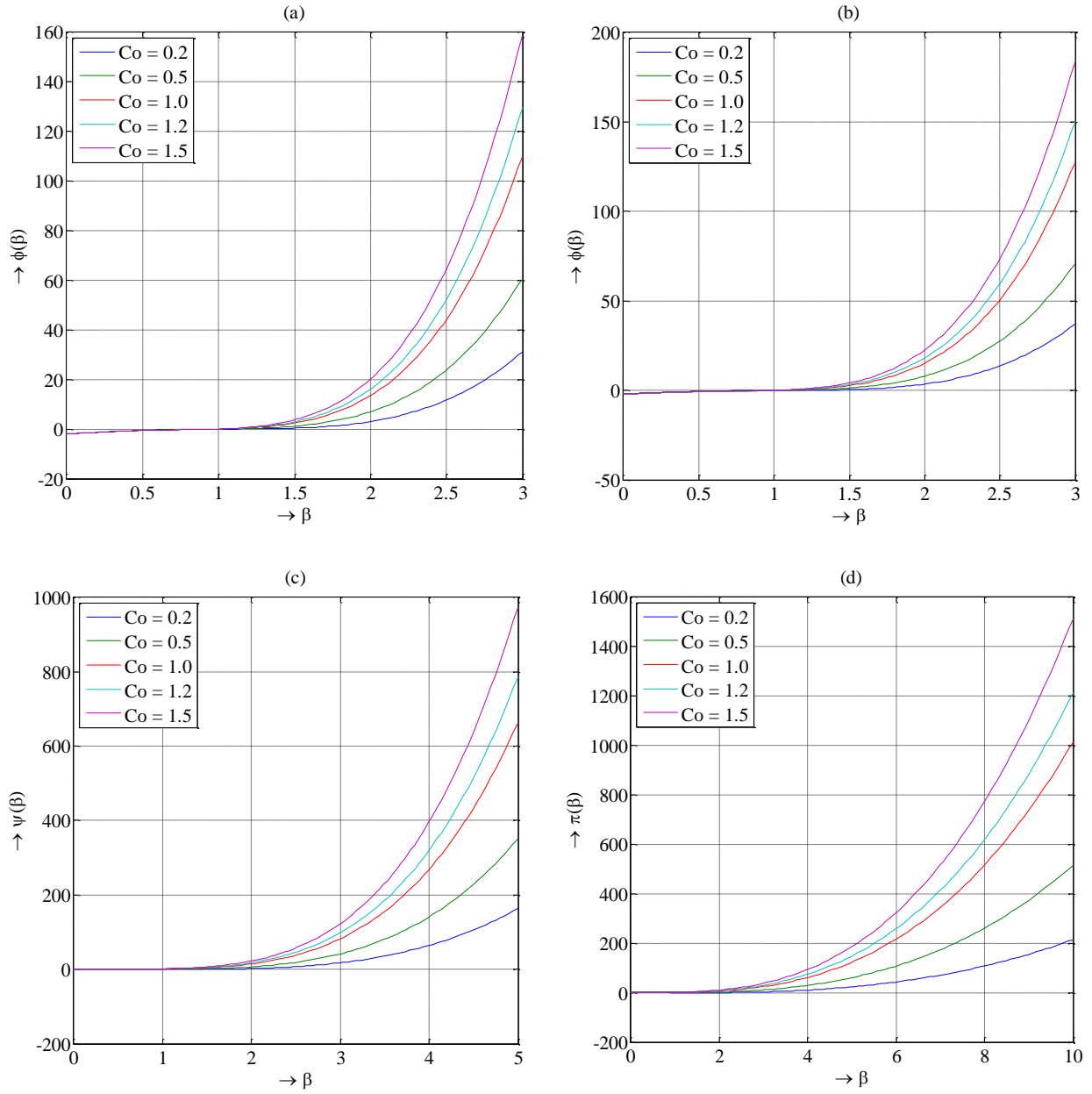


Figure 4.1. Graphical approach of ϕ , ψ , and π when $C_0 > 0.1$; (a) dusty gas for $M = 1.4$, (b) dusty gas for $M = 1.5$, (c) Royce EOS for $a = 1.0$, & $\Gamma_0 = 1.78$, and (d) perfect gas for $\gamma = 1.4$

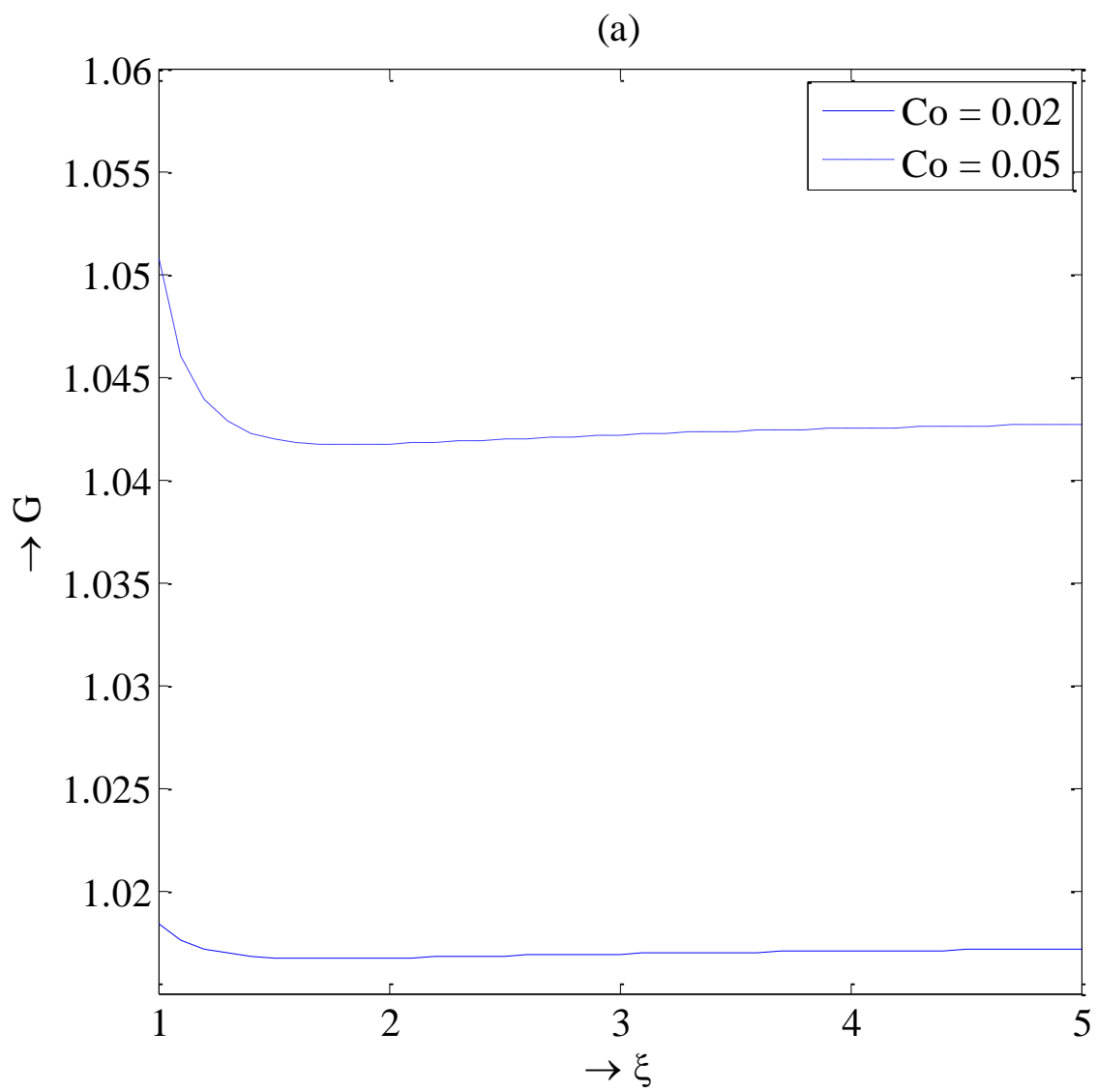


Figure 4.2(a). Density profiles for dusty gas when $M = 1.4$

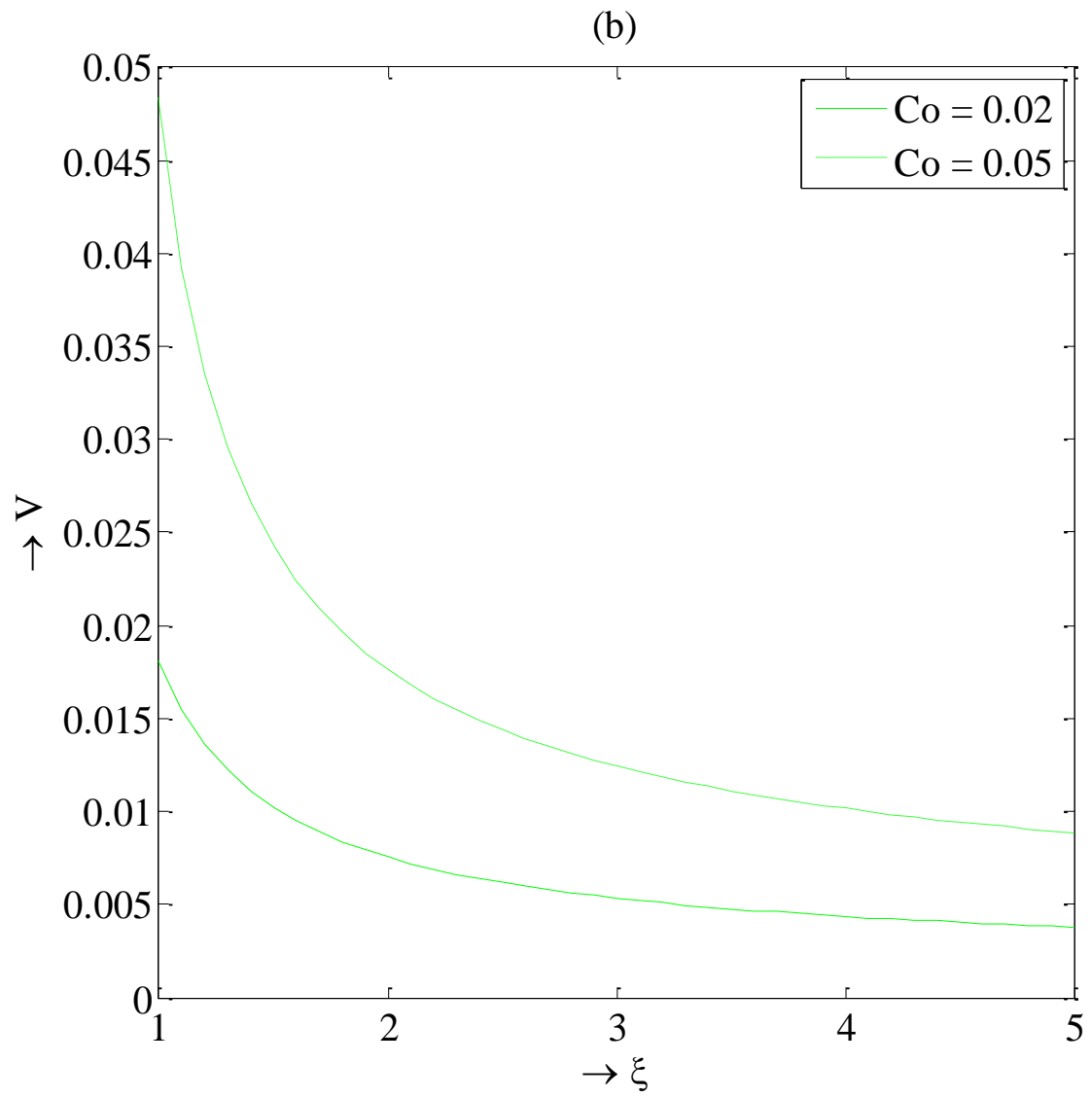


Figure 4.2(b). Velocity profiles for dusty gas when $M = 1.4$

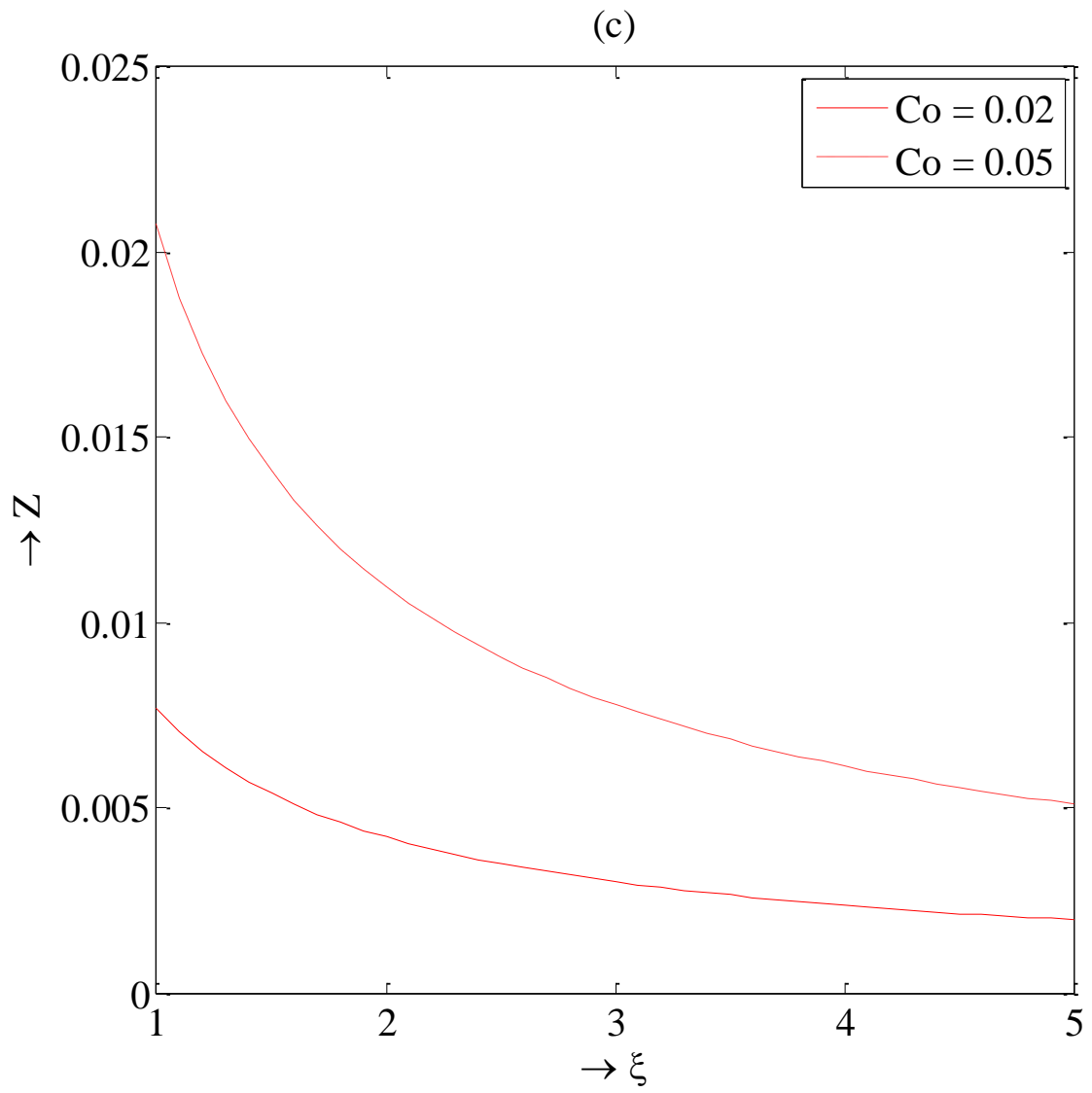


Figure 4.2(c). Pressure profiles for dusty gas when $M = 1.4$

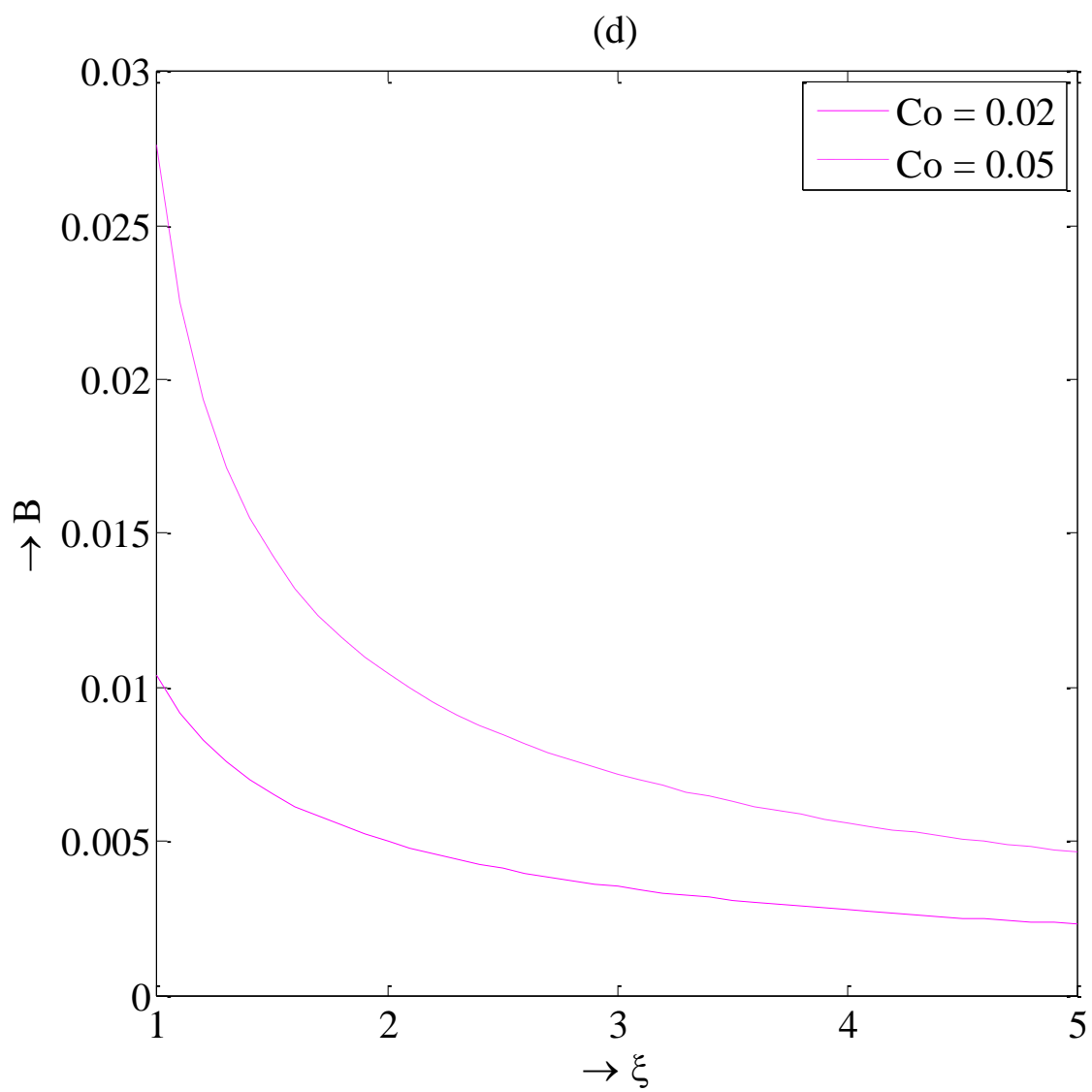


Figure 4.2(d). Magnetic pressure profiles for dusty gas when $M = 1.4$

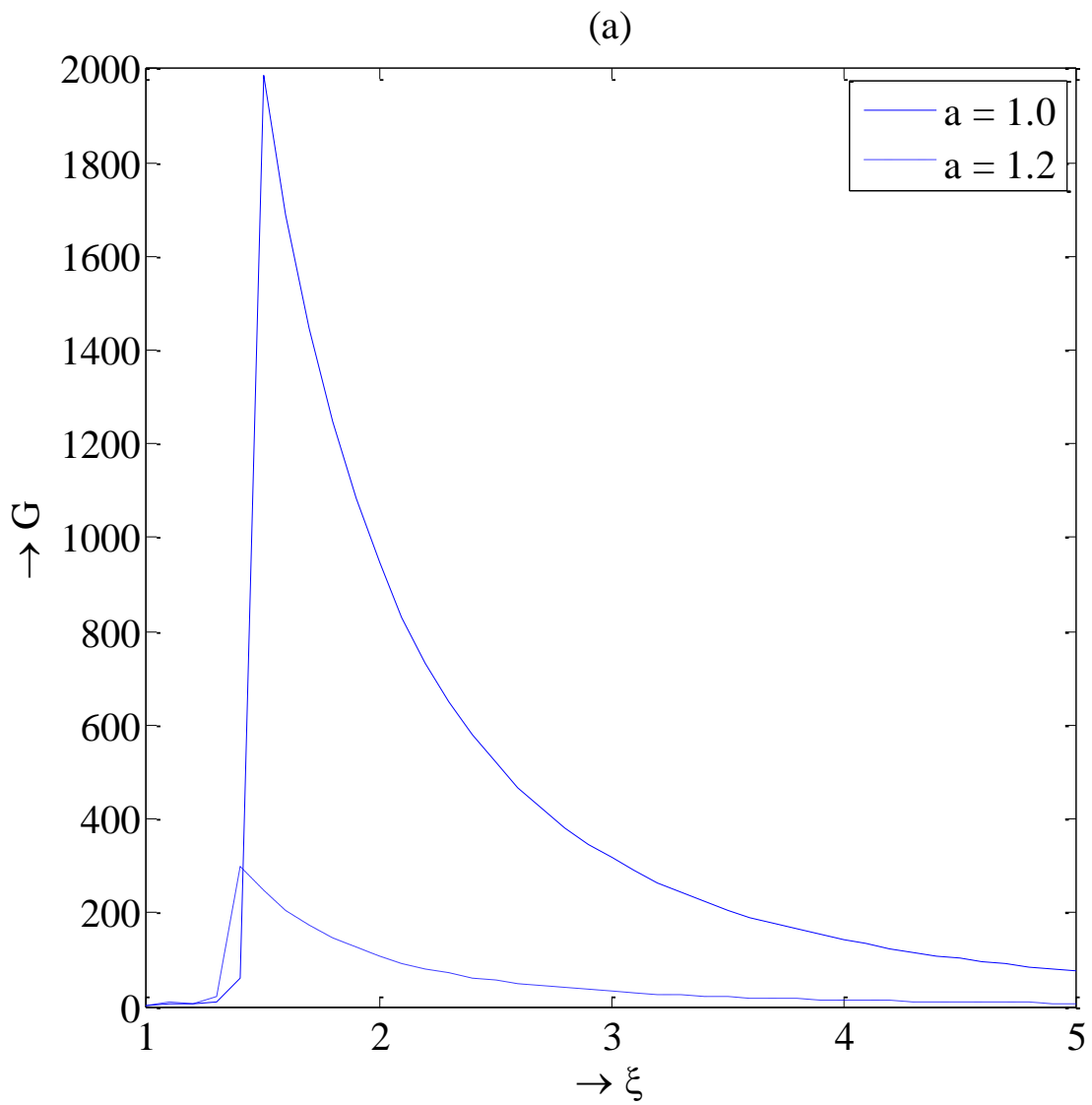


Figure 4.3(a). Density profiles for Royce EOS when $\Gamma_0 = 1.78$, $C_0 = 0.02$

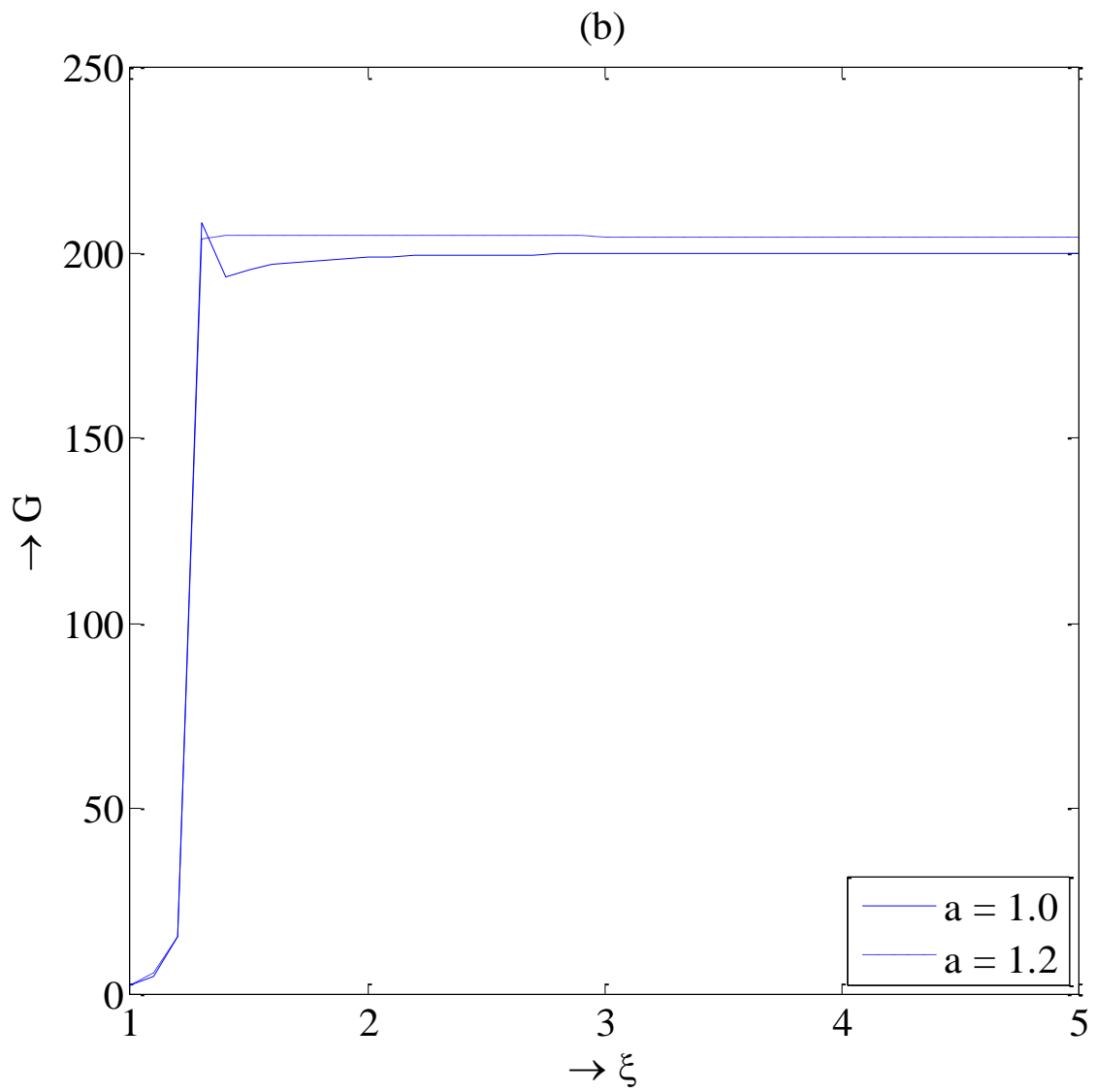


Figure 4.3(b). Density profiles for Royce EOS when $\Gamma_0 = 1.78$, $C_0 = 0.05$

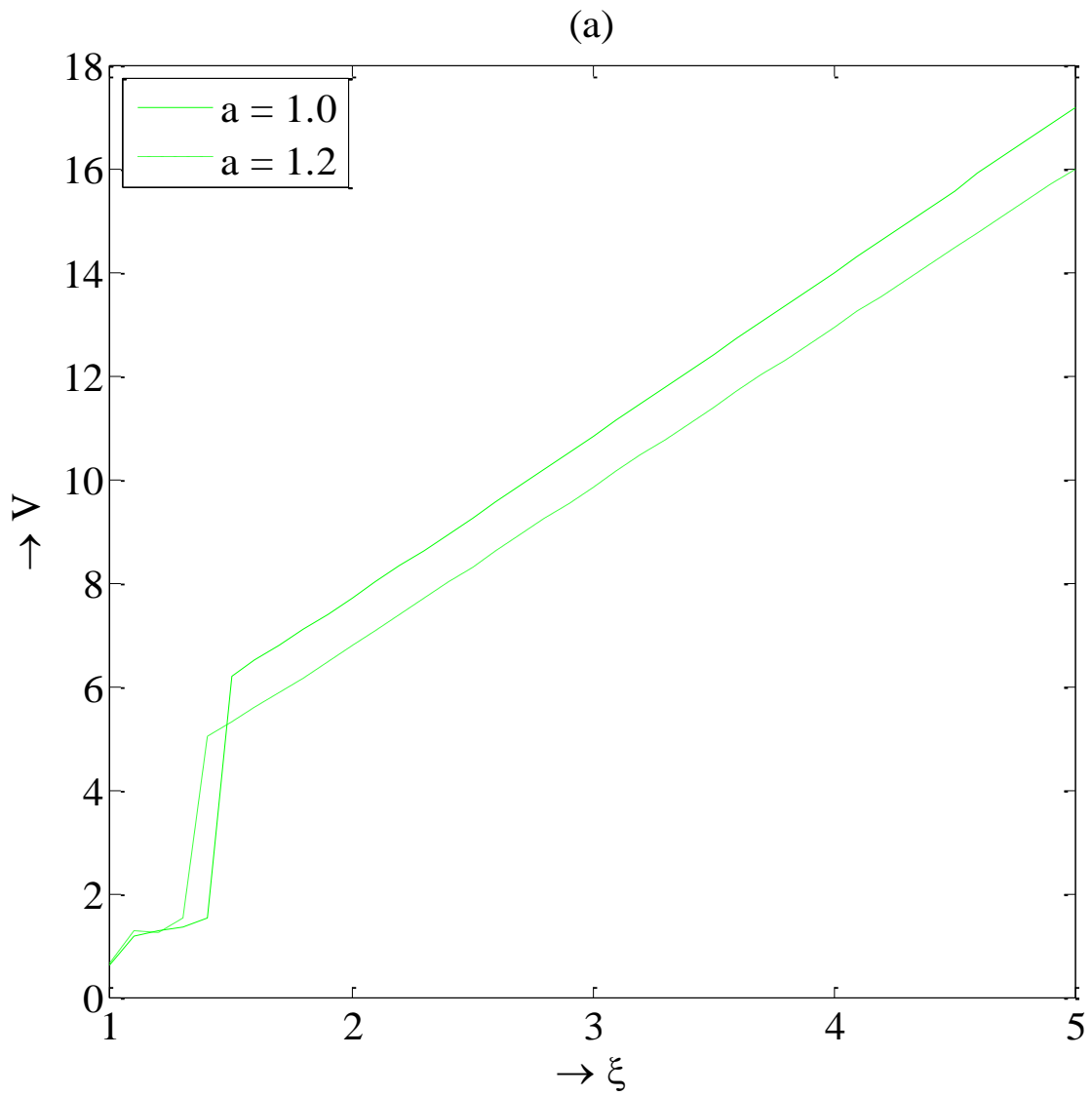


Figure 4.4(a). Velocity profiles for Royce EOS when $\Gamma_0 = 1.78$, $C_0 = 0.02$

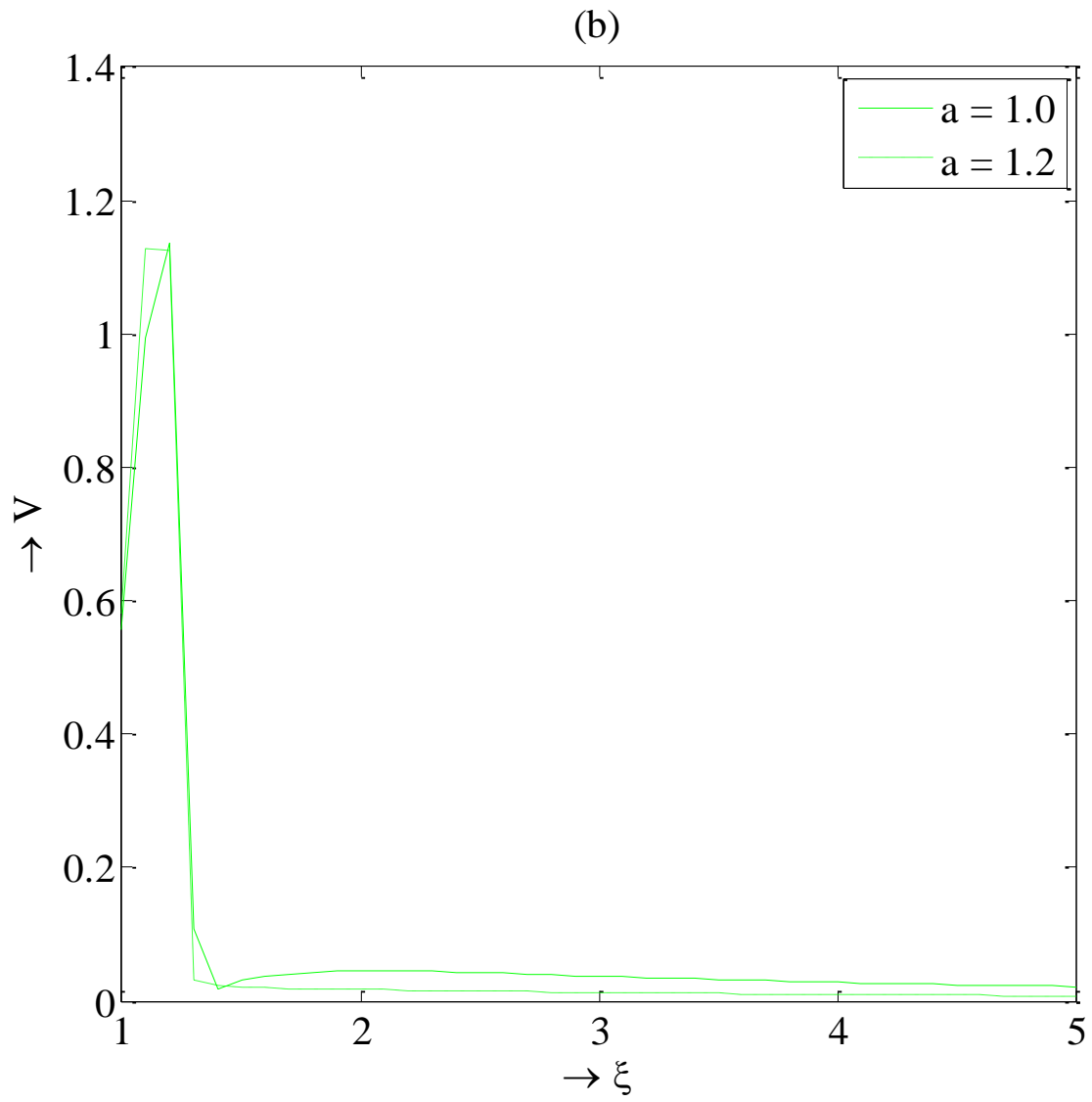


Figure 4.4(b). Velocity profiles for Royce EOS when $\Gamma_0 = 1.78$, $C_0 = 0.05$

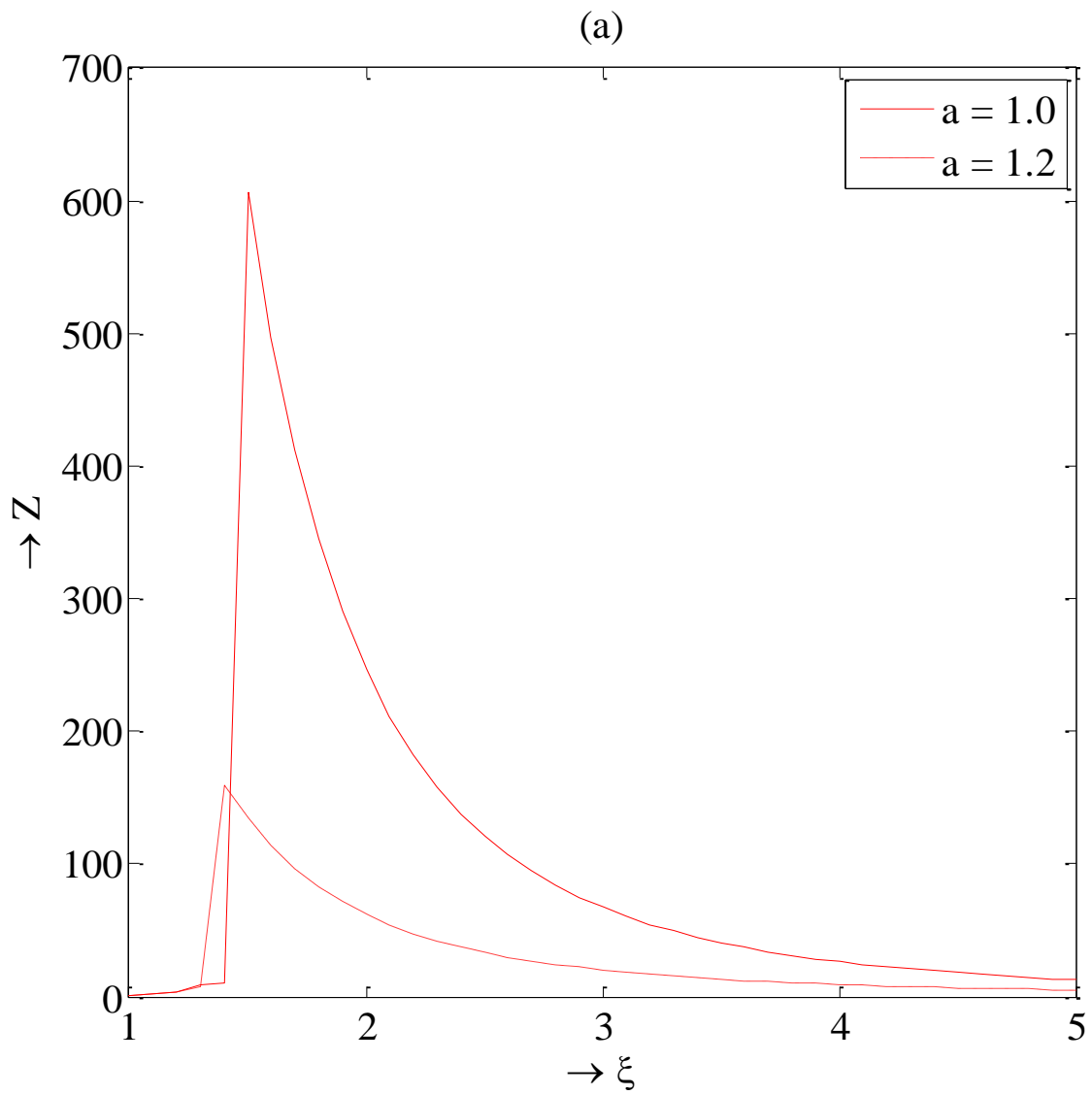


Figure 4.5(a). Pressure profiles for Royce EOS when $\Gamma_0 = 1.78$, $C_0 = 0.02$

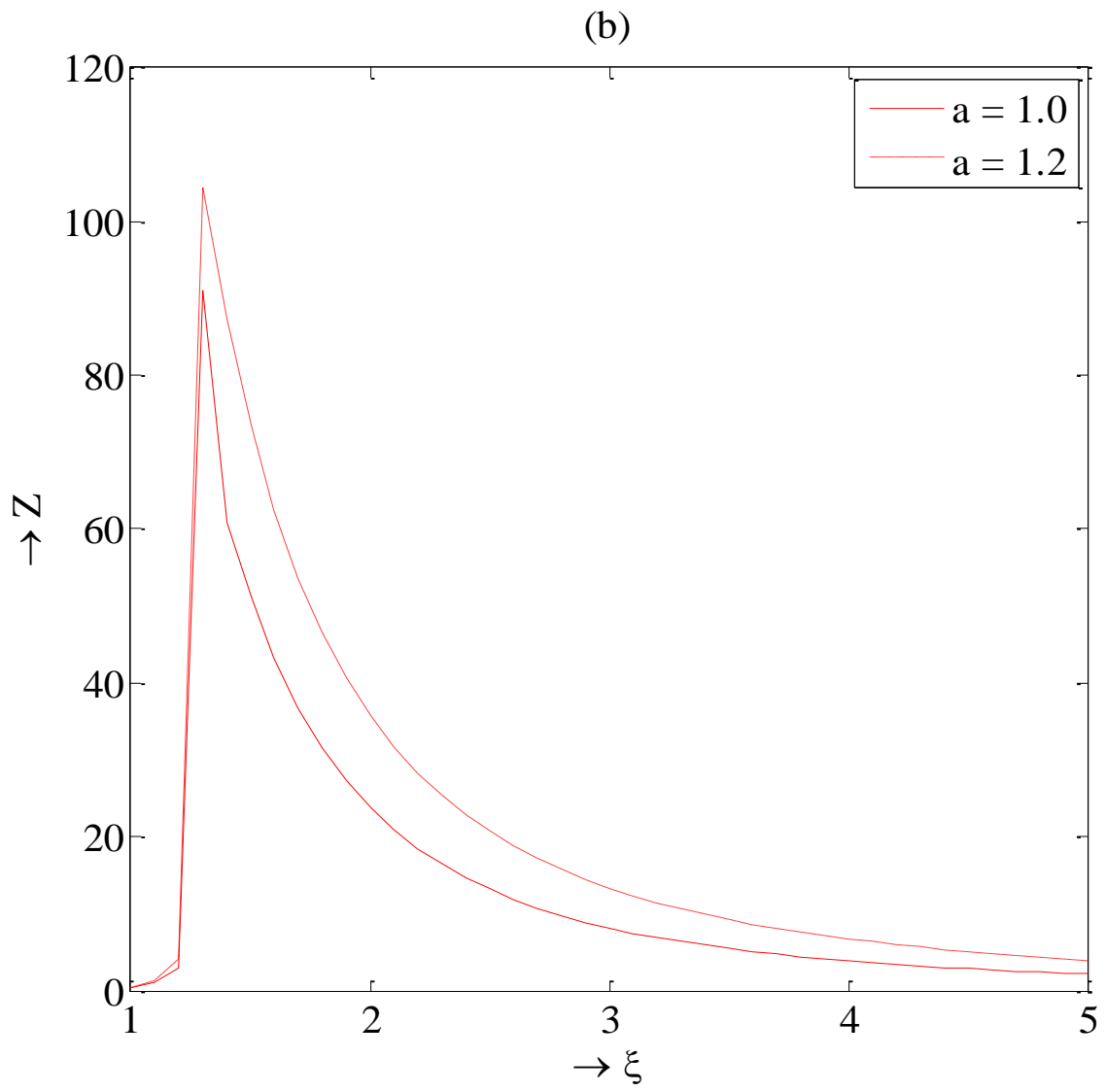


Figure 4.5(b). Pressure profiles for Royce EOS when $\Gamma_0 = 1.78$, $C_0 = 0.05$

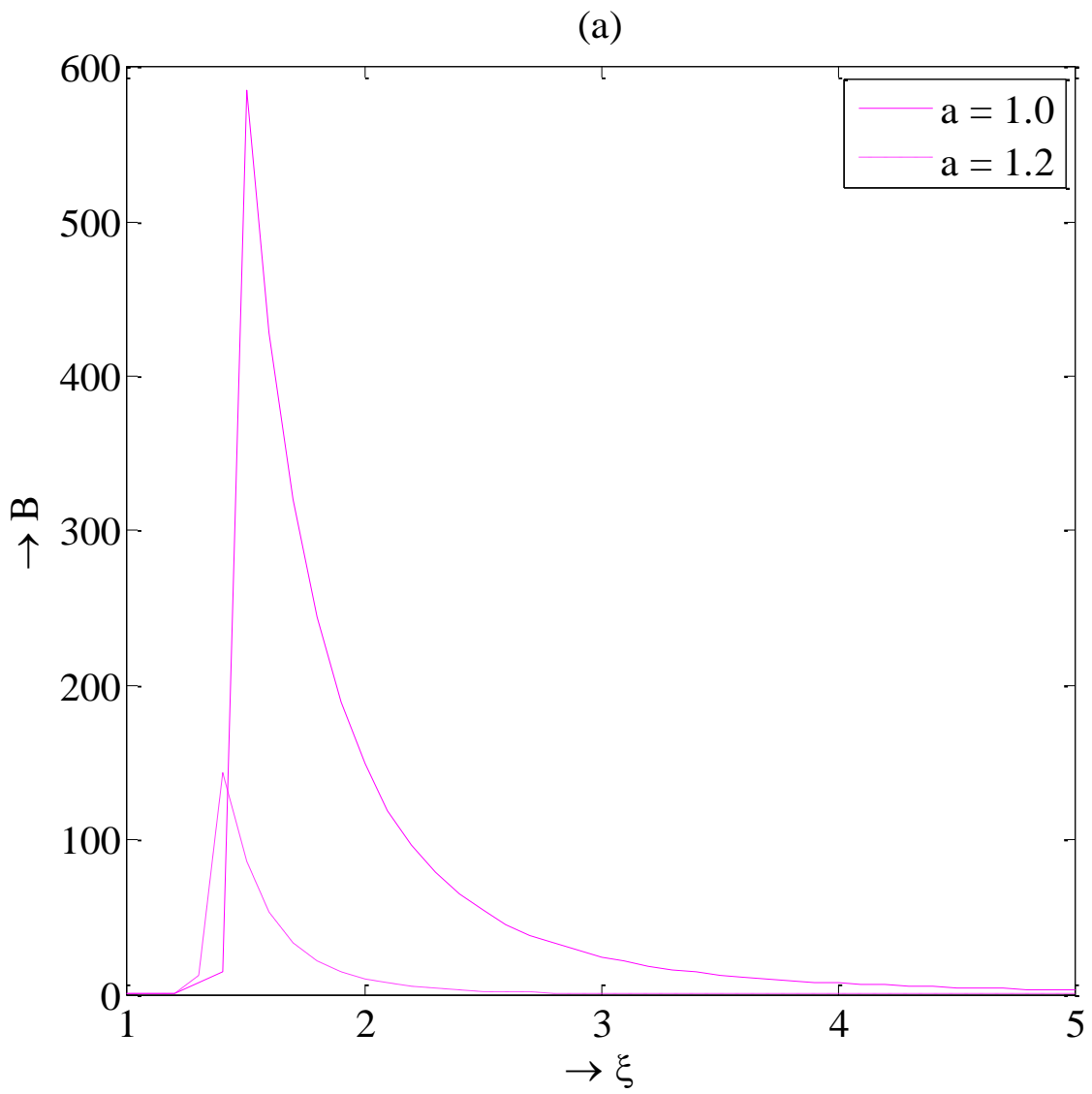


Figure 4.6(a). Magnetic pressure profiles for Royce EOS when $\Gamma_0 = 1.78$, $C_0 = 0.02$

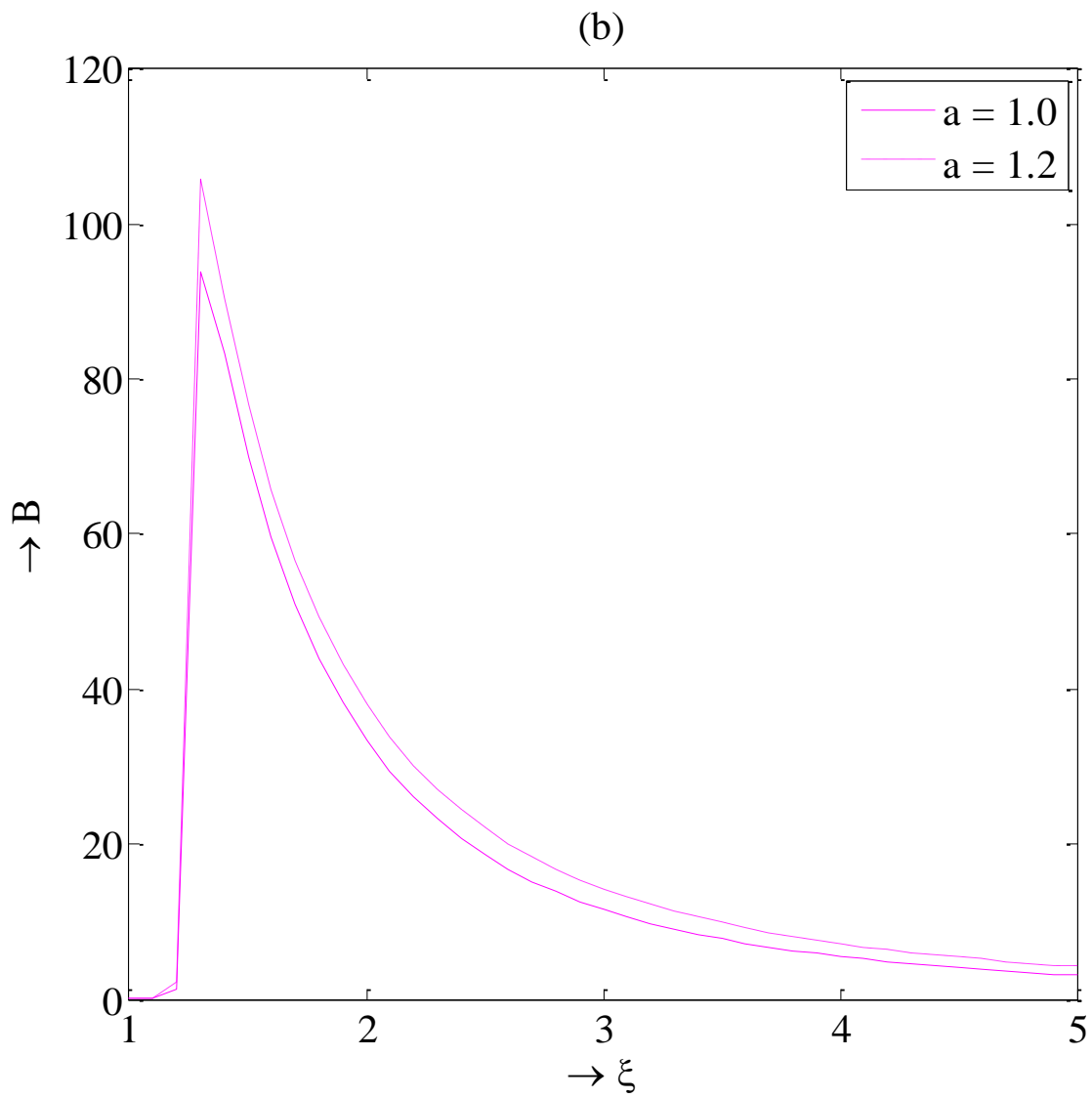


Figure 4.6(b). Magnetic pressure profiles for Royce EOS when $\Gamma_0 = 1.78$, $C_0 = 0.05$

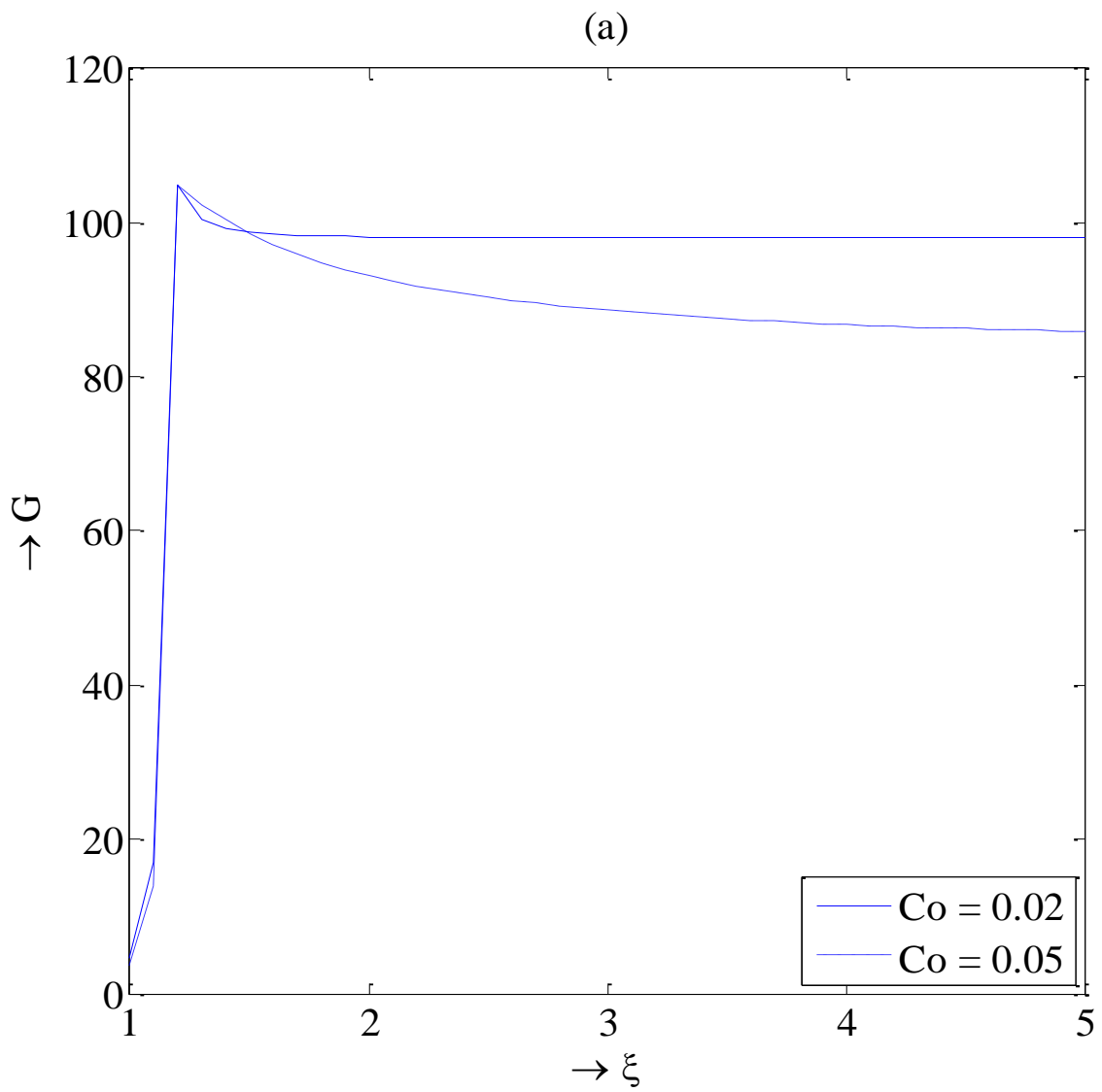


Figure 4.7(a). Density profiles for perfect gas when $\gamma = 1.4$

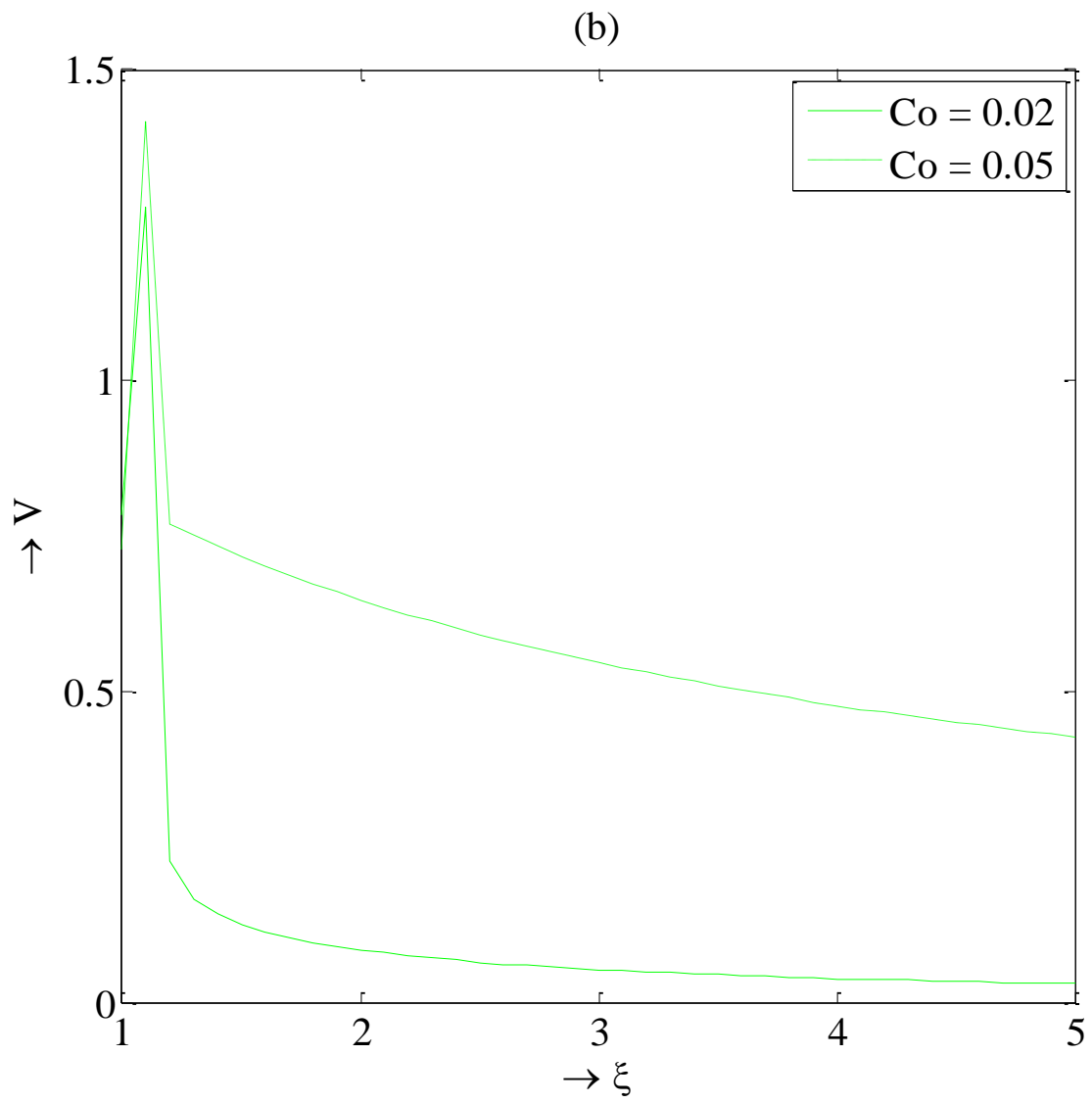


Figure 4.7(b). Velocity profiles for perfect gas when $\gamma = 1.4$

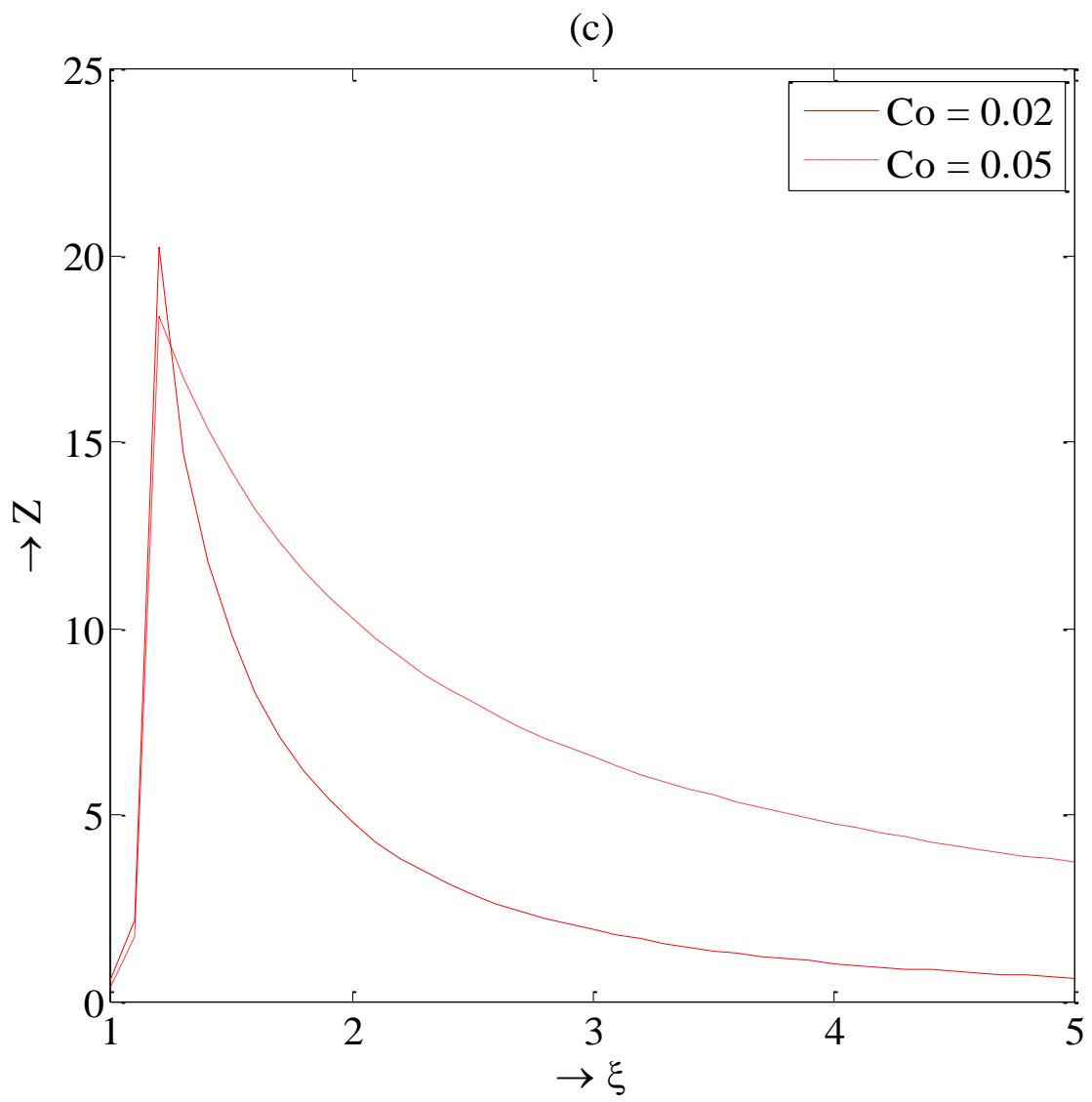


Figure 4.7(c). Pressure profiles for perfect gas when $\gamma = 1.4$

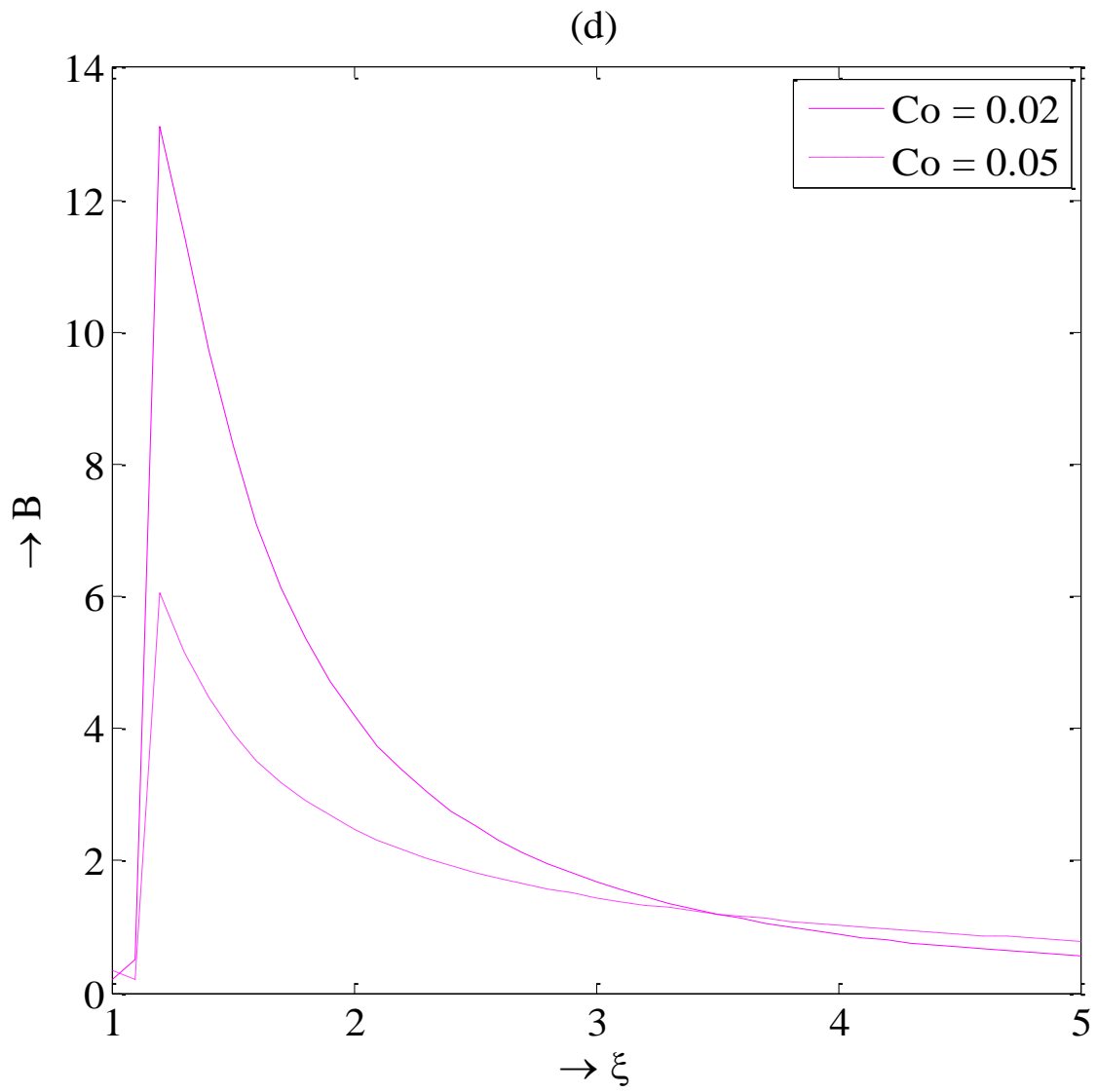


Figure 4.7(d). Magnetic pressure profiles for perfect gas when $\gamma = 1.4$

Chapter-5

Magnetogasdynamic Shock Waves a Numerical Study

5.1 Introduction

Magnetogasdynamics applies to many conductive fluid and plasma flows encountered in nature. In several circumstances, the flow is subject to a strong as well as a weak magnetic field. Such situation can be thought of occurring in earth's liquid core, and is present in solar physics such as sunspots, solar flares, solar corona, solar winds, etc. The strong magnetic fields play significant roles in the dynamics of the interstellar medium. Several authors contributed to this investigation and we mention the contributions of [6, 24, 26, 50, 54, 56, 57, 84, 96, 97, 98] for their high accuracy results and alternative approaches for the investigation of implosion problem. The propagation of shock waves under the influence of strong magnetic field is of great interest to many researchers. The areas of interest vary from astrophysics to plasma physics, to Magneto hydrodynamic (MHD) shock waves. Propagation of shock waves in magneto hydrodynamics (MHD) has been studied by several researchers. Analytical solutions were presented by Genot [33] for anisotropic MHD shocks. Hoffmann and Teller [99] developed a mathematical treatment for the motion of MHD shock waves in the very weak and very strong magnetic fields. Bazer and Ericson [100] were first among the many researchers to study the hydromagnetic shocks for

astrophysical applications. A number of approaches namely, the similarity method, power series solution method, CCW method have been used for the theoretical investigations of MHD shock waves in homogeneous and inhomogeneous media.

In the recent years much attention has been focused on the self-similar solutions because of their wide applications in determining solutions of nonlinear differential equations of physical interest. The gas attains very high temperature due to the propagation of shock waves and at such a high temperature, the gas gets ionized, hence effects of magnetic field becomes significant in the study of converging shock waves. The study of MHD shock waves in a non-ideal gas is of great scientific interest in many problems because of their applications in the areas of astrophysics, oceanography, atmospheric sciences, hypersonic aerodynamics and hypervelocity impact.

In this chapter, a model to determine the similarity solutions to the problem of gas dynamic flow under the influence of strong magnetic field is presented. The problem treated here involves distinct features: the global behavior of the physical parameter has been studied; the initial pressure ratio is confined to a moderate value. The path of the piston is imposed as boundary condition. Thus an accelerated, a decelerated or a constant velocity piston can be specified. The numerical values of similarity exponents and profiles of flow variables are obtained. These are presented through the illustrative graphs and tables. The

magnetic field effects on the flow variables through a medium and total energy under the influence of strong magnetic field is also presented.

5.2 Basic Equations and Boundary Conditions

The conservation equations governing the non-steady one dimensional flow can be written as [7, 70, 76, 81, 91, 98]

$$\frac{\partial \rho}{\partial t} + u \frac{\partial \rho}{\partial r} + \rho \frac{\partial u}{\partial r} + \frac{(m-1)\rho u}{r} = 0 \quad (5.1)$$

$$\frac{\partial u}{\partial t} + u \frac{\partial u}{\partial r} + \rho^{-1} \left(\frac{\partial p}{\partial r} + \frac{\partial h}{\partial r} \right) = 0 \quad (5.2)$$

$$\frac{\partial p}{\partial t} + u \frac{\partial p}{\partial r} - a^2 \left(\frac{\partial \rho}{\partial t} + u \frac{\partial \rho}{\partial r} \right) = 0 \quad (5.3)$$

$$\frac{\partial h}{\partial t} + u \frac{\partial h}{\partial r} + 2h \frac{\partial u}{\partial r} + 2h(m-1)u/r = 0 \quad (5.4)$$

where $\rho(r, t)$, $u(r, t)$, and $p(r, t)$ denote the density, velocity, and pressure of the gas particles behind the shock front, $h(r, t)$ is the magnetic pressure defined by $h = \frac{\mu H^2}{2}$ with μ as magnetic permeability and H is the transverse magnetic field, $a^2 = \frac{(\Gamma+1)p}{\rho}$ is the equilibrium speed of sound, Γ is the Gruneisen coefficient, $m = 2(3)$ denote shock wave in cylindrical (spherical) geometry.

It is assumed that the plasma has infinite electrical conductivity and permeated by an axial magnetic field orthogonal to the trajectories of the gas particles. Shock is assumed to be strong and propagating into a medium according to a power law $R(t) \propto (t)^\alpha$, where $R(t)$ is the position of the shock wave front from the center

at time t and $t = 0$ corresponds to the instant of the convergence when $R = 0$.

The equation of state under equilibrium condition is of Mie-Gruneisen type [57],

$$p = \rho e \Gamma (\rho/\rho_0) \quad (5.5)$$

where the function $\Gamma(\rho/\rho_0)$ is the Gruneisen parameter and e is the specific internal energy.

5.2.1 Boundary conditions

The boundary conditions at shock front due to Rankine-Hugoniot, can be written as [6, 7, 76]

$$\rho = \frac{\Gamma+2}{\Gamma} \rho_0 \left\{ 1 + \frac{2}{\Gamma} \left(\frac{a_0}{D} \right)^2 \right\} \quad \text{and} \quad u = \frac{2}{\Gamma+2} D \left(1 - \frac{a_0}{D} \right) \quad (5.6)$$

$$p = \frac{2}{\Gamma+2} \rho_0 D^2 \left\{ 1 - \frac{\Gamma}{2} \left(\frac{a_0}{D} \right)^2 \right\} - \frac{1(\Gamma+2)^2}{2\Gamma^2} C_0 \rho_0 D^2 \left\{ 1 + \frac{2}{\Gamma} \left(\frac{a_0}{D} \right)^2 \right\}^2 \quad (5.7)$$

$$h = \frac{1}{2} \left(\frac{\Gamma+2}{\Gamma} \right)^2 C_0 \rho_0 D^2 \left\{ 1 + \frac{2}{\Gamma} \left(\frac{a_0}{D} \right)^2 \right\}^2 \quad (5.8)$$

where $C_0 = \frac{2h_0}{\rho_0 D^2}$ is the shock Cowling number and D is the speed of the shock

wave defined as $D = \frac{dR}{dt}$, since the initial energy input E_0 of explosion is very

large, the shocks speed $D \gg a_0$ so that $\frac{a_0}{D} \rightarrow 0$ in the strong shock limit.

Therefore, the Rankine-Hugoniot jump conditions (5.6-5.8) in the case of strong shock waves can be written as

$$\rho = \frac{\Gamma+2}{\Gamma} \rho_0 \quad \text{and} \quad u = \frac{2}{\Gamma+2} D \quad (5.9)$$

$$p = \frac{2}{\Gamma+2} \rho_0 D^2 - \frac{1}{2} \frac{(\Gamma+2)^2}{\Gamma^2} C_0 \rho_0 D^2 \quad (5.10)$$

$$h = \frac{1}{2} \frac{(\Gamma+2)^2}{\Gamma^2} C_0 \rho_0 D^2 \quad (5.11)$$

Using equations (5.9), (5.10), and (5.11), the EOS (5.5) can be written as [57]

$$\left(2 - \frac{C_0 \beta^3}{(\beta-1)}\right) = (\beta - 1) \Gamma(\beta) \quad (5.12)$$

where $\beta(\rho/\rho_0)$ is the compression just behind the shock, which is called measure of shock strength. When $C_0 = 0$, the propagation of shock wave into a medium is without magnetic field and equation (5.12) reduces to the non-magnetic case in a non-ideal medium. The total energy E inside a blast wave is equal to the energy supplied by the explosive and thus constant. The total energy is given by the expression [7]

$$E = 4\pi \int_0^D \left(\frac{1}{2} \rho u^2 + \frac{p}{\Gamma} + h\right) R^{(m-1)} dR \quad (5.13)$$

Eliminating ρ_0 from equations (5.10) and (5.11), p and h can be written as [after using equation (5.9)]

$$p = \frac{\Gamma}{2} \rho u^2 - \frac{C_0 (\Gamma+2)^3}{8 \Gamma} \rho u^2 \quad \text{and} \quad h = \frac{1}{8} \frac{(\Gamma+2)^3}{\Gamma} C_0 \rho u^2$$

5.2.2 Conservation equations and boundary conditions

The basic equations can be made dimensionless by transforming the independent variables for space r and time t into new independent variables as follows [7]

$$p = \frac{\Gamma}{2} \rho u^2 - \frac{C_0(\Gamma+2)^3}{8} \frac{\rho u^2}{\Gamma} \quad \text{and} \quad h = \frac{1(\Gamma+2)^3}{8} \frac{C_0 \rho u^2}{\Gamma} \quad (5.14)$$

$$\rho = \rho_0 G(\xi) \quad (5.15)$$

$$u = DV(\xi) \quad (5.16)$$

where similarity variable $\xi = \frac{r}{R}$

With the help of equations (5.1) and (5.14), the governing equations (5.2-5.4) can be rewritten as follows,

$$\frac{\partial u}{\partial t} + (1 + \Gamma)u \frac{\partial u}{\partial r} + \frac{u^2}{2\rho} \left\{ \frac{(\Gamma+2)\hat{\Gamma}}{\Gamma} + \Gamma \right\} \frac{\partial \rho}{\partial r} = 0 \quad (5.17)$$

$$\frac{\partial u}{\partial t} + u \frac{\partial u}{\partial r} + \frac{u\Gamma}{2} \left\{ \frac{\partial u}{\partial r} + (m-1) \frac{u}{r} \right\} + \frac{u}{\rho} \left(\frac{N_2}{N_1} \right) \left\{ \dot{\Gamma} \frac{\partial \rho}{\partial t} + u\hat{\Gamma} \frac{\partial \rho}{\partial r} \right\} = 0 \quad (5.18)$$

$$\frac{\partial u}{\partial t} + u \frac{\partial u}{\partial r} + \frac{u}{2} \left\{ \frac{\partial u}{\partial r} + (m-1) \frac{u}{r} \right\} + \frac{u}{\rho} \left(\frac{\Gamma-1}{\Gamma^2} \right) \left\{ \dot{\Gamma} \frac{\partial \rho}{\partial t} + u\hat{\Gamma} \frac{\partial \rho}{\partial r} \right\} = 0 \quad (5.19)$$

where

$$N_1 = \left[\frac{\Gamma}{1} - \frac{C_0(\Gamma+2)^3}{4} \frac{1}{\Gamma} \right], \quad N_2 = \frac{(\Gamma+2)}{2\Gamma} \left[1 - \frac{C_0}{2\Gamma^2} (\Gamma-1)(\Gamma+2)^2 \right],$$

$$\hat{\Gamma} = \frac{\partial \Gamma}{\partial r} \quad \text{and} \quad \dot{\Gamma} = \frac{\partial \Gamma}{\partial t}$$

The derivatives in equations (5.17-5.19) change according to relations of the following type

$$\frac{\partial}{\partial r} = \frac{1}{R} \frac{\partial}{\partial \xi}, \quad \frac{\partial}{\partial t} = \frac{\partial}{\partial t} - \xi \frac{D}{R} \frac{\partial}{\partial \xi}$$

The transformed system of three ordinary differential equations in non-dimensional form depend only on the similarity variable ξ and are,

$$\{(1 + \Gamma)V - \xi\} \left(\frac{V'}{V}\right) + \frac{\Gamma V}{2} \left(\frac{G'}{G}\right) - \frac{(\Gamma+2)V}{2R} \left(\frac{G'}{G}\right)^2 = -\lambda \quad (5.20)$$

$$\left\{\left(1 + \frac{\Gamma}{2}\right)V - \xi\right\} \left(\frac{V'}{V}\right) - \frac{\Gamma\phi(\Gamma)}{R} (V + \xi^2 D) \left(\frac{G'}{G}\right)^2 = -\lambda - \frac{\Gamma V(m-1)}{2\xi} \quad (5.21)$$

$$\left(\frac{3V}{2} - \xi\right) \left(\frac{V'}{V}\right) - \frac{(\Gamma-1)}{\Gamma R} (V + \xi^2 D) \left(\frac{G'}{G}\right)^2 = -\lambda - \frac{(m-1)V}{2\xi} \quad (5.22)$$

where D is $\frac{dR}{dt} = \dot{R}$, $\lambda = \dot{D} \frac{R}{D^2}$, G, V are new dimensionless functions of density ρ and velocity u . The differentiation of the new dimensionless functions with respect to the similarity variable ξ is denoted by a prime. Further using equation (5.20), the equations (5.21) and (5.22) can be reduced into a system of two ordinary differential equations.

$$A_1 \left(\frac{G'}{G}\right) + B_1 \left(\frac{V'}{V}\right) = C_1 \quad (5.23)$$

$$A_2 \left(\frac{G'}{G}\right) + B_2 \left(\frac{V'}{V}\right) = C_2 \quad (5.24)$$

The above equations can be written in matrix form as

$$\begin{bmatrix} A_1 & B_1 \\ A_2 & B_2 \end{bmatrix} \begin{bmatrix} \frac{G'}{G} \\ \frac{V'}{V} \end{bmatrix} = \begin{bmatrix} C_1 \\ C_2 \end{bmatrix} \quad (5.25)$$

where $A_1 = \frac{(V+\xi^2 D)\Gamma^2\phi(\Gamma)}{\Gamma+2}$, $B_1 = \frac{2\{(1+\Gamma)V-\xi\}}{\Gamma V} A_1 - \frac{1}{2} \{(2 + \Gamma)V - 2\xi\}$,

$$\begin{aligned}
A_2 &= \frac{(V+\xi^2 D)(\Gamma-1)}{\Gamma+2}, & B_2 &= \frac{2\{(1+\Gamma)V-\xi\}}{\Gamma V} A_2 - \frac{1}{2}(3V - 2\xi), \\
C_1 &= \left(1 - \frac{2}{\Gamma V} A_1\right) \lambda + \frac{\Gamma V(m-1)}{2\xi}, & C_2 &= \left(1 - \frac{2}{\Gamma V} A_2\right) \lambda + \frac{V(m-1)}{2\xi}, \\
\phi(\Gamma) &= \frac{2(\Gamma+2)\Gamma^2 - C_0(\Gamma-1)(\Gamma+2)^3}{4\Gamma^4 - C_0\Gamma^2(\Gamma+2)^3}, \\
G' &= G \frac{\Delta_1}{\Delta}, & V' &= V \frac{\Delta_2}{\Delta}
\end{aligned} \tag{5.26}$$

and

$$\Delta = \frac{(V-\alpha\xi^2)}{f_3} \left[\frac{V}{2} f_1 + 6\xi f_2 \right] \tag{5.27}$$

$$\begin{aligned}
\Delta_1 &= \frac{1}{\Gamma f_3} \left[(V - \alpha\xi^2) \left\{ \lambda f_4 + (m-1) \left(1 + \frac{V}{\xi} (\Gamma+1) \right) f_5 \right\} + \frac{V}{2} f_6 \left\{ \lambda + \right. \right. \\
&\left. \left. (m-1) \left(1 - \frac{V}{\xi} \right) \right\} \right]
\end{aligned} \tag{5.28}$$

$$\Delta_2 = \frac{(V-\alpha\xi^2)}{f_3} \left[6\lambda f_7 - \frac{(m-1)V}{2\xi} f_5 \right] \tag{5.29}$$

where $f_1, f_2, f_3, f_4, f_5, f_6$, and f_7 are functions of Γ

$$f_1(\Gamma) = 2\Gamma^2(2\Gamma^2 - \Gamma - 10) - C_0\Gamma^2(\Gamma^5 + 4\Gamma^4 + \Gamma^3 - 10\Gamma^2 - 4\Gamma + 8),$$

$$f_2(\Gamma) = \Gamma^4(4 - \Gamma), \quad f_3(\Gamma) = 4\Gamma^2(\Gamma + 2) - C_0(\Gamma + 2)^4,$$

$$f_4(\Gamma) = 2(-5\Gamma^3 + 4\Gamma^2 - \Gamma - 10) - \frac{1}{\Gamma^2} f_1, \quad f_5(\Gamma) = 4\Gamma^3(\Gamma - 4) - f_4,$$

$$f_6(\Gamma) = \Gamma(\Gamma - 1)(\Gamma + 2)f_3, \quad f_7(\Gamma) = \frac{1}{\Gamma^2} f_2, \quad \text{and} \quad \lambda = 1 - \frac{1}{\alpha}$$

The transformed boundary conditions are

$$G(1) = \beta \quad \text{and} \quad V(1) = 1 - \frac{1}{\beta} \quad (5.30)$$

5.3 Solution Procedure

5.3.1 Evaluation of $\beta(\rho/\rho_0)$ the measure of shock strength

Considering the EOS of Mie-Gruneisen type [57]:

a) The McQueen defined by

$$\Gamma(G) = \frac{\Gamma_0}{G} \quad (5.31)$$

and

b) The Royce EOS defined by

$$\Gamma(G) = \Gamma_0 - b \left(1 - \frac{1}{G}\right) \quad (5.32)$$

along with equation (5.12) we obtain bi-quadratic equations in β as

$$C_0\beta^4 + (\Gamma_0 - 2)\beta^2 + 2(1 - \Gamma_0)\beta + \Gamma_0 = 0 \quad (5.33)$$

and

$$C_0\beta^4 + (\Gamma_0 - b)\beta^3 + (3b - 2 - 2\Gamma_0)\beta^2 + (2 - 3b + \Gamma_0)\beta + b = 0 \quad (5.34)$$

respectively. These equations are solved to obtain an unique value of β corresponding to the constants C_0 , Γ_0 , and b . According to Descartes's rule of signs these two equations will have at least two real and two complex roots. This was found to be true as can be seen from the solution curves and from these

solutions curves (see Figure 5.1 and Figure 5.2) it is observed that irrespective of the constants a real root is always $\beta = 1$ and this corresponds to the case where magnetic effect $C_0 = 0$. Neglecting the imaginary roots, the other roots are solved numerically using MATLAB and are tabulated in Table 5.1 and Table 5.2.

Table 5.1: Selected values of β and α for McQueen EOS for different values C_0

	$C_0 = 0.02$		$C_0 = 0.05$	
Γ_0	β	α	β	α
2.25	3.64832	0.72590123673362	2.70724	0.63062011495102
2.378	3.38294	0.704399132115852	2.58037	0.612458678406585
2.655	2.90851	0.656181343712072	2.34205	0.573023633141906
2.97	2.51656	0.602632164542073	2.12633	0.529706113350233

Table 5.2: Selected values of β and α for Royce EOS for different values of C_0 and an arbitrary constant b

		$b = 1$		$b = 1.2$		$b = 1.5$	
Γ_0	C_0	β	α	β	α	β	α
2.25	0	2.16886	0.538928284905434	2.26621	0.558734627417583	2.47481	0.595928576335153
	0.02	2.05713	0.513885850675456	2.13416	0.531431570266522	2.29118	0.563543676184324
	0.05	1.91188	0.476954620582882	1.96778	0.491813109189035	2.07584	0.518267303838446
2.378	0	2.07536	0.518155886207694	2.15239	0.535400183052328	2.30928	0.566964595025289
	0.02	1.97778	0.494382590581359	2.03990	0.509779891171136	2.16171	0.537403259456634
	0.05	1.84825	0.458947653185446	1.89427	0.472092151594018	1.98075	0.495140729521646
2.655	0	1.91908	0.478916981053421	1.96875	0.492063492063492	2.06256	0.515165619424405
	0.02	1.84246	0.457247375791062	1.88369	0.469127085666962	1.95978	0.489738644133525
	0.05	1.73720	0.424361040755238	1.76876	0.434632171690902	1.82537	0.452165862263541
2.97	0	1.79103	0.441662060378665	1.82373	0.451673219171698	1.88226	0.468723768236057
	0.02	1.72918	0.421691206236482	1.75691	0.430818880876084	1.80579	0.446225751610099
	0.05	1.64179	0.390908703305539	1.66354	0.398872284405545	1.70115	0.412162360755959

5.3.2 Numerical integration solution procedure

In order to integrate the set of non-linear ordinary differential equations (5.26), we use Runge-Kutta fourth order method with a small step size. The integration is carried out in the range, $1 \leq \xi < \infty$. Starting the integration with a known value of β and α (α is evaluated corresponding to every β iteratively), shown in Table 5.1 and Table 5.2. The whole solution procedure is repeated until the shock conditions are satisfied within the desired accuracy of error of the order of 10^{-5} .

5.4 Results and Discussion

In this chapter, the entire computational work has been carried out using MATLAB. Numerical calculations are performed for the values of non-ideal parameters $C_0 = 0.02, 0.05$; $b = 1.0, 1.2, 1.5$; and $\Gamma_0 = 2.25, 2.378, 2.655, 2.97$. The values of similarity exponent α for different values of C_0 in the case of McQueen EOS and Royce EOS are listed in Table 5.1 and Table 5.2 respectively. The variations of non-dimensional shock velocity, pressure, magnetic pressure and density with ξ for McQueen EOS are shown in Figure 5.3(a-d). It is observed that the flow variables velocity, pressure (for both cylindrical and spherical geometry) are high at the shock front (for the McQueen EOS) and increases with the increase in the non-idealness parameters and reduce gradually as ξ increases. Again from Figure 5.3(c) and Figure 5.3(d) at $\xi = 1$, magnetic pressure and energy are very high and reduce drastically with increase in ξ and become constant. Also from the Figure 5.3(e-l) for Royce EOS it can be seen that the

velocity, pressure, magnetic pressure and energy profiles, first increase with the increase in ξ and decrease with further increase in ξ . It is notable that increase in the non-idealness parameters (from Table 5.1 and Table 5.2) have effect on β . As β value increases, increase in velocity, pressure, magnetic pressure and energy is prominent for both the EOS. Thus it is observed from Figure 5.3(e-l) that increase in β does not automatically decelerate the shock front but the velocity and pressure behind the shock front increases quickly in the presence of the magnetic field and decrease slowly and become constant. Also in the presence of non-idealness parameters and in the absence of magnetic field the velocity and pressure profiles reduce gradually. It is noted from Figure 5.4(a-d) for the EOS of McQueen, density and energy increase drastically for $\xi > 2.5$ whereas with non-idealness parameters the velocity and pressure increase sharply for $\xi \geq 1$. From the Figure 5.5(a-f) with non-idealness parameters in the absence of magnetic field C_0 for the Royce EOS the velocity and pressure profiles gradually decrease (see Figure 5.5(a) and Figure 5.5(d)) and become constant, whereas pressure and energy profiles (see Figure 5.5(b, c, e, f)) initially increase with the increase in ξ and reduce slowly with increasing ξ and become constant. Also from the Figure 5.6(a-e) it is observed that shock propagates more rapidly in perfect gas in presence of the magnetic field. It is interesting to note that the rate of rise in the flow variables increase with the increase in the strength of magnetic field. The results of the study can be summarized as follows.

1. The flow variables velocity, pressure for both cylindrical and spherical geometry are high at the shock front for the McQueen EOS increases with the increase in the non-idealness parameters and reduce gradually as ξ increases.
2. At $\xi = 1$, magnetic pressure and energy are very high and reduce drastically with increase in ξ and become constant. The velocity, pressure, magnetic pressure and energy profiles, first increase with ξ and then decrease with further increase in ξ for Royce EOS.
3. It is notable that increase in the non-idealness parameters has effect on β . Increase in β does not automatically decelerate the shock front but the velocity and pressure behind the shock front increases quickly in the presence of the magnetic field and decrease slowly and become constant.
4. In the presence of non-idealness parameters and in the absence of magnetic field the velocity and pressure profiles reduce gradually. In the EOS of McQueen, density and energy increase drastically for $\xi > 2.5$ whereas with non-idealness parameters the velocity and pressure increase sharply for $\xi \geq 1$.
5. With non-idealness parameters in the absence of magnetic field C_0 for the Royce EOS the velocity and pressure profiles gradually decrease and become constant, whereas pressure and energy profiles initially increase

with the increase in ξ and reduce slowly with increasing ξ and become constant.

- In the presence of the magnetic field the shock propagates more rapidly in perfect gas. It is interesting to note that the rate of rise in the flow variables increase with the increase in the strength of magnetic field.

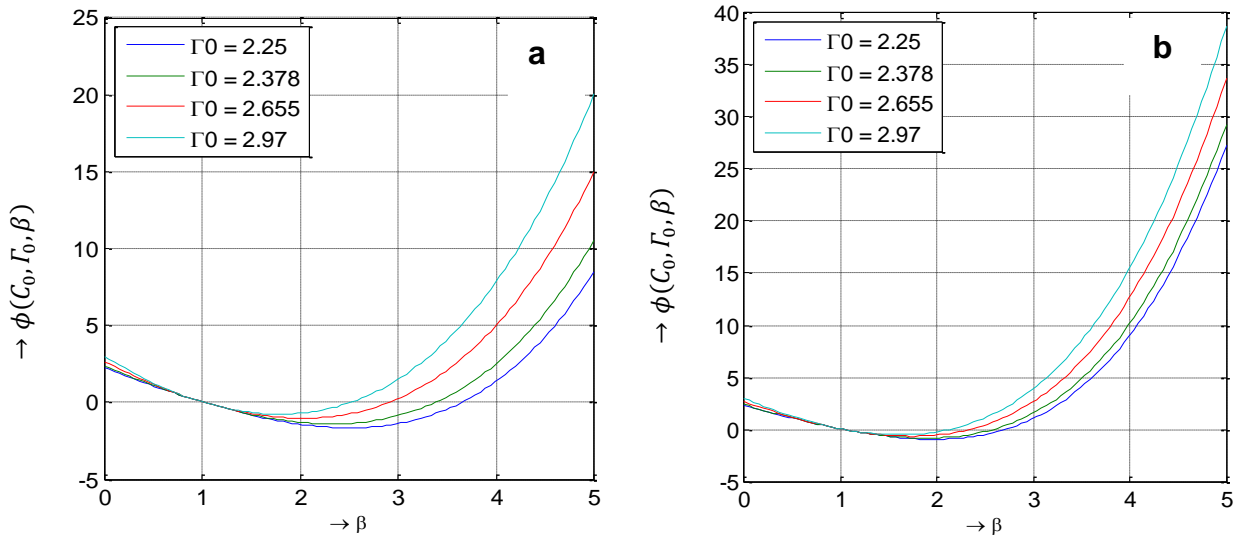


Figure 5.1. Graphical approach to estimate positive roots of equation $\phi(C_0, \Gamma_0, \beta) = 0$ in the case of McQueen EOS; when (a) $C_0 = 0.02$ and (b) $C_0 = 0.05$

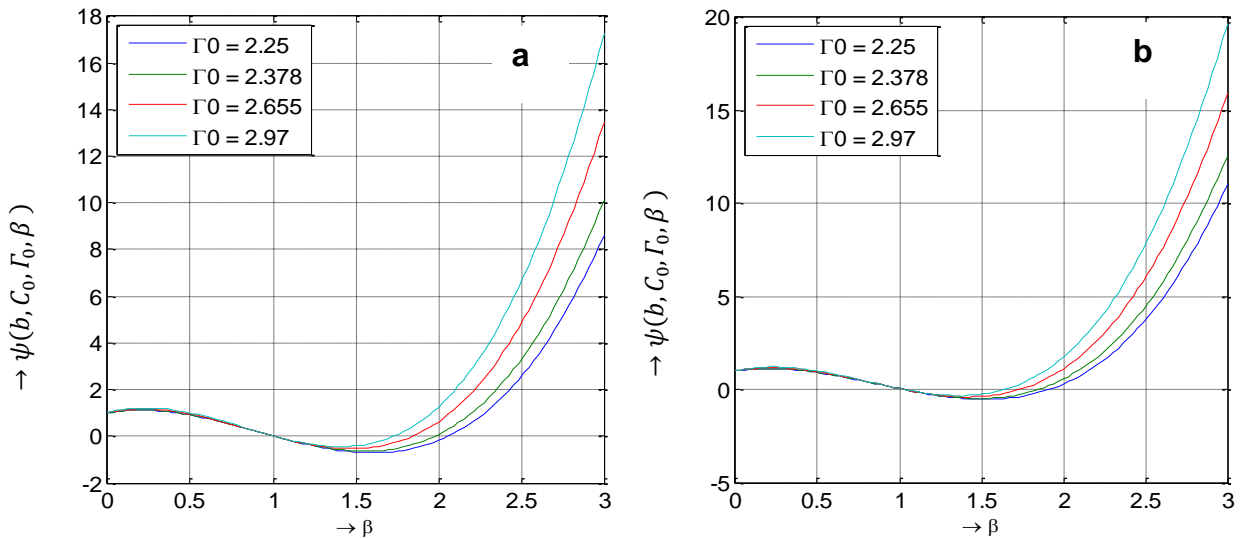


Figure 5.2. Graphical approach to estimate positive roots of equation $\psi(b, C_0, \Gamma_0, \beta) = 0$ in the case of Royce EOS; when (a) $C_0 = 0.02$ and (b) $C_0 = 0.05$

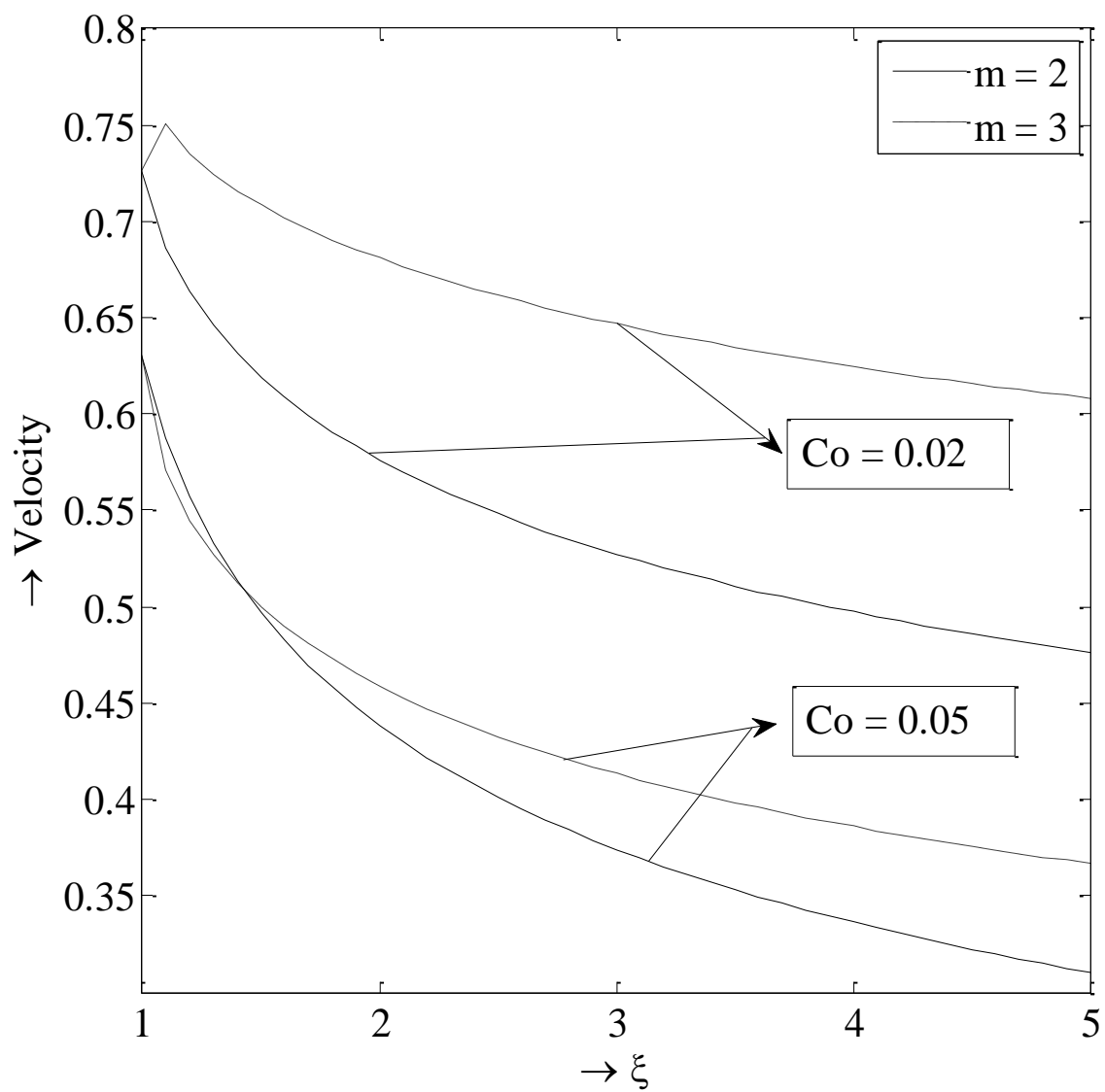


Figure 5.3(a). Velocity profiles of Mc Queen EOS for $\Gamma_0 = 2.25$ and different values of C_0

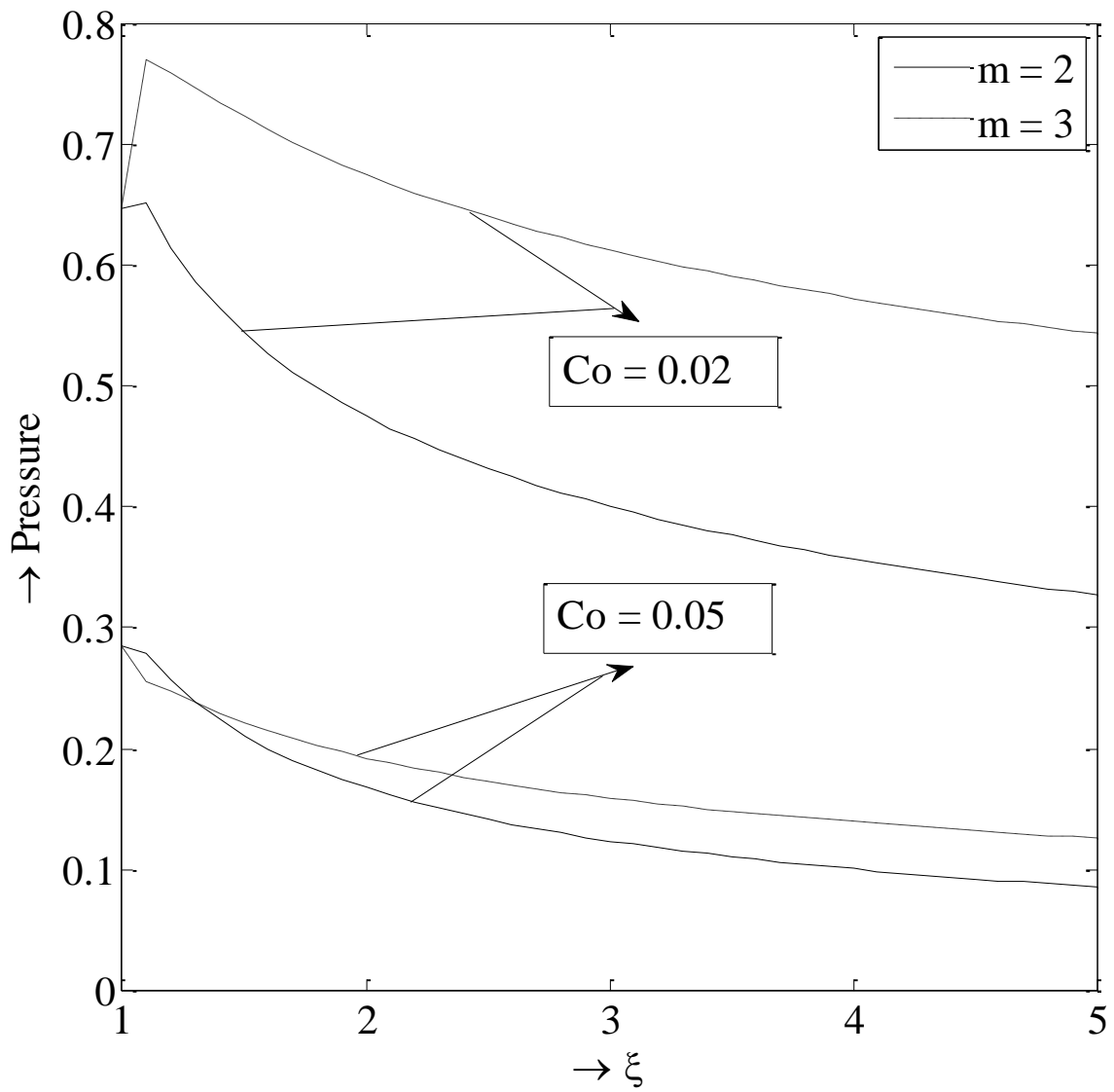


Figure 5.3(b). Pressure profiles of Mc Queen EOS for $\Gamma_0 = 2.25$ and different values of C_0

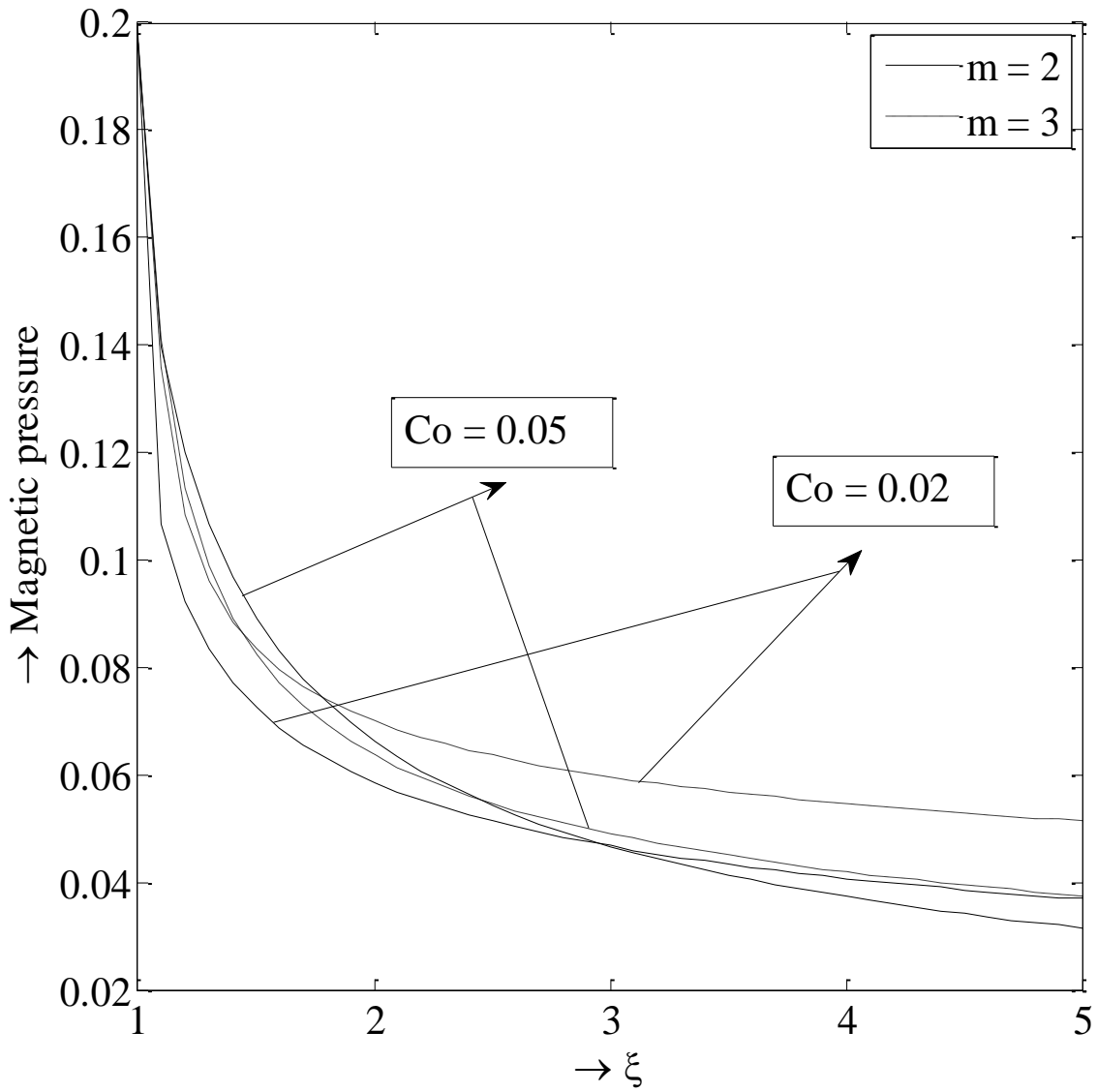


Figure 5.3(c). Magnetic pressure profiles of Mc Queen EOS for $\Gamma_0 = 2.25$ and different values of C_0

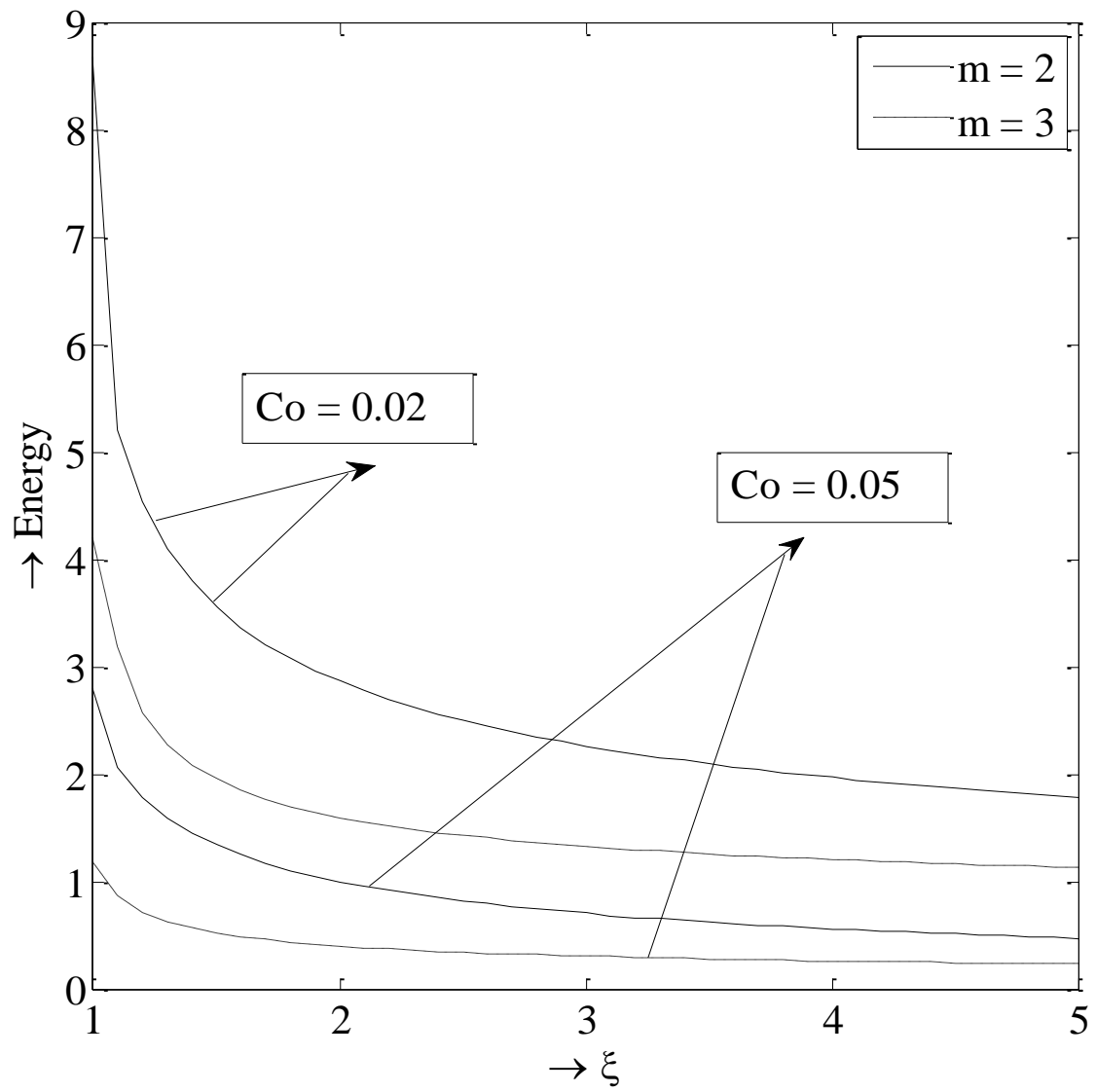


Figure 5.3(d). Energy profiles of Mc Queen EOS for $\Gamma_0 = 2.25$ and different values of C_0

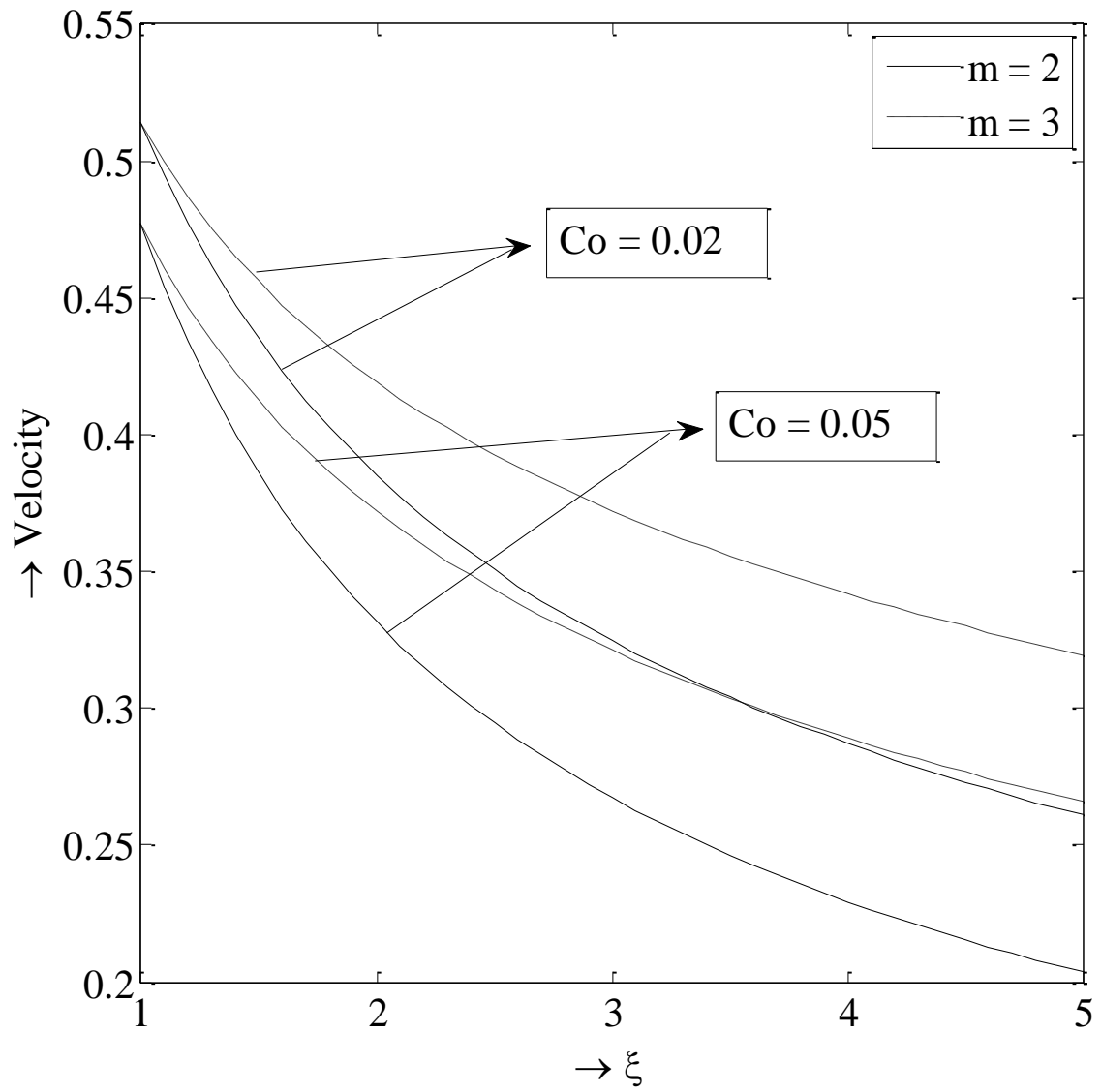


Figure 5.3(e). Velocity profiles of Royce EOS for $b = 1.0$, $\Gamma_0 = 2.25$, and different values of C_0

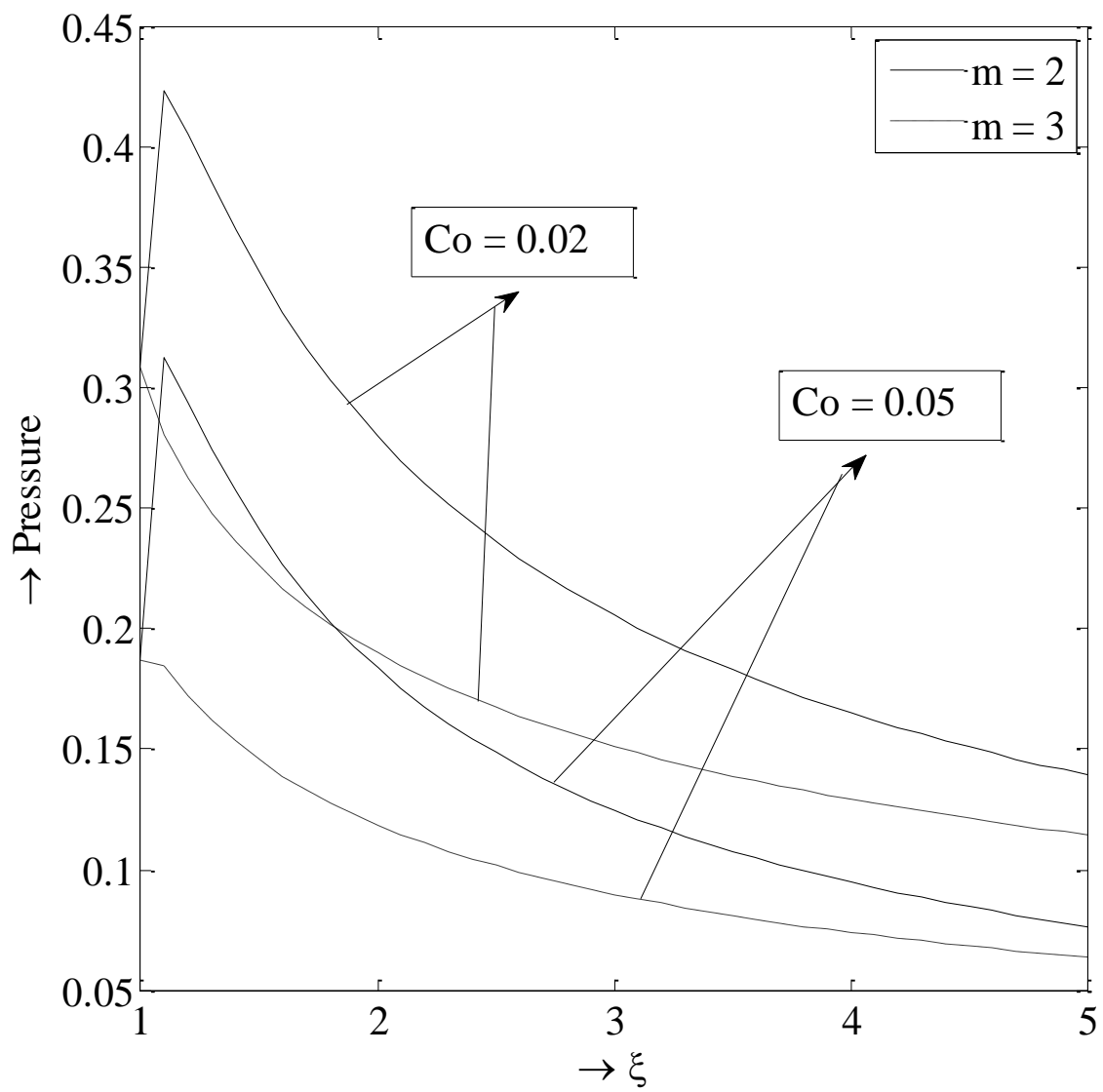


Figure 5.3(f). Pressure profiles of Royce EOS for $b = 1.0$, $\Gamma_0 = 2.25$, and different values of C_0

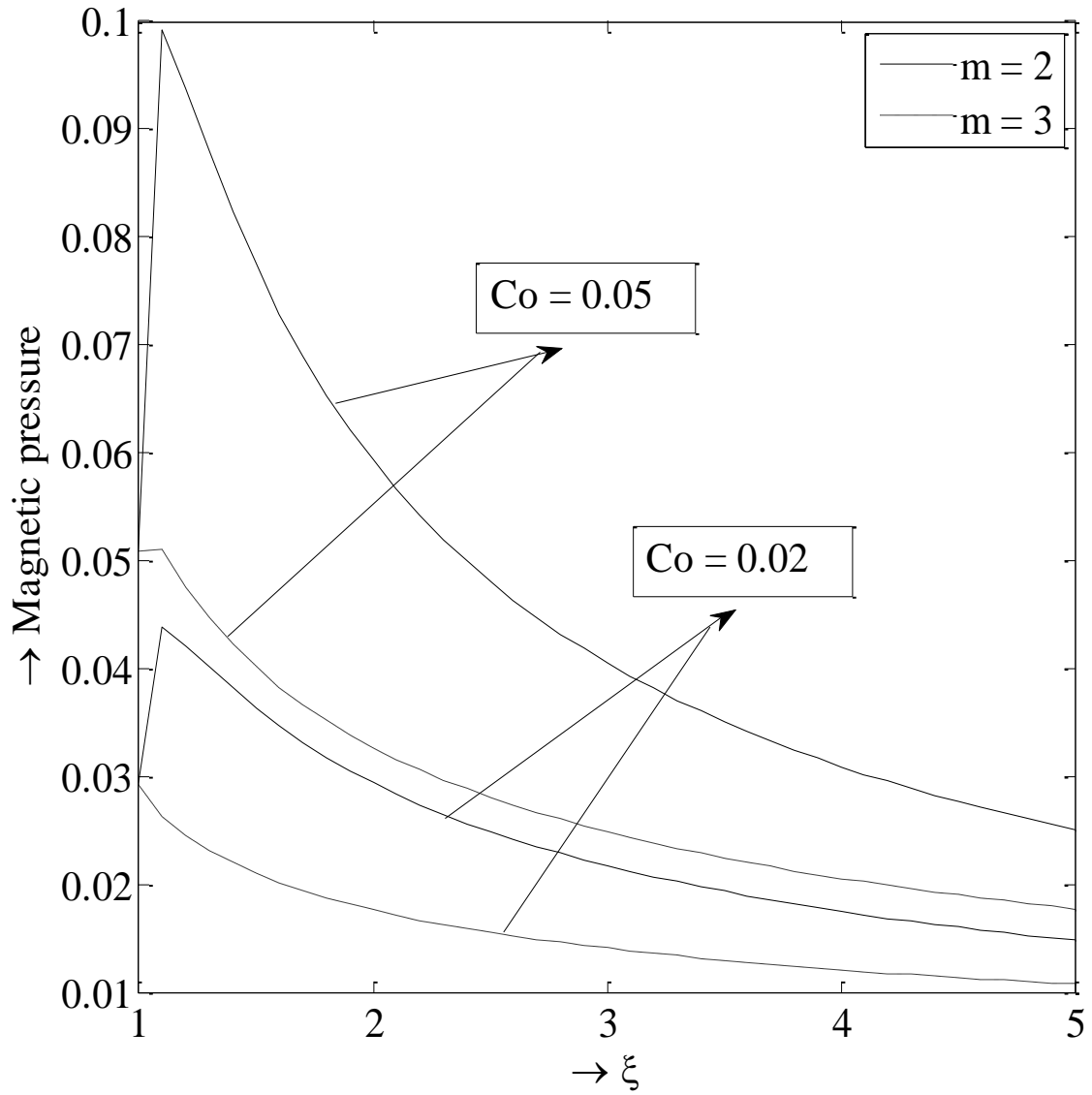


Figure 5.3(g). Magnetic pressure profiles of Royce EOS for $b = 1.0$, $\Gamma_0 = 2.25$, and different values of C_0

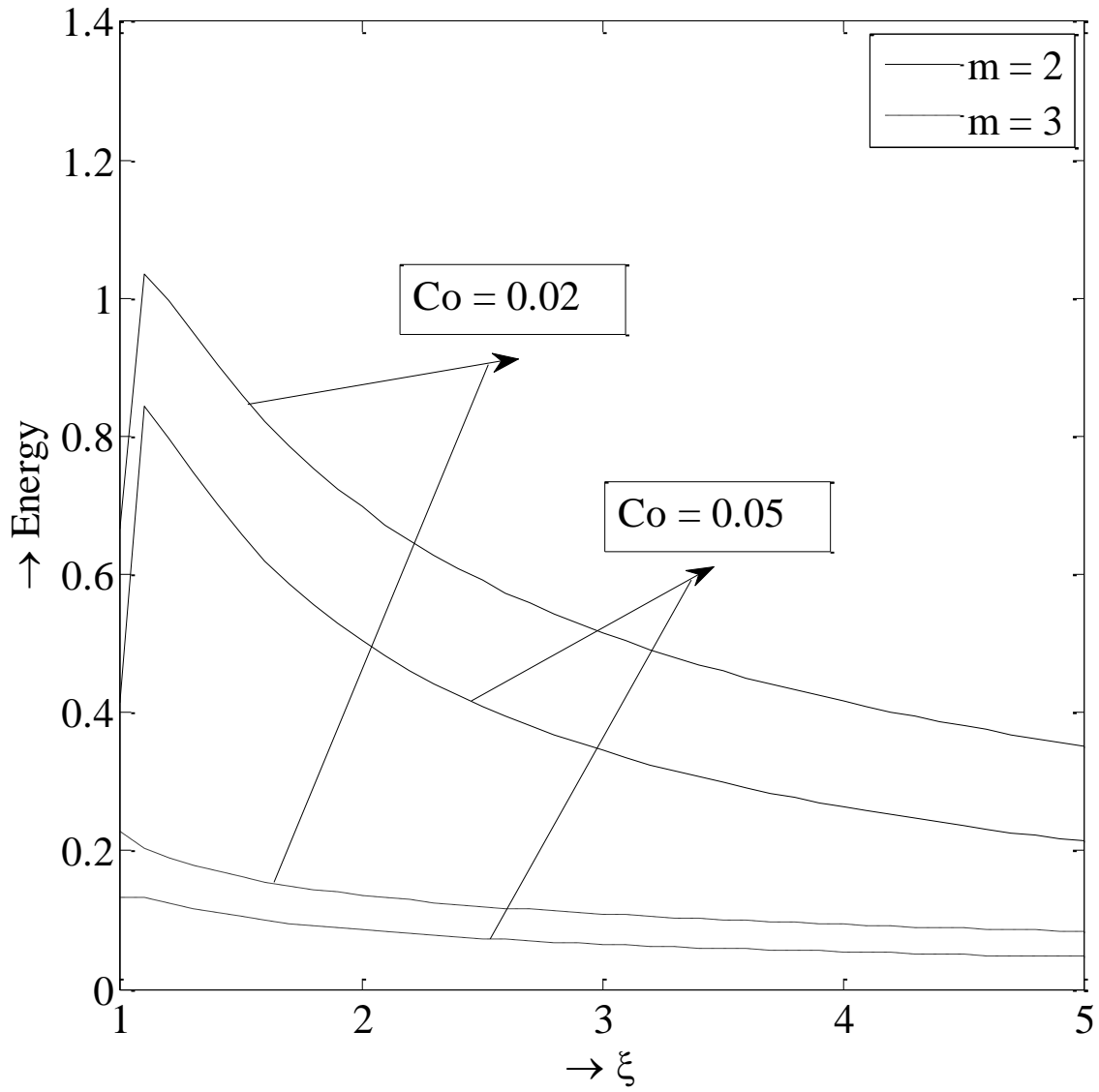


Figure 5.3(h). Energy profiles of Royce EOS for $b = 1.0$, $\Gamma_0 = 2.25$, and different values of C_0

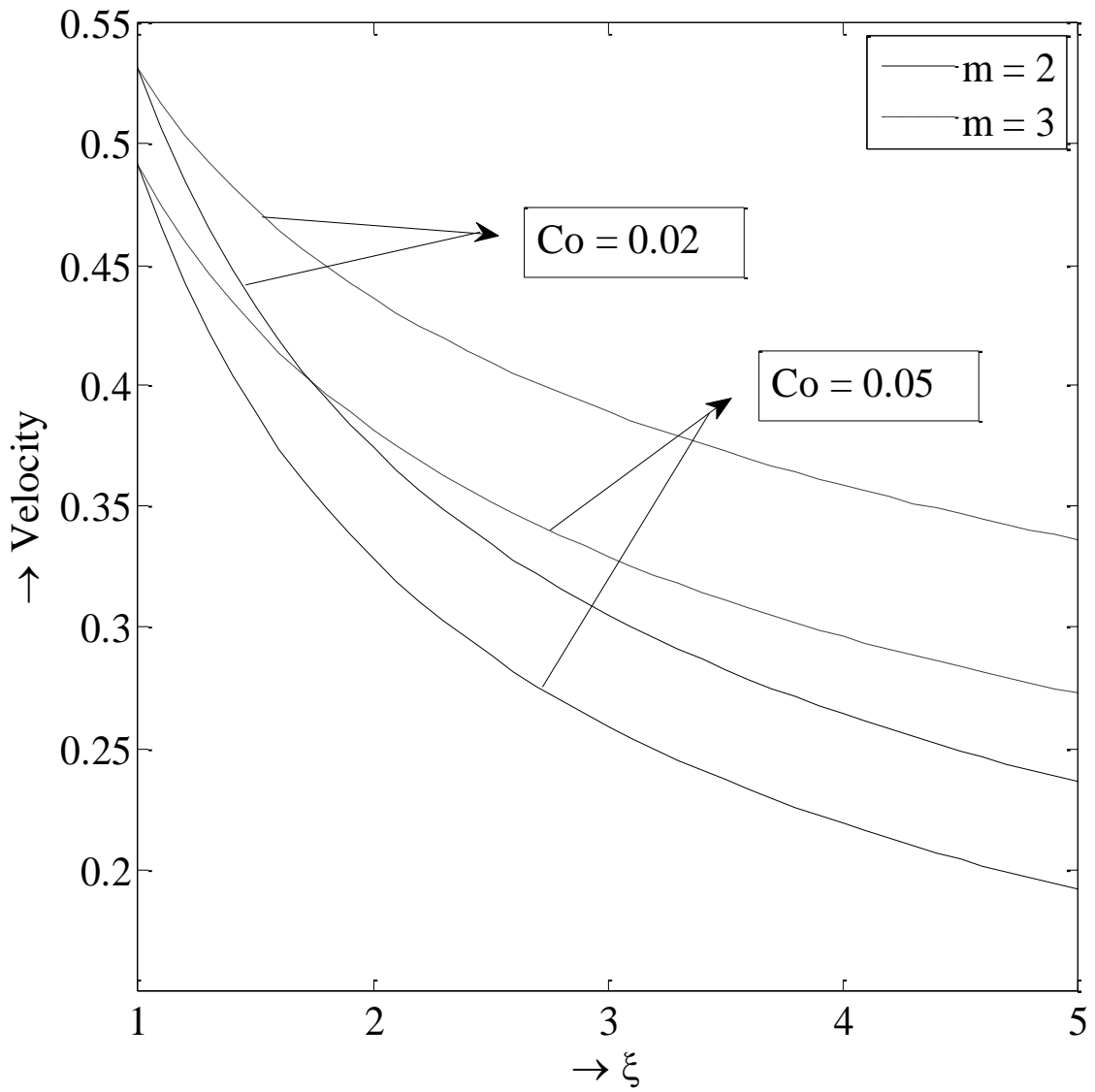


Figure 5.3(i). Velocity profiles of Royce EOS for $b = 1.2$, $\Gamma_0 = 2.25$, and different values of C_0

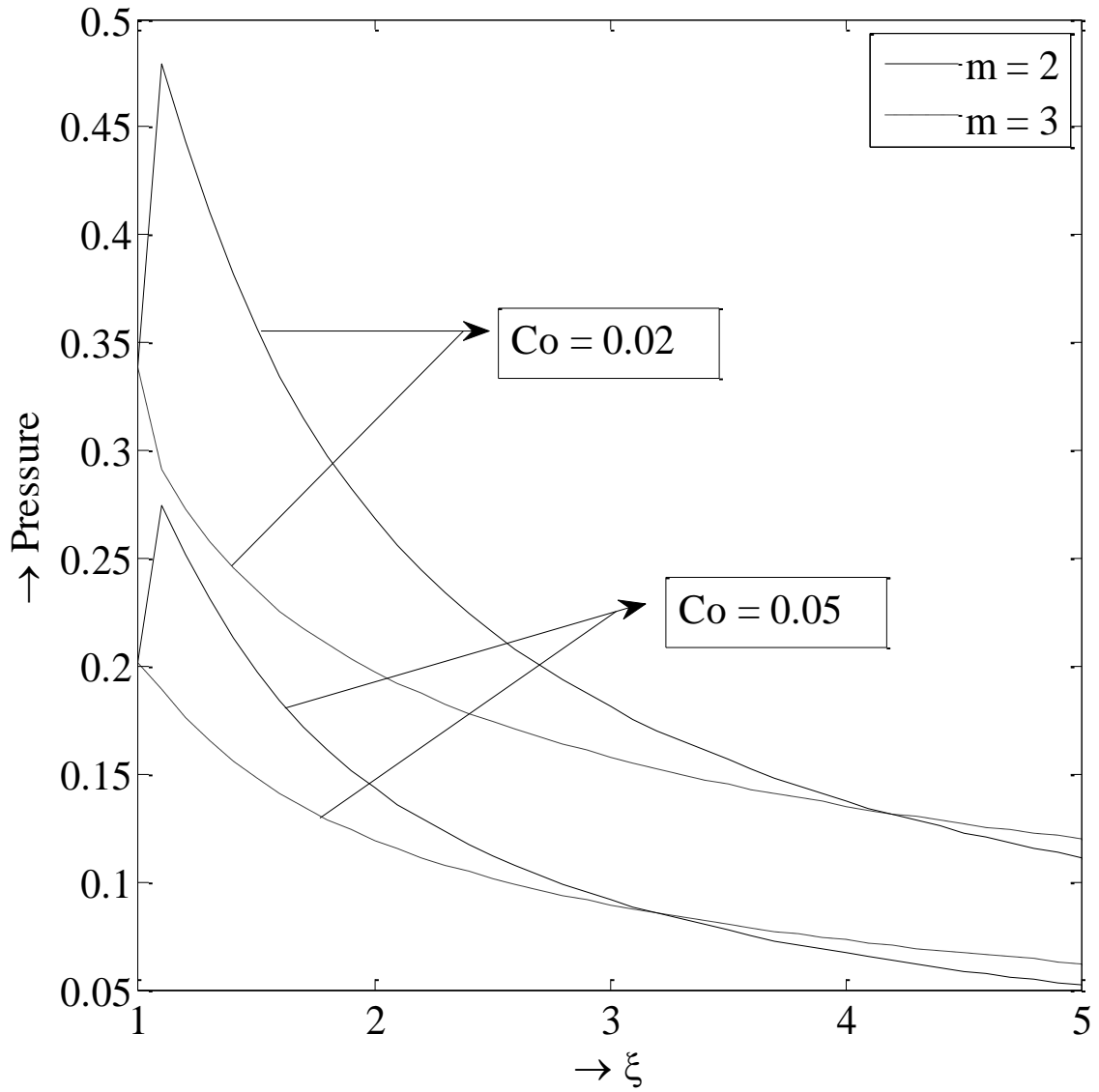


Figure 5.3(j). Pressure profiles of Royce EOS for $b = 1.2$, $\Gamma_0 = 2.25$, and different values of C_0

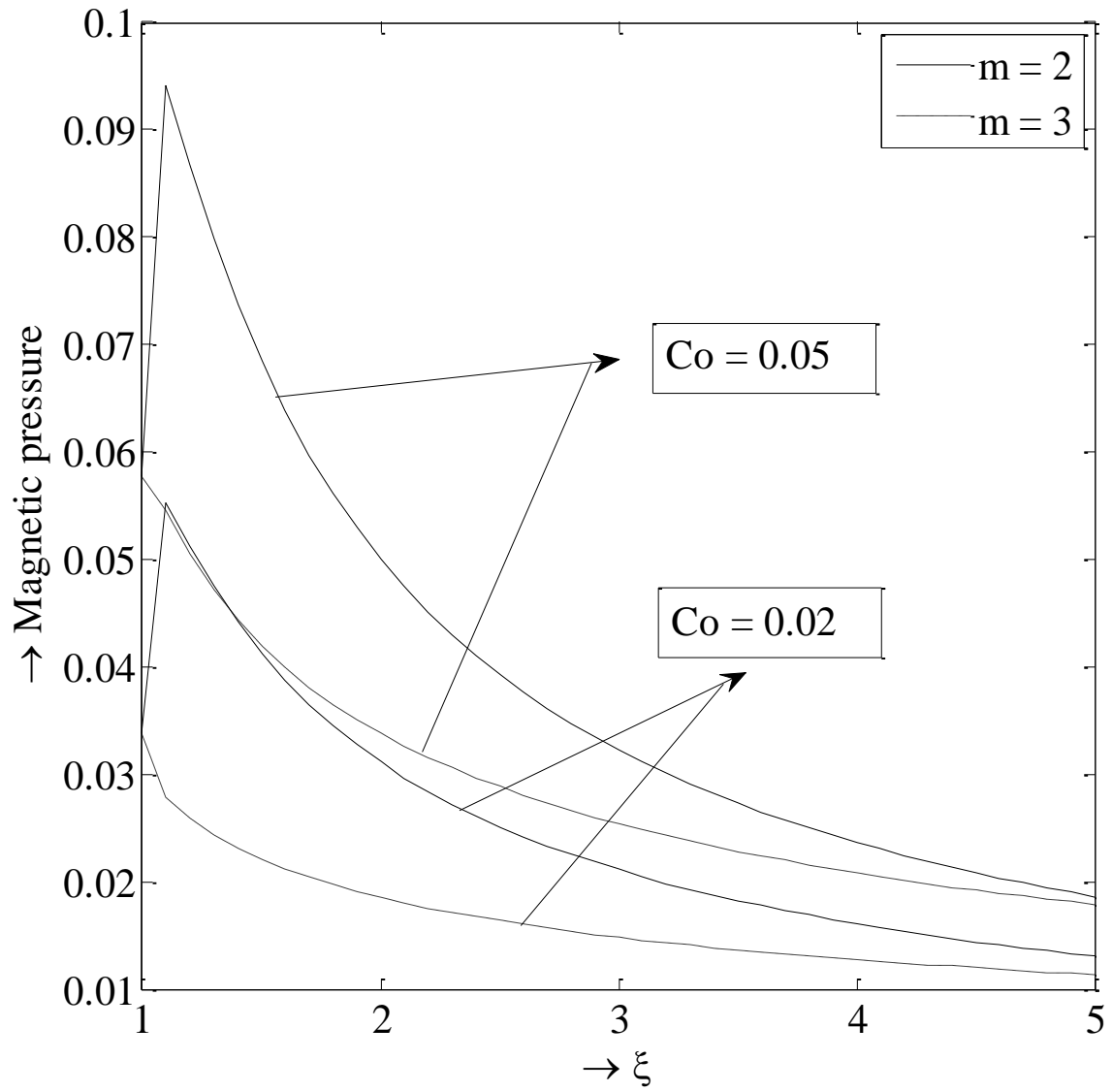


Figure 5.3(k). Magnetic pressure profiles of Royce EOS for $b = 1.2$, $\Gamma_0 = 2.25$, and different values of C_0

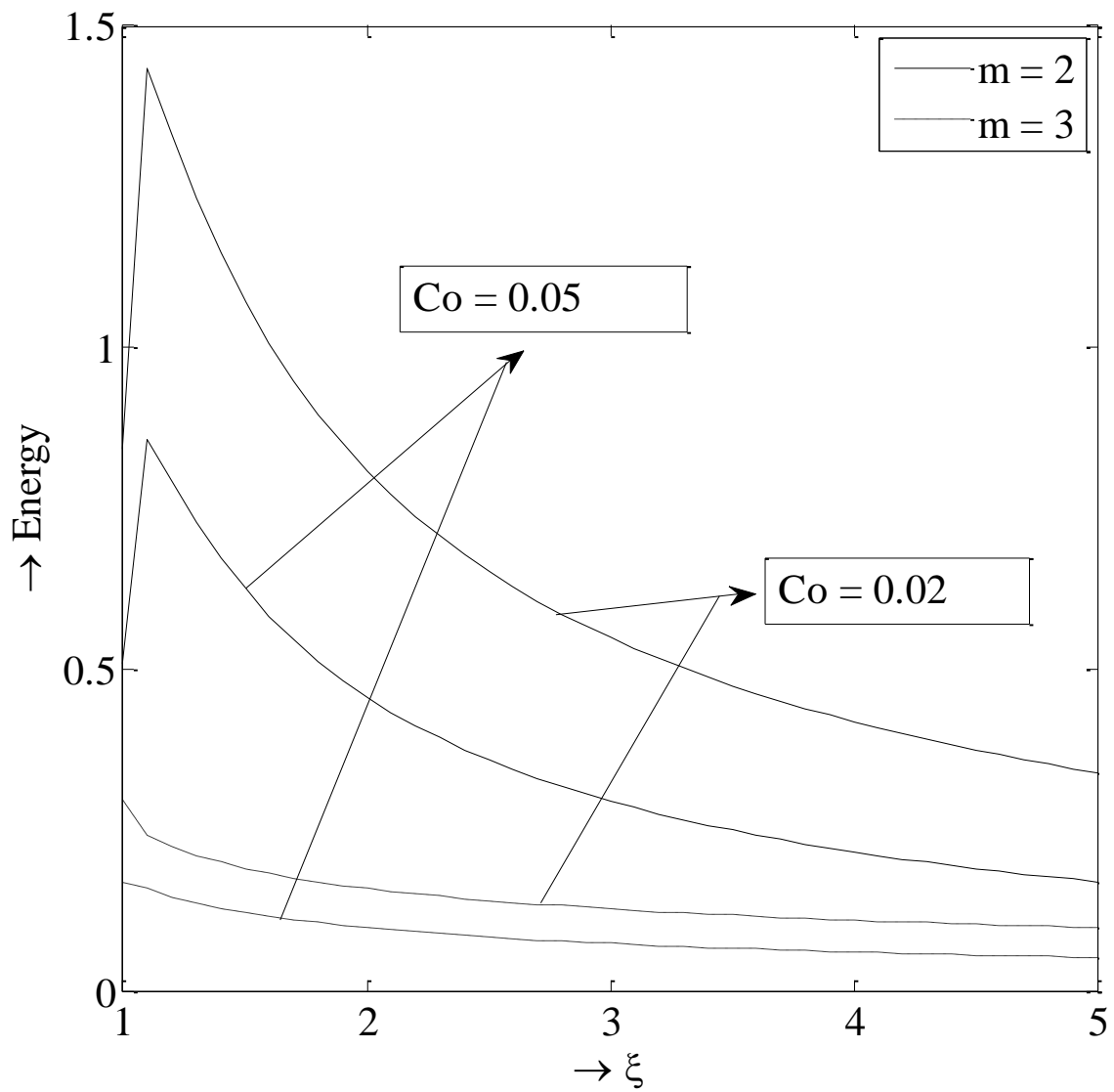


Figure 5.3(1). Energy profiles of Royce EOS for $b = 1.2$, $\Gamma_0 = 2.25$, and different values of C_0

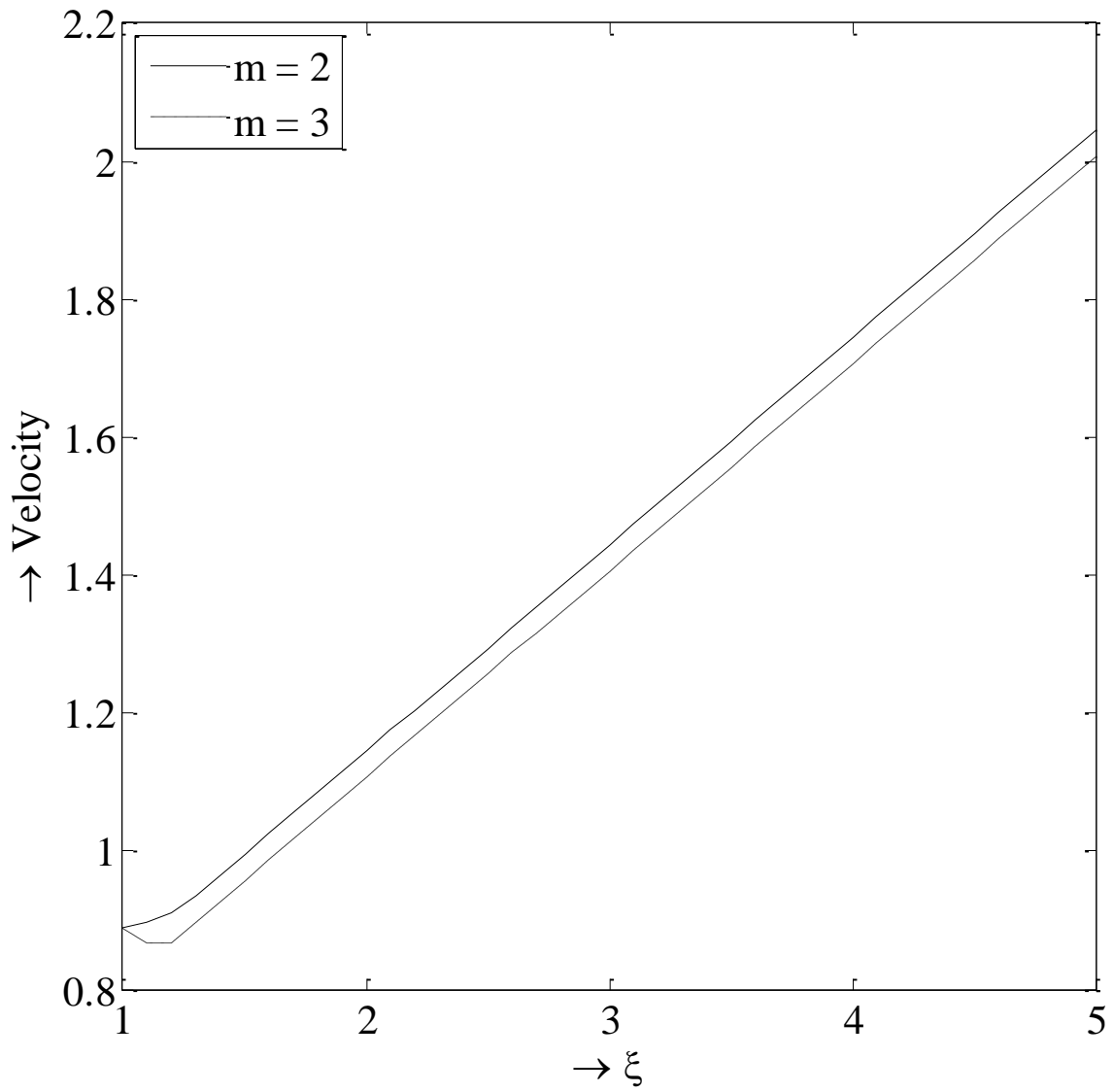


Figure 5.4(a). Velocity profiles of Mc Queen EOS for $\Gamma_0 = 2.25$, magnetic effect $C_0 = 0$, and $m = 2, 3$

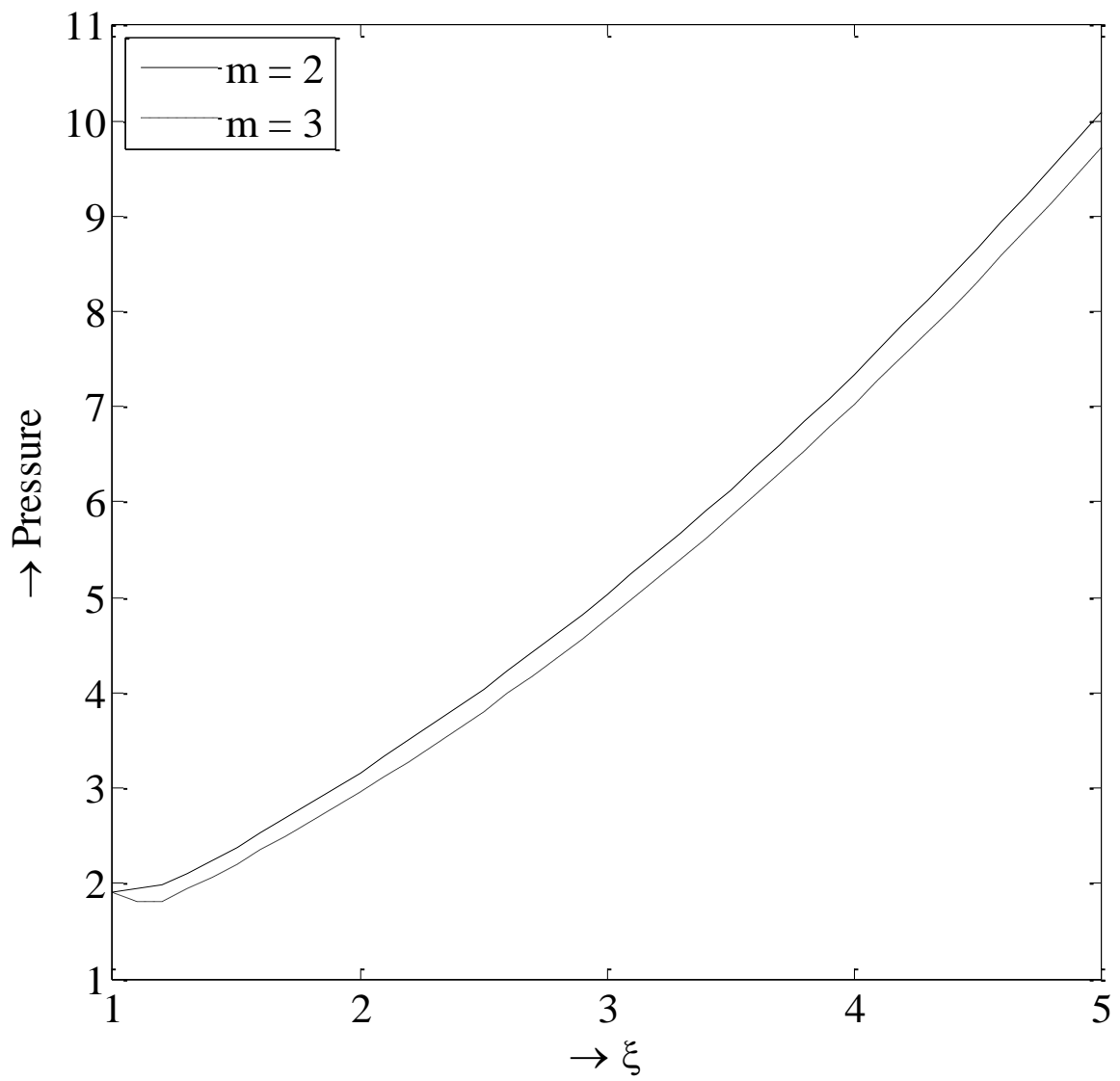


Figure 5.4(b). Pressure profiles of Mc Queen EOS for $\Gamma_0 = 2.25$, magnetic effect $C_0 = 0$, and $m = 2, 3$

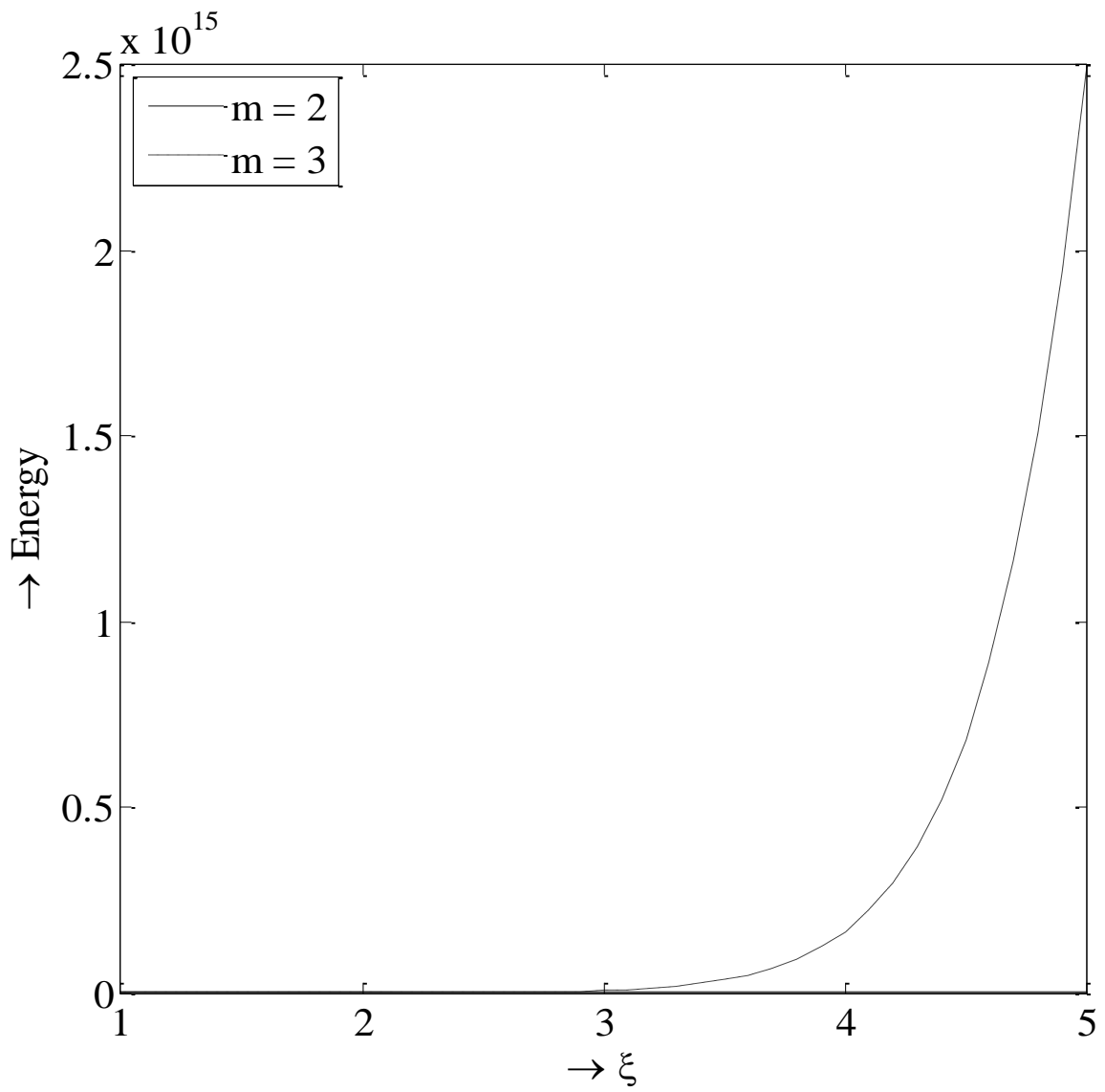


Figure 5.4(c). Energy profiles of Mc Queen EOS for $\Gamma_0 = 2.25$, magnetic effect $C_0 = 0$, and $m = 2, 3$

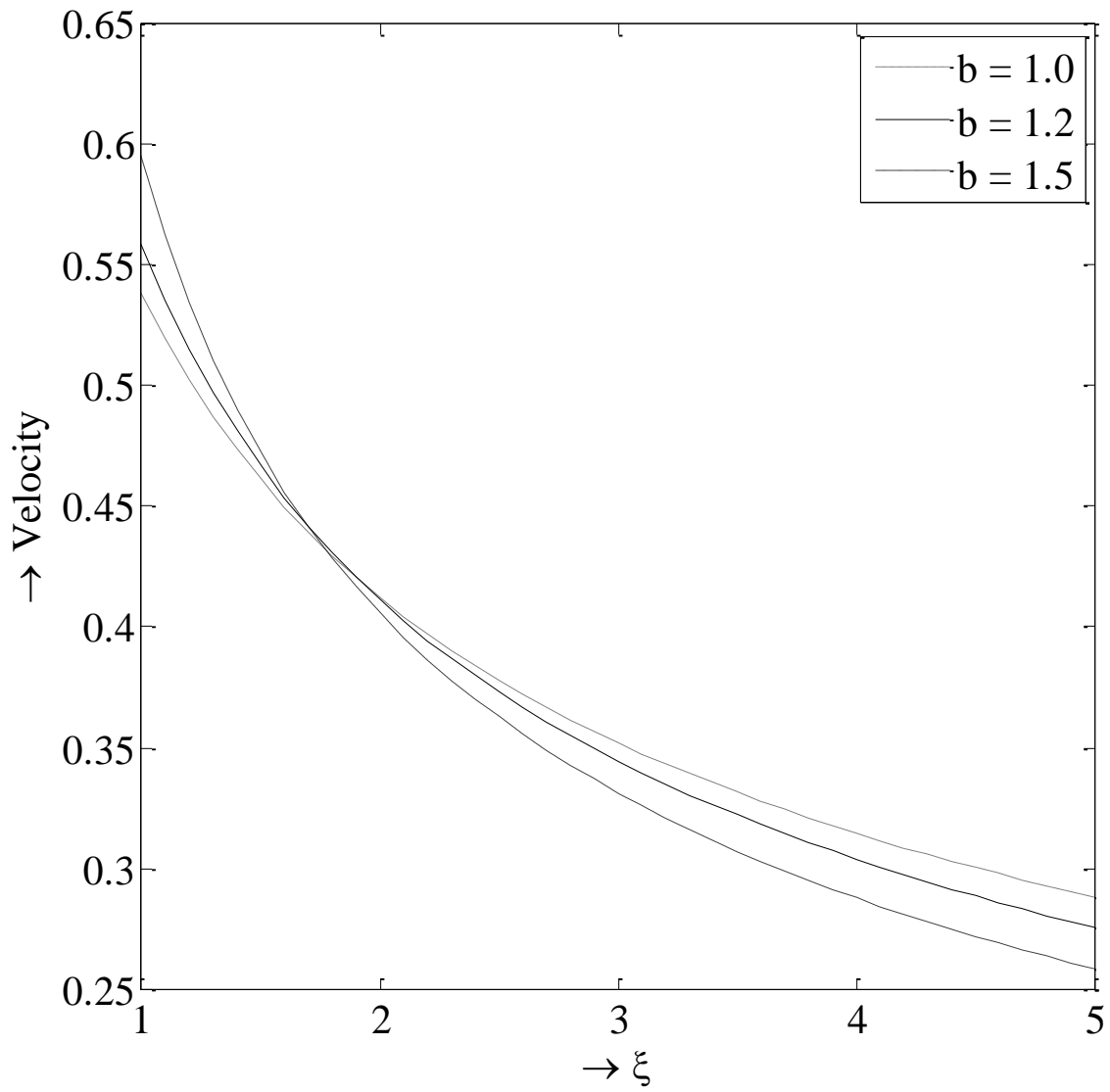


Figure 5.5(a). Velocity profiles of Royce EOS for $\Gamma_0 = 2.25$, magnetic effect $C_0 = 0$, $m = 2$, and different values of b

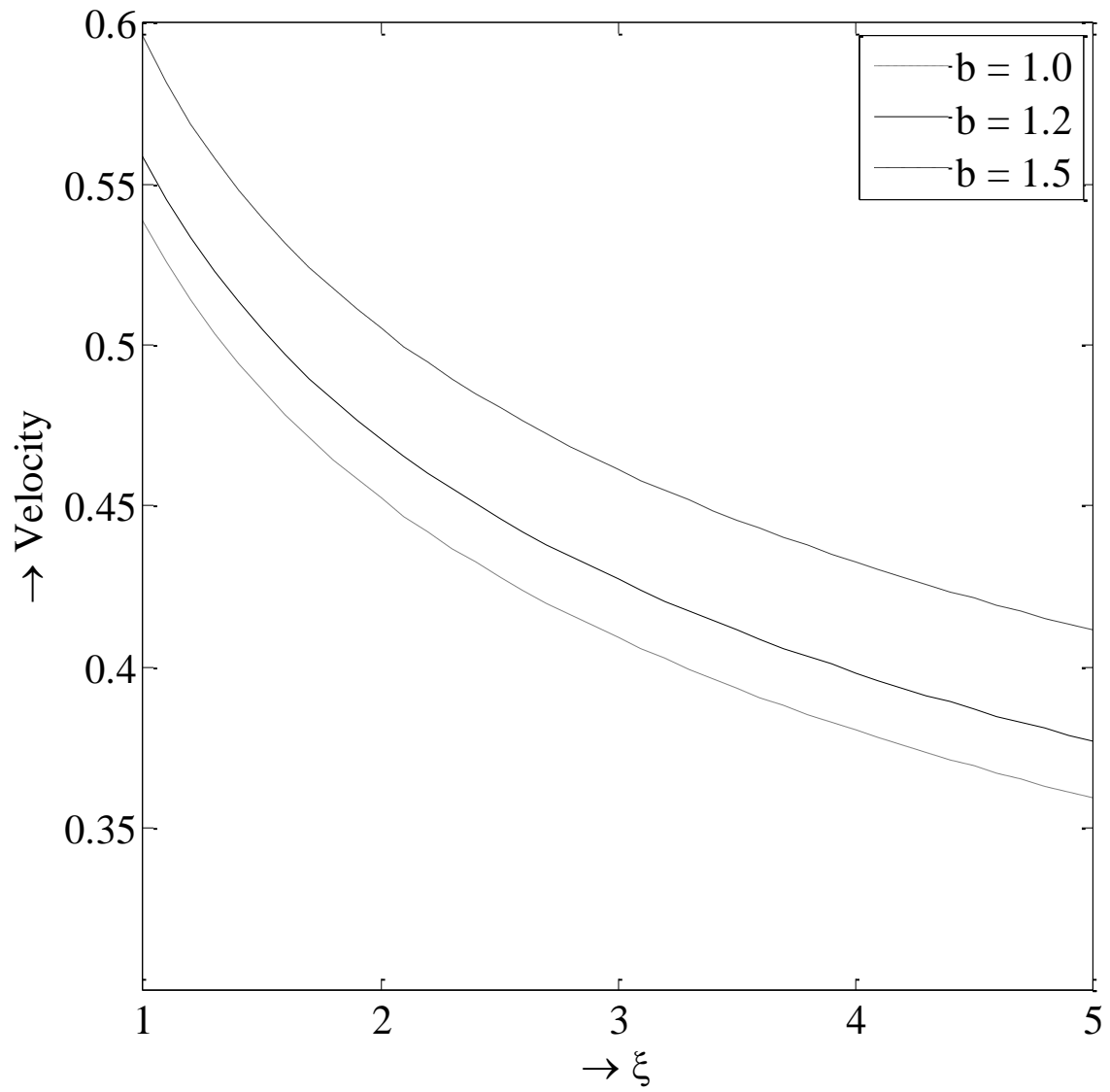


Figure 5.5(b). Velocity profiles of Royce EOS for $\Gamma_0 = 2.25$, magnetic effect $C_0 = 0$, $m = 3$, and different values of b

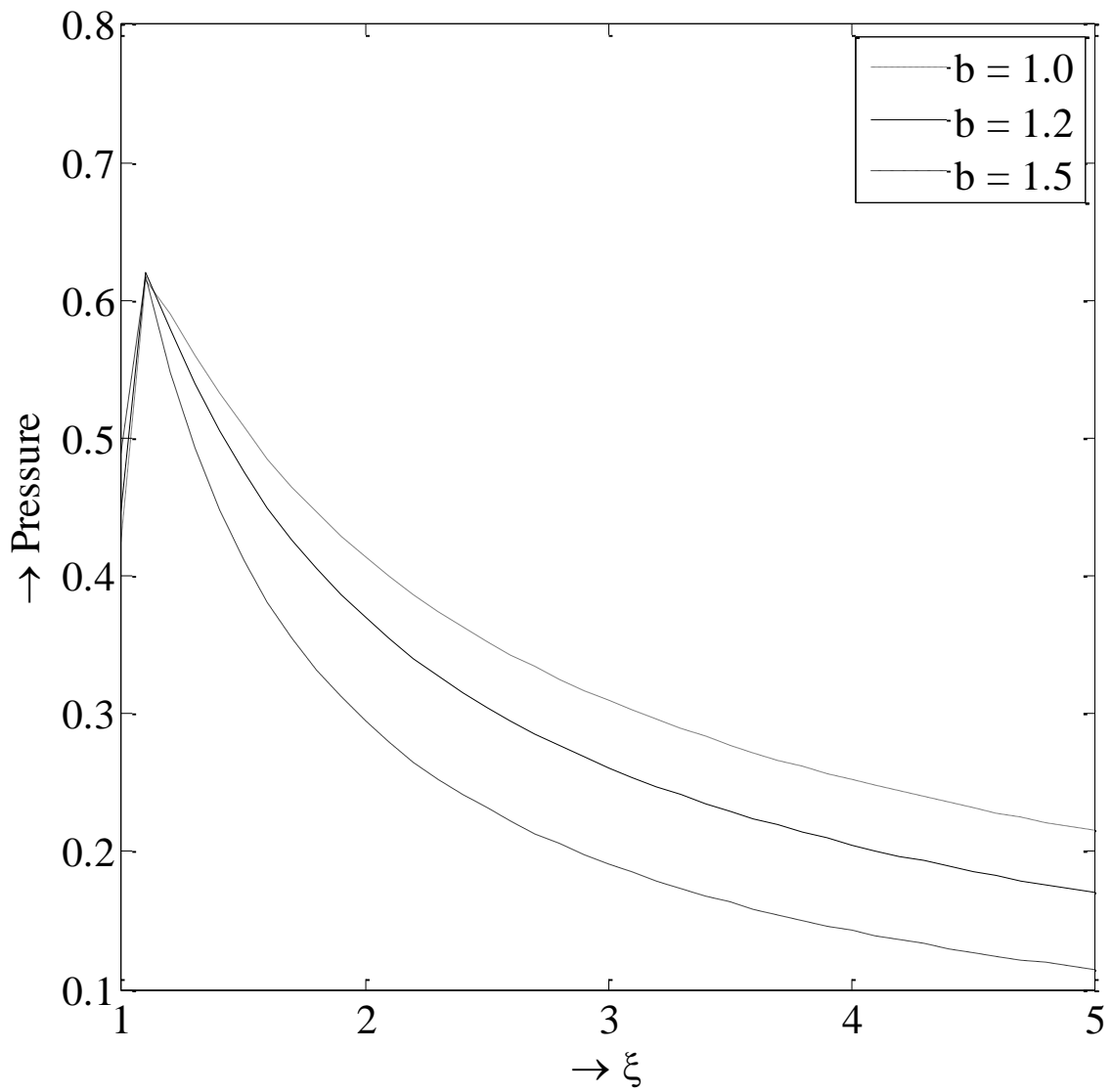


Figure 5.5(c). Pressure profiles of Royce EOS for $\Gamma_0 = 2.25$, magnetic effect $C_0 = 0$, $m = 2$, and different values of b

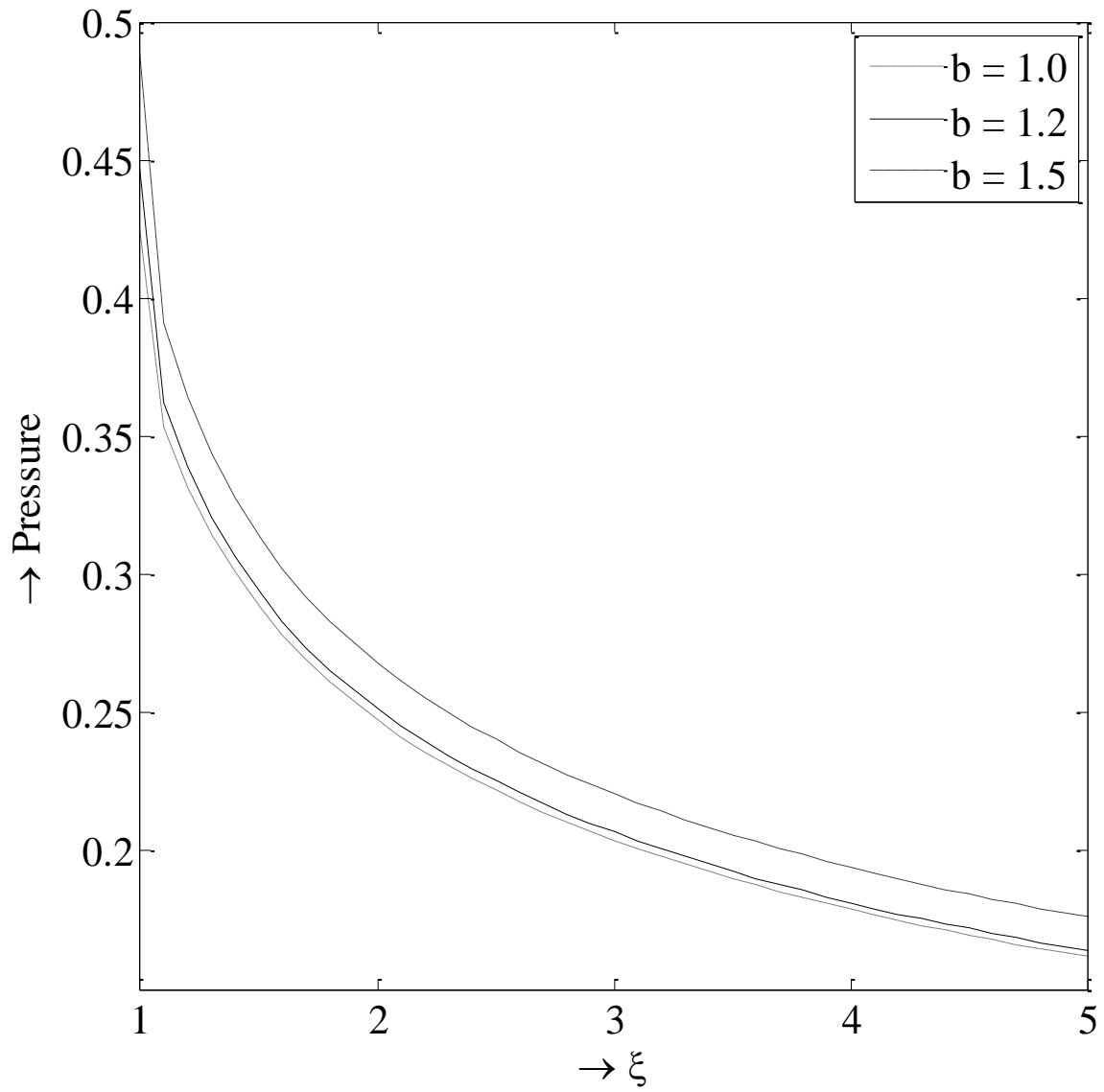


Figure 5.5(d). Pressure profiles of Royce EOS for $\Gamma_0 = 2.25$, magnetic effect $C_0 = 0$, $m = 3$, and different values of b

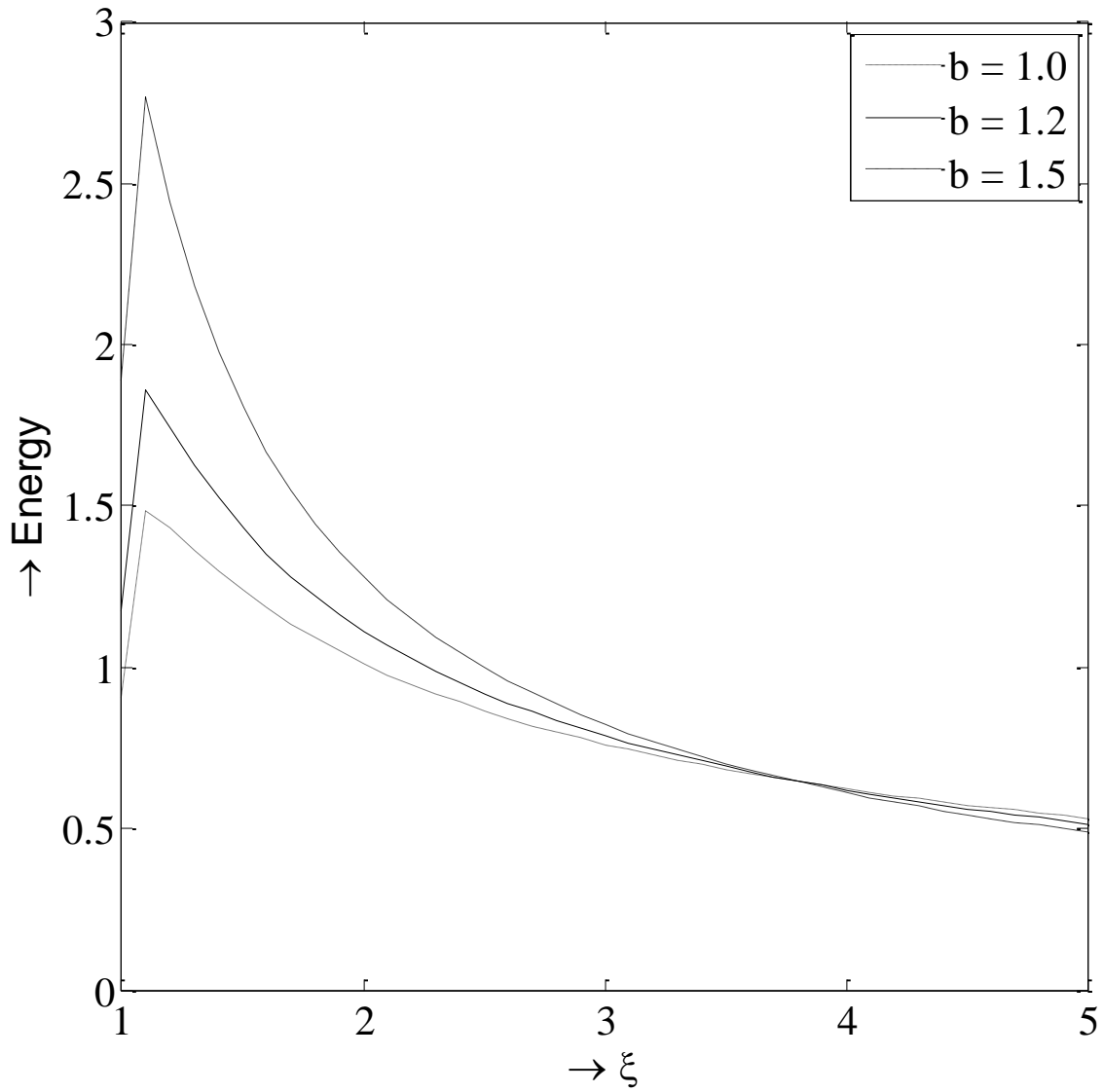


Figure 5.5(e). Energy profiles of Royce EOS for $\Gamma_0 = 2.25$, magnetic effect $C_0 = 0$, $m = 2$, and different values of b

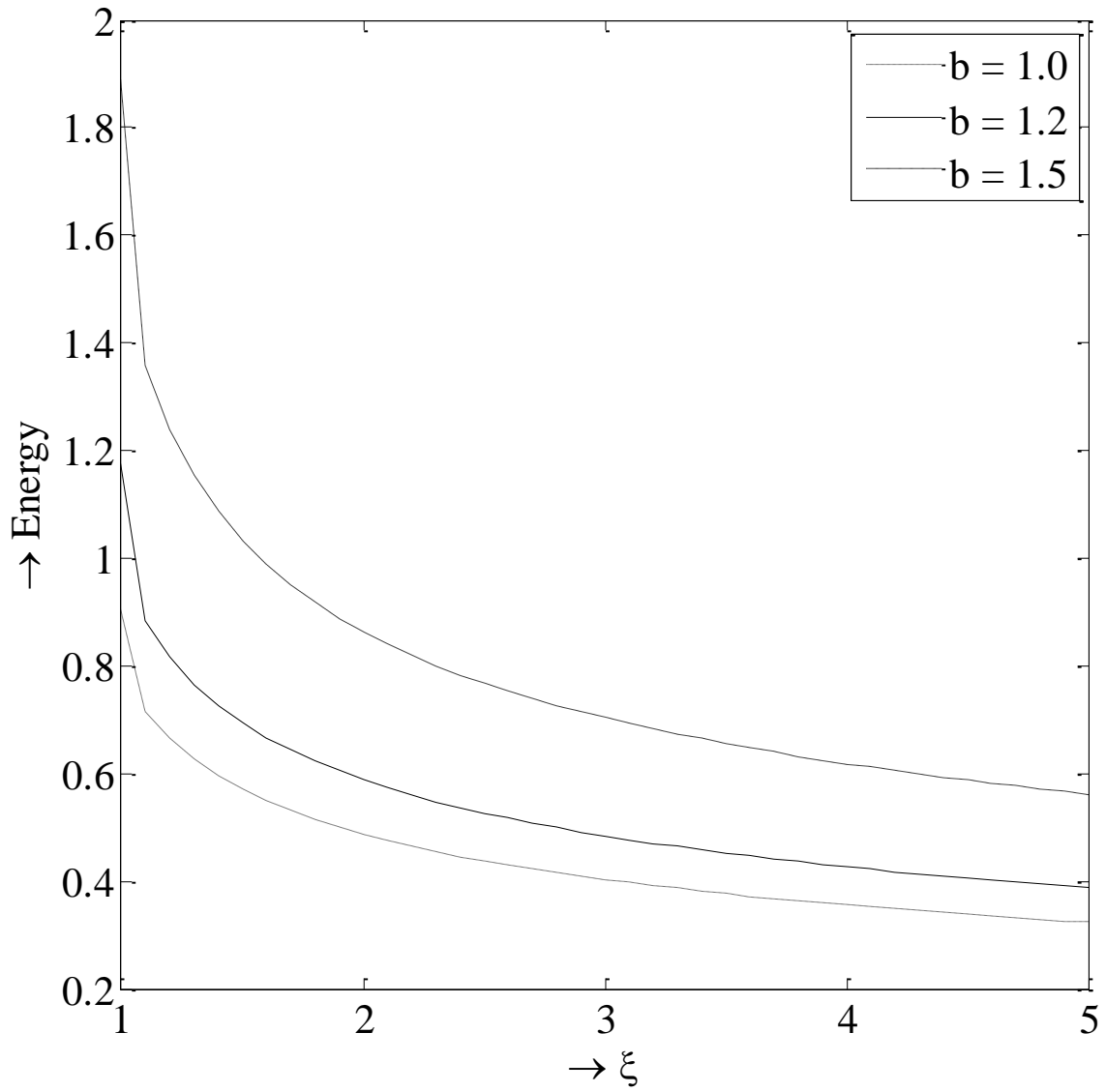


Figure 5.5(f). Energy profiles of Royce EOS for $\Gamma_0 = 2.25$, magnetic effect $C_0 = 0$, $m = 3$, and different values of b

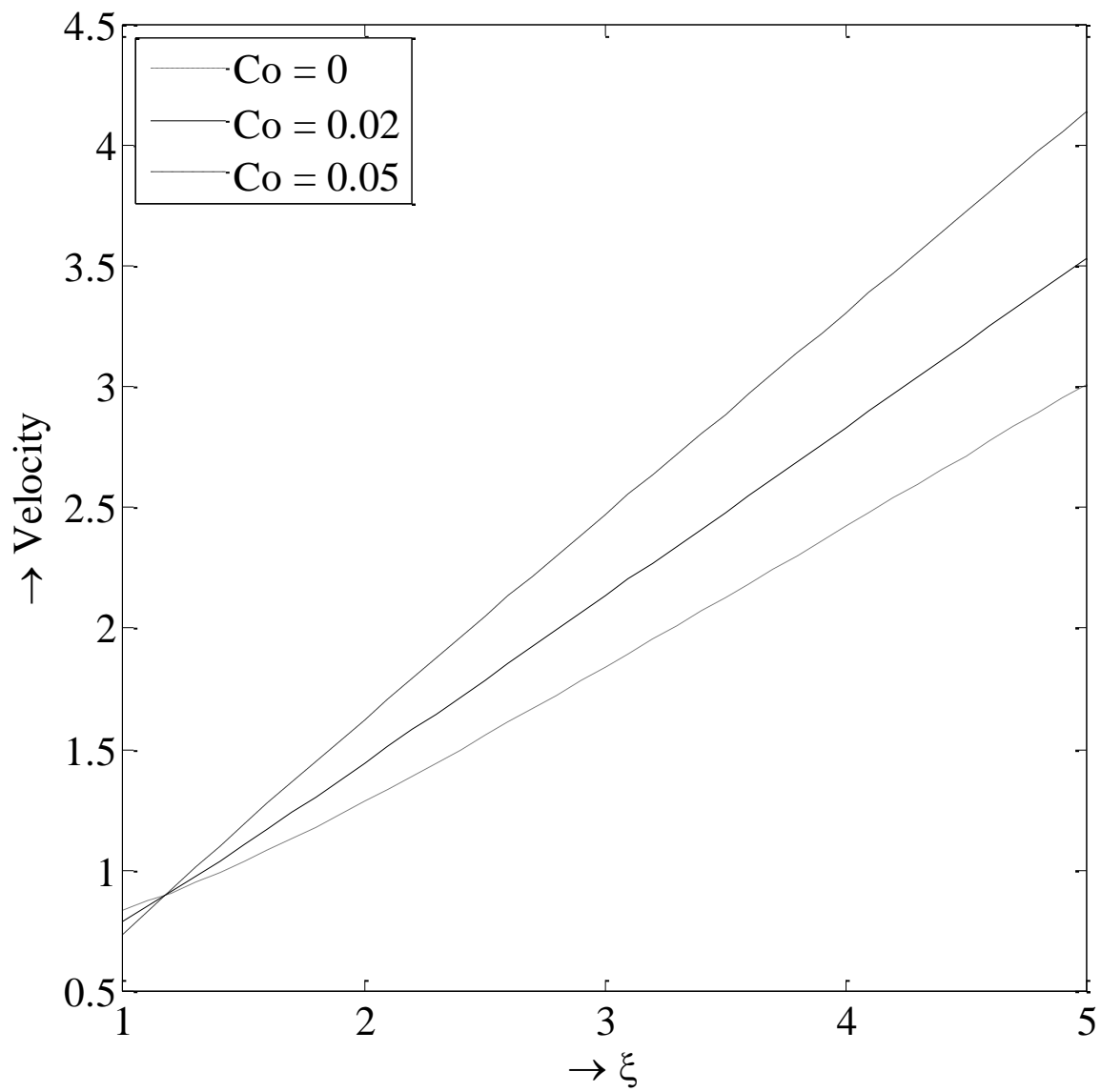


Figure 5.6(a). Velocity profiles of perfect gas EOS for $\gamma = 1.4$, $m = 2$, and different values of C_0

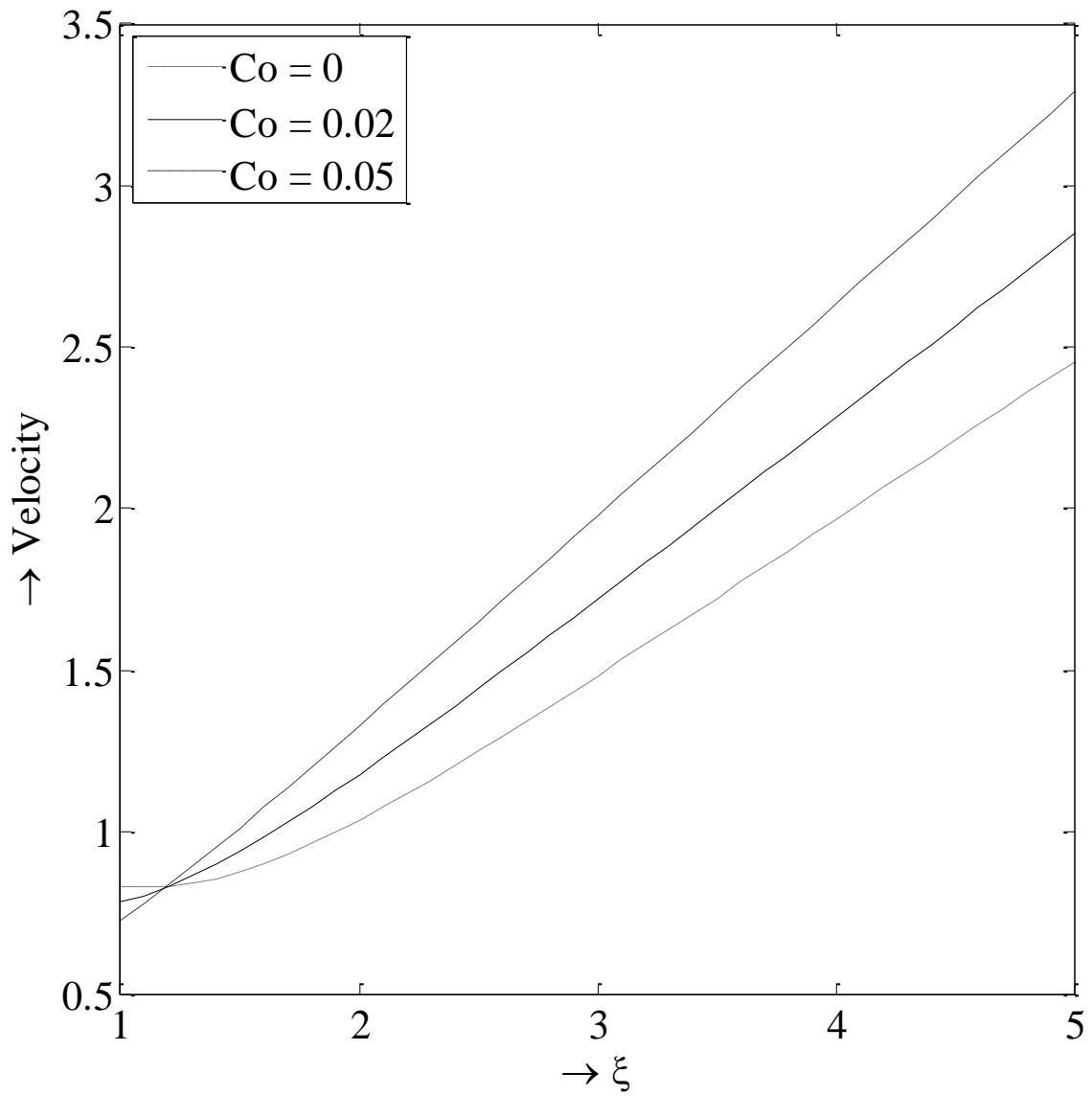


Figure 5.6(b). Velocity profiles of perfect gas EOS for $\gamma = 1.4$, $m = 3$, and different values of C_0

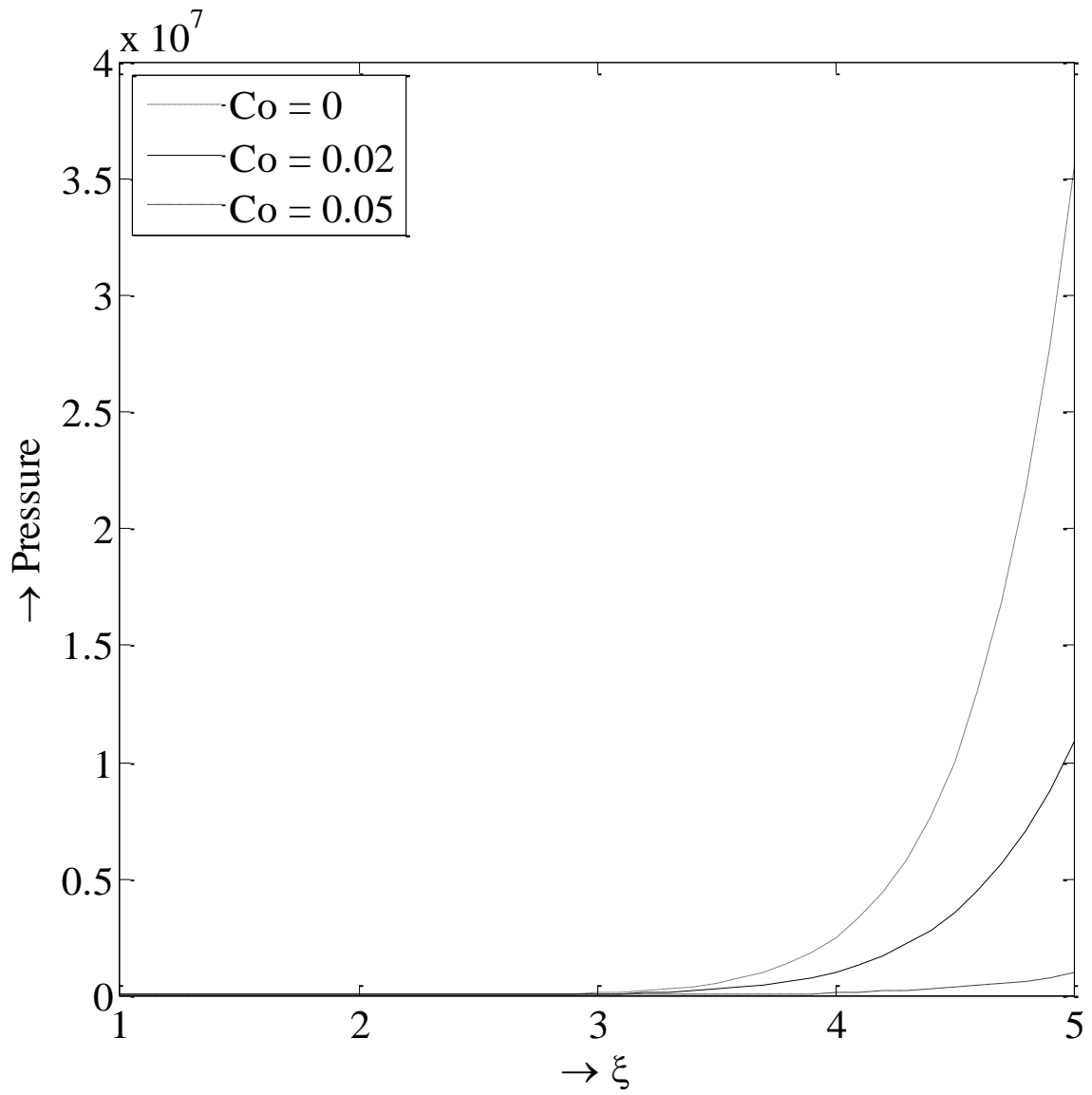


Figure 5.6(c). Pressure profiles of perfect gas EOS for $\gamma = 1.4$, $m = 2$, and different values of C_0

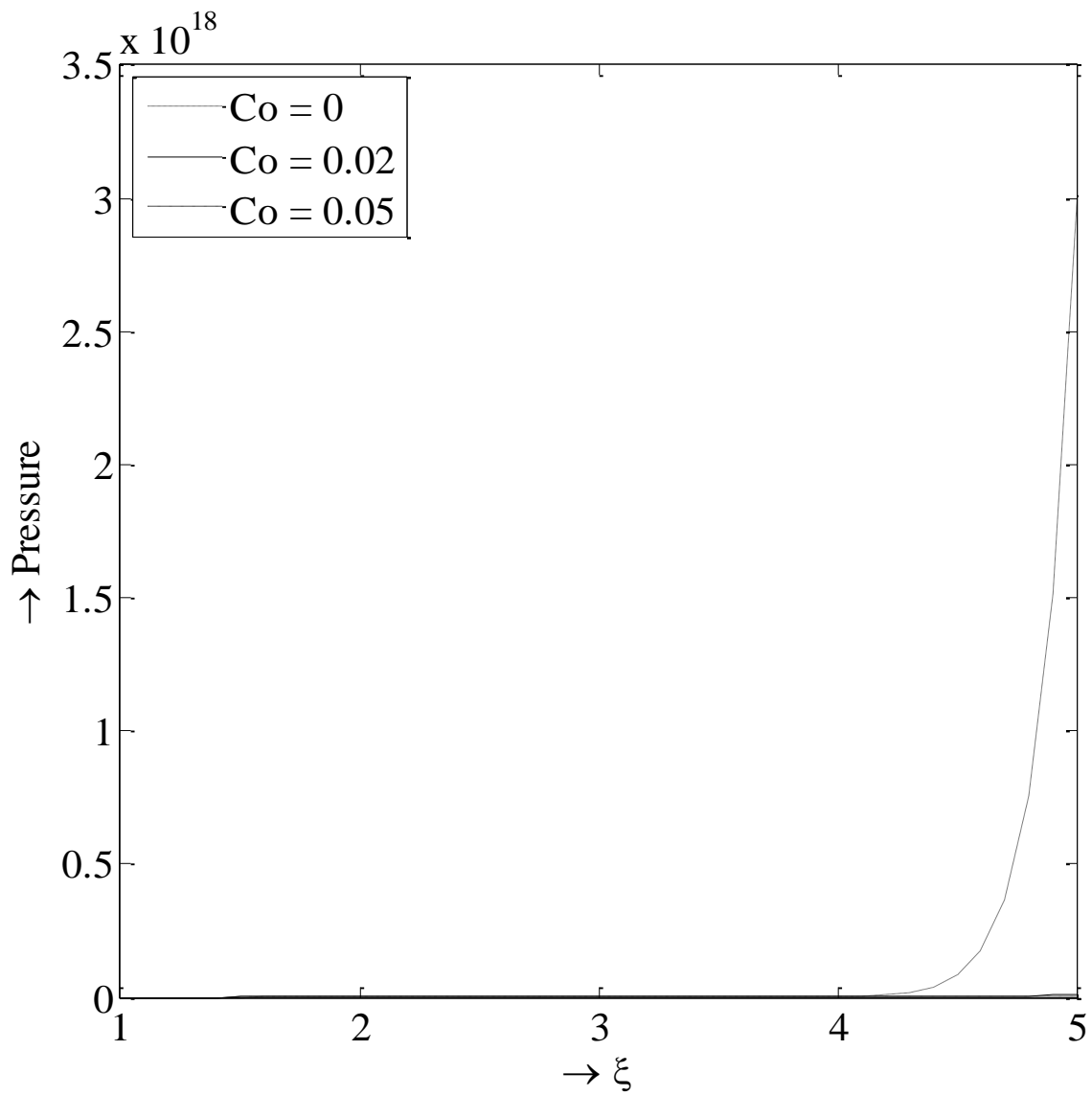


Figure 5.6(d). Pressure profiles of perfect gas EOS for $\gamma = 1.4$, $m = 3$, and different values of C_0

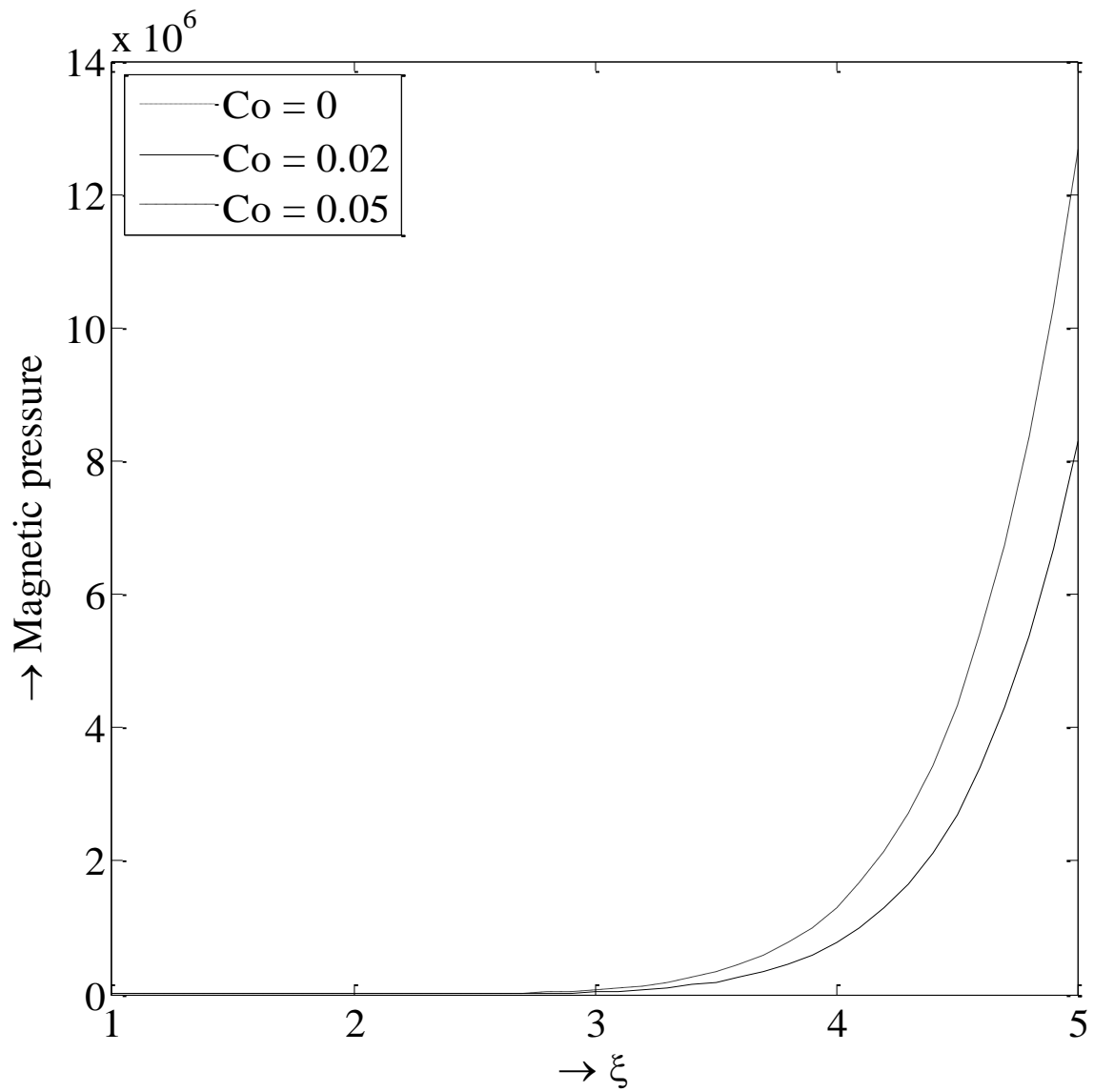


Figure 5.6(e). Magnetic pressure profiles of perfect gas EOS for $\gamma = 1.4$, $m = 2$, and different values of C_0

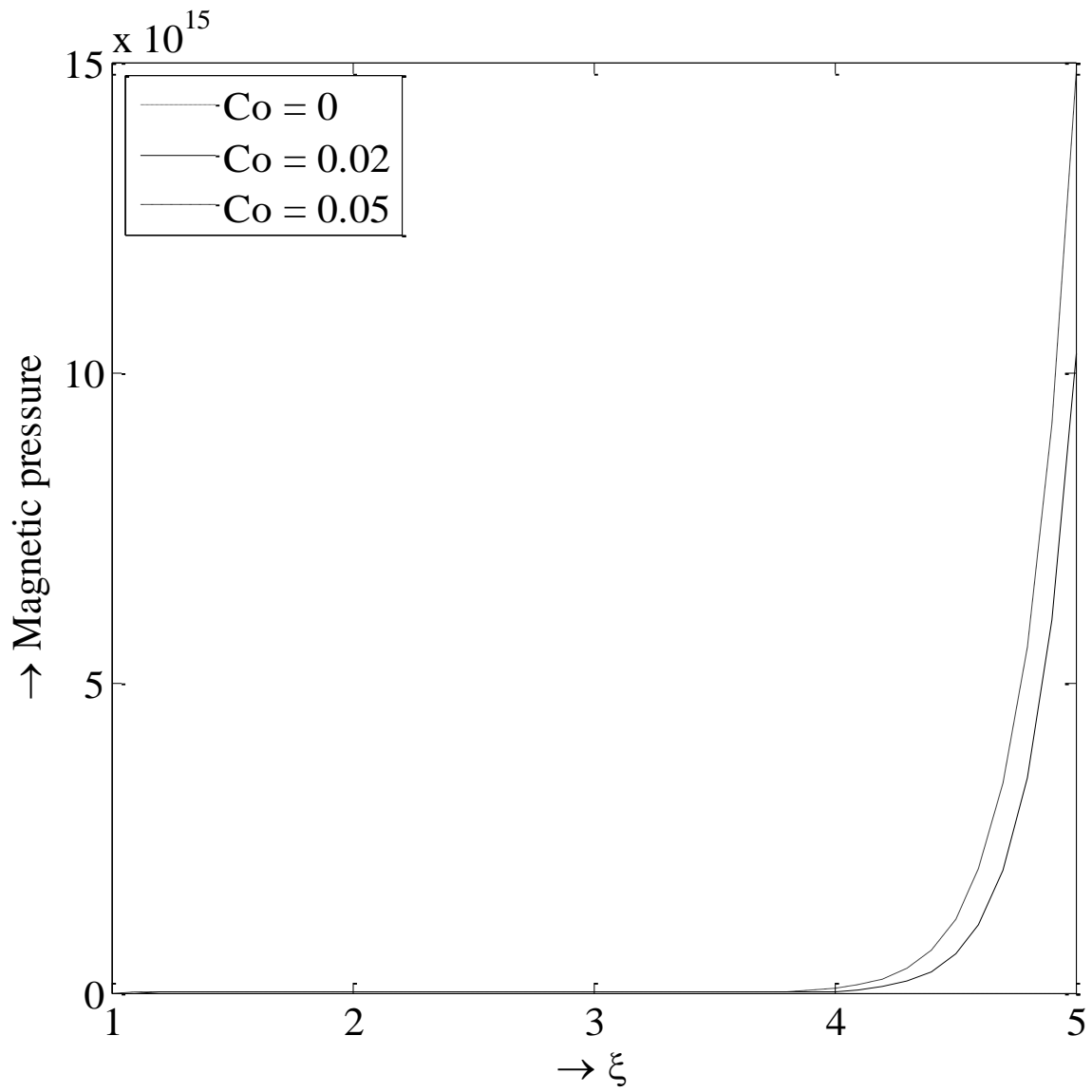


Figure 5.6(f). Magnetic pressure profiles of perfect gas EOS for $\gamma = 1.4$, $m = 3$, and different values of C_0

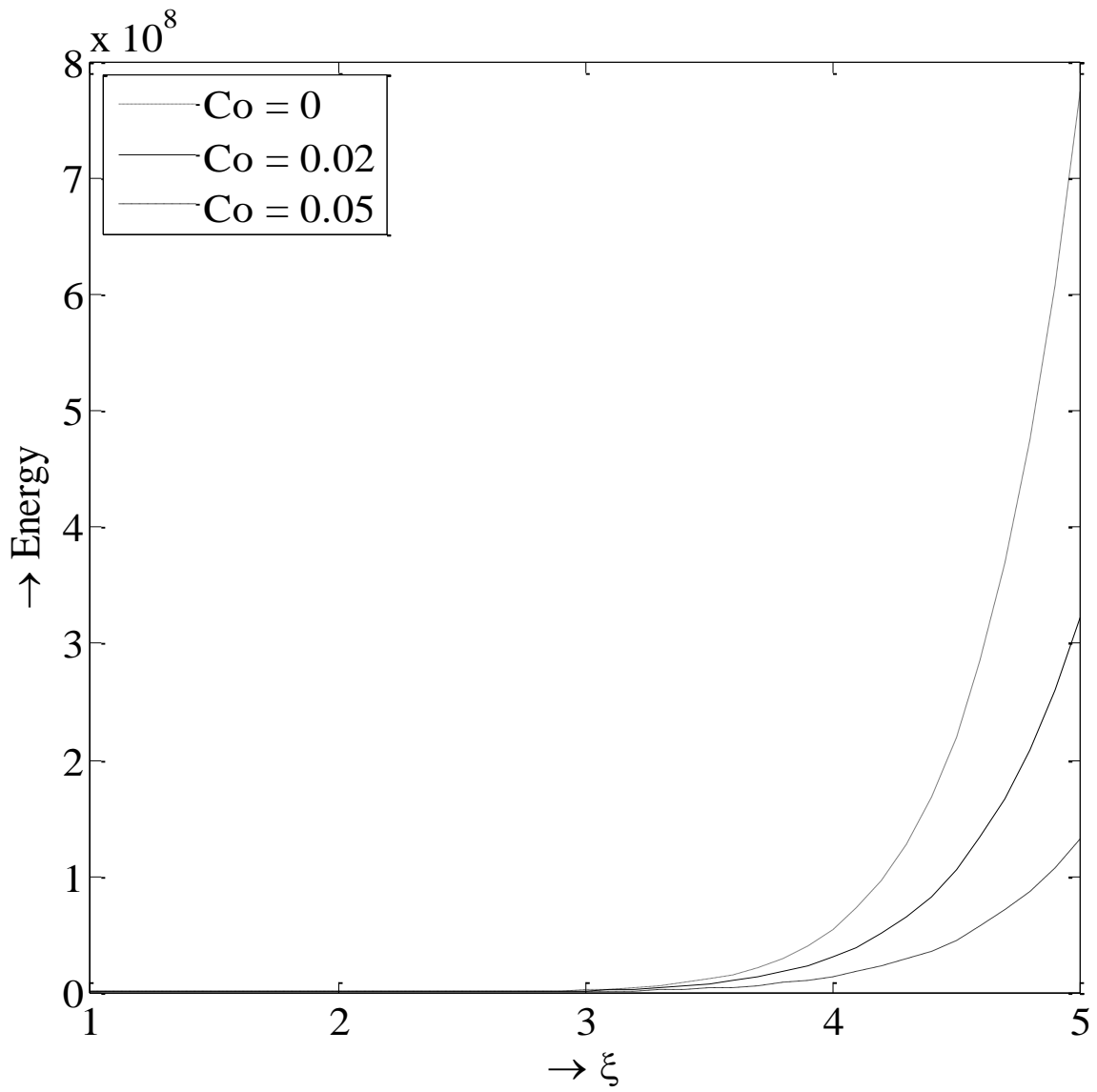


Figure 5.6(g). Energy profiles of perfect gas EOS for $\gamma = 1.4$, $m = 2$, and different values of C_0

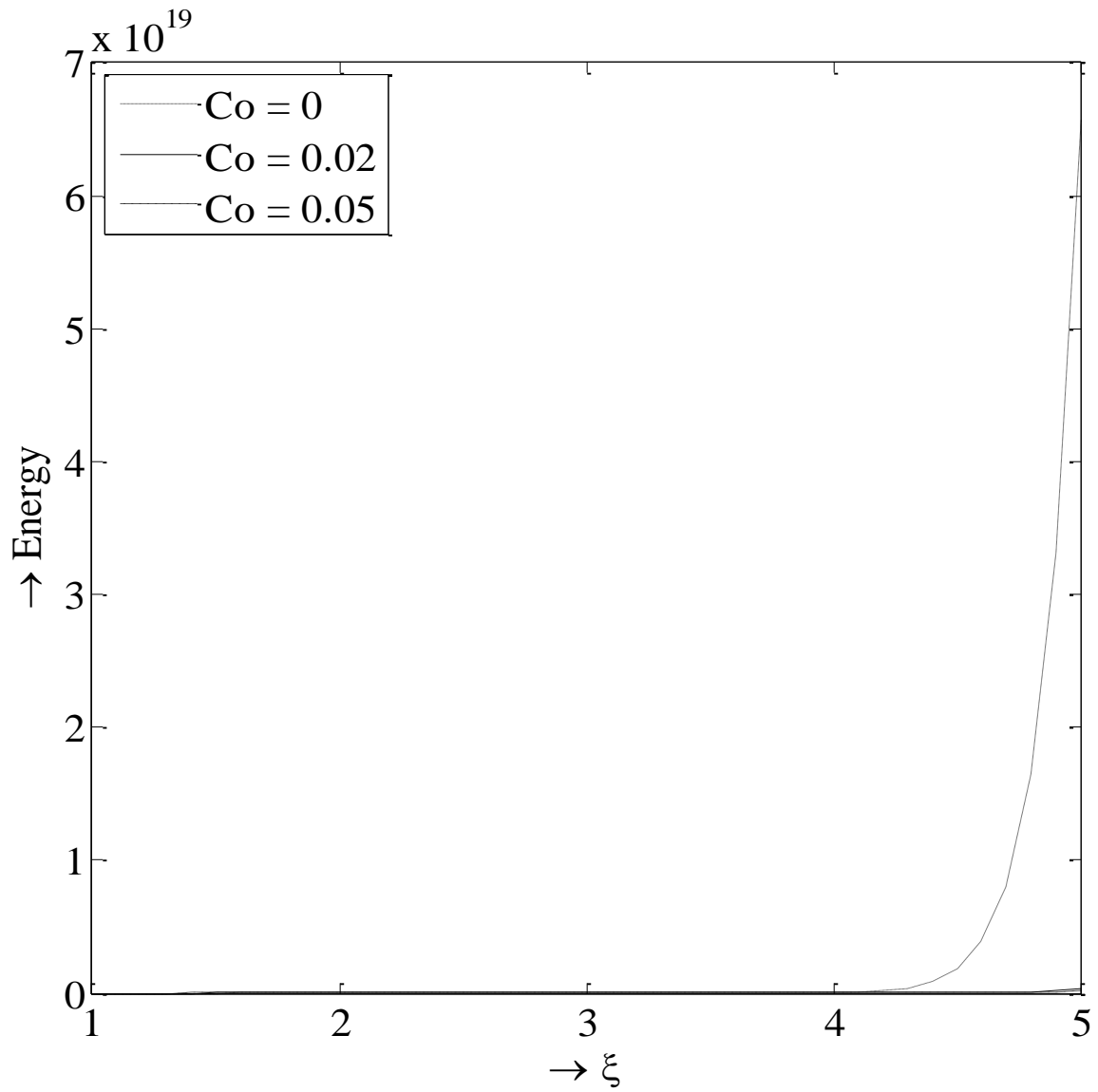


Figure 5.6(h). Energy profiles of perfect gas EOS for $\gamma = 1.4$, $m = 3$, and different values of C_0

Chapter-6

Similarity Solution of Spherical Shock Waves - Effect of Viscosity

6.1 Introduction

Shock waves are very common phenomenon in the supersonic flow of any fluid. Shock process occurs naturally that are related to hydrodynamics, aerodynamics, astrophysics, nuclear engineering and space science. Shock waves are mathematically treated as discontinuities, further shock wave is not a true physical discontinuity, but a very narrow transition zone whose thickness is of the order of a few molecular mean-free paths. In a shocked medium, particles behind the shock front experience compressive as well as shear forces thus the particles move away from their equilibrium position. The similarity solutions of converging spherical and cylindrical shock wave problems with different equation of states (EOS) were investigated by several authors [1, 24, 33, 50, 54, 57, 70, 84, 97]. The existence and effects of the viscous forces for the similarity solutions to shock wave problems were studied by several researchers [101-104]. Zeldovich and Raizer [7] and Landau and Lifshitz [91] have studied the entropy production in a viscous medium and developed an analytical model for the shock process based on Hugoniot curves considering the effects of viscosity and heat conduction.

The role of viscosity in physics and mathematical investigation of model problems suggest that the presence of viscosity implies the existence of a continuous, differentiable solution. This mathematical theory does not guarantee this in general. The actual formulation of artificial viscosity introduced by Von Neumann and Richtmyer [40] involved adding a viscosity term to the momentum equation, that augments the pressure in the instance there is shock compression and is independent of shock strength. The new system will satisfy the Rankine-Hugoniot jump conditions [41] in the shock region and has little effect outside the shock layer. The resistance to variations in distribution of cohesive forces in fluids experienced result in removing the inhomogeneities in velocities. These types of resistances result in the phenomenon of viscosity in fluid motions [42]. This viscosity effect was found to be one of the most important effects in the equations of motion. The shock heating of solar corona discussed by Orta et al. [43] have shown that the shock thickness and profile depend on viscosity and resistivity and as a consequence heating ultimately occurs. Ballai et al. [44] in the study of dispersive shock waves concluded that the effect of dispersion will alter the amplitude and propagation speed of a shock wave and also discussed in detail the viscosity effect. The supersonic flows exhibit an important property i.e., the coexistence of shock waves with viscous effects for many fluid dynamic systems [45]. In the supersonic regime of compressible gas flow the interaction of shock waves with viscosity is a very important problem. Mathematically this can be approximated to a hydrodynamic case.

Several astrophysical and geophysical phenomena occur due to the Magnetohydrodynamic (MHD) shockwaves. Some of the applications by the application of external magnetic field are drag reduction in duct flows, design of coolant blankets for fusion reactors, control of turbulence of immersed jets during continuous casting of steel, advanced flow control schemes for hypersonic vehicles and missiles.

The main purpose of this work in this chapter is to describe complete mechanism of shock wave problem, which include viscous terms and study the dissipation effects on the propagation of shock waves including viscosity under the effect of magnetic field. Also to study and confirm the effect of (i) the non-idealness parameter and the viscosity parameters on the shock strength and the flow variables respectively, (ii) effect of discontinuities of the physical parameters due to viscosity and (iii) complete flow field depending on the magnitude of the viscosity. To define this type of shock process spherically symmetric conservation equations are considered. The viscosity term (suggested by Von Neumann and Richtmyer [40]) is included into the hydrodynamic equations for spherically symmetric flow (Figure 6.1). The main advantage of artificial viscosity approach is its simplicity thereby high computational efficiency and oscillations in the flow profiles dampen and the smoothness in the profiles increases.

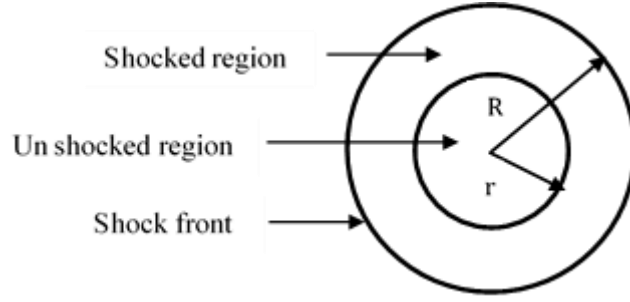


Figure 6.1. Schematic diagram of spherical shock wave propagation

6.2 Formulation of the Problem

The viscosity term (suggested by Von Neumann and Richtmyer [40]) is included into the hydrodynamic equations for spherically symmetric flow in magnetogasdynamics regime, can be written in Eulerian form as [7, 40, 76, 81, 91, 92]

$$\frac{\partial \rho}{\partial t} + u \frac{\partial \rho}{\partial r} + \rho \frac{\partial u}{\partial r} + \frac{2\rho u}{r} = 0 \quad (6.1)$$

$$\frac{\partial u}{\partial t} + u \frac{\partial u}{\partial r} + \frac{1}{\rho} \left(\frac{\partial p}{\partial r} + \frac{\partial q}{\partial r} + \frac{\partial h}{\partial r} \right) = 0 \quad (6.2)$$

$$\frac{\partial e}{\partial t} + u \frac{\partial e}{\partial r} - \frac{1}{\rho^2} (p + q) \left(\frac{\partial \rho}{\partial t} + u \frac{\partial \rho}{\partial r} \right) = 0 \quad (6.3)$$

$$\frac{\partial h}{\partial t} + u \frac{\partial h}{\partial r} + 2h \frac{\partial u}{\partial r} + \frac{4hu}{r} = 0 \quad (6.4)$$

where r and t are independent space and time coordinates ρ , u , p , q and e are density, velocity, pressure, artificial viscosity, and internal energy per unit mass respectively and $h = \frac{\mu H^2}{2}$ is the magnetic pressure, H and μ being magnetic field strength and the magnetic permeability respectively. The shock position is given

by $R_s(t)$ and its velocity is $D = \frac{dR_s(t)}{dt}$. Originally, Von Neumann and Richtmyer

[40] proposed the following expression for the viscosity term:

$$\left. \begin{aligned} q &= -\rho K^2 (\Delta x)^2 \left(\frac{\partial u}{\partial x} \right)^2, \quad \text{if } \frac{\partial u}{\partial x} < 0 \text{ or } \frac{\partial \rho}{\partial t} > 0 \\ q &= 0, \quad \text{otherwise} \end{aligned} \right\} \quad (6.5)$$

Here, u is the fluid velocity, ρ is the density, Δx is spacial interval and K is a constant parameter whose value is conveniently adjusted in every numerical experiment. This parameter K controls the number of zones in which the shock waves are spread. The form of q adopted for the present problem is consistent with Richard Latter [103] requirements and is

$$q = \frac{1}{2} K^2 \rho r^2 \frac{\partial u}{\partial r} \left(\left| \frac{\partial u}{\partial r} \right| - \frac{\partial u}{\partial r} \right) \quad (6.6)$$

The expression for q denotes a non-linear dissipative mechanism, which is effective in the shock layer and negligible elsewhere.

6.2.1 Boundary conditions

The boundary conditions at shock front due to the Rankine-Hugoniot jump relations, under the strong shock limit can be written into the following form [6, 7]

$$\left. \begin{aligned} \rho_1 &= \rho_0 \beta, \quad u_1 = \left(1 - \frac{1}{\beta} \right) D, \\ p_1 &= \left(1 - \frac{1}{\beta} - \frac{c_0 \beta^2}{2} \right) \rho_0 D^2, \quad h_1 = \frac{c_0 \beta^2}{2} \rho_0 D^2 \end{aligned} \right\} \quad (6.7)$$

The equation of state (EOS) is of Mie-Gruneisen type [57] of following form

$$p = [\Gamma(\rho/\rho_0) - 1]\rho e - \Pi(\rho/\rho_0) \quad (6.8)$$

where Γ and Π are functions to be determined according to the EOS under consideration and each Γ and Π gives a different EOS.

Using the strong shock relations (6.7) in equation (6.8), we get

$$2 - \frac{c_0\beta^3}{(\beta-1)} + \frac{2\beta}{(\beta-1)}\Pi(\beta) = (\beta - 1)(\Gamma(\beta) - 1) \quad (6.9)$$

where β is the measure of shock strength.

6.2.2 Transformation of basic equations

We consider a set of suitable similarity transformations

$$\left. \begin{aligned} \rho &= \rho_0\psi(\xi), \quad u = D\phi(\xi), \quad p = \rho_0D^2f(\xi), \\ h &= \rho_0D^2l(\xi), \quad q = \rho_0D^2g(\xi) \end{aligned} \right\} \quad (6.10)$$

where $\xi = \frac{r}{R}$, ξ is the similarity variable and $R = A(t)^\alpha$ (shock propagation follows a power law), ψ , ϕ , f , l and g are dimensionless density, velocity, pressure, magnetic pressure and viscosity term (which are functions of ξ) respectively. In general these terms are termed as reduced functions. Along with the reduced functions we consider a similar set of transformations for convenience such as,

$$\left. \begin{aligned} \psi(\xi) &= \Psi(\xi), \quad \phi(\xi) = \frac{\xi}{\alpha} \Phi(\xi), \quad f(\xi) = \frac{\xi^2}{\alpha^2} F(\xi), \\ l(\xi) &= \frac{\xi^2}{\alpha^2} L(\xi), \quad g(\xi) = \frac{\xi^2}{\alpha^2} G(\xi) \end{aligned} \right\} \quad (6.11)$$

where Ψ , Φ , F , L and G are new unknown reduced functions for the reduced density, velocity, pressure, magnetic pressure and viscosity term functions respectively. Using the transformations (6.10) and (6.11), the equations (6.1-6.4, 6.6) can be written in the following non-dimensional form:

$$(\Phi - \alpha) \frac{d \ln \Psi}{d \ln \xi} + \frac{d \Phi}{d \ln \xi} + 3\Phi = 0 \quad (6.12)$$

$$\frac{1}{\Psi} \frac{dF}{d \ln \xi} + (\Phi - \alpha) \frac{d\Phi}{d \ln \xi} + \frac{1}{\Psi} \frac{dG}{d \ln \xi} + \frac{1}{\Psi} \frac{dL}{d \ln \xi} + \frac{2}{\Psi} (F + G + L) + \Phi(\Phi - 1) = 0 \quad (6.13)$$

$$\frac{dF}{d \ln \xi} + Y(\Psi, F, G) \frac{d \ln \Psi}{d \ln \xi} + 2F \left[1 + \frac{(\alpha - 1)}{(\Phi - \alpha)} \right] = 0 \quad (6.14)$$

$$(\Phi - \alpha) \frac{dL}{d \ln \xi} + 2L \frac{d\Phi}{d \ln \xi} + 2L[4\Phi - 1] = 0 \quad (6.15)$$

$$G = \frac{K^2}{2} \Psi (\xi \Phi)' [|(\xi \Phi)'| - (\xi \Phi)'] \quad (6.16)$$

where prime (') denotes differentiation with respect to ξ and

$$Y(\Psi, F, G) = \frac{\alpha^2}{\xi^2} \left[\Pi' \Psi - \Pi \left(\frac{\Gamma' \Psi}{(\Gamma - 1)} + 1 \right) \right] - F \left(\frac{\Gamma' \Psi}{(\Gamma - 1)} + \Gamma \right) - (\Gamma - 1)G \quad (6.17)$$

and the transformed boundary conditions are

$$\left. \begin{aligned} \Psi(1) &= \beta, \quad \Phi(1) = \left(1 - \frac{1}{\beta}\right), \quad F(1) = \left(1 - \frac{1}{\beta} - \frac{c_0\beta^2}{2}\right), \\ L(1) &= \frac{c_0\beta^2}{2}, \quad G(1) = 0 \end{aligned} \right\} \quad (6.18)$$

The numerical solution of equations (6.12-6.16) will be obtained by considering two cases. Firstly considering the regions where the viscosity is absent and secondly when it is present. Thus the flow field defines two regions based on the gradient of the term $(\xi\Phi)$. The region $(\xi\Phi)' \leq 0$ means that the viscous effect is present in the flow field (Figure 6.2) that comprises of transition flow field between the undisturbed medium and the shock front.

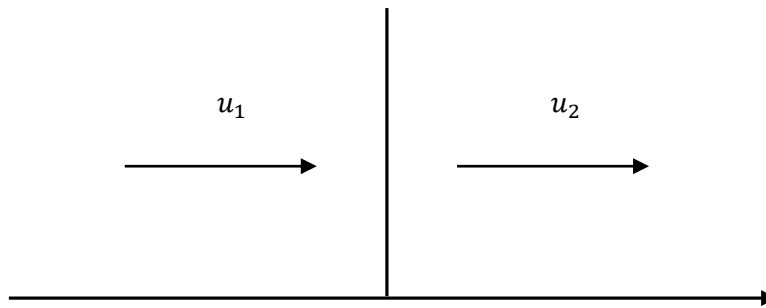


Figure 6.2. Flow with shock wave

Thus the equation (6.16) may be rewritten as follows,

$$\frac{d\Phi}{d\xi} = \frac{-1}{\xi K(\Psi/G)^{1/2}} - \frac{\Phi}{\xi} \quad (6.19)$$

For the region $(\xi\Phi)' > 0$, the viscosity term of equation (6.16) is zero (i.e., $G = 0$) and the remaining equations defining the flow can be written in matrix form for convenience as

$$\begin{pmatrix} \Phi - \alpha & 1 & 0 & 0 \\ 0 & \Phi - \alpha & \frac{1}{\psi} & \frac{1}{\psi} \\ Z & 0 & 1 & 0 \\ 0 & 2L & 0 & \Phi - \alpha \end{pmatrix} \begin{pmatrix} \frac{d \ln \Psi}{d \ln \xi} \\ \frac{d \Phi}{d \ln \xi} \\ \frac{d F}{d \ln \xi} \\ \frac{d L}{d \ln \xi} \end{pmatrix} = \begin{pmatrix} -3\Phi \\ -\frac{2}{\psi}(F + L) - \Phi(\Phi - 1) \\ -2F \left[1 + \frac{(\alpha - 1)}{(\Phi - \alpha)} \right] \\ -2L[4\Phi - 1] \end{pmatrix} \quad (6.20)$$

where

$$Z(\Psi, F) = \frac{\alpha^2}{\xi^2} \left[\Pi' \Psi - \Pi \left(\frac{\Gamma' \Psi}{(\Gamma - 1)} + 1 \right) \right] - F \left(\frac{\Gamma' \Psi}{(\Gamma - 1)} + \Gamma \right) \quad (6.21)$$

The numerical solution procedure involves in writing equation (6.20) as follows:

$$\frac{d \Psi}{d \xi} = \frac{\Psi \Delta_1}{\xi \Delta}, \quad \frac{d \Phi}{d \xi} = \frac{\Delta_2}{\xi \Delta}, \quad \frac{d F}{d \xi} = \frac{\Delta_3}{\xi \Delta}, \quad \frac{d L}{d \xi} = \frac{\Delta_4}{\xi \Delta} \quad (6.22)$$

where

$$\Delta = (\Phi - \alpha)^2 + \frac{1}{\psi}(Z - 2L) \quad (6.23)$$

$$\Delta_1 = \Phi(\Phi - 1) - 3\Phi(\Phi - \alpha) - \frac{2}{\psi}(L + F) \frac{(\alpha - 1)}{(\Phi - \alpha)} \quad (6.24)$$

$$\Delta_2 = \frac{2}{\psi} \{ F(\alpha - 1) - L(\Phi - \alpha) \} - \Phi(\Phi - 1)(\Phi - \alpha) + \frac{2L}{\psi} \{ 4\Phi - 1 \} - \frac{3\Phi Z}{\psi} \quad (6.25)$$

$$\Delta_3 = 3\Phi Z(\Phi - \alpha) - \Phi(\Phi - 1) - \frac{2}{\psi}(F + L) + \frac{2LZ(\Phi - 1)}{\psi(\Phi - \alpha)} + 2F \left(1 + \frac{(\alpha - 1)}{(\Phi - \alpha)} \right) \left\{ \frac{2L}{\psi} - (\Phi - \alpha)^2 \right\} \quad (6.26)$$

$$\Delta_4 = 2L\Phi(\Phi - 1) + \frac{4L}{\psi} \left\{ L - F \frac{(\alpha - 1)}{(\Phi - \alpha)} \right\} - 2 \frac{ZL(\Phi - 1)}{\psi(\Phi - \alpha)} - 2L(\Phi - \alpha) \{ 4\Phi - 1 \} \quad (6.27)$$

6.3 Solution Procedure

The solution procedure involves the following.

- (a) Evaluation of β the measure of shock strength for the considered non-idealness parameters.
- (b) Solutions of the transformed system of differential equations with and without viscosity.

6.3.1 Evaluation of β

The two EOS of Mie-Gruneisen type, Royce [57], van der Waals [97] are considered:

- a) putting $\Gamma(\Psi) = \Gamma_0 + 1 - d \left(1 - \frac{1}{\Psi}\right)$ and $\Pi(\Psi) = 0$ in equation (6.8), the Royce EOS can be written as,

$$p = \rho e \left[\Gamma_0 - d \left(1 - \frac{1}{\Psi}\right) \right] \quad (6.28)$$

where $d > 0$ is an arbitrary constant and Γ_0 is non-ideal parameter. Again,

- b) putting $\Gamma(\Psi) = 1 + \frac{(\gamma-1)}{(1-b\Psi)}$ and $\Pi = \left[1 - \frac{(\gamma-1)}{(1-b\Psi)}\right] a\Psi^2$ in equation (6.8), the van der Waals EOS can be written as,

$$p = \left(\frac{\gamma-1}{1-B\rho}\right) (\rho e + A\rho^2) - A\rho^2 \quad (6.29)$$

where $a = A\rho_0^2$, $b = B\rho_0$, e denotes the specific internal energy, γ is the ratio of specific heats ($\gamma > 1$), and the quantities A , B are the van der Waals gas constants for molecular cohesive forces and finite size of molecules ($A \geq 0$ and $0 \leq B < 1/\rho$) respectively. Substituting equation (6.28) and (6.29) in equation (6.9), we obtain the following two biquadratic equations in terms of β respectively.

$$M(\beta) \equiv C_0\beta^4 + (\Gamma_0 - d)\beta^3 + (3d - 2 - 2\Gamma_0)\beta^2 + (2 - 3d + \Gamma_0)\beta + d = 0 \quad (6.30)$$

$$N(\beta) \equiv b(2a - C_0)\beta^4 + \{C_0 - a(4 - 2\gamma)\}\beta^3 + (2b + \gamma - 1)\beta^2 - 2(\gamma + b)\beta + (\gamma + 1) = 0 \quad (6.31)$$

Using MATLAB these equations are solved for β corresponding to the constants (a , b , C_0 , d , γ and Γ_0). Descartes' rule of signs suggest that the polynomial $M(\beta)$ has two negative and two positive roots whereas $N(\beta)$ has one negative and three positive roots. This can also be seen from the solution curves (Figures 6.3 and 6.4). We observed from these figures that there is always one real root ($\beta = 1$) irrespective of the constants considered. This corresponds to case of no magnetic effect ($C_0 = 0$). Neglecting the negative roots subsequent computations are performed.

6.3.2 Solutions of the transformed equations

The solution of the non-linear system of ordinary differential equations is obtained by considering the two cases, (i) without viscosity ($K = 0$) and (ii) with viscosity ($K \neq 0$).

6.3.3 Numerical solution without viscosity ($K = 0$)

To obtain the solution without viscosity with the known values of β , Γ_0 and γ , the system of equations (6.22) are solved numerically where α is unknown. Substituting the boundary conditions (6.18) into the equations (6.22) and using the method of shock fitting we obtain the following simplified equations

$$P_1\alpha^2 + Q_1\alpha + R_1 = 0 \quad (\text{Royce EOS}) \quad (6.32)$$

$$P_2\alpha^2 + Q_2\alpha + R_2 = 0 \quad (\text{van der Waals EOS}) \quad (6.33)$$

where α_i 's are the roots of the equations (6.32, 6.33) and

$$P_1 = 2[d\beta^3 + (\Gamma_0 - d)\beta^4]$$

$$Q_1 = 4[d\beta^2 + (\Gamma_0 - 2d)\beta^3 - (\Gamma_0 - d)\beta^4]$$

$$R_1 = 2d^2 + 2d(2\Gamma_0 - 3d + 1)\beta + 2\{(\Gamma_0 - 3d)(\Gamma_0 - d + 1) + (\Gamma_0 - d)\}\beta^2$$

$$+ \{C_0d^2 - 2(\Gamma_0 - d)(\Gamma_0 - d + 1) + 2(3d - 2\Gamma_0)\}\beta^3$$

$$+ 2\{(\Gamma_0 - d)(1 + dC_0) - dC_0\}\beta^4 + C_0(\Gamma_0 - d)(\Gamma_0 - d + 1)\beta^5$$

$$P_2 = 2\beta^2 + \{a(4 - 2\gamma) - 4b\}\beta^3 + \{ab(2\gamma - 8) + 2b^2\}\beta^4 + 4ab^2\beta^5$$

$$Q_2 = 4\beta - (8b + 4)\beta^2 + (4b^2 + 8b)\beta^3 - 4b^2\beta^4$$

$$\begin{aligned} R_2 = & 2(1 + \gamma) - 2(2 + \gamma)(1 + b)\beta + 2\{1 + (4 + \gamma)b + b^2\}\beta^2 \\ & + \{(\gamma - 2)C_0 - 4b - 4b^2\}\beta^3 + \{(4 - \gamma)bC_0 + 2b^2\}\beta^4 \\ & - 2C_0b^2\beta^5 \end{aligned}$$

The roots of the biquadratic equations (6.30), (6.31) and the quadratic equations (6.32), (6.33) for different non-ideal parameters are shown in Tables 6.1 and 6.2.

6.3.4 Numerical solution with viscosity (K)

The presence of viscosity is expected to damp the amplitude of oscillations near the discontinuities in the physical quantities and thereby the Rankine-Hugoniot conditions do not show any special significance in the viscosity formalism. The system of equations (6.12-6.15, 6.19) are solved numerically with the known values of β , Γ_0 , γ , α (obtained previously) and viscosity K ($= 0.003439, 0.0349$ and 0.349) [103].

To integrate the set of non-linear ordinary differential equations without and with viscosity we use Runge-Kutta fourth order method with small step size. The integration is carried out in the range, $1 \leq \xi < \infty$. Starting the integration with a known value of β and α (α is evaluated corresponding to every β iteratively), shown in Tables 6.1 and 6.2, the whole solution procedure is repeated until the shock conditions are satisfied within the desired accuracy.

6.4 Results and Discussion

In this chapter, the entire computational work has been carried out using MATLAB. Numerical calculations are performed for the values of non-ideal parameters $d = 0.1, 0.3, 0.5, 0.7, 1.0$; $C_0 = 0.02, 0.05$; $b = 0.0004, 0.001, 0.005, 0.01, 0.03$; $\Gamma_0 = 1.78, 2.12$, and $\gamma = 1.4, 1.6$. The values of similarity exponent α for different values of β in the case of Royce and van der Waals EOS are listed in Tables 6.1 and 6.2 respectively. The variations of non-dimensional density, shock velocity, pressure and magnetic pressure with ξ for Royce and van der Waals EOS in the absence of viscosity ($K = 0$) and with viscosity ($K = 0.00349, 0.0349, \text{ and } 0.349$) are investigated in detail and are shown in Figures 6.5-6.16. The results of the study in both EOSs (Royce and van der Waals) are summarized as follows:

The increase in the non-idealness parameters d , a and b , has effect on the measure of shock strength β . It is notable that increase in magnitude of β in case of Royce EOS and decrease in the van der Waals EOS respectively (Tables 6.1 and 6.2).

In the absence of viscosity ($K = 0$), from Figure 6.5(a-d) it is observed that the density, velocity, pressure, and magnetic pressure distributions for Royce EOS decreases with the increasing values of d (non-idealness parameter) and β (measure of shock strength). Whereas in the case of van der Waals EOS, the flow variables density, velocity, and pressure increase with an increasing values of non-idealness parameter b , and for decrease in measure of shock strength β as

shown in Figure 6.9(a-d). In both the EOS under consideration the flow variables developed sharp edge profiles. This can be attributed to the excitation of oscillations in molecules through shock front. The change in magnetic pressure is negligible with change of non-idealness parameter b . This phenomenon is observed to be more prominent in case of van der Waals EOS than Royce EOS. Similar trend in the velocity and density profiles were reported by Khodadad and Khazraiyani [105], Lee and Whalen [106] respectively.

It is very important to observe that in the presence of viscosity formalism (i.e., $K \neq 0$) the profiles of the flow field could lead to continuous shock flow fields in which the sharp edged continuous profiles at the shock wave reduce and change to smooth curves. Flow variables (physical parameters) changed rapidly, but smoothly for both EOS. It is to be noted that the effect on flow variables (physical parameters) in the medium of van der Waals EOS is appreciable for small values of non-idealness parameter b , while for large values of non-idealness parameter b , it is very small. Similar trend in the pressure profiles were reported by Chikitkin et al. [107] and density profiles by Chikitkin et al. [107], Lee and Whalen [106].

It is observed that in the presence of non-idealness parameters d and b along with the introduction of artificial viscosity ($K = 0.00349$) during the numerical integration process the nature of the profiles of both the EOS change from being sharp edged to smooth curves (Figures 6.6(a-d) and 6.10(a-d)). The smoothness

in the flow parameters further improved by increasing the value of viscosity i.e., $K = 0.0349$ to 0.349 in both the EOS (Figures 6.6(a-d), 6.7(a-d), 6.11(a-d) and 6.12(a-d)). With the non-idealness parameter $d(= 0.1, 0.3, 0.5)$ and $K = 0.0349$, from Figure 6.7(a-d) for Royce EOS the density, velocity, pressure and magnetic profiles gradually increase with increase in ξ and decrease slowly and become constant. This behavior continues to remain the same with sharp edges becoming smoother with increase in the value of $K (= 0.349)$ (see Figure 6.8(a-d)). Thus we conclude that along with the non-idealness parameters and with the introduction of artificial viscosity ($K = 0.00349, 0.0349,$ and 0.349) the excitation of oscillations in the molecules dampen and the smoothness in the profiles increases. With the non-idealness parameter $b(= 0.001, 0.005, 0.01)$ and $K = 0.0349$, from Figure 6.11(a-d) for van der Waals EOS the density, velocity, pressure and magnetic profiles gradually increase with increase in ξ and slowly and become constant. This behavior remains unaltered with the value of $K > 0.349$ (Figure 6.12(a-d)).

It is observed that spread of flow variables increases with increase in the range of the non-idealness parameter b and fixed values of viscosity parameter K . Thus, the thickness of MHD shock front increases with increase in the value of non-idealness parameter b . The thickness of MHD shock wave depends only on its strength and is constant with increase in reduced distance ξ . However, the increase in the thickness of shock front with increase in the non-idealness

parameter b is more notable for certain range of values of viscosity parameter K for both EOS of Royce and van der Waals.

Numerical computations revealed that the change in the flow variables with the non-idealness parameters d , and b is constant and independent of large values of viscosity parameter K for Royce and van der Waals EOS respectively. Thus artificial viscosity has no effect along a wave front of constant phase. This is because the velocity component tangential to a shock front is continuous in the limit of arbitrary grid refinement in this direction. This type of behavior is called wave front invariance.

In particular, we observed that for smaller values of magnitude of viscosity parameter K the effect on flow variables velocity, pressure are constant initially with the increase in ξ and decreases more rapidly with increasing values of non-idealness parameter b and fixed values of non-idealness parameter a in the EOS of van der Waals. Also it is observed that the thickness of MHD shock front is maximum for small values of non-idealness parameter b , which increases more with increasing values of non-idealness a and fixed values of non-idealness parameter b (Figures 6.13-6.16).

We concluded that artificial viscosity could distinguish between shock-wave and adiabatic compression. It vanishes for uniform compression and rigid rotation and also vanishes along a surface of constant phase. Along such a surface the velocity field has a constant magnitude, and is also continuous, but may vary in direction.

Moreover, artificial viscosity produce forces that go to zero continuously as compression goes to zero for expansion, so that latter is a reversible process.

The values of similarity exponent α for different values of β for Royce EOS and van der Waals EOS are evaluated. The conclusions of the study are summarized as follows:

- 1) It is noted that the increase in the non-idealness parameters d , a and b , have effect on the measure of shock strength β , i.e., increase in magnitude of β in case of Royce EOS and decrease in the van der Waals EOS respectively.
- 2) In the presence of non-idealness parameters and in the absence of viscosity ($K = 0$) the density, velocity, pressure, and magnetic pressure distributions for Royce EOS observed to decrease with the increasing values of non-idealness parameter d , and for increasing values of measure of shock strength β .
- 3) In the case of van der Waals EOS, the flow variables density, velocity, and pressure increase with an increasing values of non-idealness parameter b , and for decrease in measure of shock strength β .
- 4) In both the EOS under consideration it is observed that the flow variables have sharp edge profiles. The change in magnetic pressure is negligible in case of van der Waals EOS than Royce EOS.

- 5) It is notable that in the presence of non-idealness parameters d and b and with the introduction of artificial viscosity ($K = 0.00349, 0.0349,$ and 0.349) during the numerical integration process the nature of the profiles of both the EOS change from being sharp edged to smooth curves.
- 6) It is observed that the large value of artificial viscosity has no effect along a wave front of constant phase because the velocity component tangential to a shock front is continuous in the limit of arbitrary grid refinement in this direction.
- 7) With the non-idealness parameter $b(= 0.001, 0.005, 0.01)$ and $K = 0.0349$, for van der Waals EOS the density, velocity, pressure and magnetic profiles gradually increases with increase in ξ and slowly and become constant. This behaviour remains unaltered with the value of $K > 0.349$.
- 8) We conclude that with the non-idealness parameters and with the introduction of artificial viscosity ($K = 0.00349, 0.0349,$ and 0.349) the excitation of oscillations in the molecules dampen and the smoothness in the profiles increases.
- 9) It is observed that spread of flow variables increases with increase in the range of the non-idealness parameter b and fixed values of viscosity parameter K .
- 10) The thickness of MHD shock front increases with increase in the value of non-idealness parameter b . It is observed that the thickness of MHD

shock wave depends only on its strength and is constant with increase in reduced distance ξ .

- 11) It is observed that for smaller values of viscosity parameter K the effect on flow variables is constant initially with the increase in ξ and decreases more rapidly with increasing values of non-idealness parameter b and fixed values of non-idealness parameter a in the EOS of van der Waals. Also it is observed that the thickness of MHD shock front is maximum for small values of non-idealness parameter b , which increases more with an increasing values of non-idealness parameter a and fixed values of non-idealness parameter b .
- 12) We conclude that artificial viscosity distinguishes between shock-wave and adiabatic compression. It vanishes for uniform compression and rigid rotation and also vanishes along a surface of constant phase. Along such a surface the velocity field has a constant magnitude, and is also continuous, but may vary in direction.

Table 6.1: Similarity exponent α for Royce EOS when $\Gamma_0 = 1.78, 2.12$

d	C_0	$\Gamma_0 = 1.78$		$\Gamma_0 = 2.12$	
		β	α	β	α
0.1	0.02	2.06157	1.32738	1.89160	1.33130
	0.05	1.93154	1.28273	1.78867	1.28039
0.3	0.02	2.12842	1.31746	1.93417	1.32320
	0.05	1.98290	1.27537	1.82234	1.27433
0.5	0.02	2.20935	1.30624	1.98357	1.31420
	0.05	2.04357	1.26708	1.86077	1.26760
0.7	0.02	2.31003	1.29336	2.04184	1.30411
	0.05	2.11673	1.25770	1.90523	1.26008
1.0	0.02	2.52063	1.26985	2.15300	1.28631
	0.05	2.26132	1.24099	1.98726	1.24694

Table 6.2: Similarity exponent α for van der Waals EOS when $\gamma = 1.4, 1.6$

b	C_0	$a = 0.0025$				$a = 0.0075$			
		$\gamma = 1.4$		$\gamma = 1.6$		$\gamma = 1.4$		$\gamma = 1.6$	
		β	α	β	α	β	α	β	α
0.0004	0.02	4.76932	1.28941	3.75301	1.30083	5.10068	1.26749	3.85936	1.29204
	0.05	3.74624	1.29955	3.16116	1.29411	3.89914	1.28819	3.22478	1.28893
0.001	0.02	4.76157	1.28987	3.74788	1.30124	5.08995	1.26821	3.85327	1.29259
	0.05	3.74301	1.29974	3.15846	1.29433	3.89516	1.28848	3.22168	1.28921
0.005	0.02	4.71012	1.29296	3.71393	1.30403	5.01922	1.27300	3.81306	1.29624
	0.05	3.72142	1.30106	3.14044	1.29578	3.86863	1.29045	3.20107	1.29113
0.01	0.02	4.64644	1.29693	3.67204	1.30757	4.93287	1.27906	3.76379	1.30083
	0.05	3.69427	1.30279	3.11794	1.29765	3.83541	1.29300	3.17541	1.29356
0.03	0.02	4.39947	1.31395	3.51064	1.32218	4.60935	1.30386	3.57709	1.31937
	0.05	3.58427	1.31055	3.02839	1.30565	3.70229	1.30415	3.07413	1.30382

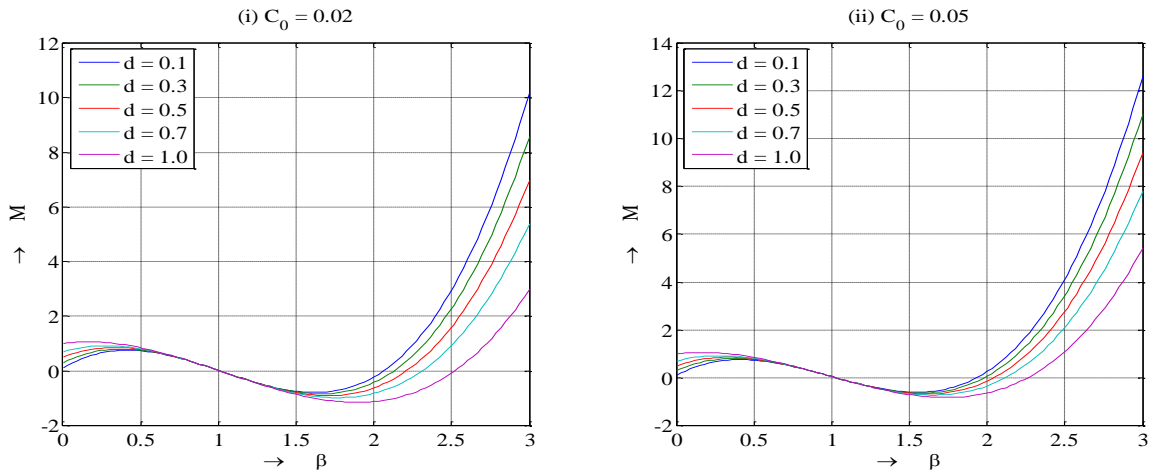


Figure 6.3. Graphical approach of $M(\beta)$ for Royce EOS when $\Gamma_0 = 1.78$ and various values of d

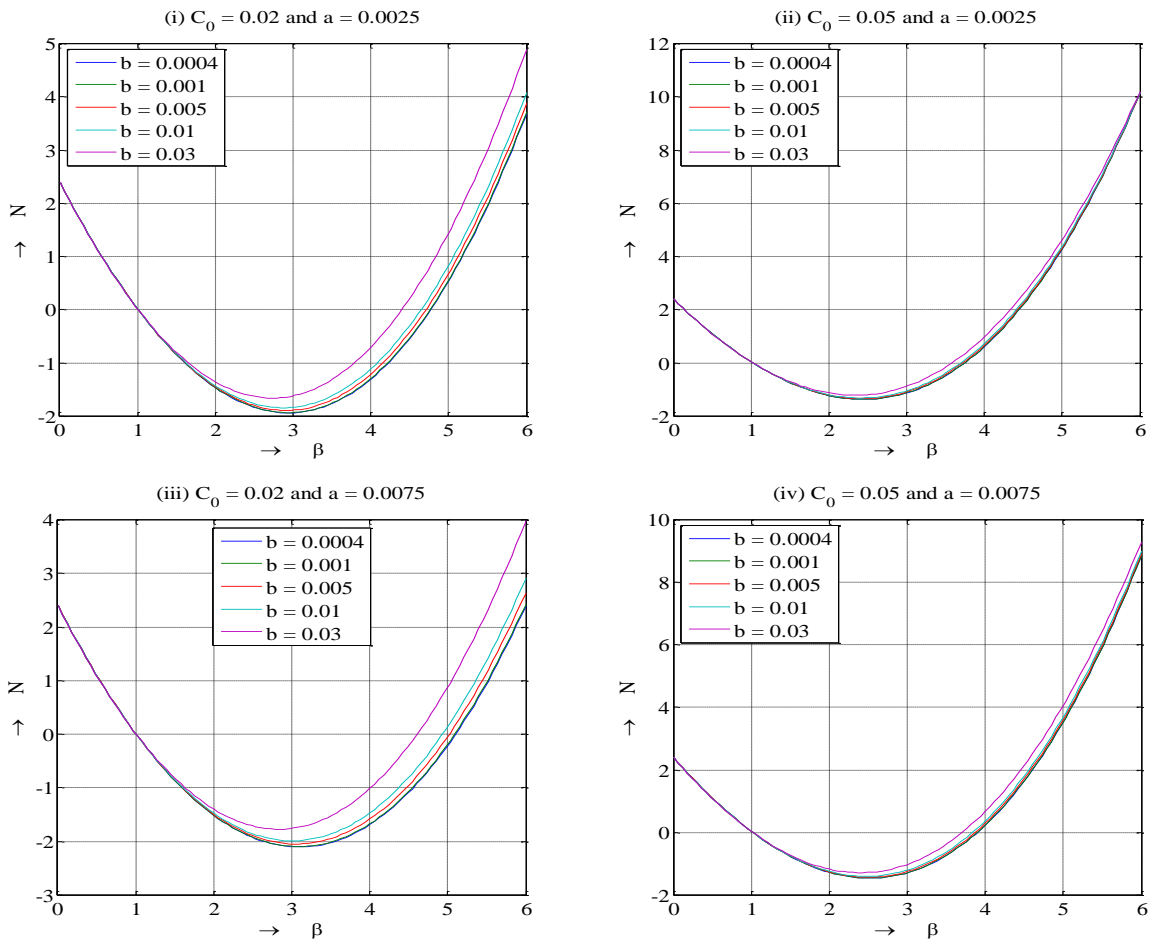


Figure 6.4. Graphical approach of $N(\beta)$ for van der Waals EOS when $\gamma = 1.4$ and various values of b

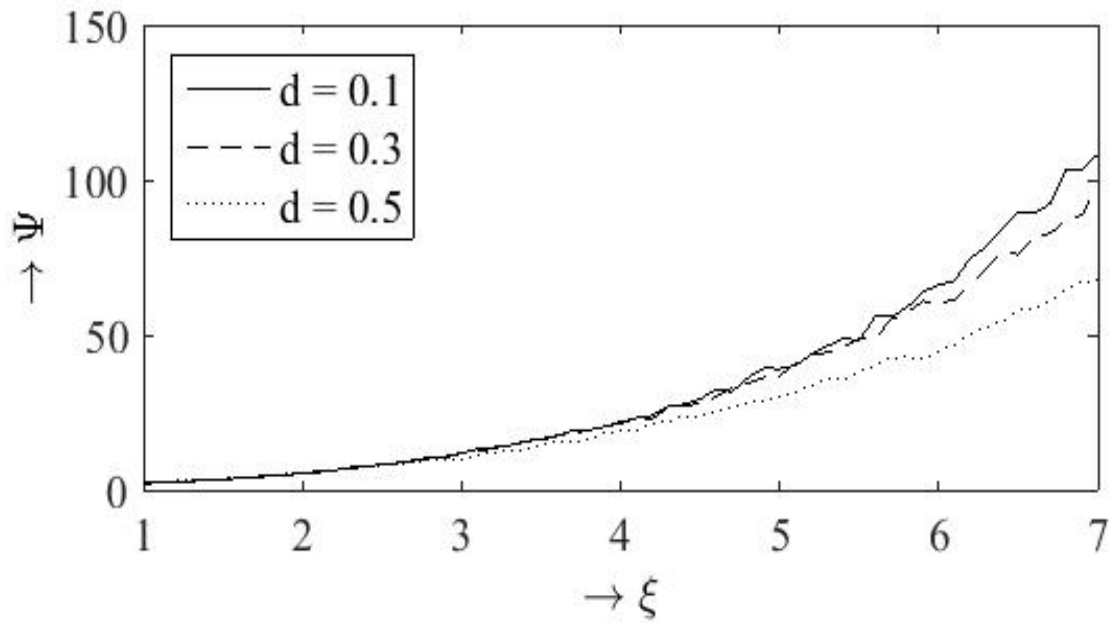


Figure 6.5(a). Density profiles for Royce EOS when $\Gamma_0 = 1.78$, $K = 0$

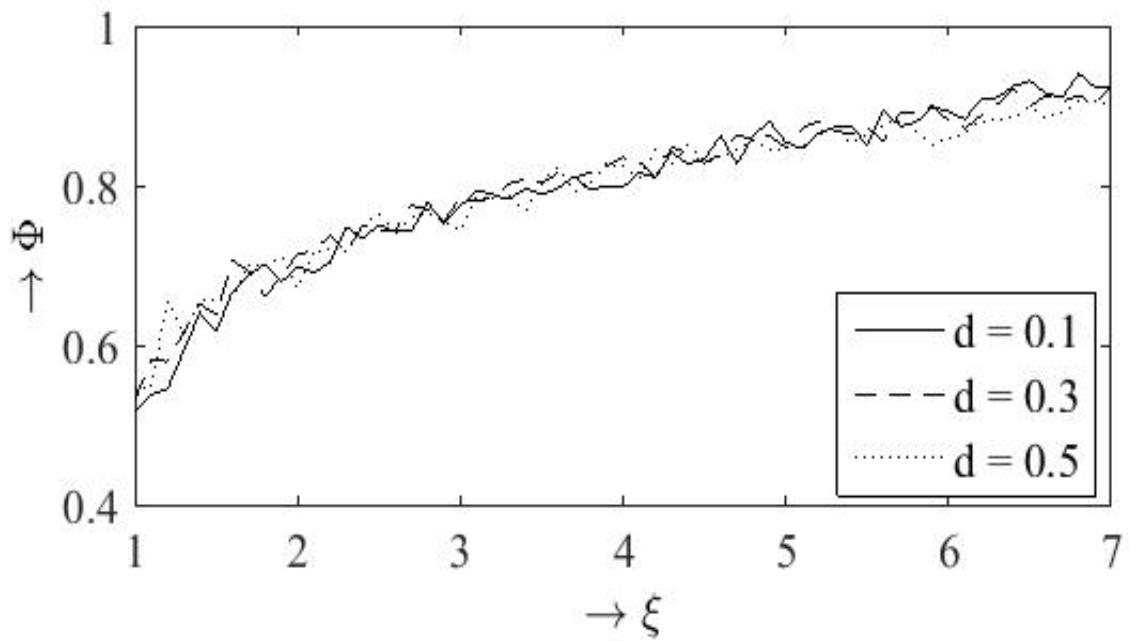


Figure 6.5(b). Velocity profiles for Royce EOS when $\Gamma_0 = 1.78$, $K = 0$

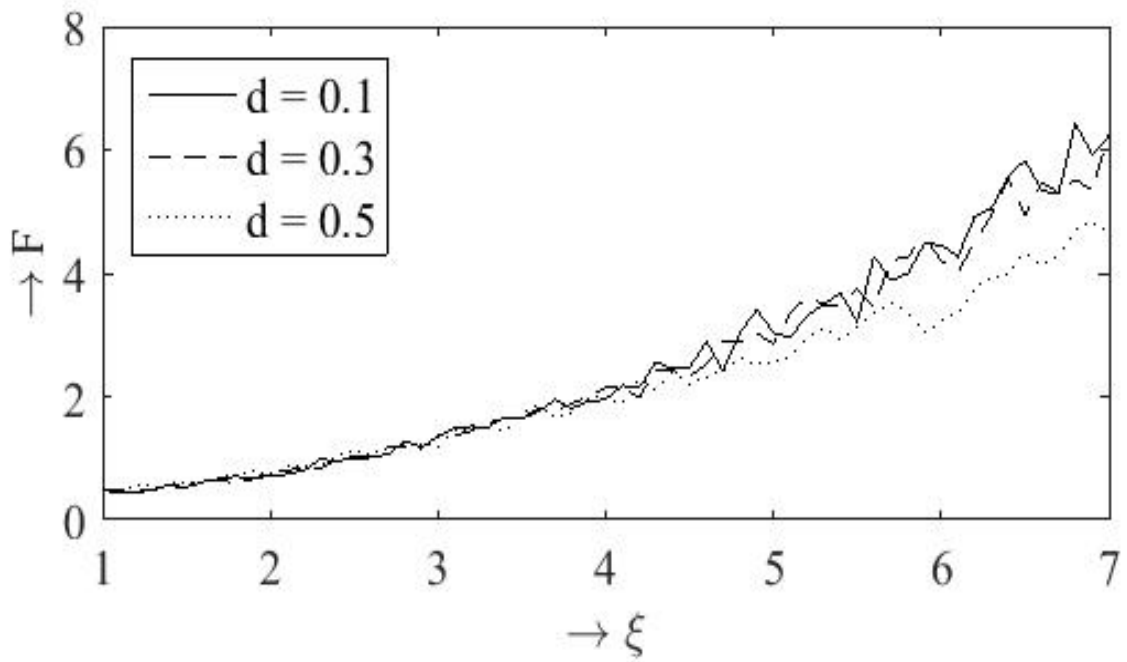


Figure 6.5(c). Pressure profiles for Royce EOS when $\Gamma_0 = 1.78$, $K = 0$

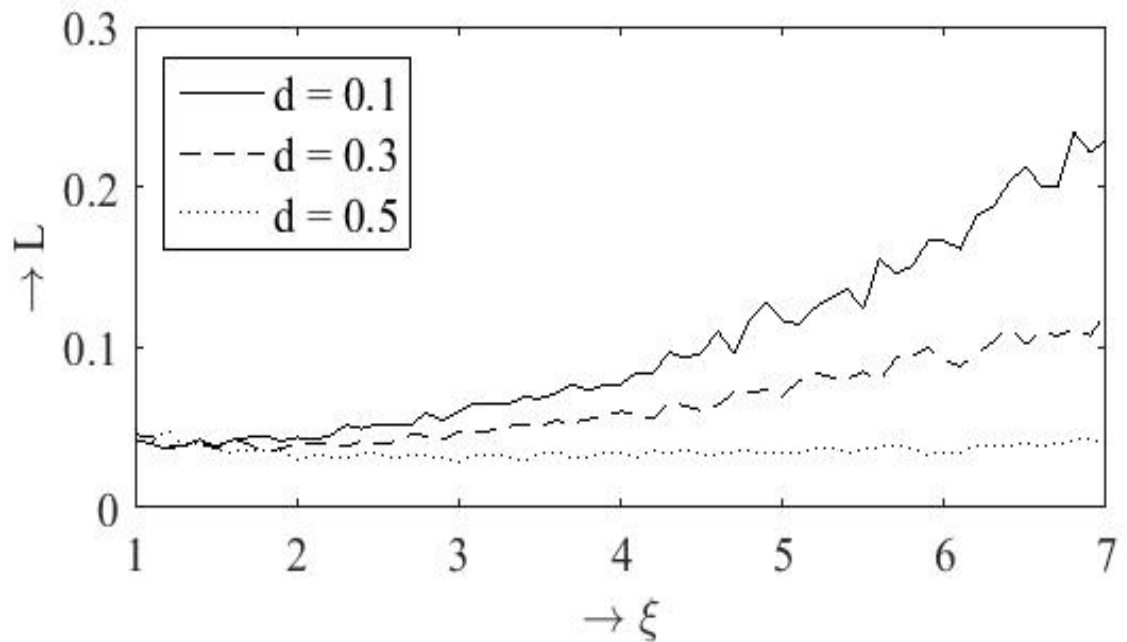


Figure 6.5(d). Magnetic pressure profiles for Royce EOS when $\Gamma_0 = 1.78$, $K = 0$

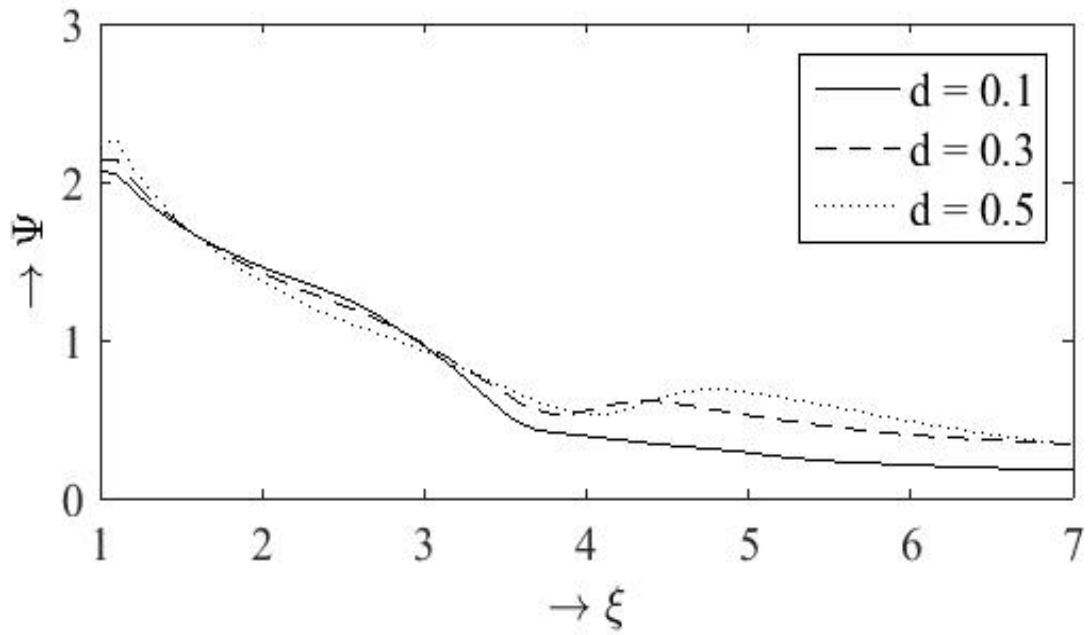


Figure 6.6(a). Density profiles for Royce EOS when $\Gamma_0 = 1.78$, $K = 0.00349$

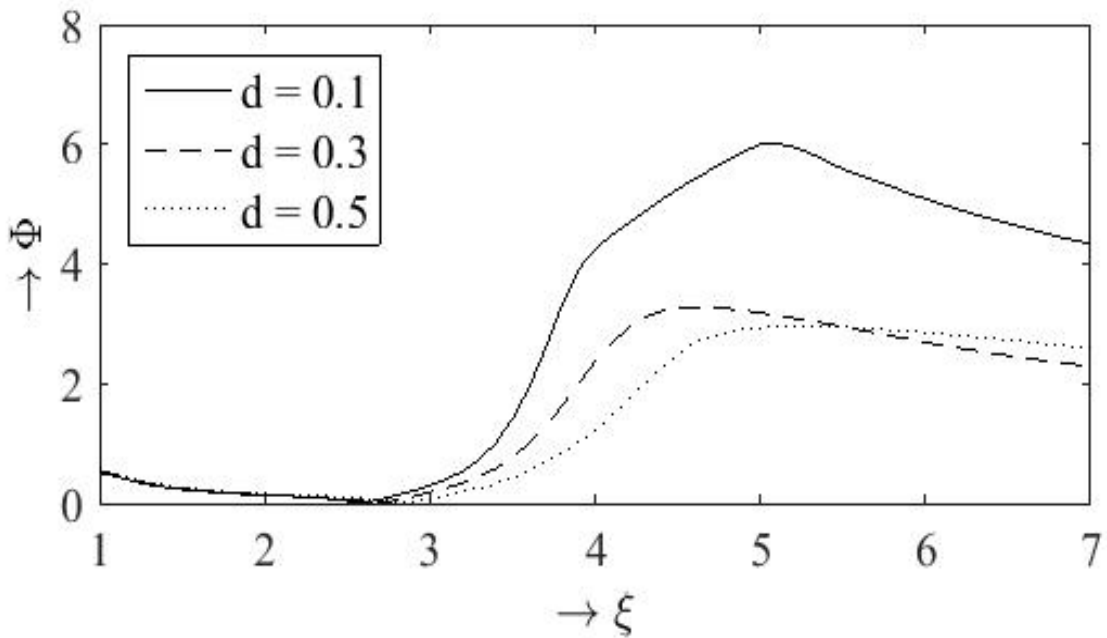


Figure 6.6(b). Velocity profiles for Royce EOS when $\Gamma_0 = 1.78$, $K = 0.00349$

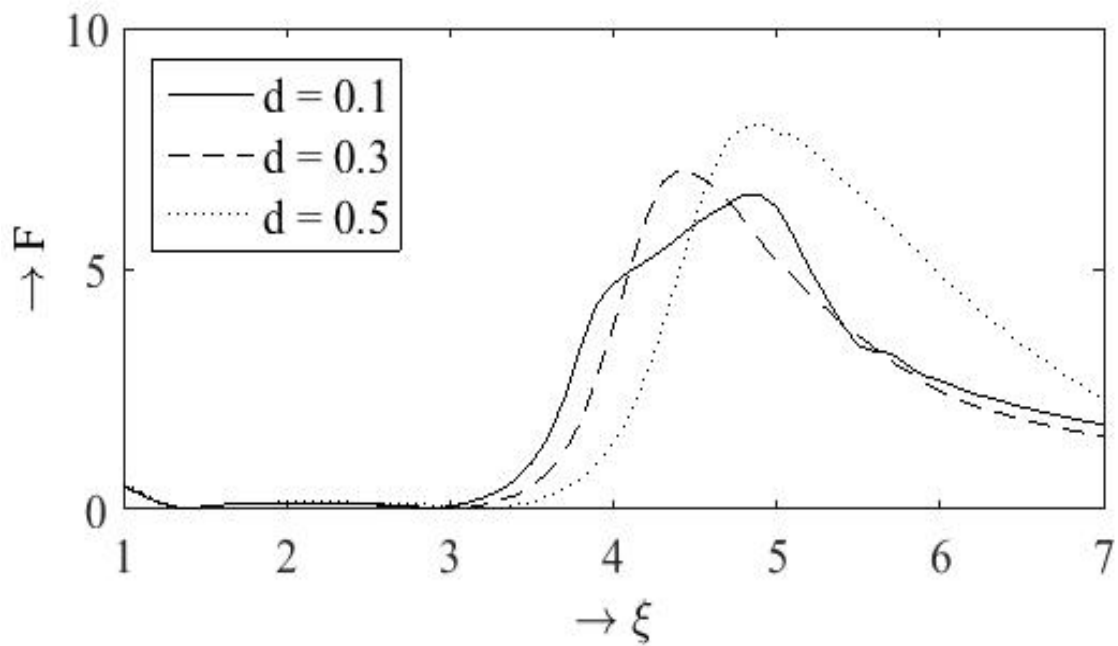


Figure 6.6(c). Pressure profiles for Royce EOS when $\Gamma_0 = 1.78$, $K = 0.00349$

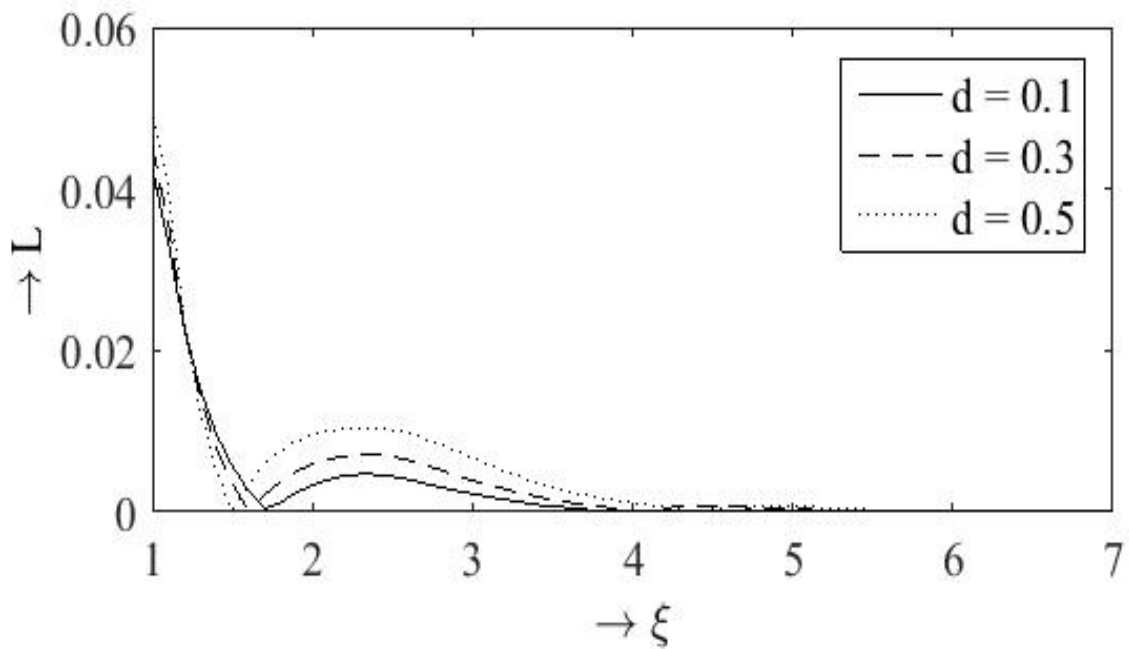


Figure 6.6(d). Magnetic pressure profiles for Royce EOS when $\Gamma_0 = 1.78$, $K = 0.00349$

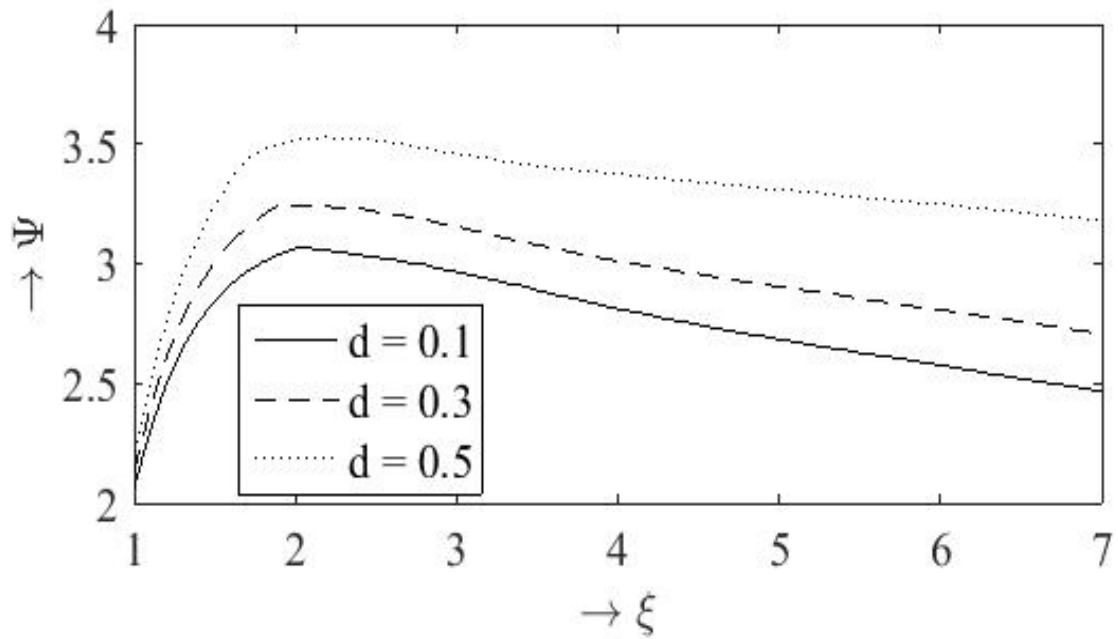


Figure 6.7(a). Density profiles for Royce EOS when $\Gamma_0 = 1.78$, $K = 0.0349$

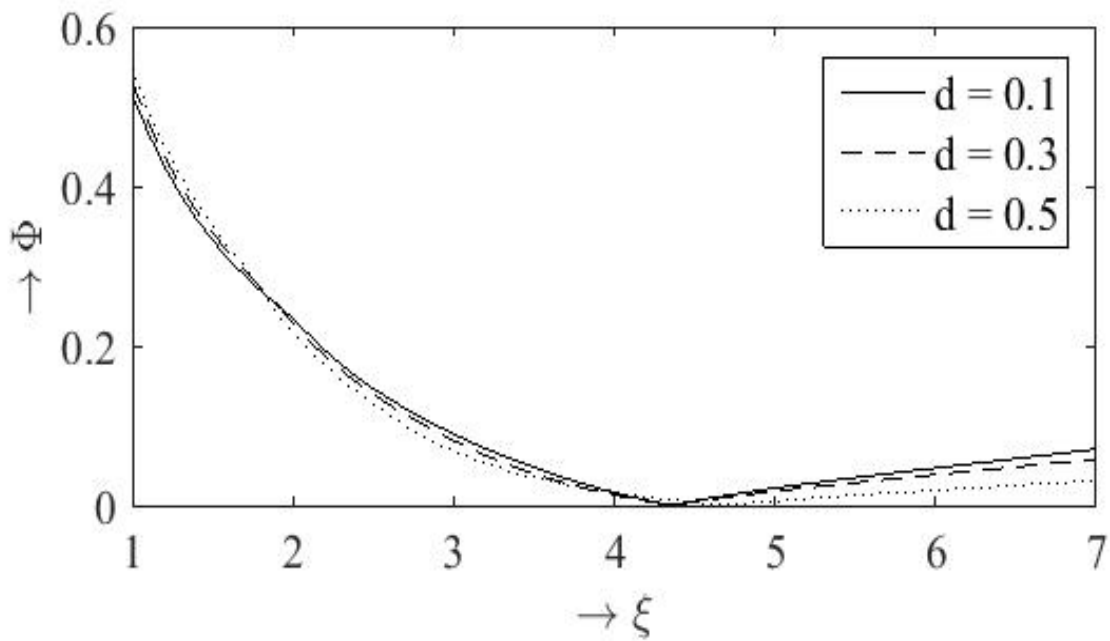


Figure 6.7(b). Velocity profiles for Royce EOS when $\Gamma_0 = 1.78$, $K = 0.0349$

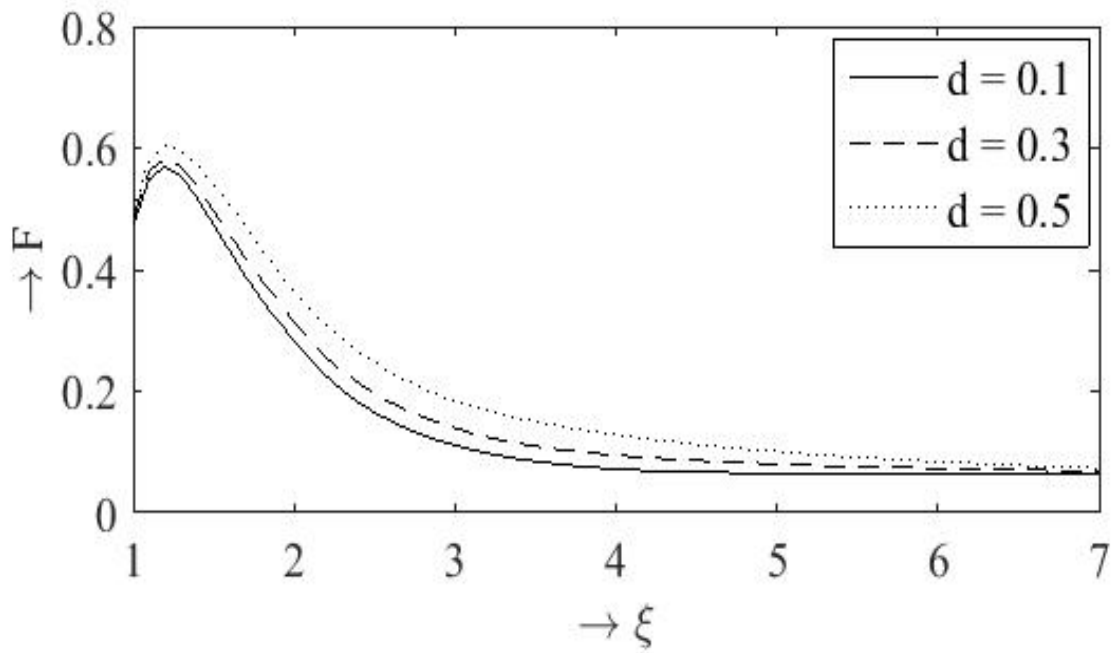


Figure 6.7(c). Pressure profiles for Royce EOS when $\Gamma_0 = 1.78$, $K = 0.0349$

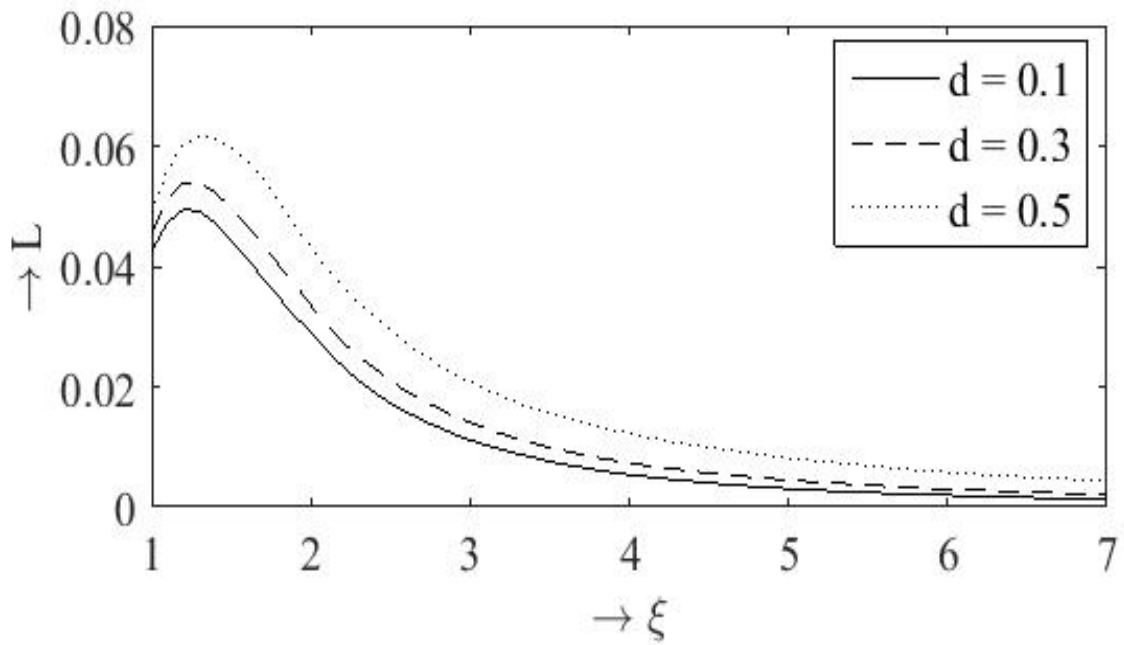


Figure 6.7(d). Magnetic pressure profiles for Royce EOS when $\Gamma_0 = 1.78$, $K = 0.0349$

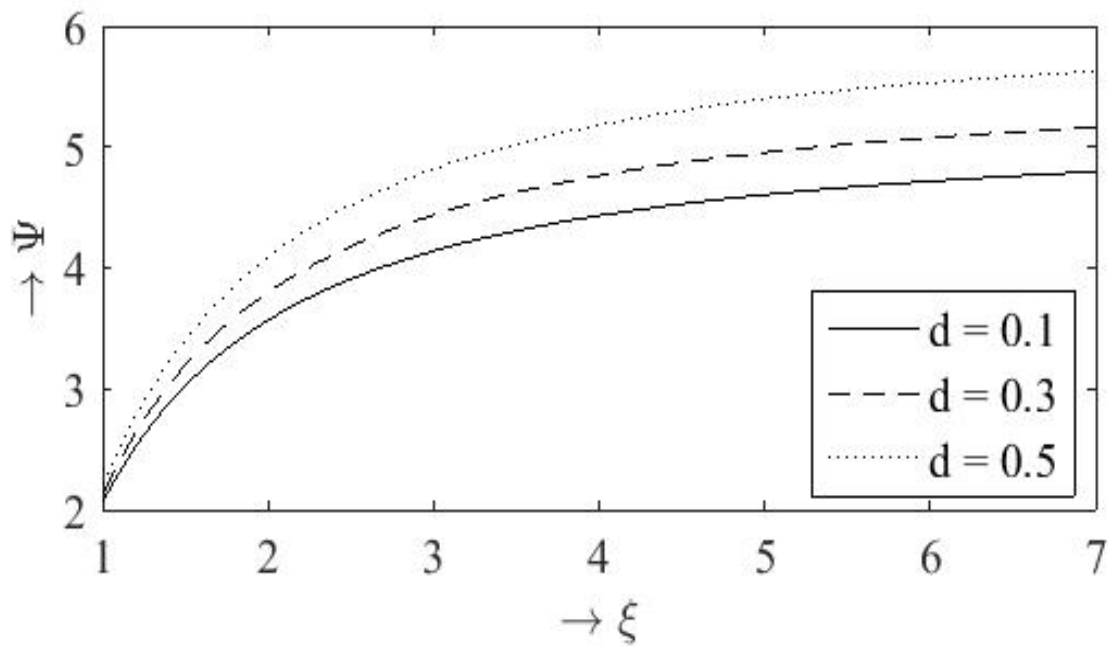


Figure 6.8(a). Density profiles for Royce EOS when $\Gamma_0 = 1.78$, $K = 0.349$

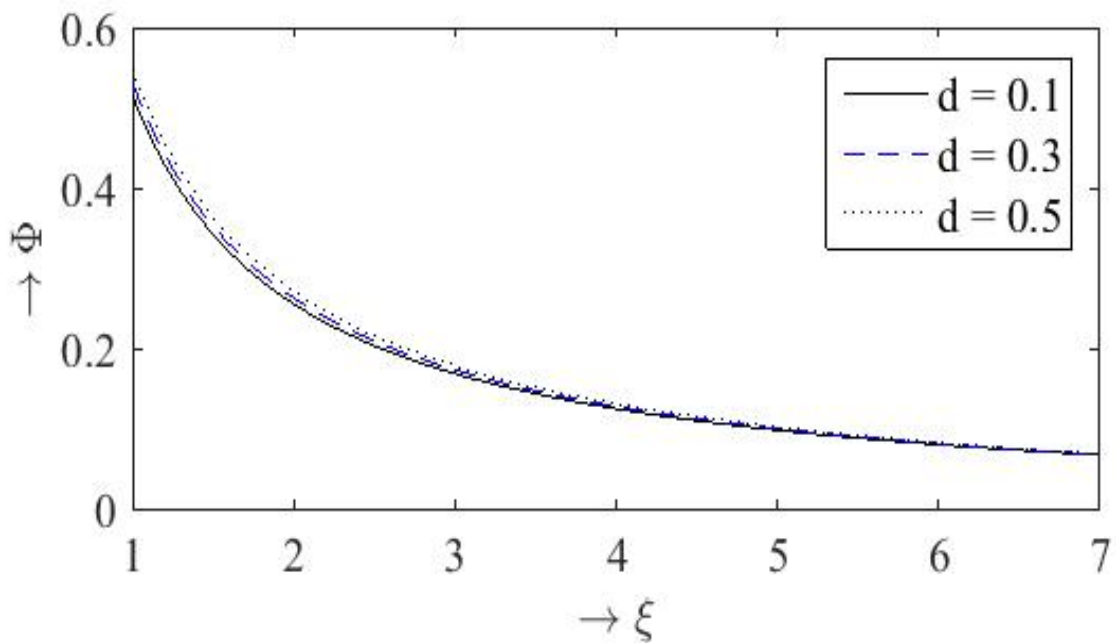


Figure 6.8(b). Velocity profiles for Royce EOS when $\Gamma_0 = 1.78$, $K = 0.349$

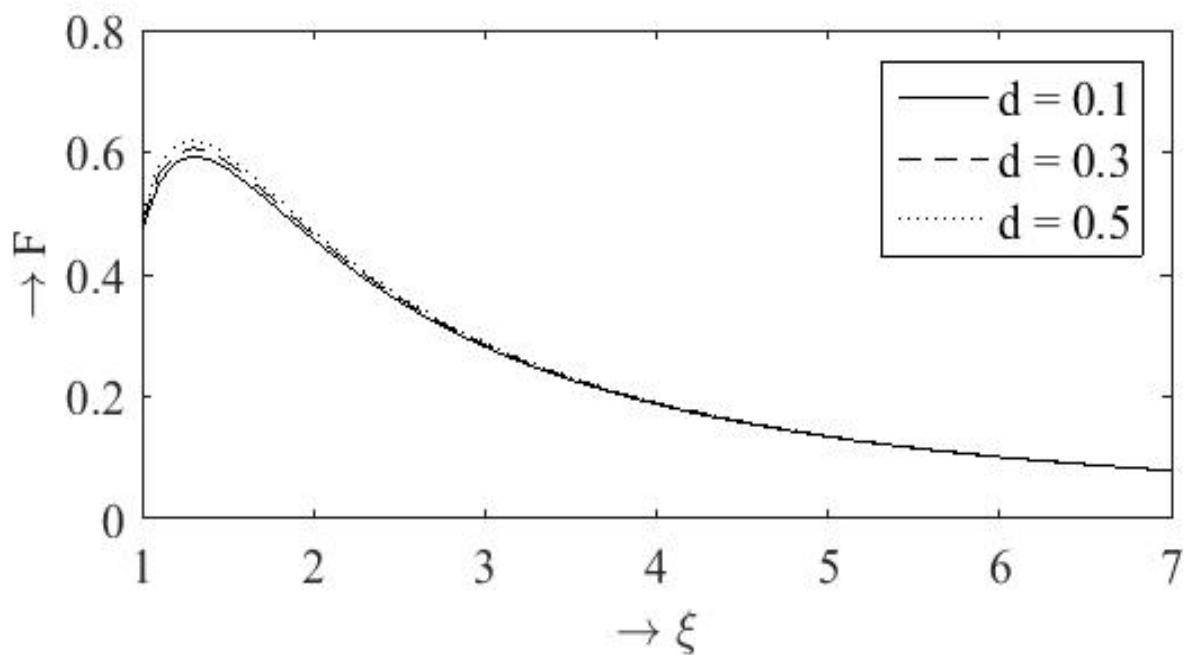


Figure 6.8(c). Pressure profiles for Royce EOS when $\Gamma_0 = 1.78$, $K = 0.349$

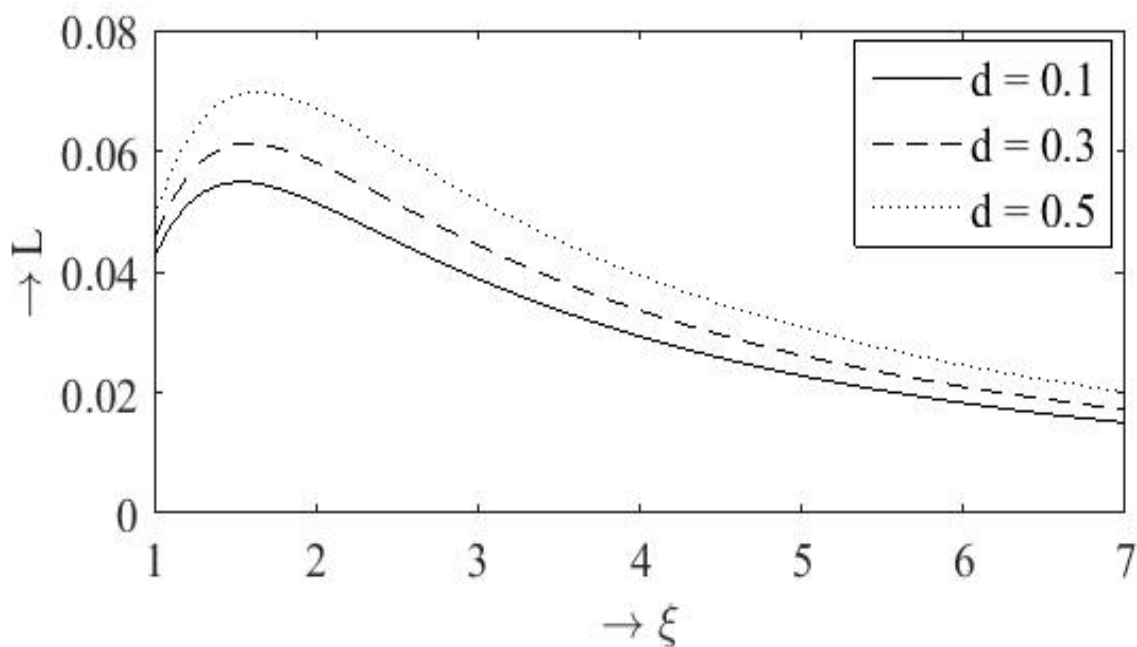


Figure 6.8(d). Magnetic pressure profiles for Royce EOS when $\Gamma_0 = 1.78$, $K = 0.349$

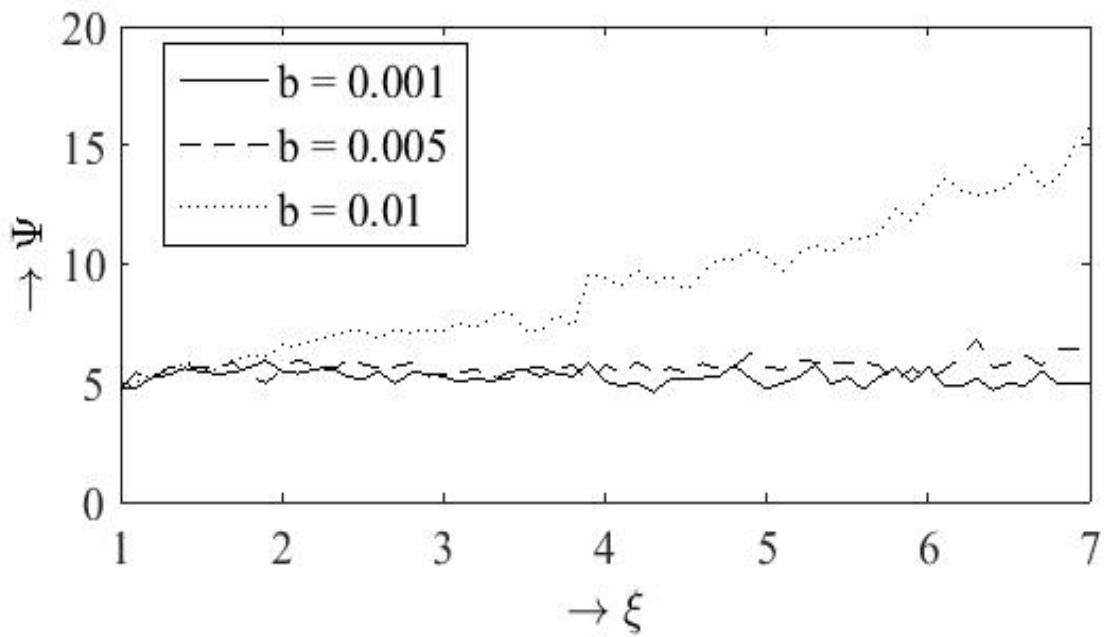


Figure 6.9(a). Density profiles for van der Waals EOS when $\gamma = 1.4$, $K = 0$ and $a = 0.0025$

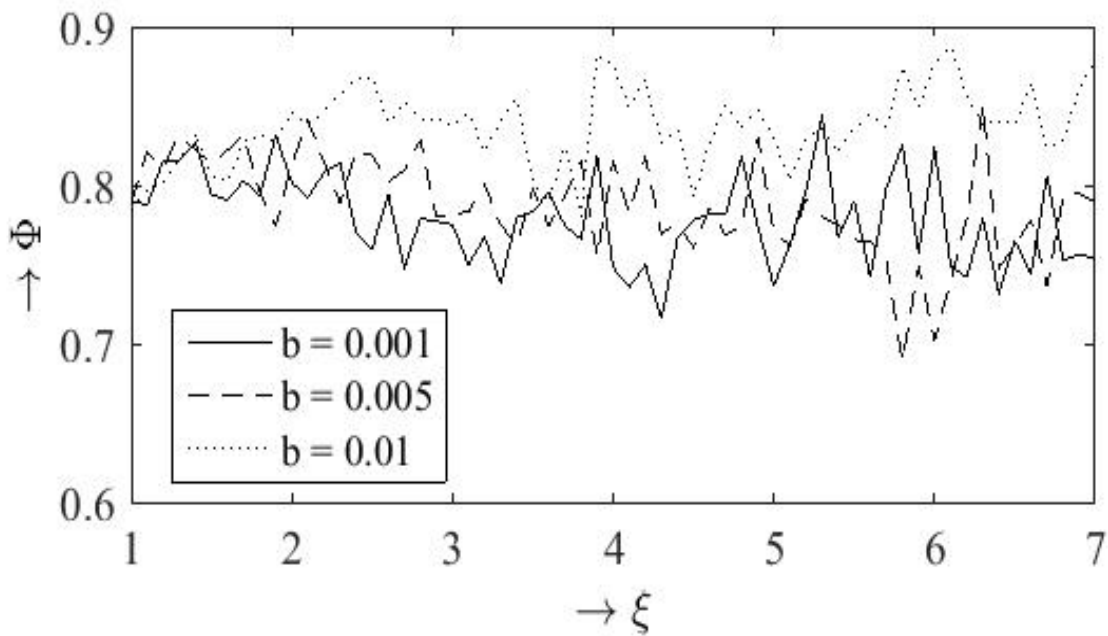


Figure 6.9(b). Velocity profiles for van der Waals EOS when $\gamma = 1.4$, $K = 0$ and $a = 0.0025$

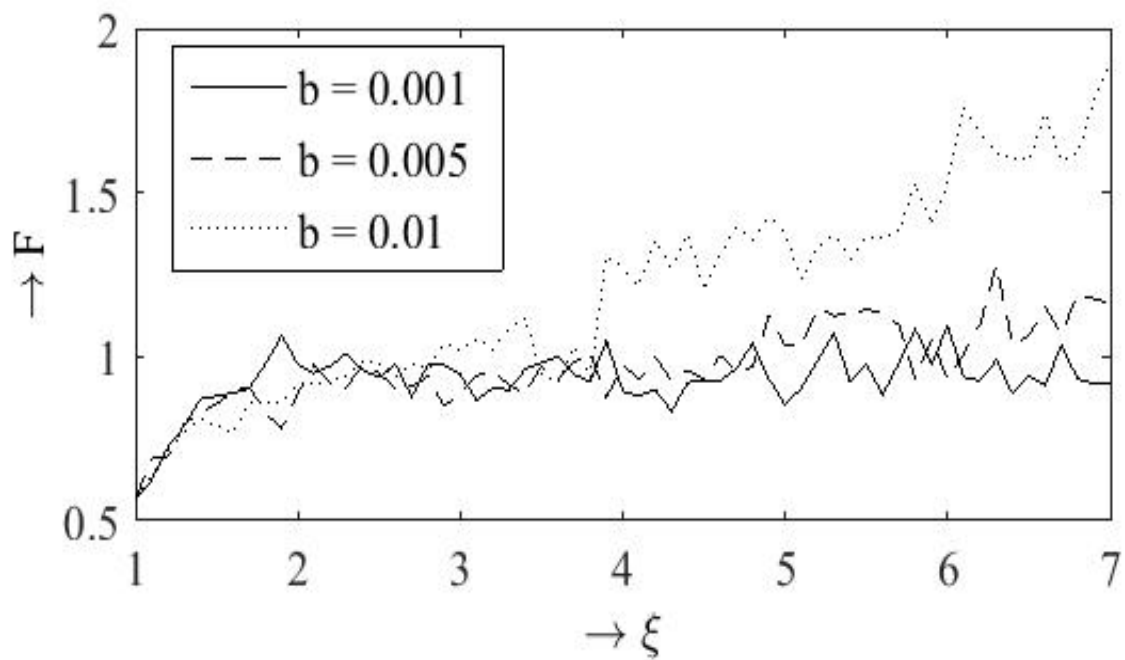


Figure 6.9(c). Pressure profiles for van der Waals EOS when $\gamma = 1.4$, $K = 0$ and $a = 0.0025$

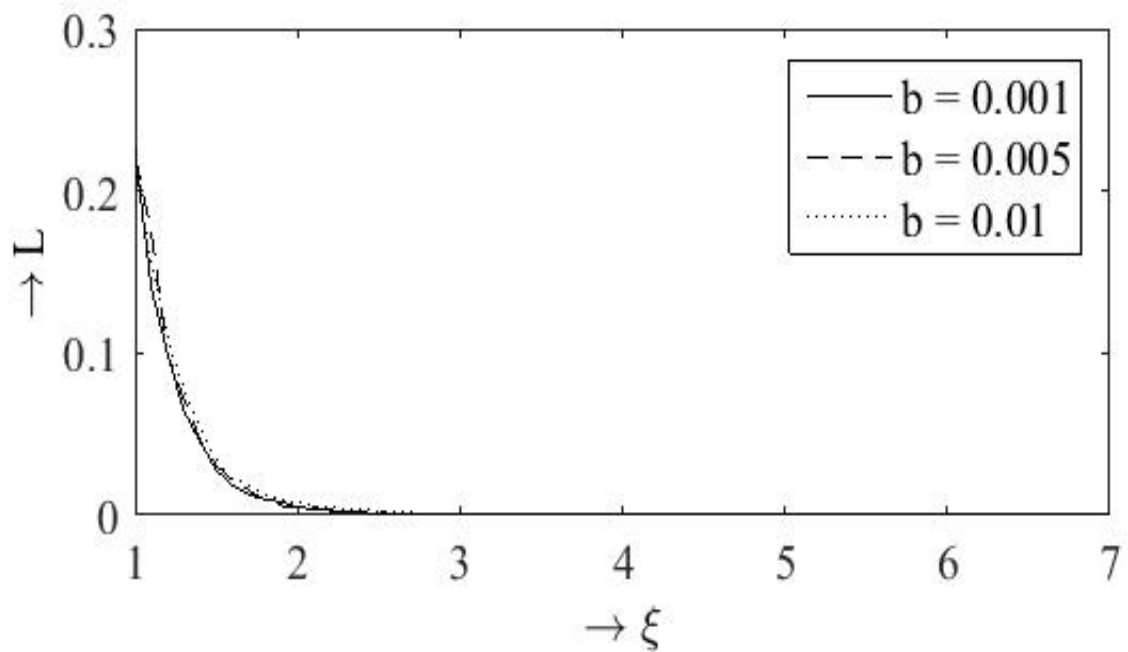


Figure 6.9(d). Magnetic pressure profiles for van der Waals EOS when $\gamma = 1.4$, $K = 0$ and $a = 0.0025$

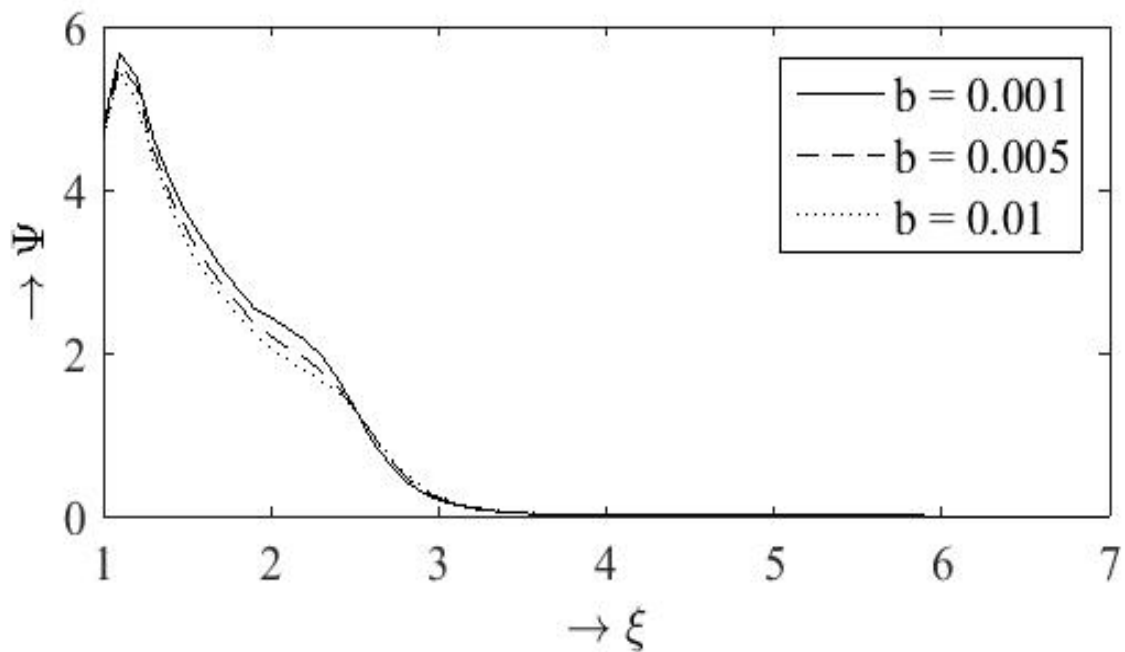


Figure 6.10(a). Density profiles for van der Waals EOS when $\gamma = 1.4$, $K = 0.00349$ and $a = 0.0025$

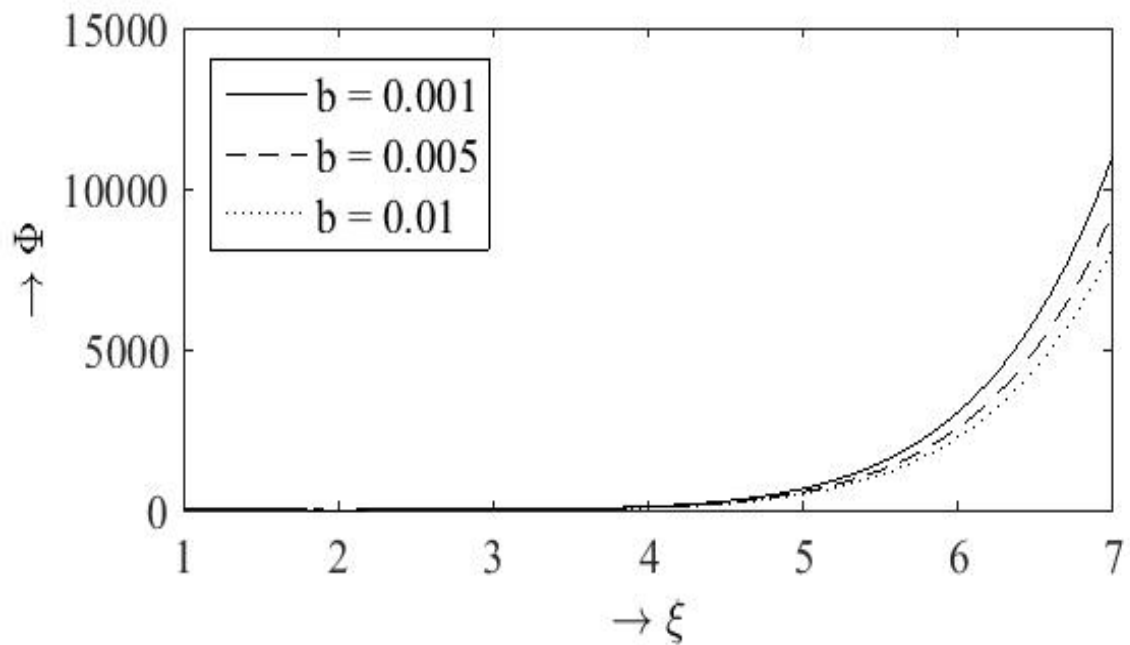


Figure 6.10(b). Velocity profiles for van der Waals EOS when $\gamma = 1.4$, $K = 0.00349$ and $a = 0.0025$

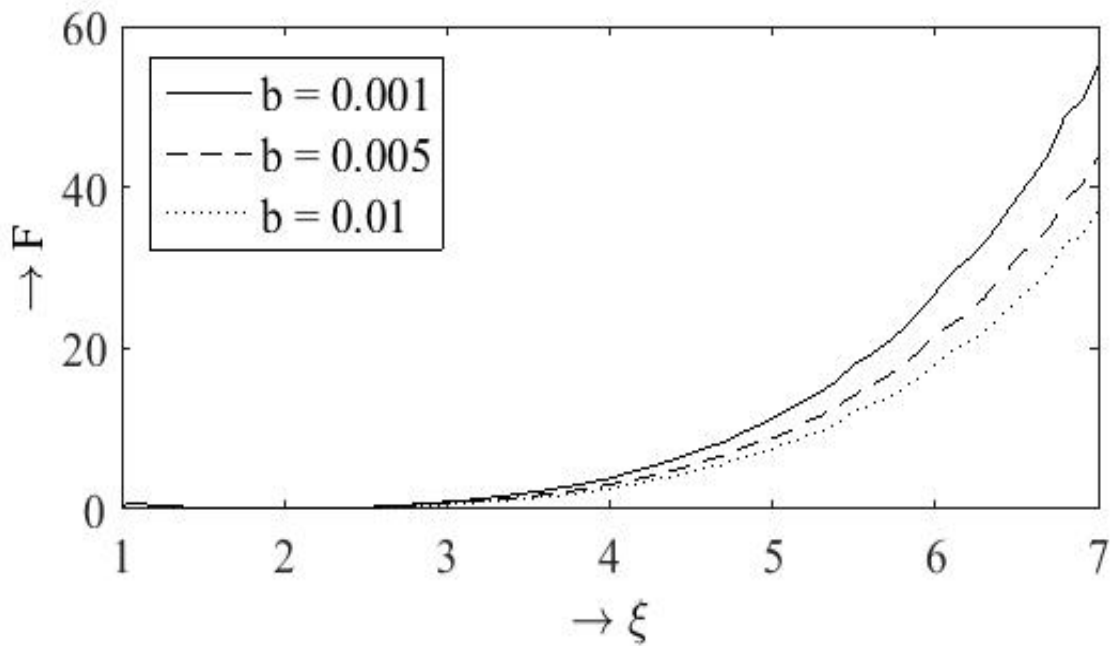


Figure 6.10(c). Pressure profiles for van der Waals EOS when $\gamma = 1.4$, $K = 0.00349$ and $a = 0.0025$

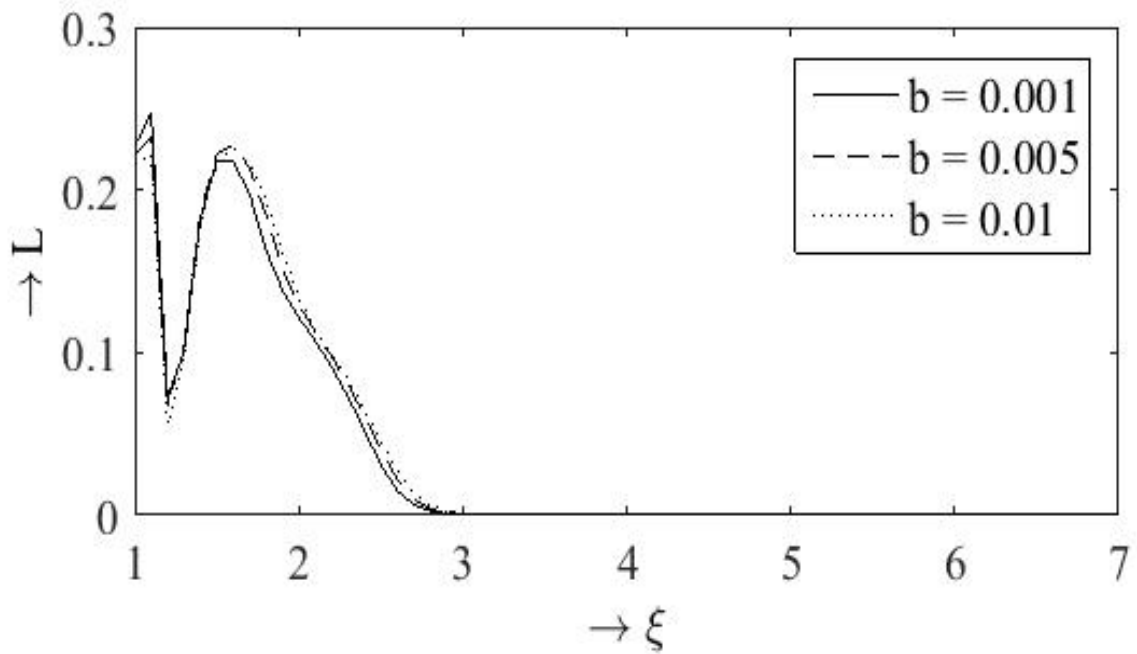


Figure 6.10(d). Magnetic pressure profiles for van der Waals EOS when $\gamma = 1.4$, $K = 0.00349$ and $a = 0.0025$

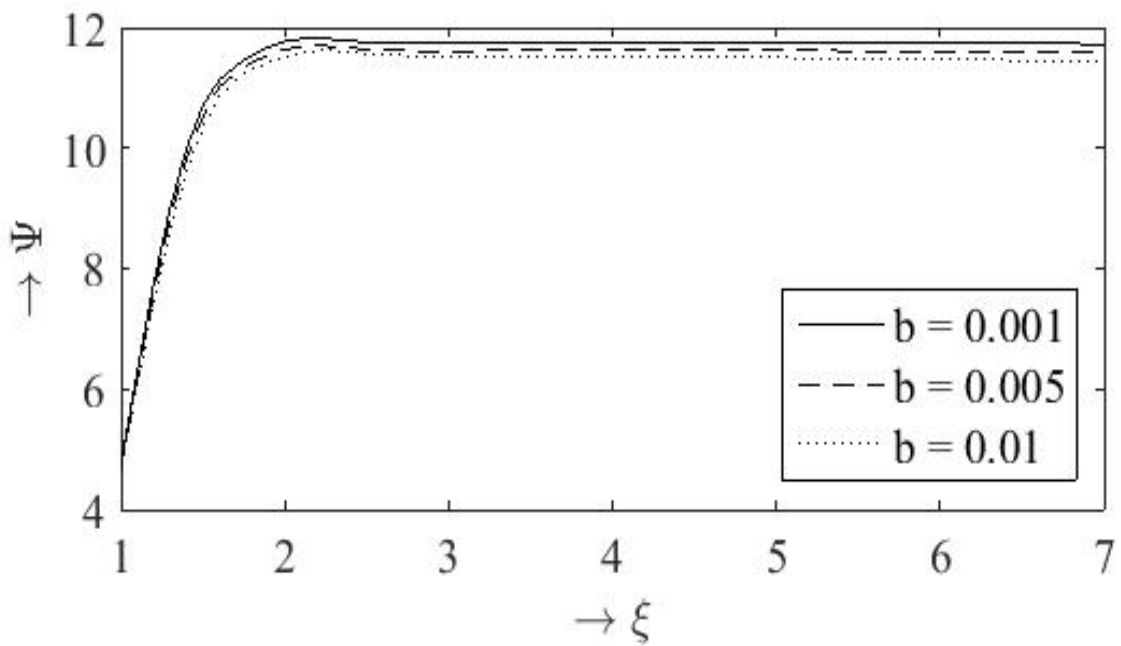


Figure 6.11(a). Density profiles for van der Waals EOS when $\gamma = 1.4$, $K = 0.0349$ and $a = 0.0025$

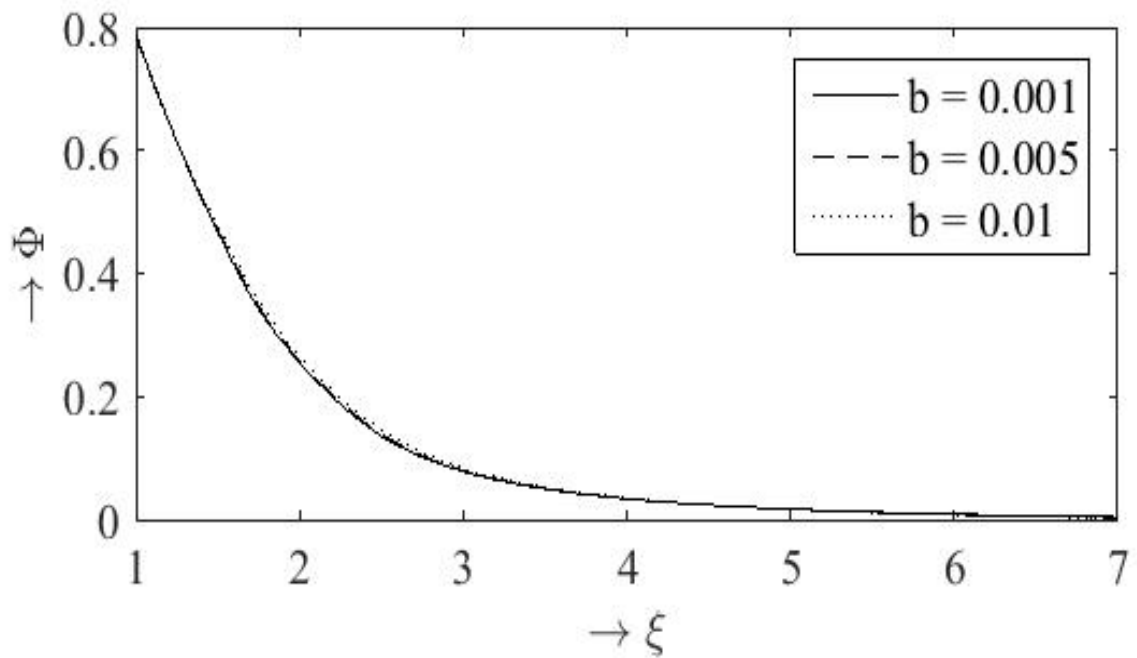


Figure 6.11(b). Velocity profiles for van der Waals EOS when $\gamma = 1.4$, $K = 0.0349$ and $a = 0.0025$

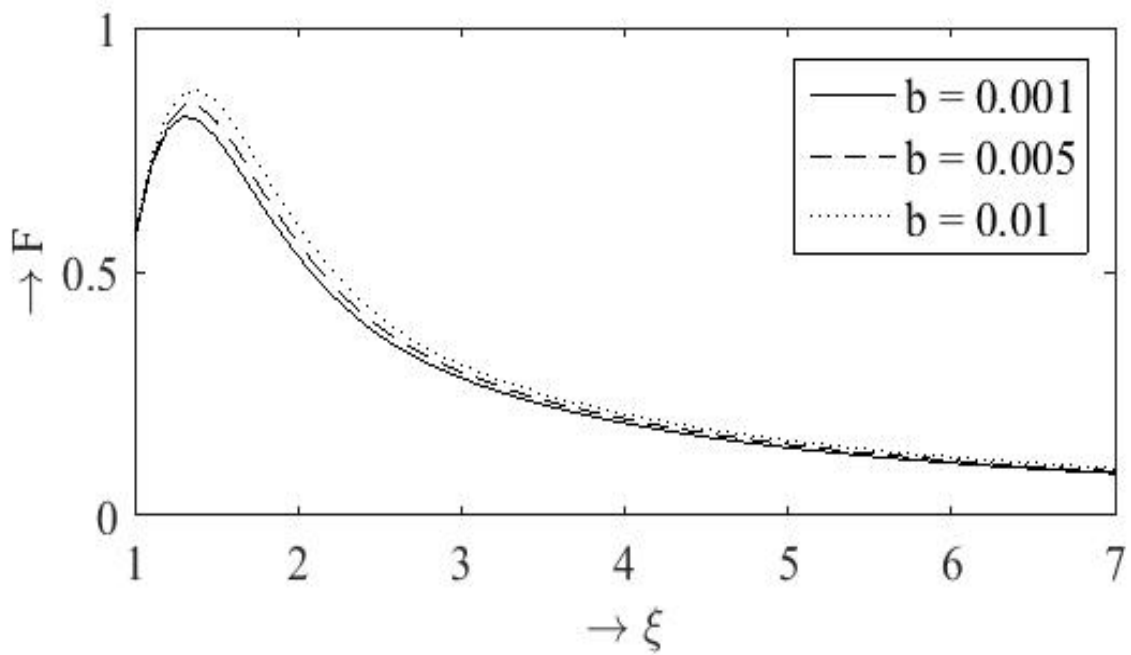


Figure 6.11(c). Pressure profiles for van der Waals EOS when $\gamma = 1.4$, $K = 0.0349$ and $a = 0.0025$

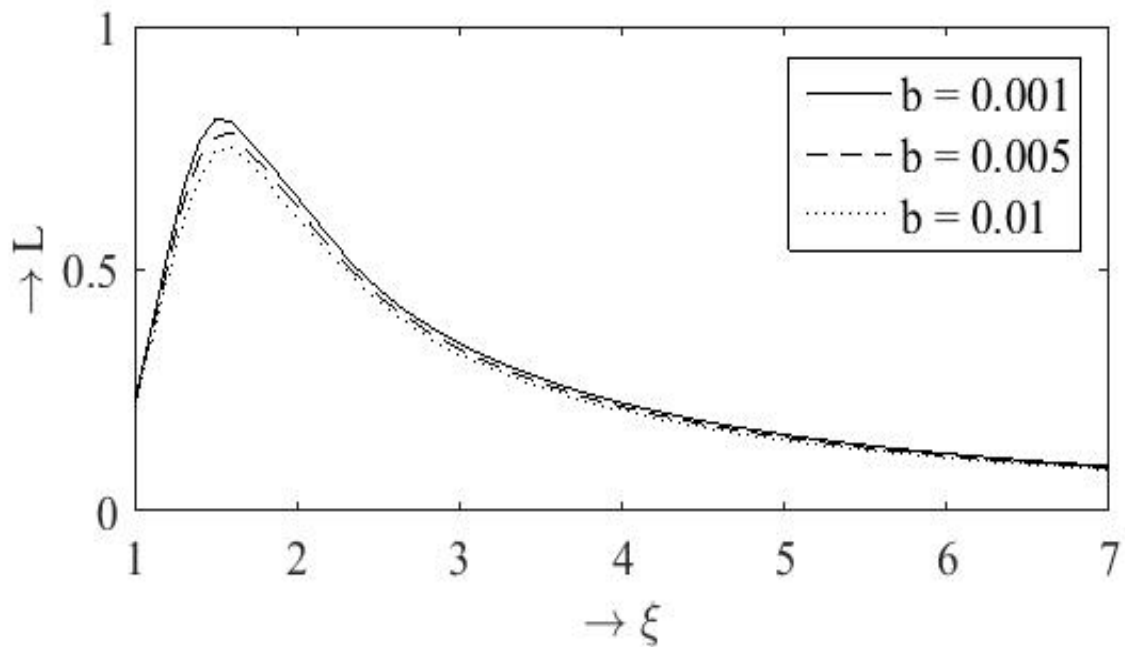


Figure 6.11(d). Magnetic pressure profiles for van der Waals EOS when $\gamma = 1.4$, $K = 0.0349$ and $a = 0.0025$

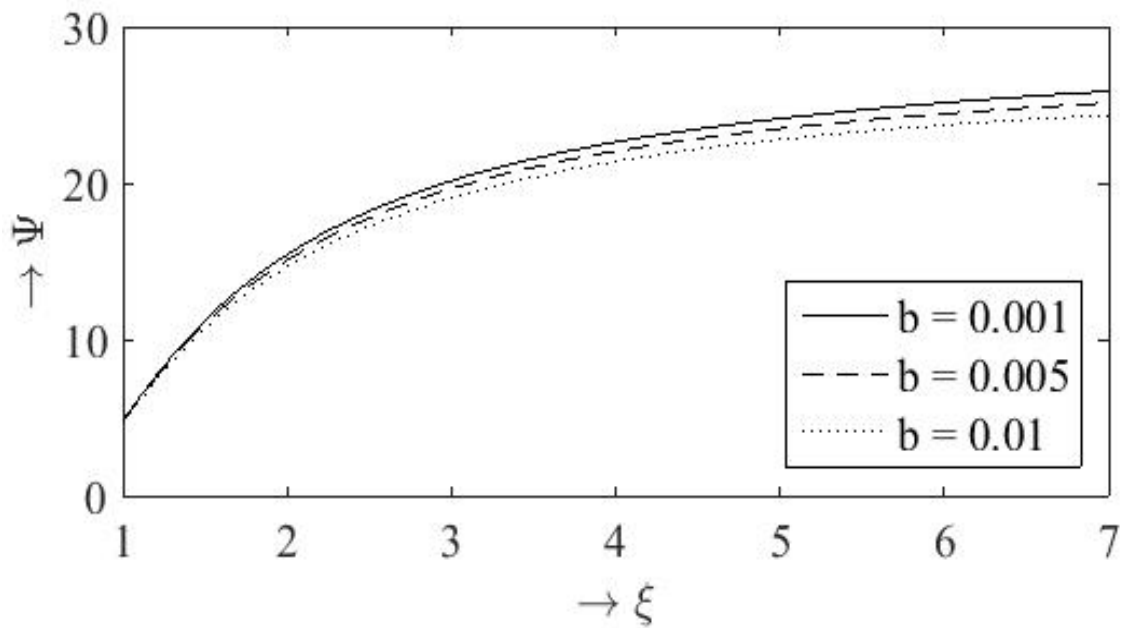


Figure 6.12(a). Density profiles for van der Waals EOS when $\gamma = 1.4$, $K = 0.349$ and $a = 0.0025$

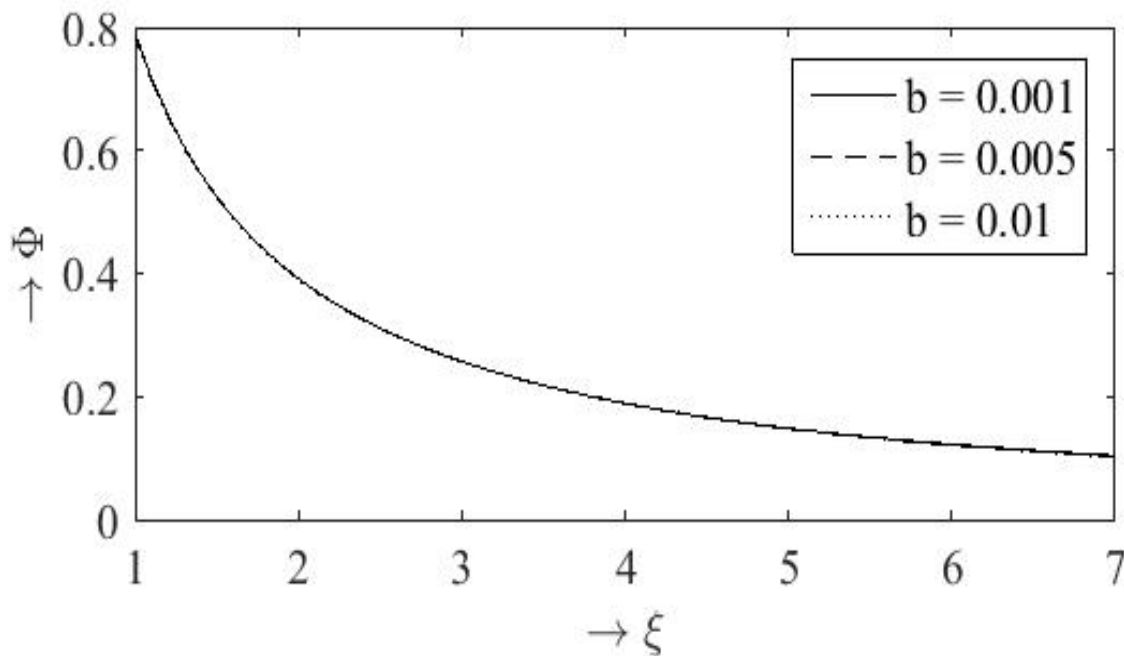


Figure 6.12(b). Velocity profiles for van der Waals EOS when $\gamma = 1.4$, $K = 0.349$ and $a = 0.0025$

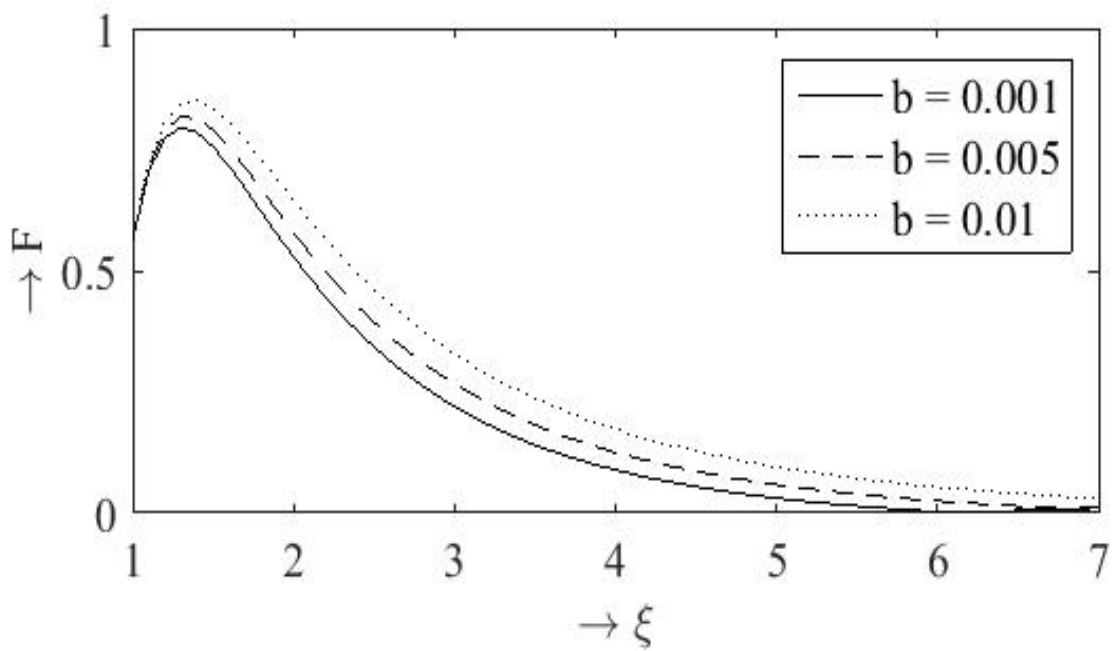


Figure 6.12(c). Pressure profiles for van der Waals EOS when $\gamma = 1.4$, $K = 0.349$ and $a = 0.0025$

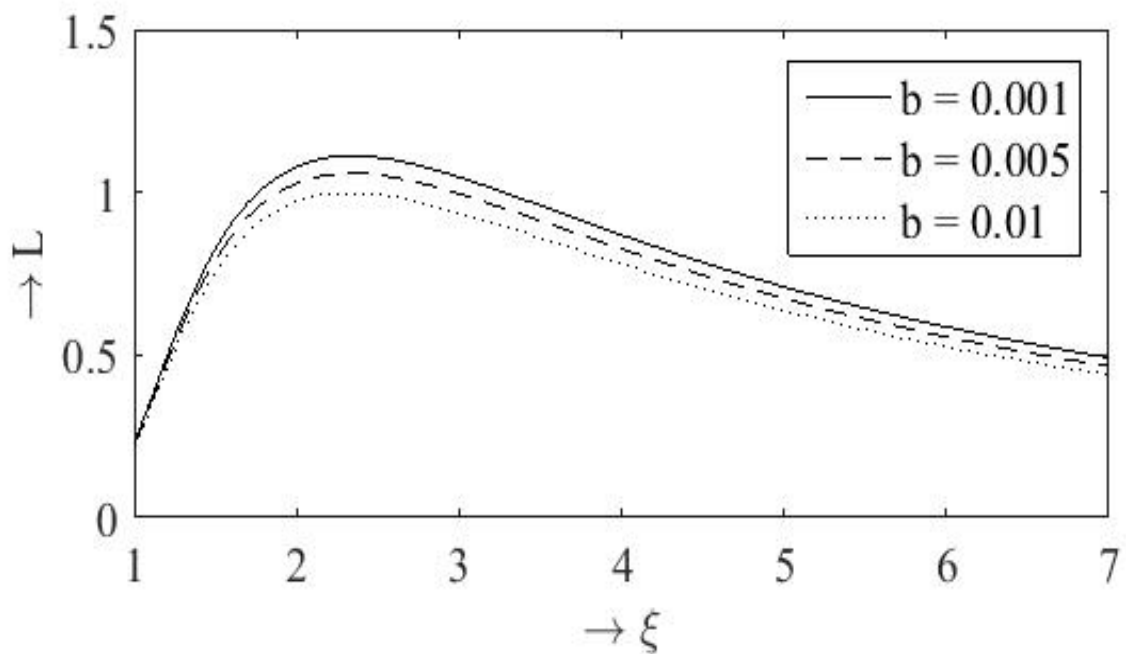


Figure 6.12(d). Magnetic pressure profiles for van der Waals EOS when $\gamma = 1.4$, $K = 0.349$ and $a = 0.0025$

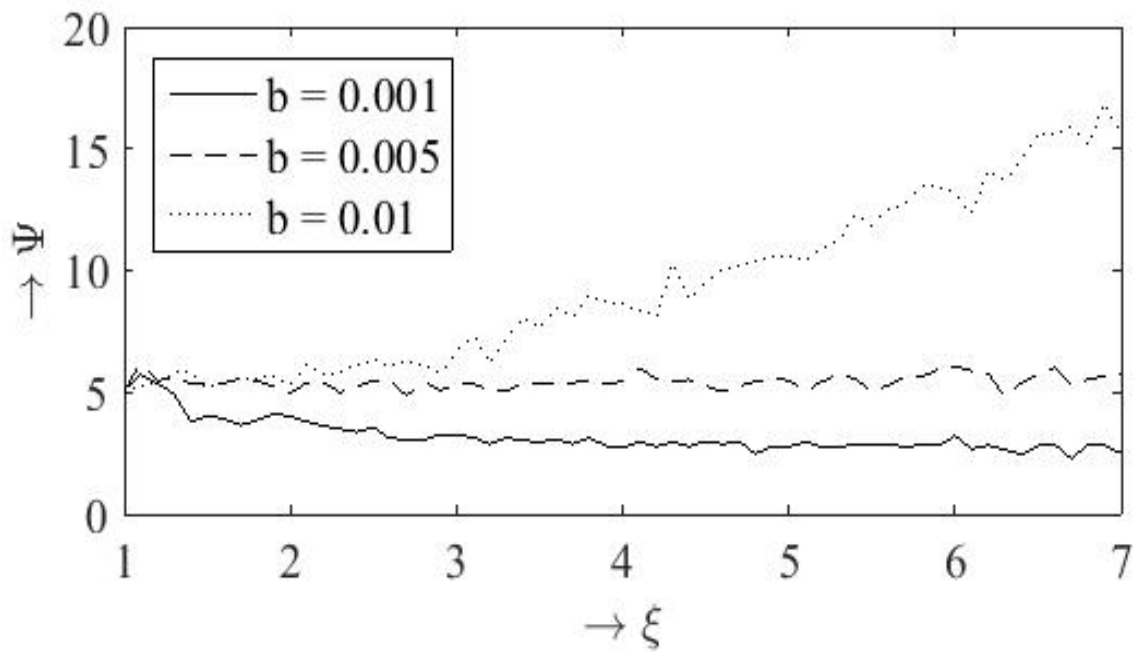


Figure 6.13(a). Density profiles for van der Waals EOS when $\gamma = 1.4$, $K = 0$ and $a = 0.0075$

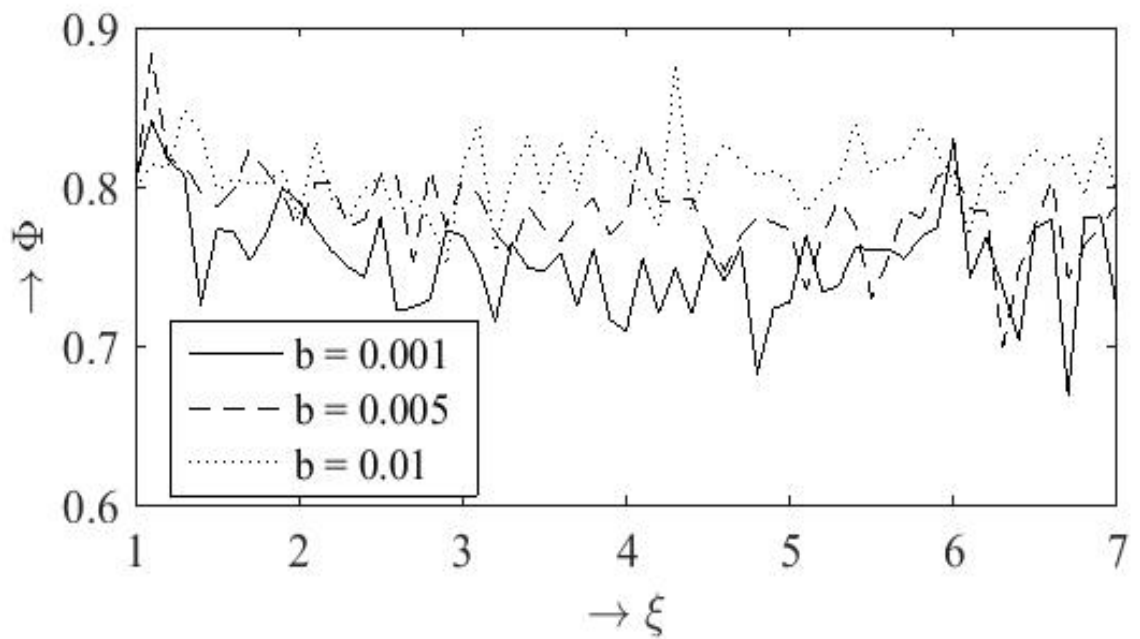


Figure 6.13(b). Velocity profiles for van der Waals EOS when $\gamma = 1.4$, $K = 0$ and $a = 0.0075$

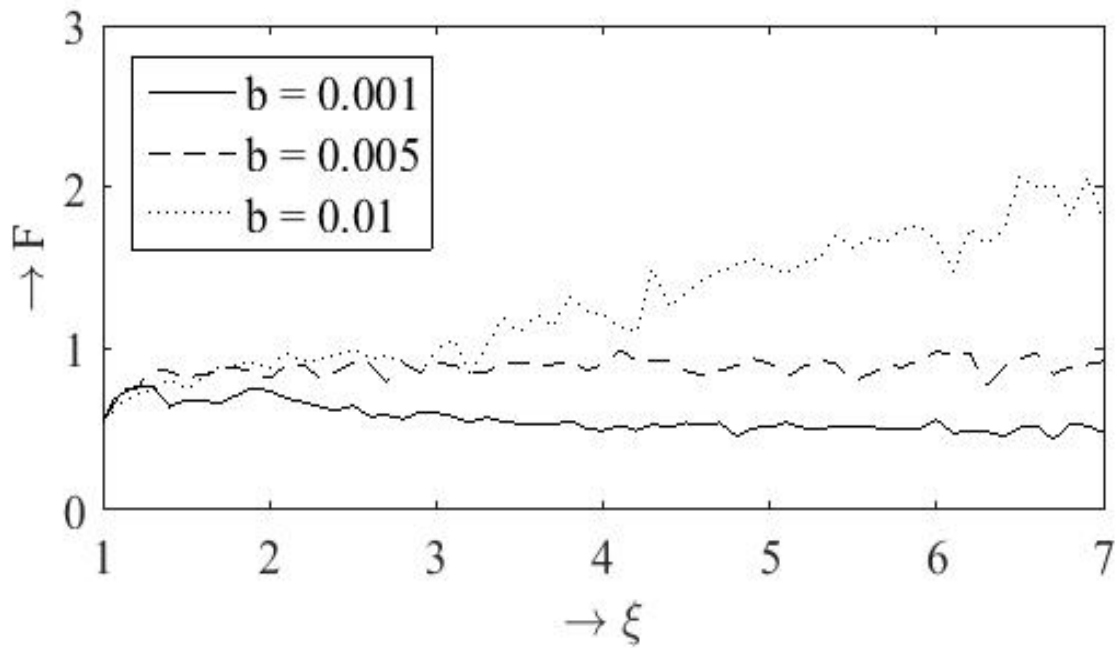


Figure 6.13(c). Pressure profiles for van der Waals EOS when $\gamma = 1.4$, $K = 0$ and $a = 0.0075$

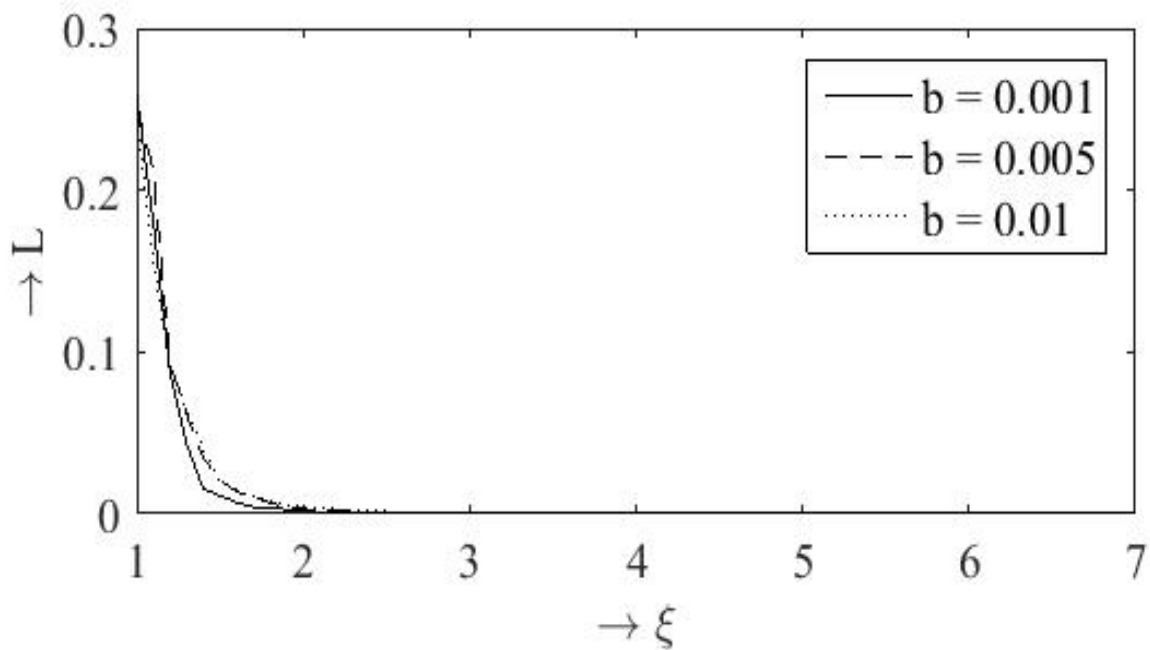


Figure 6.13(d). Magnetic pressure profiles for van der Waals EOS when $\gamma = 1.4$, $K = 0$ and $a = 0.0075$

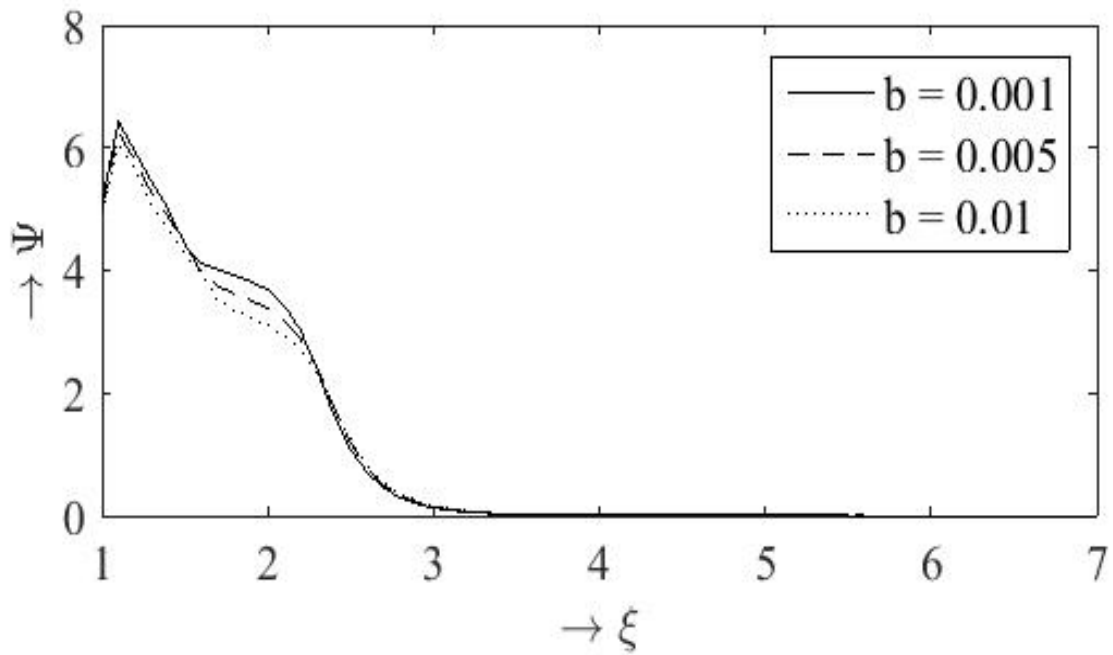


Figure 6.14(a). Density profiles for van der Waals EOS when $\gamma = 1.4$, $K = 0.00349$ and $a = 0.0075$

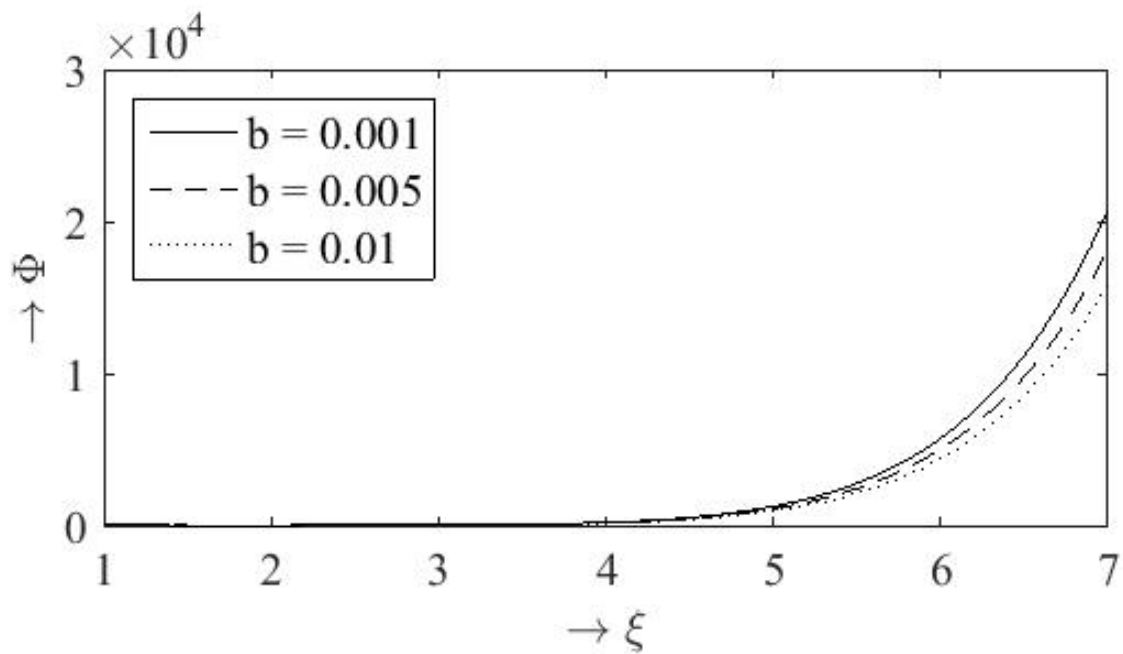


Figure 6.14(b). Velocity profiles for van der Waals EOS when $\gamma = 1.4$, $K = 0.00349$ and $a = 0.0075$

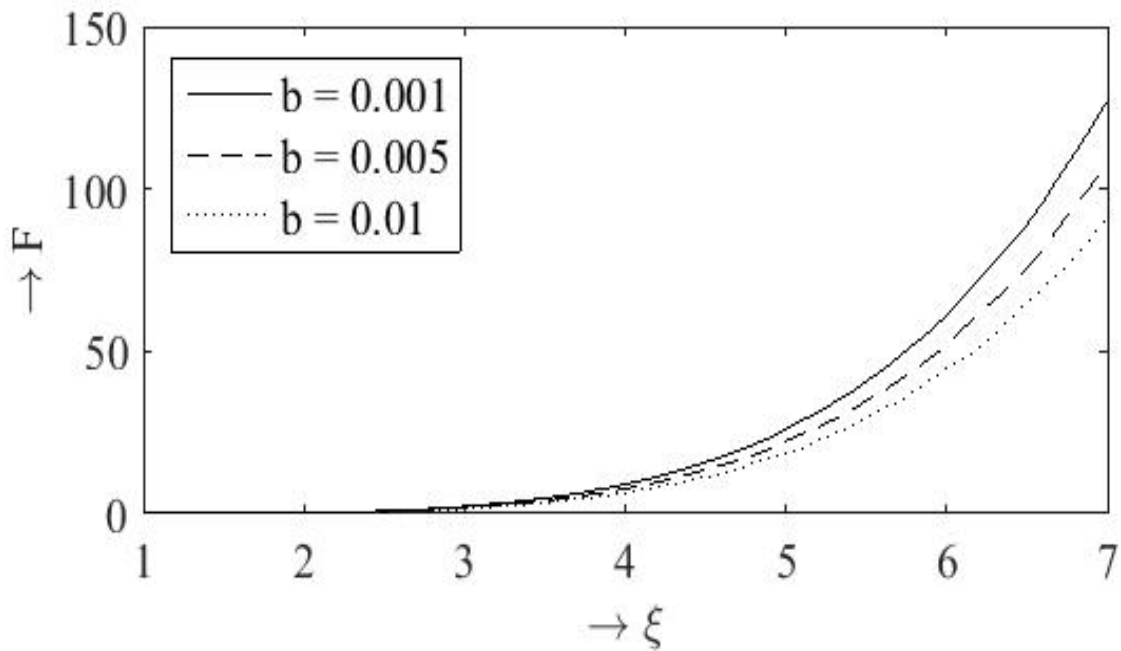


Figure 6.14(c). Pressure profiles for van der Waals EOS when $\gamma = 1.4$, $K = 0.00349$ and $a = 0.0075$

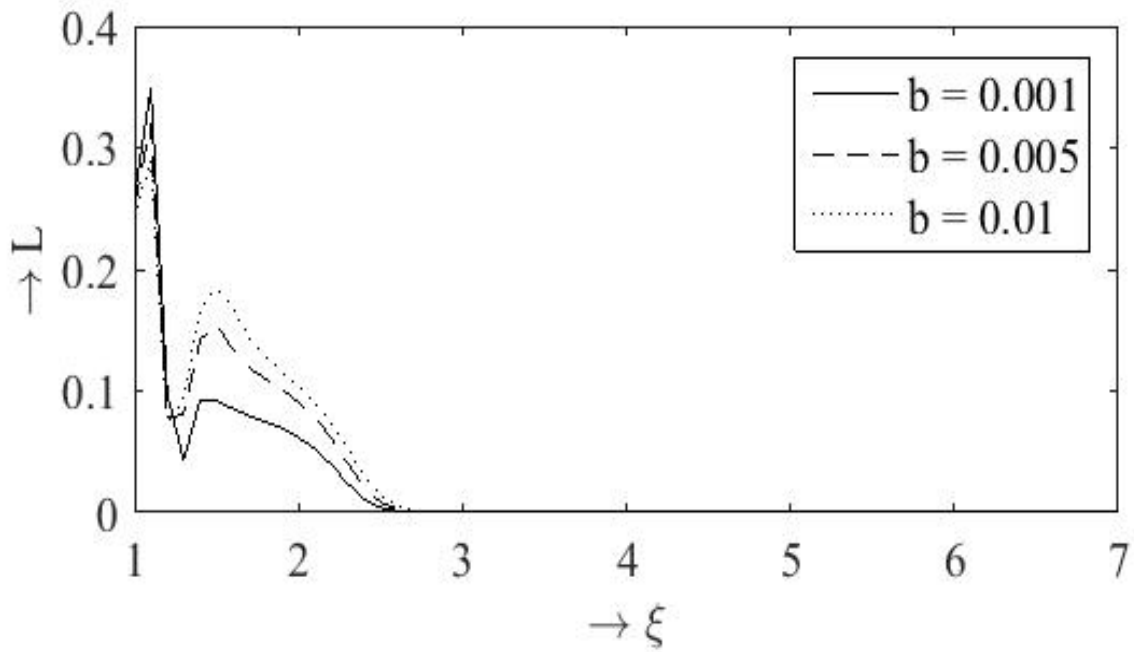


Figure 6.14(d). Magnetic pressure profiles for van der Waals EOS when $\gamma = 1.4$, $K = 0.00349$ and $a = 0.0075$

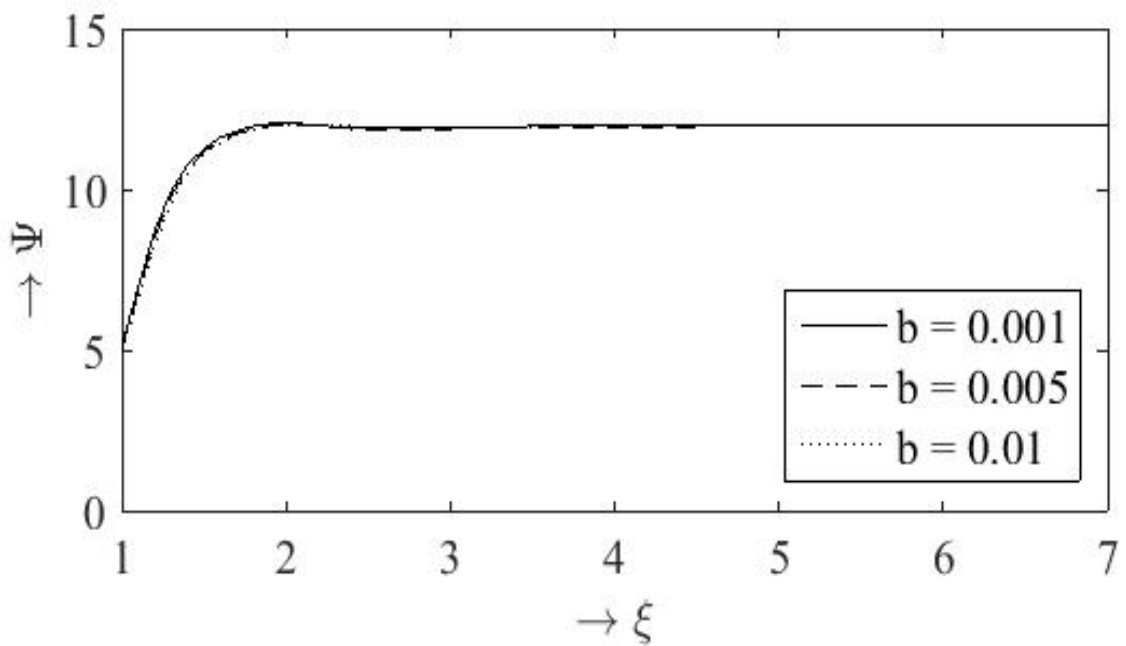


Figure 6.15(a). Density profiles for van der Waals EOS when $\gamma = 1.4$, $K = 0.0349$ and $a = 0.0075$

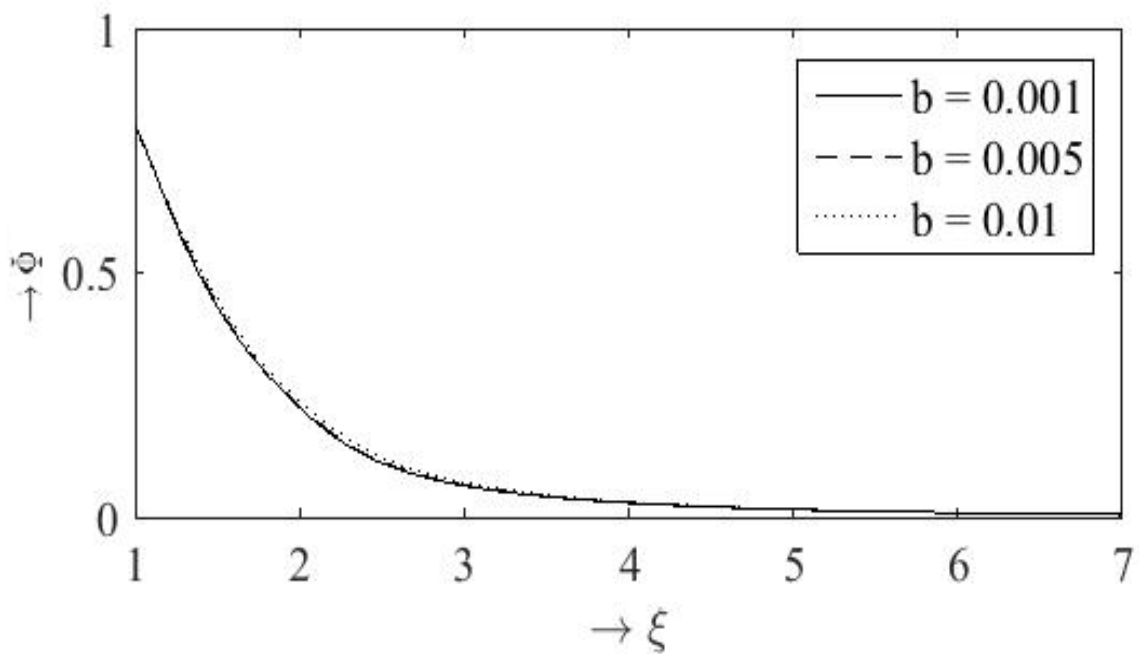


Figure 6.15(b). Velocity profiles for van der Waals EOS when $\gamma = 1.4$, $K = 0.0349$ and $a = 0.0075$

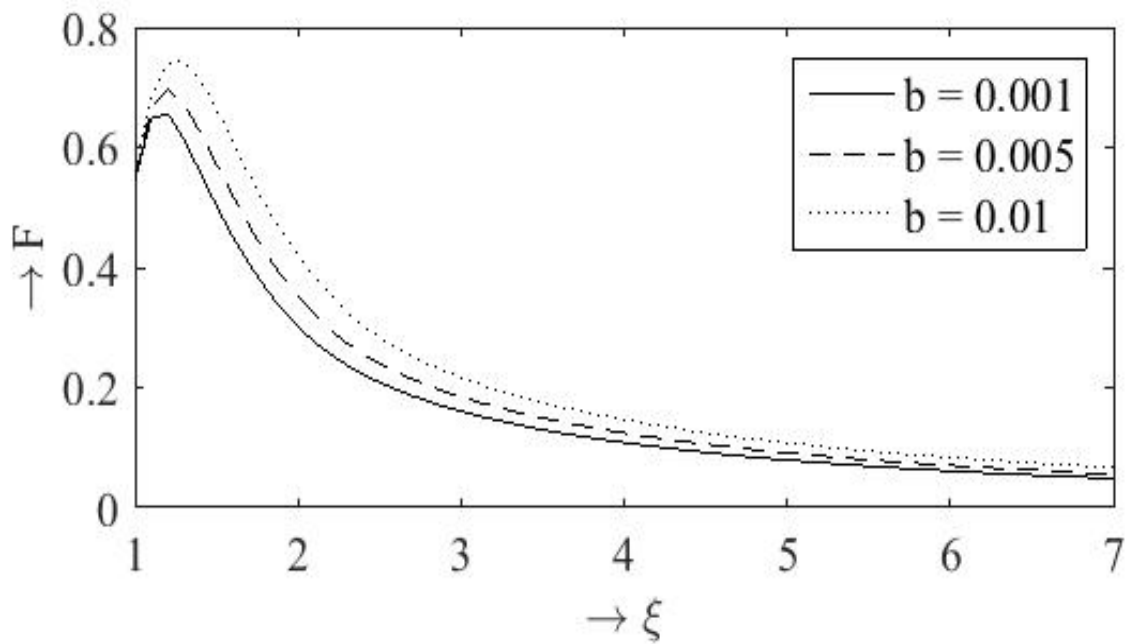


Figure 6.15(c). Pressure profiles for van der Waals EOS when $\gamma = 1.4$, $K = 0.0349$ and $a = 0.0075$

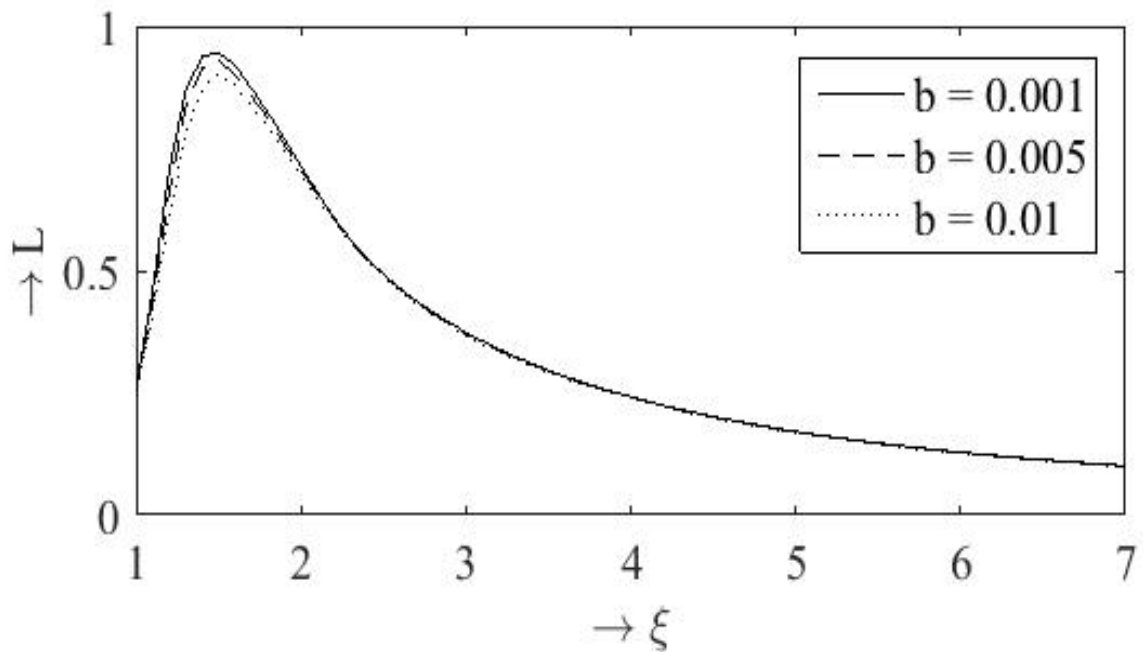


Figure 6.15(d). Magnetic pressure profiles for van der Waals EOS when $\gamma = 1.4$, $K = 0.0349$ and $a = 0.0075$

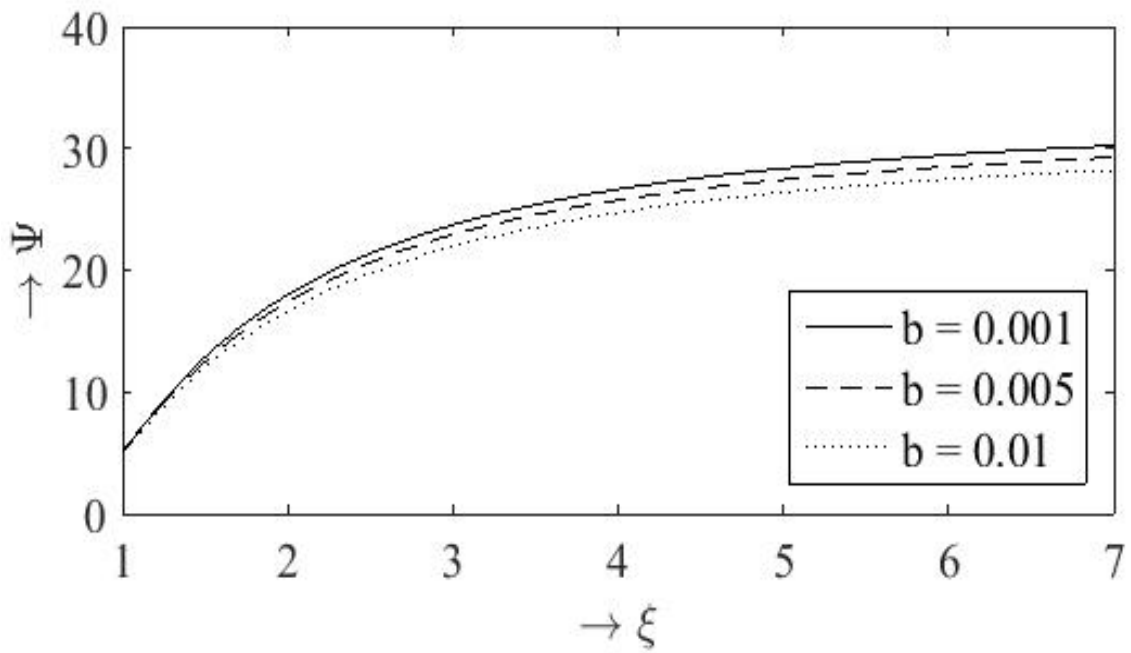


Figure 6.16(a). Density profiles for van der Waals EOS when $\gamma = 1.4$, $K = 0.349$ and $a = 0.0075$

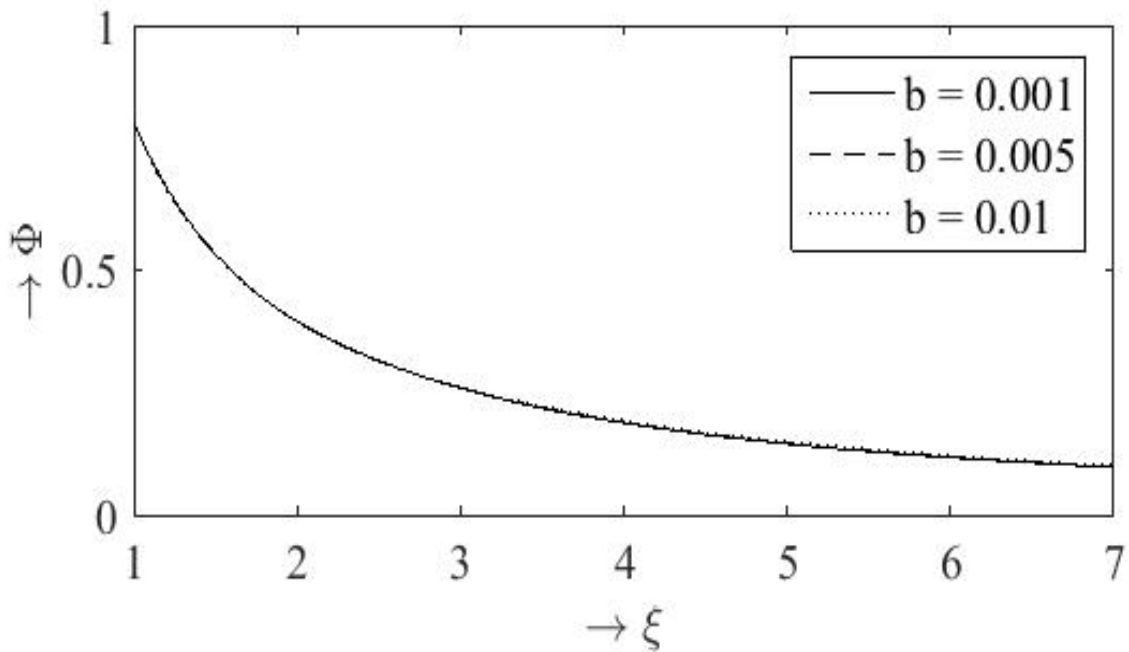


Figure 6.16(b). Velocity profiles for van der Waals EOS when $\gamma = 1.4$, $K = 0.349$ and $a = 0.0075$

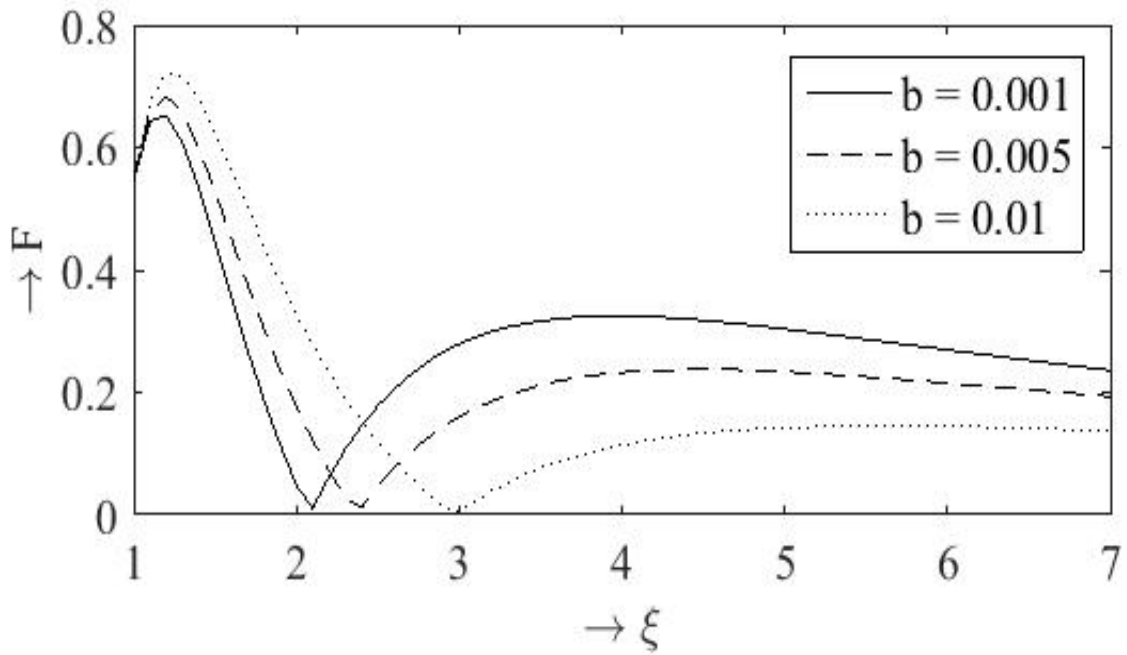


Figure 6.16(c). Pressure profiles for van der Waals EOS when $\gamma = 1.4$, $K = 0.349$ and $a = 0.0075$

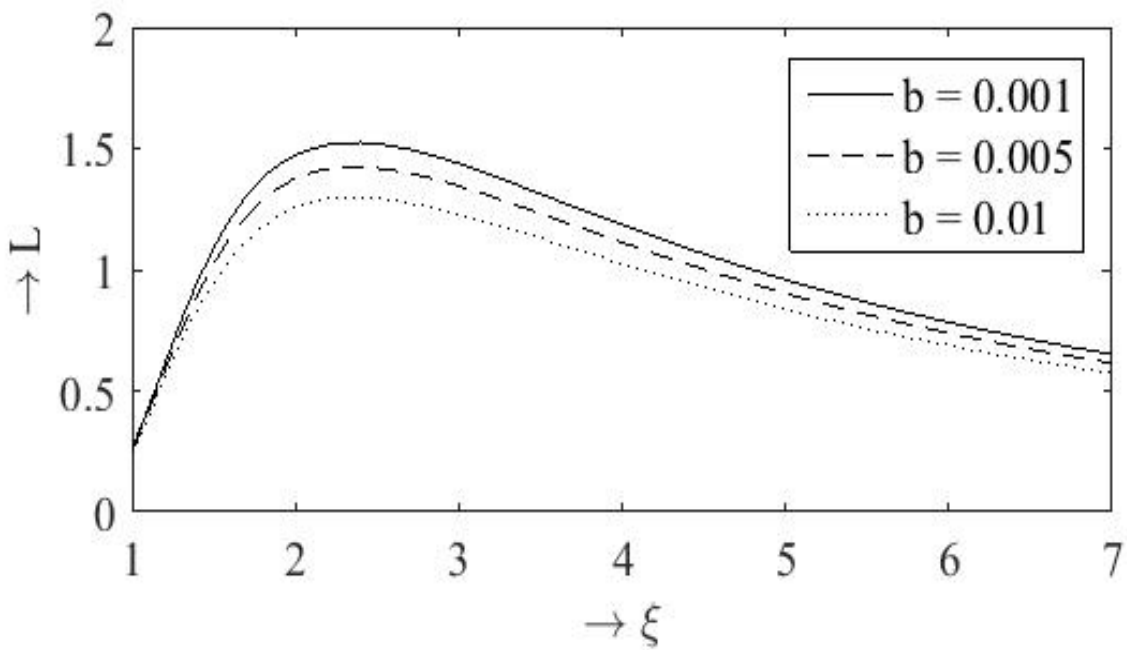


Figure 6.16(d). Magnetic pressure profiles for van der Waals EOS when $\gamma = 1.4$, $K = 0.349$ and $a = 0.0075$

Chapter-7

Self-Similar Motion of Strong Converging Cylindrical and Spherical Shock Waves in Non-ideal Stellar Medium

7.1 Introduction

Shock processes occurs naturally in various processes which are related to hydrodynamics, astrophysical situations such as supernova explosions, photo-ionized gas, stellar winds, interstellar gas etc. They are considered to be discontinuities in mathematical point of view but shock wave is not a true physical discontinuity. The study of converging spherical and cylindrical shock waves in non-ideal stellar atmosphere under the action of monochromatic radiation is of importance because of its applications in the areas of nuclear engineering, cavitation, astrophysics, radioactively driven outflows, stellar convection, and inertial confinement fusion. The theory of radiation hydrodynamics plays an important role in studying phenomena in plasma physics. These shock fronts have a more complex structure than ordinary hydrodynamical shocks. In recent years, the problems of high-temperature gas dynamics have attracted much attention. The high temperatures generated in gases by shock waves give rise to physical and chemical phenomena such as molecular vibrational excitation, dissociation, ionization, chemical reactions, and inherently

related radiation. In continuum regime, these processes start from the wave front, so that generally the gaseous media behind the shock waves may be in thermodynamic and chemical non-equilibrium state. In the flow field of a gas at very high temperatures, the gas may be ionized and the radiation transfer is important. In classical gas dynamics the transfer of radiation is usually neglected, however, when the temperature of the gas is high, radiation can be considered as an important mode of energy transport. The gas temperature behind such a shock could depart strongly from that predicted by the standard Rankine-Hugoniot law.

Gail et al. [46] discussed applications to weak and strong shocks in a stellar atmosphere due to a shock wave trains. The effect of non-linear interactions of one dimensional adiabatic or isothermal hydrodynamic shock waves in the solar atmosphere have been studied by Fleck and Schmitz [47]. Barnwal and Srivastava [48] have investigated the general Rankine-Hugoniot jump relations for a 3-dimensional shock in dusty gas in the presence of radiation. Several authors [5, 49, 108-111] studied the shock wave problem with thermal radiation by similarity method in perfect gas. Marshak [112] studied the effect of radiation on the shock propagation by introducing the radiation diffusion approximation. Elliott [108] discussed the conditions leading to self-similarity with a specified functional form of the mean free-path of radiation and obtained a solution for self-similar explosion. Hirschler and Gretler [113] studied similarity solutions of converging spherical shock wave with radiation effect by assuming medium to be optically

thick. Khudyakov [114] discussed the self-similar problem of motion of a gas under the action of monochromatic radiation.

In recent times considerable study for the self-similar solutions in the process occurring under the action of monochromatic radiation of gaseous substances in the stellar regions has gained importance. Several problems relating to shock wave propagation in perfect gas and non-ideal gas with radiative and magneto hydrodynamic effects have been studied by Zedan [115], Leygnac et al. [116], Sampaio [117], Taylor and Ryan [118]. All the work is under the assumption that the medium in an astrophysical environment is ideal gas. This may not be true in reality and it is necessary to analyze the gas dynamic processes in a non-ideal medium with monochromatic radiation.

In the present problem a model to determine the self-similar solutions for converging spherical and cylindrical strong shock waves in stellar atmosphere under the action of monochromatic radiation in non-uniform stellar interiors with constant intensity on a unit area. It is assumed that the medium into which propagation takes place to be a non-ideal gas. Shock is assumed to be strong and obeys a power law. It is assumed that the radiation flux moves through the gas with constant intensity on a unit area of the shock wave propagation in a direction opposite to the radiation flux. The medium of flow is assumed to be obeying the EOS of Mie-Gruneisen type i.e., Royce EOS [57]. The perfect gas EOS results

too are obtained from Royce EOS as a special case, and were found to match very closely with the literature.

7.2 Formulation of the Problem

The basic equations for one-dimensional unsteady motion of cylindrical and spherical strong converging shock waves into the radiation hydrodynamic regime with the medium neglecting viscosity, heat conduction, and magnetic field characterized by the EOS of Mie-Gruneisen type can be written in Eulerian form [94, 111]

$$\frac{D\rho}{Dt} + \rho(\nabla \cdot u) + (\Omega - 1) \frac{\rho u}{r} = 0 \quad (7.1)$$

$$\frac{Du}{Dt} + \frac{1}{\rho} \nabla p = 0 \quad (7.2)$$

$$\frac{De}{Dt} - \frac{p}{\rho} \frac{D}{Dt} \left[\ln \left(\frac{\rho}{\rho_0} \right) \right] + \frac{1}{\rho r} \nabla(jr) = 0 \quad (7.3)$$

$$\nabla j = Kj \quad (7.4)$$

where $\frac{D}{Dt} = \frac{\partial}{\partial t} + (u \cdot \nabla)$ is the substantial derivative, which is the sum of local and convective derivatives. $\Omega = 2, 3$ denote the cylindrical and spherical cases of the shock waves respectively. $\rho, \rho_0, u, p, e, j, K$ denote the density of gas, density of unperturbed medium, velocity of gas particles, pressure, SIE per unit mass of volume, the flux of monochromatic radiation per unit area at radial distance r from the axis at time t and absorption coefficient respectively.

The EOS under equilibrium condition is of Mie-Gruneisen type [57, 92, 119]

$$e = \frac{p}{\rho \Gamma(\rho/\rho_0)} \quad (7.5)$$

where

$\Gamma(\rho/\rho_0)$ is the Gruneisen coefficient.

The above governing equations (7.1-7.4) can be written in matrix equation as follows

$$F_t + AF_r + B = 0 \quad (7.6)$$

where F , A , and B are given by

$$F = \begin{bmatrix} \rho \\ u \\ e \\ 0 \end{bmatrix}, \quad A = \begin{bmatrix} u & \rho & 0 & 0 \\ 0 & u & 1/\rho & 1/\rho \\ 0 & p/\rho & u & 1/\rho \\ 0 & 0 & 0 & 1 \end{bmatrix}, \quad \text{and} \quad B = \begin{bmatrix} \frac{(\Omega-1)\rho u}{r} \\ 0 \\ \frac{(\Omega-1)pu}{\rho r} + \frac{j}{\rho r} \\ -Kj \end{bmatrix}$$

F_t and F_r are partial derivatives with respect to time t and spacial coordinate r .

The absorption coefficient K is considered to vary as [114]

$$K = K_0 \rho^n p^m j^q r^s t^l \quad (7.7)$$

where the numbers n , m , q , s , l are rational exponents and

$$[K_0] = M^{-n-m-q} L^{3n+m-s} T^{2m+3q-l} \quad (7.8)$$

for the present problem, the quantities p_0 , ρ_0 , j_0 , and K_0 are dimensional constants, in which p_0 , ρ_0 , and j_0 are dependent given by

$$j_0 = [p_0]^{3/2} [\rho_0]^{-1/2} \quad (7.9)$$

The radiation absorption coefficient K depends on dimensions of j_0 , ρ_0 , which is equivalent $s + l = -1$.

7.2.1 Rankine-Hugoniot relations

The jump conditions across a shock wave propagating in an electrically conducting and radiating gas are given by Ramu et al. [92] and Narsimhulu et al. [119]

$$[(u - W)\rho]_1^2 = 0 \quad (7.10)$$

$$[p + \rho u^2]_1^2 = 0 \quad (7.11)$$

$$\left[e + \frac{p}{\rho} + \frac{1}{2}(u - W)^2 \right]_1^2 = 0 \quad (7.12)$$

$$[j]_1^2 = 0 \quad (7.13)$$

where the symbol $[...]_1^2$ represents the difference between the values of ahead upstream and behind downstream regions across shock wave respectively and W represents the scale of velocity. We assume that shock is propagating into a non-ideal stellar medium at rest with gas density varying as the power law given by Ramu and Rangarao [57],

$$R_s(t) = \mathring{A}(-t)^\alpha \quad (7.14)$$

where the function $R_s(t)$ is the time-dependent radius of the shock wave, \mathring{A} is proportionality constant and α is similarity exponent. It is assumed that the radiation pressure and radiation energy are very small in comparison to the material pressure and energy, hence neglected. For the case of strong shocks, the upstream medium can be approximated as a cold fluid ($T \sim 0$). The upstream pressure can therefore be neglected in comparison to other quantities appearing

in the Rankine-Hugoniot jump conditions (7.10-7.13). Setting $p_1 = 0$, $u_1 = 0$ in the above equations, Rankine-Hugoniot jump conditions become

$$\frac{\rho_2}{\rho_1} = \beta^{-1} \quad (7.15)$$

$$u_2 = (1 - \beta)W \quad (7.16)$$

$$p_2 = \rho_1(1 - \beta)W^2 \quad (7.17)$$

$$e_2 = \frac{1}{2}(1 - \beta)^2W^2 \quad (7.18)$$

$$j_1 = j_0 \quad (7.19)$$

where β is the shock density ratio and its magnitude is dependent on the EOS and $W = \frac{dR_s}{dt}$. The effect of ionization, dissociation, and the interaction with radiation become important on the Rankine-Hugoniot jump relations when the shock is strong. Along with the strong shock relations (7.15-7.19) and the EOS (7.5), we get

$$(\beta - 1)\Gamma(\beta) = 2 \quad (7.20)$$

7.2.2 One-dimensional self-similar motion

The basic equations are non-dimensionalized by using dimensionless functions of the similarity variable λ [7, 57, 92] are

$$\rho = \rho_0 g(\lambda) \quad (7.21.a)$$

$$u = v(\lambda)W \quad (7.21.b)$$

$$p = \rho_0 W^2 \pi(\lambda) \quad (7.21.c)$$

$$j = j_0 \psi(\lambda) \quad (7.21.d)$$

where g , v , π , and ψ are non-dimensional density, velocity, pressure, and radiation flux of similarity variable λ respectively. For computational convenience, we consider another set of transformations along with the above transformations as

$$g(\lambda) = G(\lambda) \quad (7.22.a)$$

$$v(\lambda) = \frac{\lambda}{\alpha} U(\lambda) \quad (7.22.b)$$

$$\pi(\lambda) = \frac{\lambda^2}{\alpha^2} P(\lambda) \quad (7.22.c)$$

$$\psi(\lambda) = J(\lambda) \quad (7.22.d)$$

and $Y(\lambda) = P(\lambda)/G(\lambda)$, where G , U , P , and J are new reduced density, velocity, pressure, and radiation flux functions in terms of similarity variable λ respectively.

Applying the similarity transformations, the equations of motion take the form

$$\frac{(U-\alpha)}{G} \frac{dG}{d\lambda} + \frac{dU}{d\lambda} + \frac{\Omega U}{\lambda} = 0 \quad (7.23)$$

$$\frac{1}{G} \frac{dG}{d\lambda} + (U - \alpha) \frac{dU}{d\lambda} + \frac{dY}{d\lambda} + \frac{1}{\lambda} [2Y + U(U - 1)] = 0 \quad (7.24)$$

$$\frac{Y\Phi(G)}{G} \frac{dG}{d\lambda} + \frac{dY}{d\lambda} + \left[\frac{2(U-1)Y}{\lambda(U-\alpha)} + \frac{\alpha^3 \Gamma(G)(U-1)YJ}{(U-\alpha)^2 R^3 \lambda^4 \rho_0 G(J'+1)} \right] = 0 \quad (7.25)$$

$$\frac{dJ}{d\lambda} - \alpha \lambda^s G^n P^m J^{q+1} = 0 \quad (7.26)$$

where

$$\Phi(G) = -\Gamma(G) - \frac{G}{\Gamma(G)} \frac{d\Gamma(G)}{dG} \quad \text{and} \quad 1 - \Phi(G) = \sigma \quad (7.27)$$

where σ is the material property. At the shock front, the boundary conditions (7.15-7.19) are transformed into the following form

$$G(1) = \frac{1}{\beta} \quad (7.28)$$

$$U(1) = (1 - \beta)\alpha \quad (7.29)$$

$$P(1) = \beta(1 - \beta)\alpha^2 \quad (7.30)$$

$$J(1) = 1 \quad (7.31)$$

7.3 Numerical Solution

7.3.1 Finite difference formulation

An explicit finite difference method is employed in solving system of equations (7.23-7.26). The solution domain (Figure 7.1) is discretized by a one-dimensional set of discrete grid points, with the grid points equally spaced having uniform spacing $\Delta\lambda$.

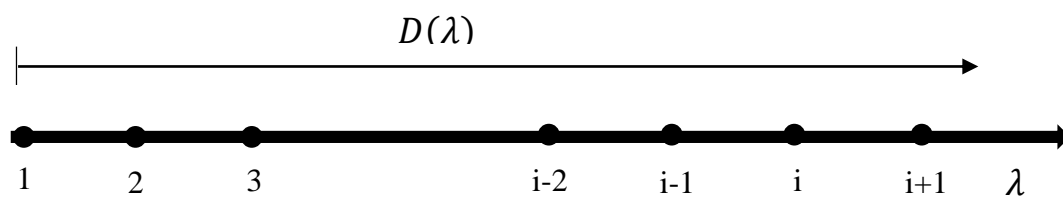


Figure 7.1. Solution domain $D(\lambda)$ and discrete finite difference

The finite difference approximations of the transformed system of equations (7.23-7.26) are given by

$$\frac{dG}{d\lambda} = \frac{G_{i+1} - G_i}{\Delta\lambda} \quad (7.32)$$

$$\frac{dU}{d\lambda} = \frac{U_{i+1} - U_i}{\Delta\lambda} \quad (7.33)$$

$$\frac{dY}{d\lambda} = \frac{Y_{i+1} - Y_i}{\Delta\lambda} \quad (7.34)$$

$$\frac{dJ}{d\lambda} = \frac{J_{i+1} - J_i}{\Delta\lambda} \quad (7.35)$$

Substituting equations (7.32-7.35) into equations (7.23-7.26) the resulting system of equations can be written in the following matrix form,

$$[C_i][X_{i+1}] = [D_i] \quad (7.36)$$

where $[C_i]$, $[X_{i+1}]$, and $[D_i]$ are 4x4, 4x1 and 4x1 matrices respectively.

$$[C_i] = \begin{bmatrix} (U_i - \alpha) & G_i & 0 & 0 \\ 1 & G_i(U_i - \alpha) & G_i & 0 \\ Y_i\Phi(G_i)/G_i & 0 & 1 & 0 \\ 0 & 0 & 0 & 1 \end{bmatrix} \quad (7.37)$$

$$[X_{i+1}] = [G_{i+1} \quad U_{i+1} \quad Y_{i+1} \quad J_{i+1}]^T \quad (7.38)$$

and

$$[D_i] = \begin{bmatrix} \left(2 - \frac{h\Omega}{\lambda_i}\right) G_i U_i - \alpha G_i \\ \left(1 - \frac{2h}{\lambda_i}\right) G_i Y_i - \frac{h}{\lambda_i} G_i U_i (U_i - 1) + G_i U_i (U_i - \alpha) + G_i \\ \frac{-h}{\lambda_i} Y_i \left\{ \frac{2(U_i - 1)}{(U_i - \alpha)} + \frac{\alpha^3 J_i (U_i - 1) \Gamma(G_i)}{(U_i - \alpha)^3 R^3 \lambda_i^3 \rho_0 G_i (J_i' + 1)} \right\} + Y_i \{1 + \Phi(G_i)\} \\ h\alpha \lambda_i^s G_i^n P_i^m J_i^{q+1} + J_i \end{bmatrix} \quad (7.39)$$

Crout's reduction technique [93] is employed to evaluate the flow parameters such as density (G_{i+1}), velocity (U_{i+1}), pressure (Y_{i+1}), and radiation flux (J_{i+1}).

where

$$G_{i+1} = \frac{(U_i - \alpha)(D_{11})^{(i)} - (D_{21})^{(i)} + G_i(D_{31})^{(i)}}{[(U_i - \alpha)^2 + Y_i \Phi(G_i) - 1]} \quad (7.40)$$

$$Y_{i+1} = \frac{\{(D_{21})^{(i)} - (U_i - \alpha)(D_{11})^{(i)}\} Y_i \Phi(G_i) + G_i \{(U_i - \alpha)^2 - 1\} (D_{31})^{(i)}}{[(U_i - \alpha)^2 + Y_i \Phi(G_i) - 1] G_i} \quad (7.41)$$

$$U_{i+1} = \frac{\{Y_i \Phi(G_i) - 1\} (D_{11})^{(i)} + (U_i - \alpha) (D_{21})^{(i)} - G_i (U_i - \alpha) (D_{31})^{(i)}}{[(U_i - \alpha)^2 + Y_i \Phi(G_i) - 1] G_i} \quad (7.42)$$

$$J_{i+1} = (D_{41})^{(i)} \quad (7.43)$$

where the superscript i refers to the location in the discretizing continuous solution domain and it is a positive integer. Numerical solution of system of equations (7.40-7.43) along with boundary conditions (7.28-7.31) are obtained for a step size of $h = 10^{-4}$.

7.3.2 Evaluation of $\beta(\rho/\rho_0)$ the measure of shock strength

Considering the EOS of Mie-Gruneisen type [57]:

The Royce EOS defined by

$$\Gamma(G) = \Gamma_0 - b \left(1 - \frac{1}{G}\right) \quad (7.44)$$

where b is constant such that $b > 0$ and Γ_0 is the non-idealness parameter.

Using equation (7.44) in equation (7.20), gives a quadratic expression in terms of β and it can be written as

$$Z(\beta) \equiv (\Gamma_0 - b)\beta^2 + (2b - \Gamma_0 - 2)\beta - b = 0 \quad (7.45)$$

The equation (7.44) reduces to perfect gas EOS when $\Gamma_0 = (\gamma - 1)$, $b = 0$ and along with equation (7.5) which is

$$p(\rho, e) = \rho e(\gamma - 1) \quad (7.46)$$

the measure of shock strength β defined by the following relation

$$\beta = \frac{\gamma+1}{\gamma-1}, \text{ provided } \beta \neq 0 \quad (7.47)$$

Positive roots are only considered in the subsequent computation. The solution curves of the polynomial $Z(\beta)$ for two different values of non-idealness parameter Γ_0 are shown in Figure 7.2. The values of measure of the shock strength β , similarity exponent α along with the known values of non-idealness parameter Γ_0 , adiabatic index γ , and constant parameter b are presented in Tables 7.1 and 7.2 for Royce and perfect gas EOS respectively.

Table 7.1: Selected values of similarity exponent α for Royce EOS

b	$\Gamma_0 = 1.4$		$\Gamma_0 = 2.0$	
	β	α	β	α
0.1	2.49240	0.43013641	2.02598	0.45569195
0.3	2.64843	0.42271081	2.08465	0.45215384
0.5	2.86086	0.41332599	2.15470	0.44806368
0.7	3.17237	0.40085328	2.24035	0.44324870
1.0	4.10850	0.37023692	2.41421	0.43404715

Table 7.2: Selected values of similarity exponent α for perfect gas

γ	β	α
1.2	11.0000	0.24828372
1.4	6.00000	0.32571203
1.6	4.33333	0.3779717
1.8	3.50000	0.41763534
2.0	3.00000	0.44948974

7.3.3 Numerical solution of flow parameters

The numerical solution of the problem involves in applying Crout's reduction technique [93] to evaluate the flow parameters such as density (G_{i+1}), velocity (U_{i+1}), pressure (Y_{i+1}), and radiation flux (J_{i+1}), from equations (7.40-7.43) using MATLAB with a step size of $\Delta h = 10^{-4}$ and an error tolerance of 10 significant digits. The whole solution procedure is repeated until the shock conditions are satisfied within the said accuracy.

7.4 Results and Discussion

Numerical calculations are performed for the values of non-ideal parameters $\rho_0 = 1$, $R = 1$, $m = 3/2$, $n = -1/2$, $s = 1$, $q = 0$ and $\sigma = 1.42$. The similarity exponent α for various values of constant parameter b and fixed values of non-idealness parameter Γ_0 are listed in Tables 7.1 and 7.2. We observe from Table 7.1, decrease in the values of similarity exponent α and increase in the measure of shock strength β with increasing values of constant parameter b and for fixed values of non-idealness parameter Γ_0 . Also from Table 7.2, for perfect gas case a

reverse trend is observed in the values of similarity exponent α and measure of shock strength β for various values of adiabatic exponent γ . The variations of non-dimensional flow variables and radiation flux for the considered non-idealness parameters for both Royce and ideal gas EOSs are shown in Figures 7.3-7.14.

It is observed from Figures 7.3 and 7.4 that the flow variable density (for both cylindrical and spherical geometry) is high at the shock front (for the Royce EOS) reduces with the increase in the non-idealness parameters and reduce gradually as λ increases. It is observed that at the shock front discontinuity appeared in density profiles is subject to physical requirement that the radiation flux cannot change across it and the mean collision time of particles is proportional to the gas density.

Also from Figures 7.5 and 7.6, it is observed for Royce EOS for the cylindrical and spherical geometries for different values of non-ideal parameters a sharp increase in velocity profiles for $\lambda = 1$ for a short range of λ and decrease steadily with the variation in λ . It is notable that increase in the non-idealness parameters (from Tables 7.1 and 7.2) have effect on β . As β value increases, increase in velocity, pressure is prominent for both the EOS. Thus it is observed from Figure 7.4, that increase in β does not automatically decelerate the shock front but the velocity and pressure behind the shock front increases quickly in the presence of monochromatic radiation and decrease slowly and become constant. The

variation in shock velocity causes the shock transition to expand to a scale larger than that of the system, so that the shock enters a different regime for real systems such as stellar atmosphere (Farnsworth and Clarke [120]). Hence, the shock velocity will increase as cryogenic implosion performance improves allowing access to the radiative pressure regime.

The effect of non-idealness parameters b on the pressure distribution in the presence of fixed non-idealness parameter Γ_0 is presented in Figures 7.7 and 7.8. The pressure distribution $Y(\lambda)$ increases as the constant parameter b increases. This is in agreement with physical fact that the velocity distribution increases with increasing b and also it is found that increase in pressure profiles has insignificant effect with increasing values of λ for both cases of geometry $\Omega = 2, 3$ and also the gas pressure decreases with increase in λ . A similar trend is observed in the radiation profiles from Figures 7.9 and 7.10.

The density, velocity, and pressure profiles for ideal gas equation of state are presented in Figures 7.11-7.14 respectively for various values of γ . Figures 7.11(a) and 7.11(b) depict density profiles of both cylindrical, spherical geometry for different values of adiabatic index γ respectively. We observe from Figure 7.11 that density distribution increases with the increase of γ and decreases in a short range of λ and a small increase is seen as a bounce and then reduces along the λ . The velocity profiles for different values of adiabatic index γ presented in Figure 7.12. A sharp rise in the velocity profiles is observed initially and decrease

rapidly along λ -axis for both cases of geometry $\Omega = 2, 3$ respectively. Moreover, this behavior is similar to the case of Royce EOS for fixed values of adiabatic index γ and non-idealness parameter b but it is just an opposite trend for different values of adiabatic index γ . Figures 7.13(a) and 7.13(b) represent pressure profiles versus λ , for various values of adiabatic index γ . The radiation flux profiles for perfect gas are presented in Figure 7.14. It is observed that initially no variation in radiation flux distribution but then it is more with an increasing values of λ . It is observed that effect of radiation from the volume of a gas becomes important at distances away from the initial point and it modifies the shock structure.

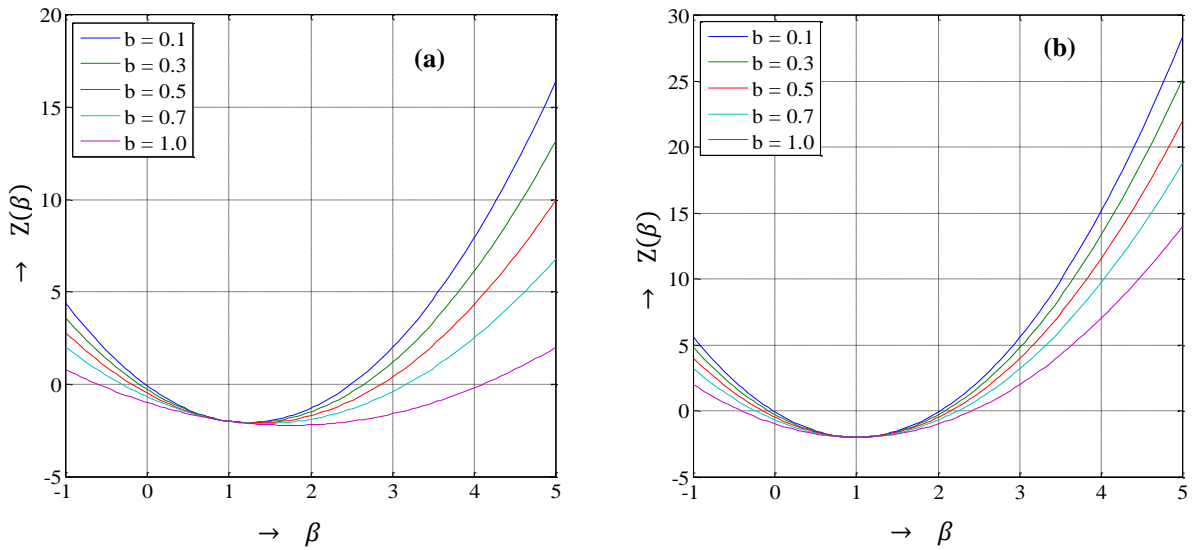


Figure 7.2. Graphical approach of $Z(\beta)$ in the case of Royce EOS; (a) $\Gamma_0 = 1.4$ and (b) $\Gamma_0 = 2.0$

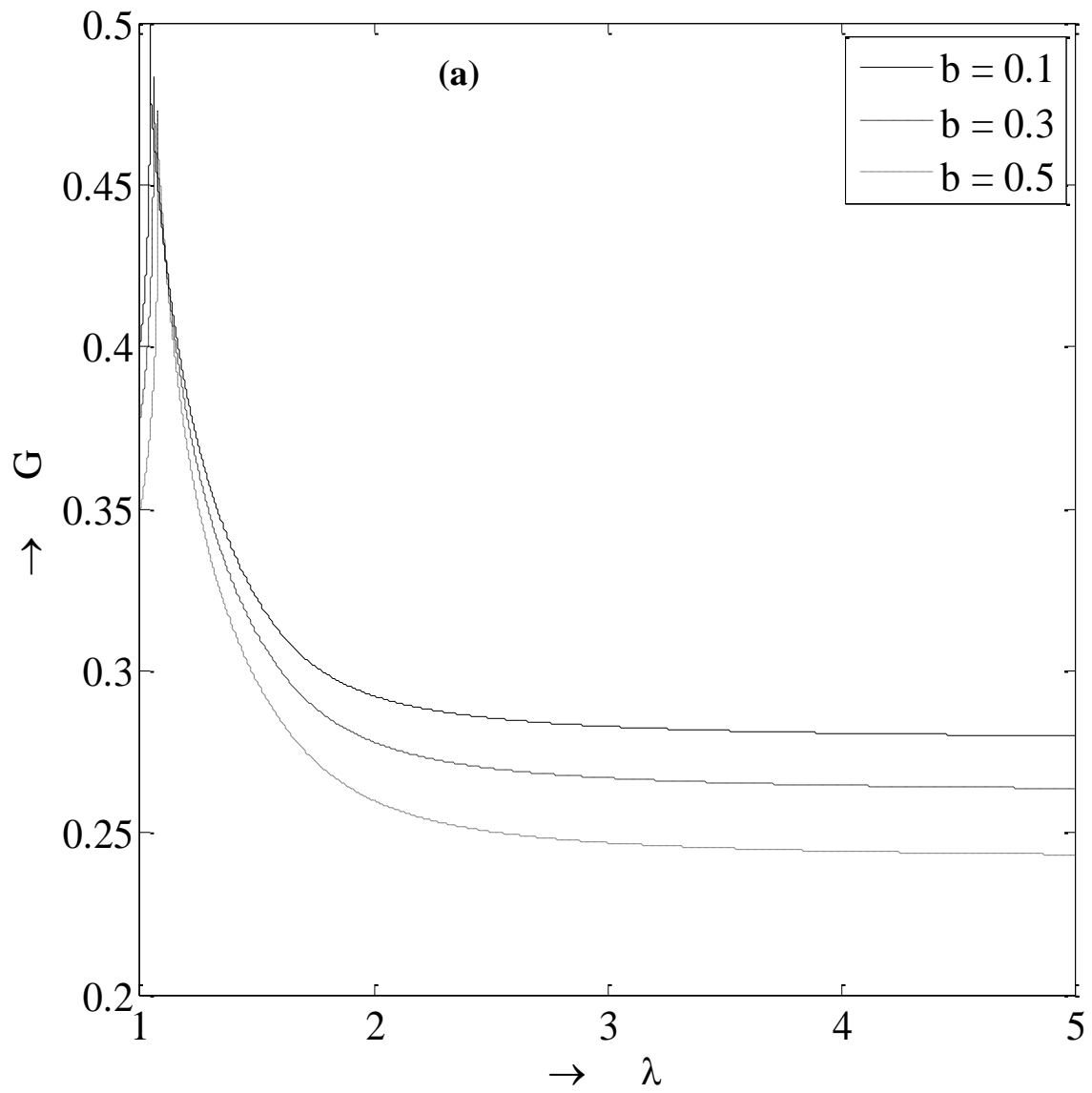


Figure 7.3(a). Density profiles for Royce EOS when $\Gamma_0 = 1.4$, $\sigma = 1.42$, and $\Omega = 2$

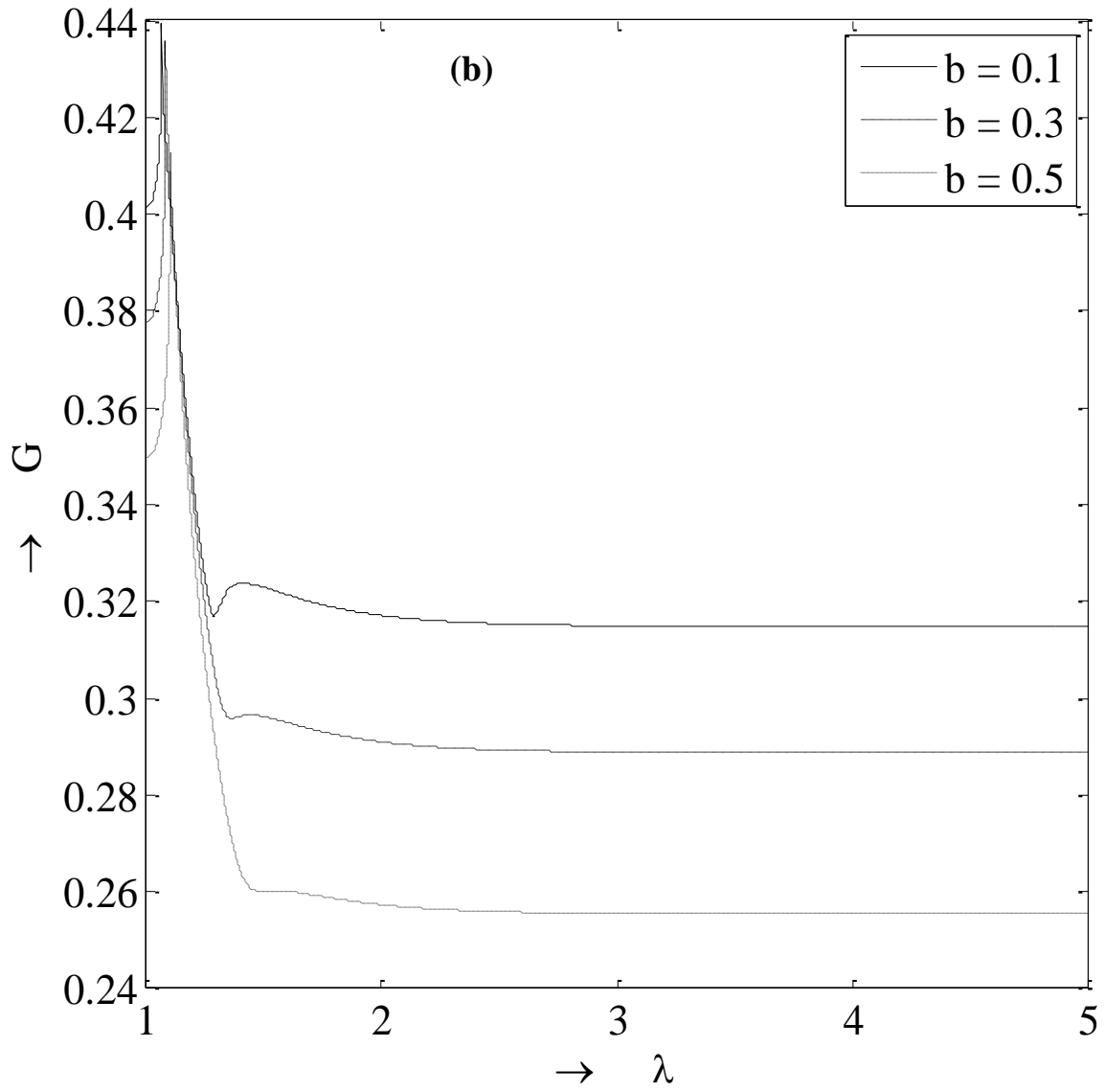


Figure 7.3(b). Density profiles for Royce EOS when $\Gamma_0 = 1.4$, $\sigma = 1.42$, and $\Omega = 3$

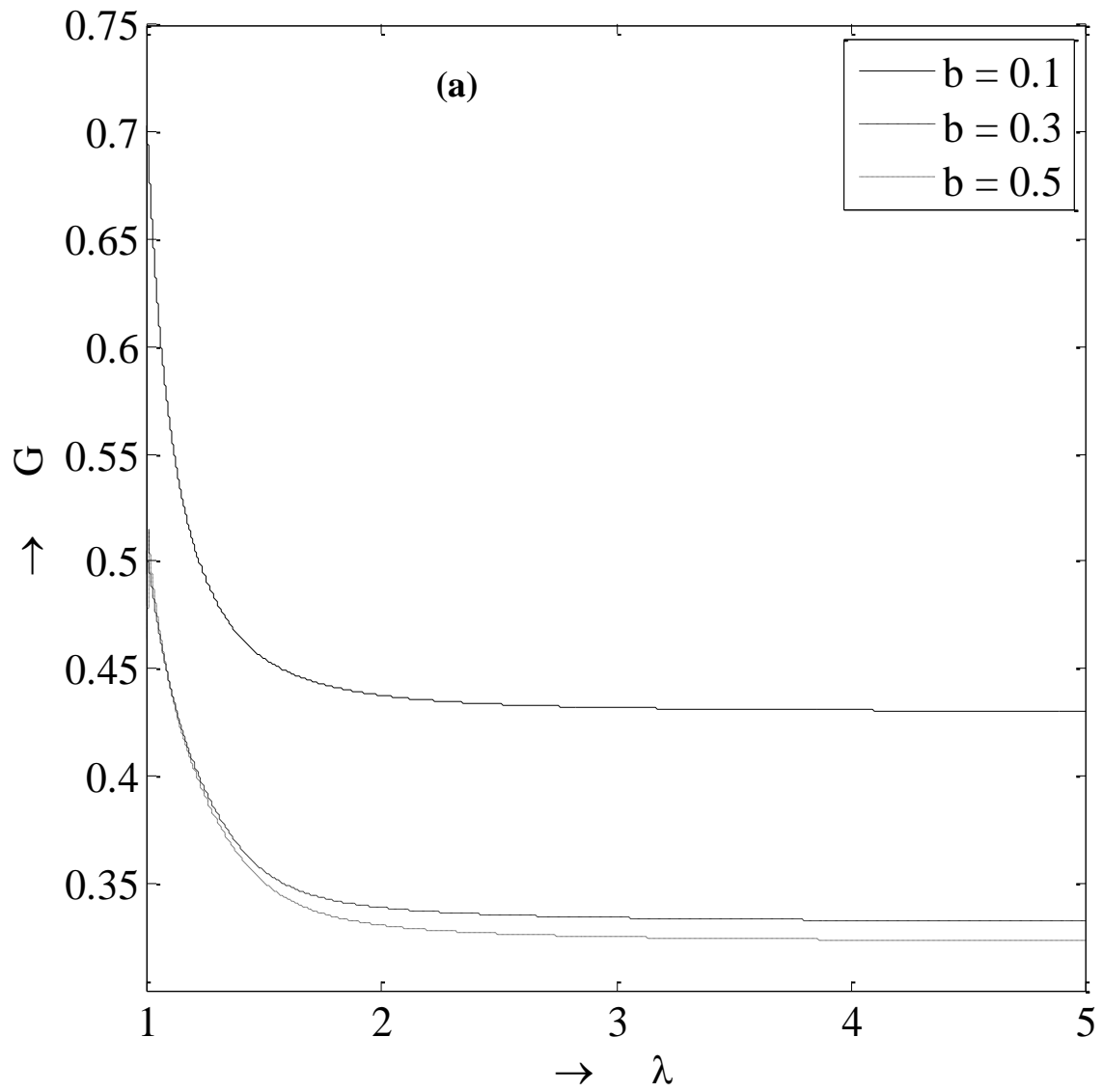


Figure 7.4(a). Density profiles for Royce EOS when $\Gamma_0 = 2.0$, $\sigma = 1.42$, and $\Omega = 2$

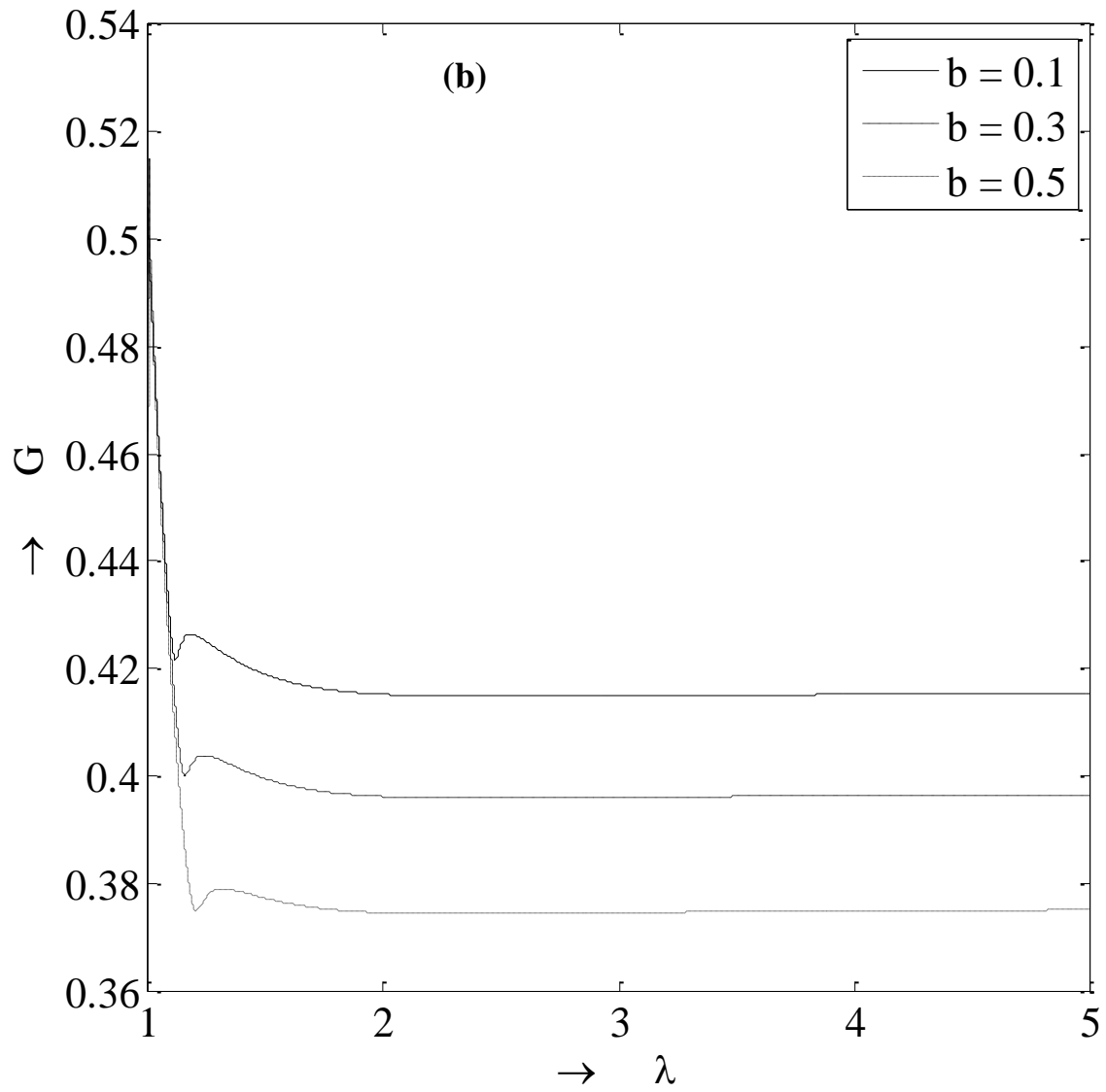


Figure 7.4(b). Density profiles for Royce EOS when $\Gamma_0 = 2.0$, $\sigma = 1.42$, and $\Omega = 3$

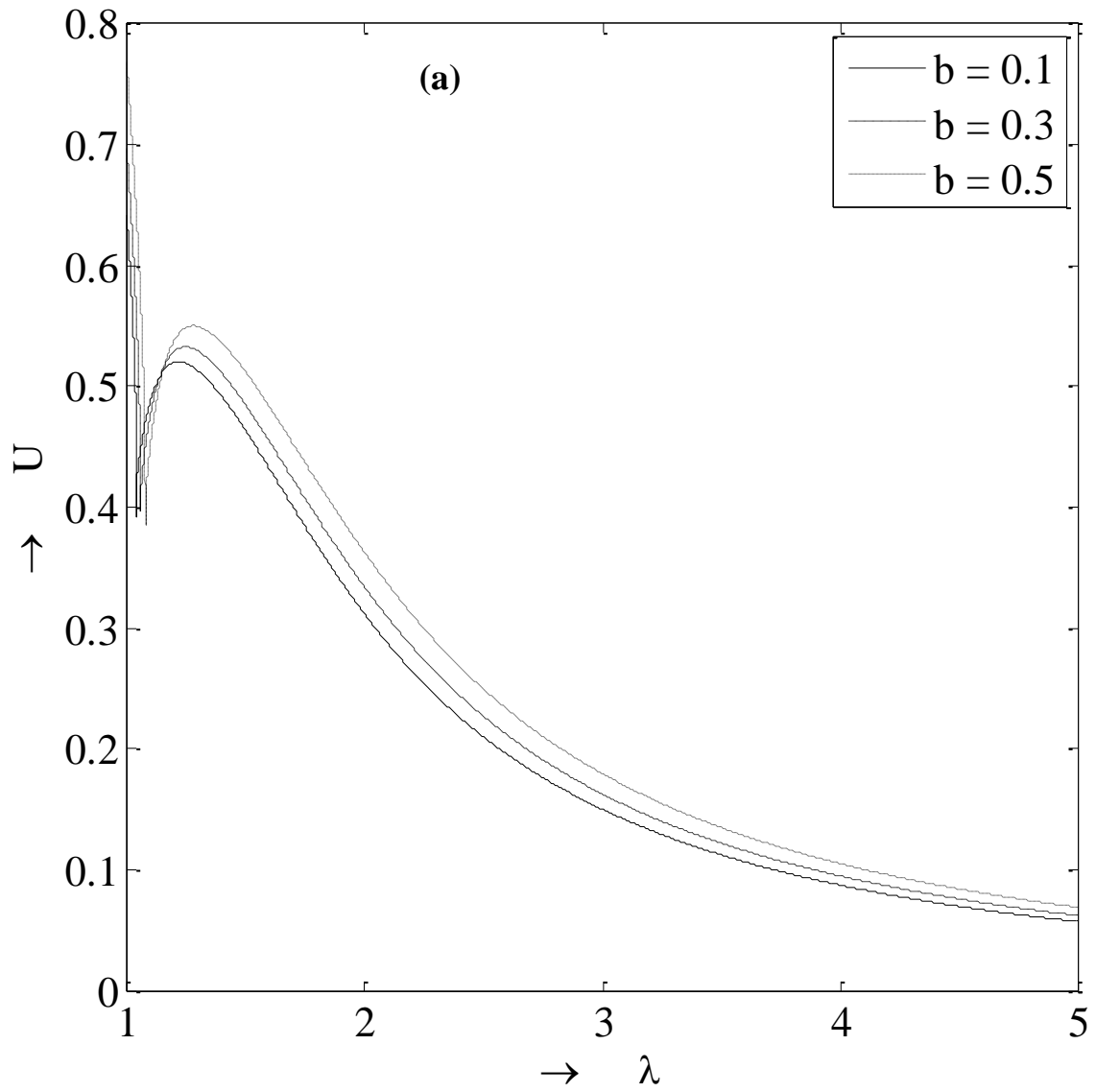


Figure 7.5(a). Velocity profiles for Royce EOS when $\Gamma_0 = 1.4$, $\sigma = 1.42$, and $\Omega = 2$

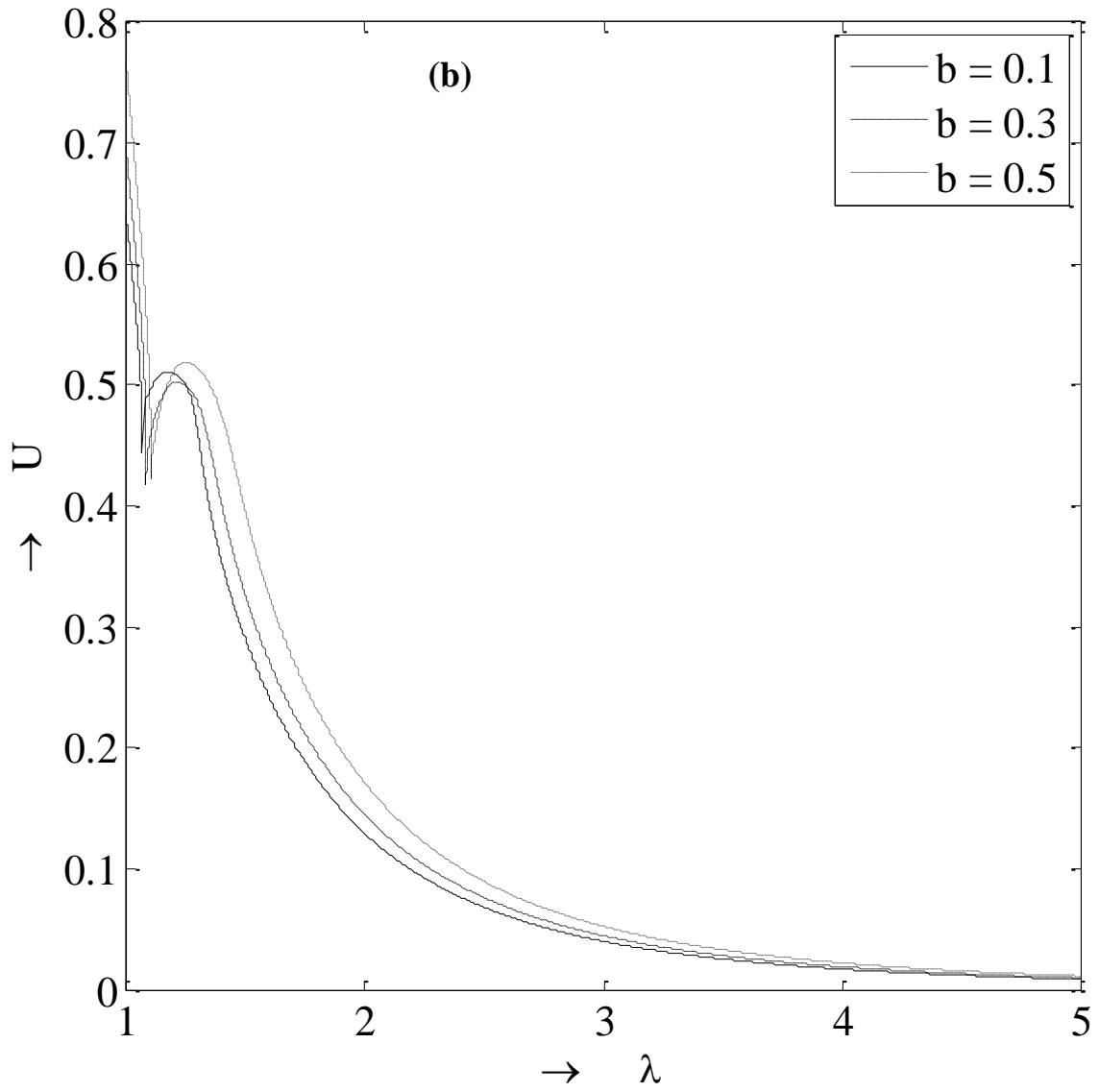


Figure 7.5(b). Velocity profiles for Royce EOS when $\Gamma_0 = 1.4$, $\sigma = 1.42$, and $\Omega = 3$

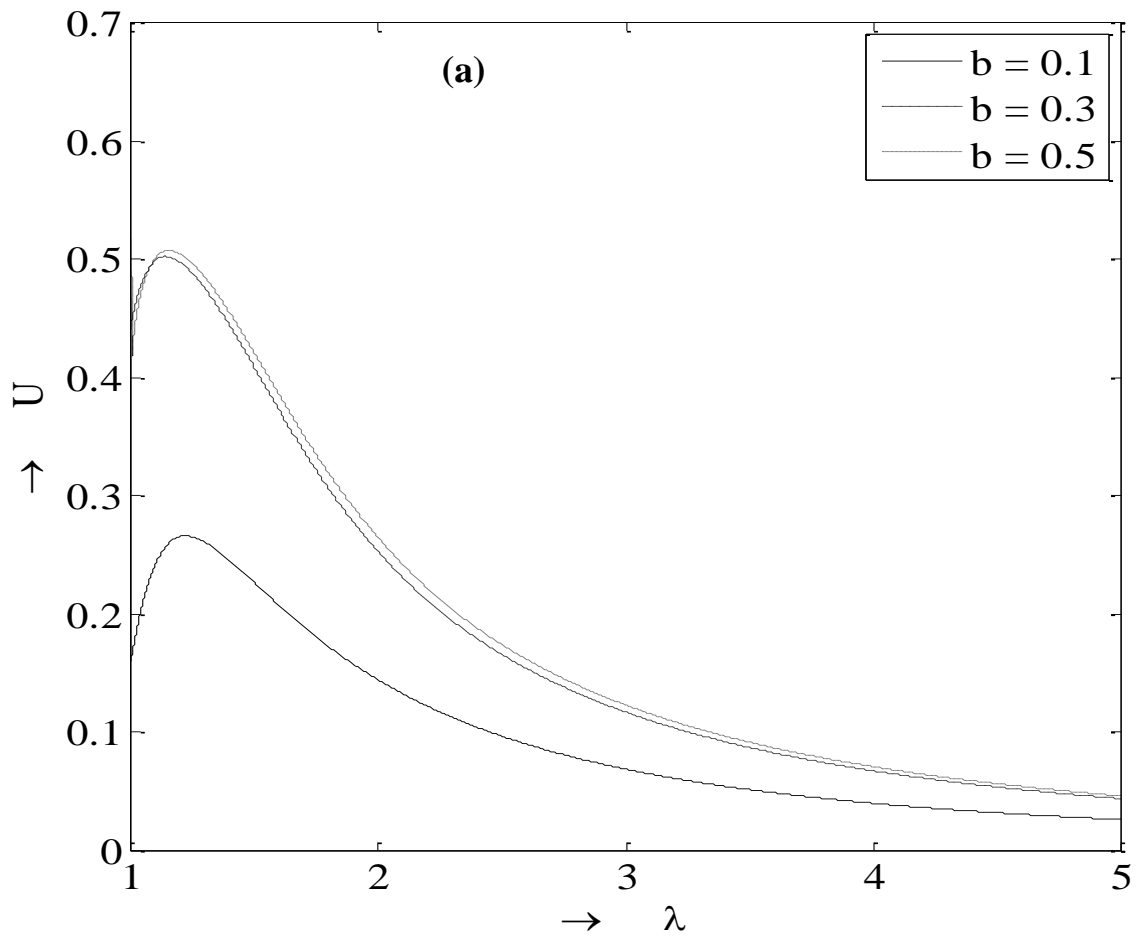


Figure 7.6(a). Velocity profiles for Royce EOS when $\Gamma_0 = 2.0$, $\sigma = 1.42$, and $\Omega = 2$

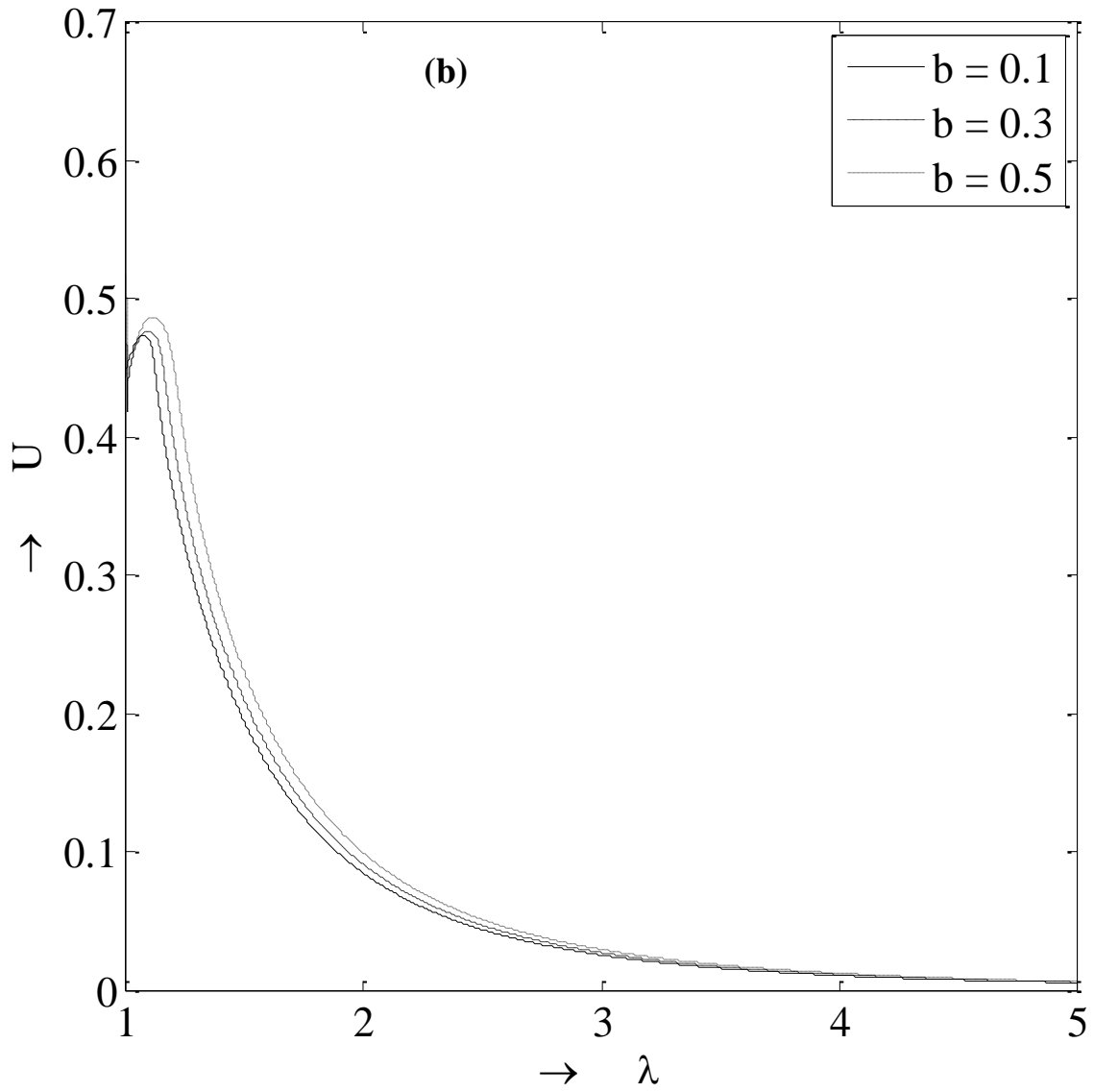


Figure 7.6(b). Velocity profiles for Royce EOS when $\Gamma_0 = 2.0$, $\sigma = 1.42$, and $\Omega = 3$

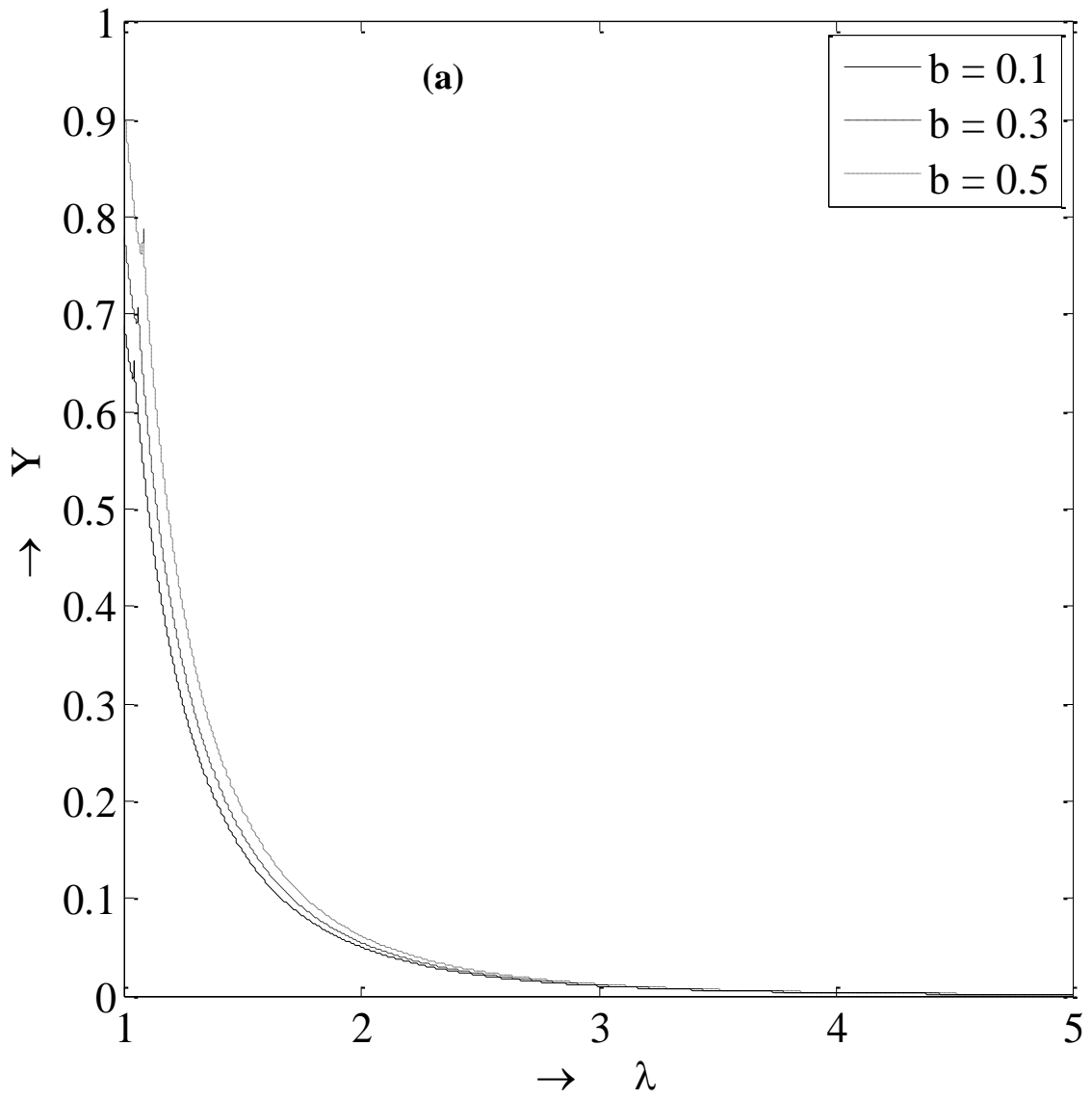


Figure 7.7(a). Pressure profiles for Royce EOS when $\Gamma_0 = 1.4$, $\sigma = 1.42$, and $\Omega = 2$

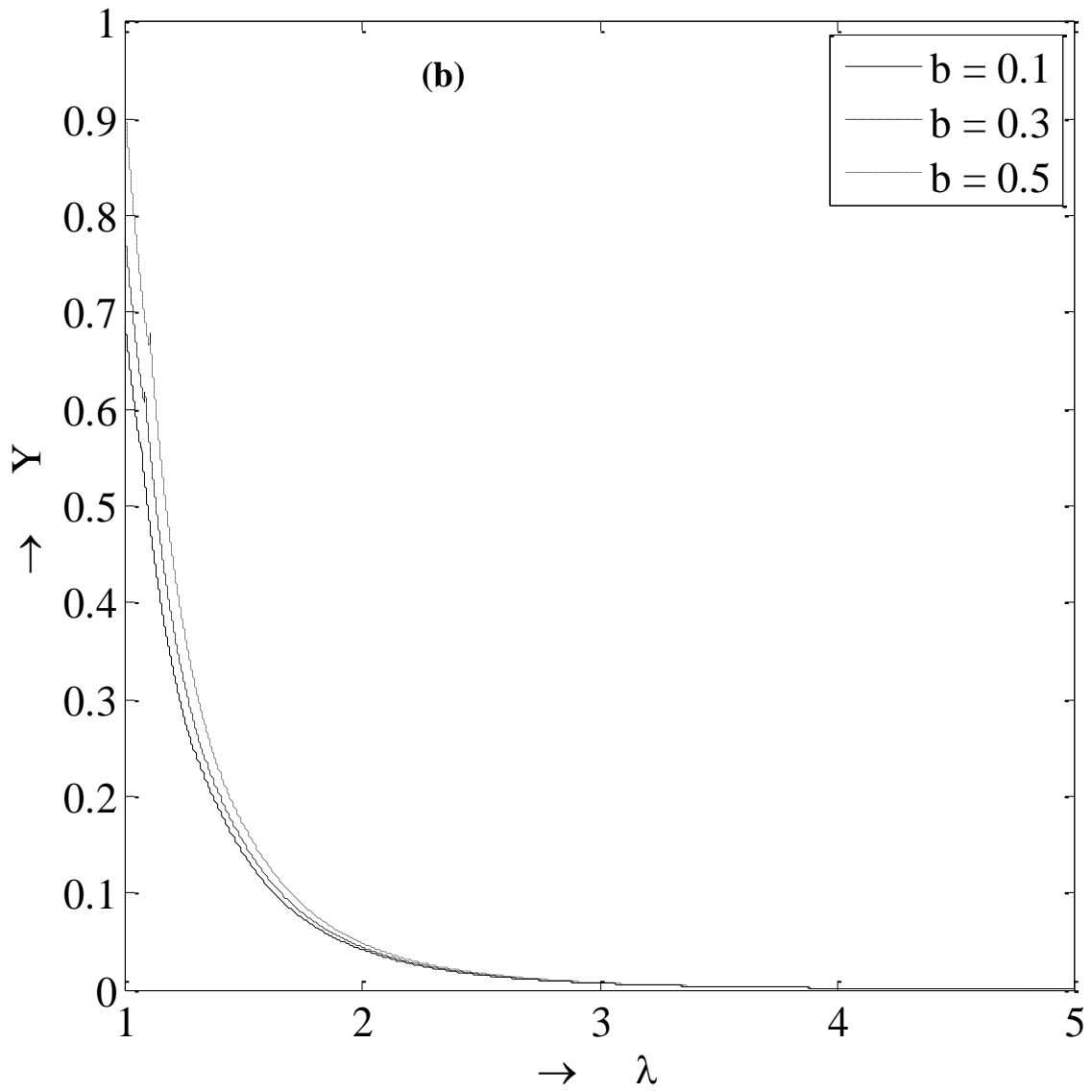


Figure 7.7(b). Pressure profiles for Royce EOS when $\Gamma_0 = 1.4$, $\sigma = 1.42$, and $\Omega = 3$

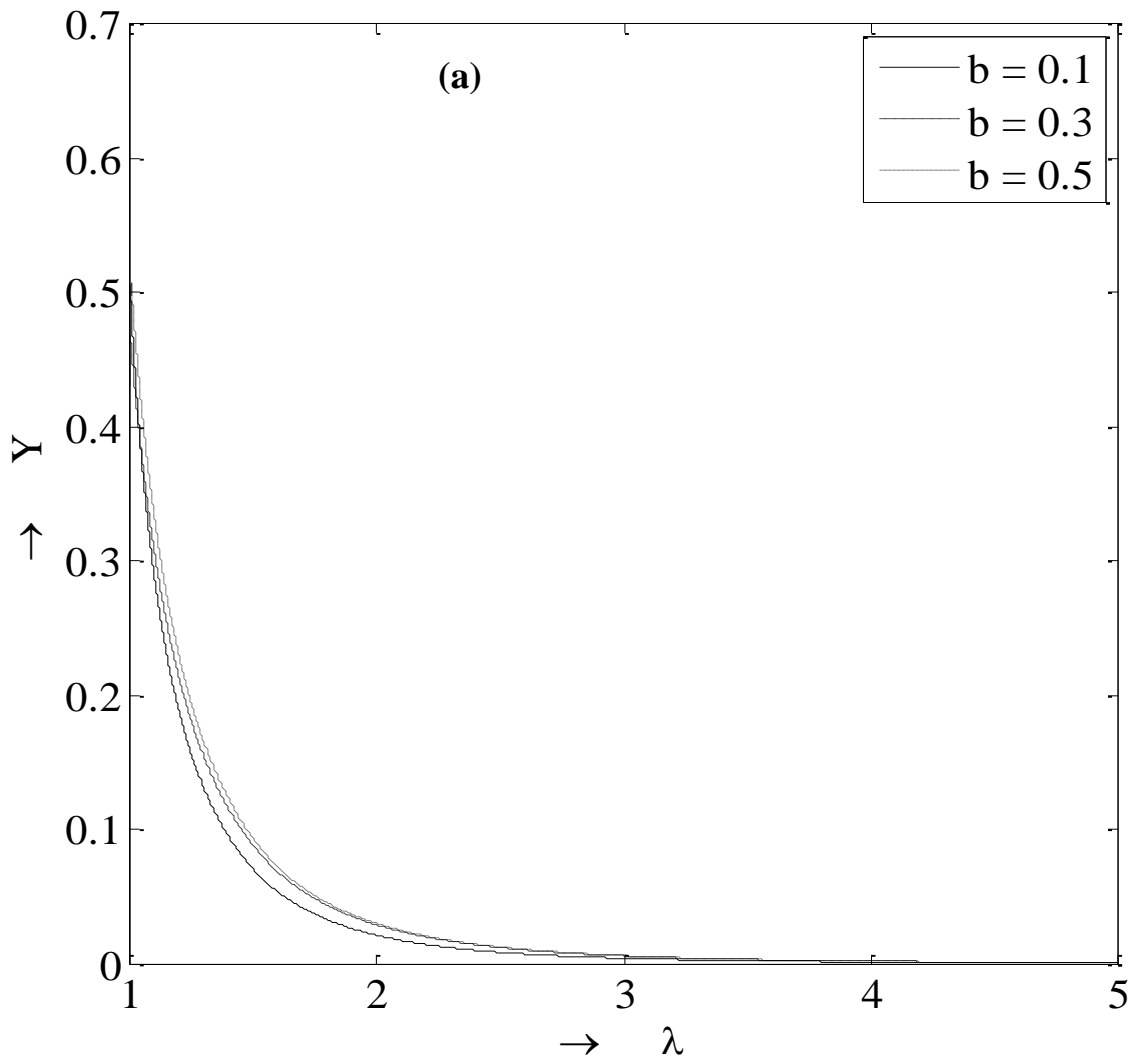


Figure 7.8(a). Pressure profiles for Royce EOS when $\Gamma_0 = 2.0$, $\sigma = 1.42$, and $\Omega = 2$

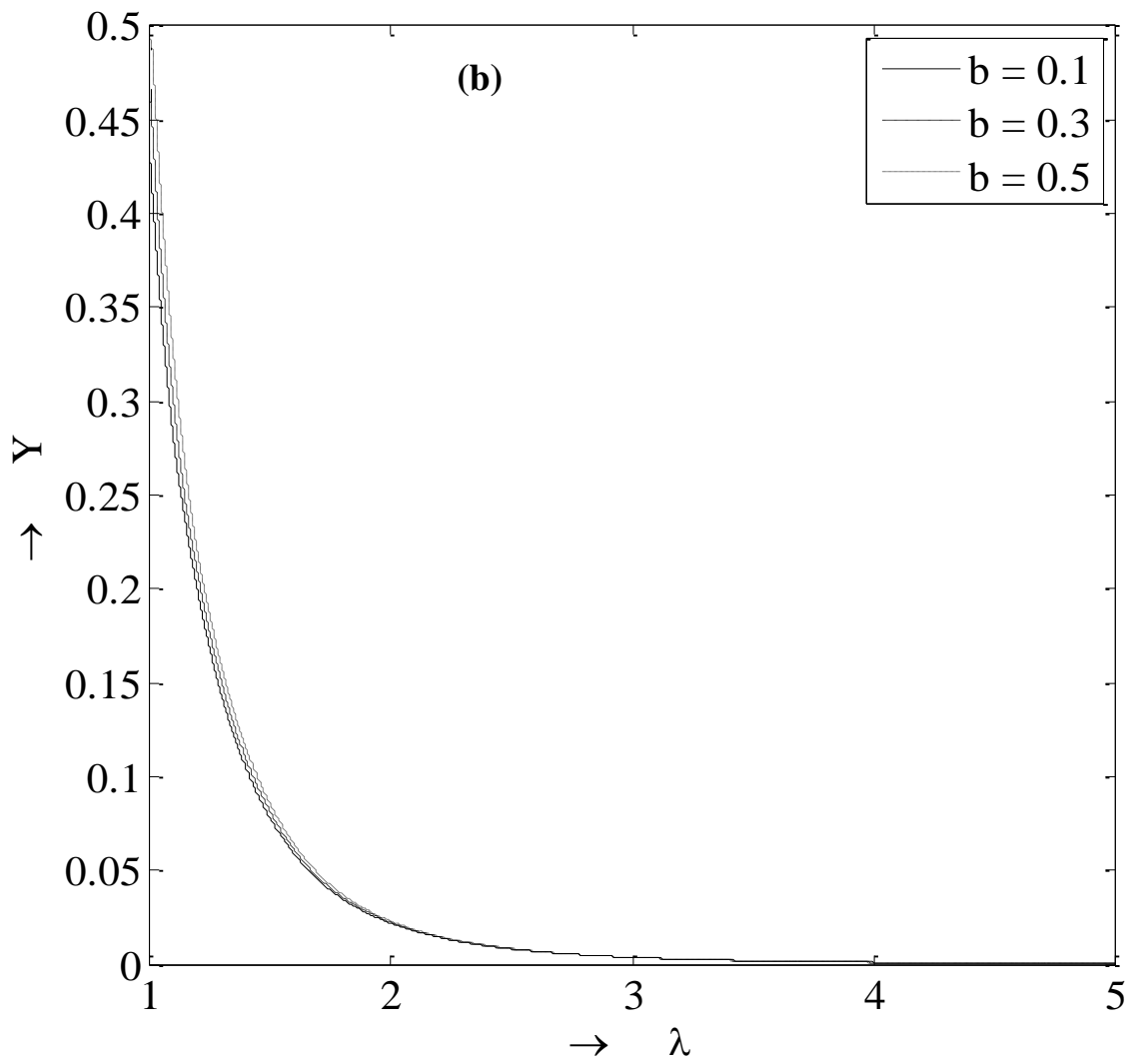


Figure 7.8(b). Pressure profiles for Royce EOS when $\Gamma_0 = 2.0$, $\sigma = 1.42$, and $\Omega = 3$

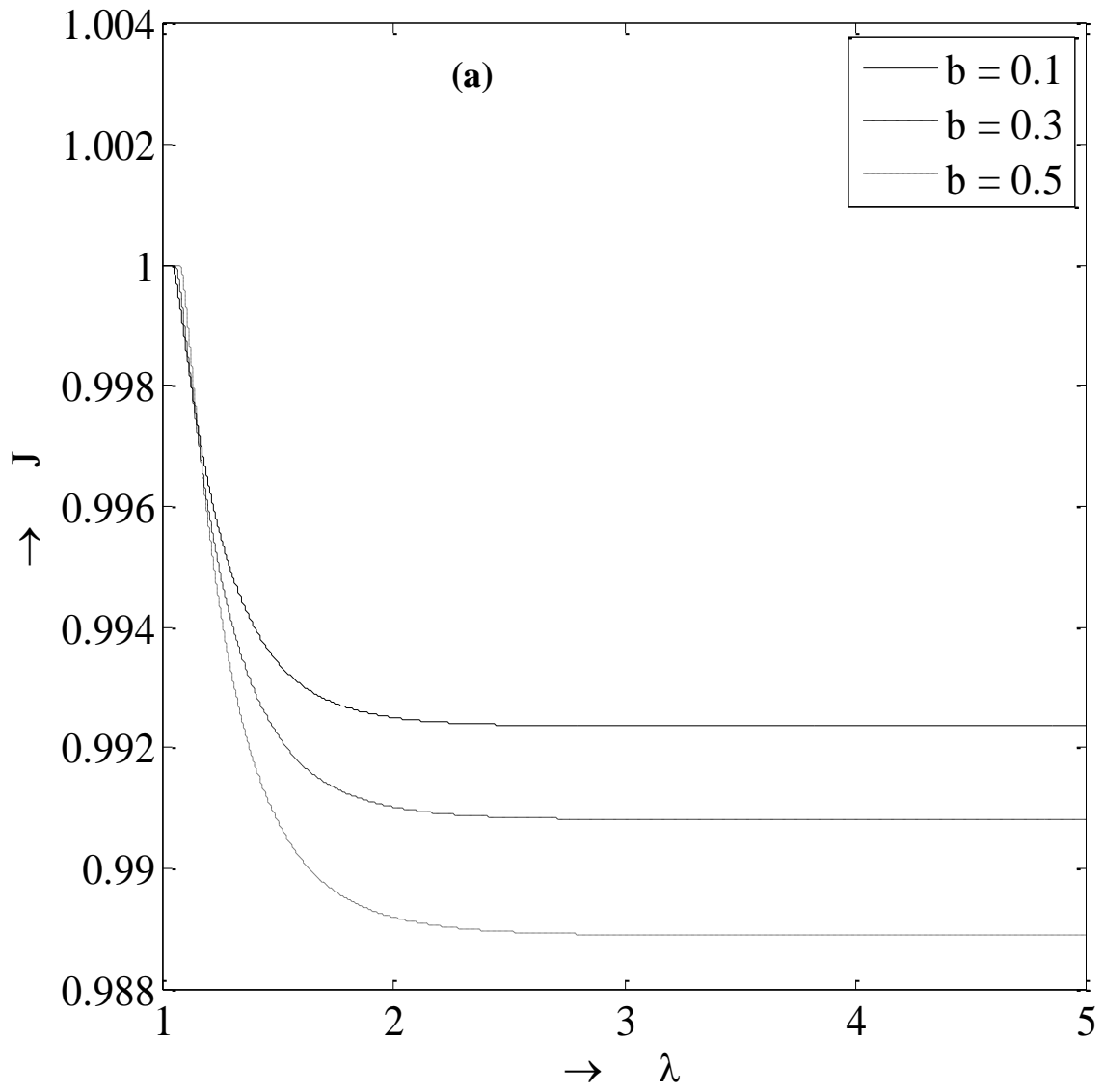


Figure 7.9(a). Radiation profiles for Royce EOS when $\Gamma_0 = 1.4$, $\sigma = 1.42$, and $\Omega = 2$

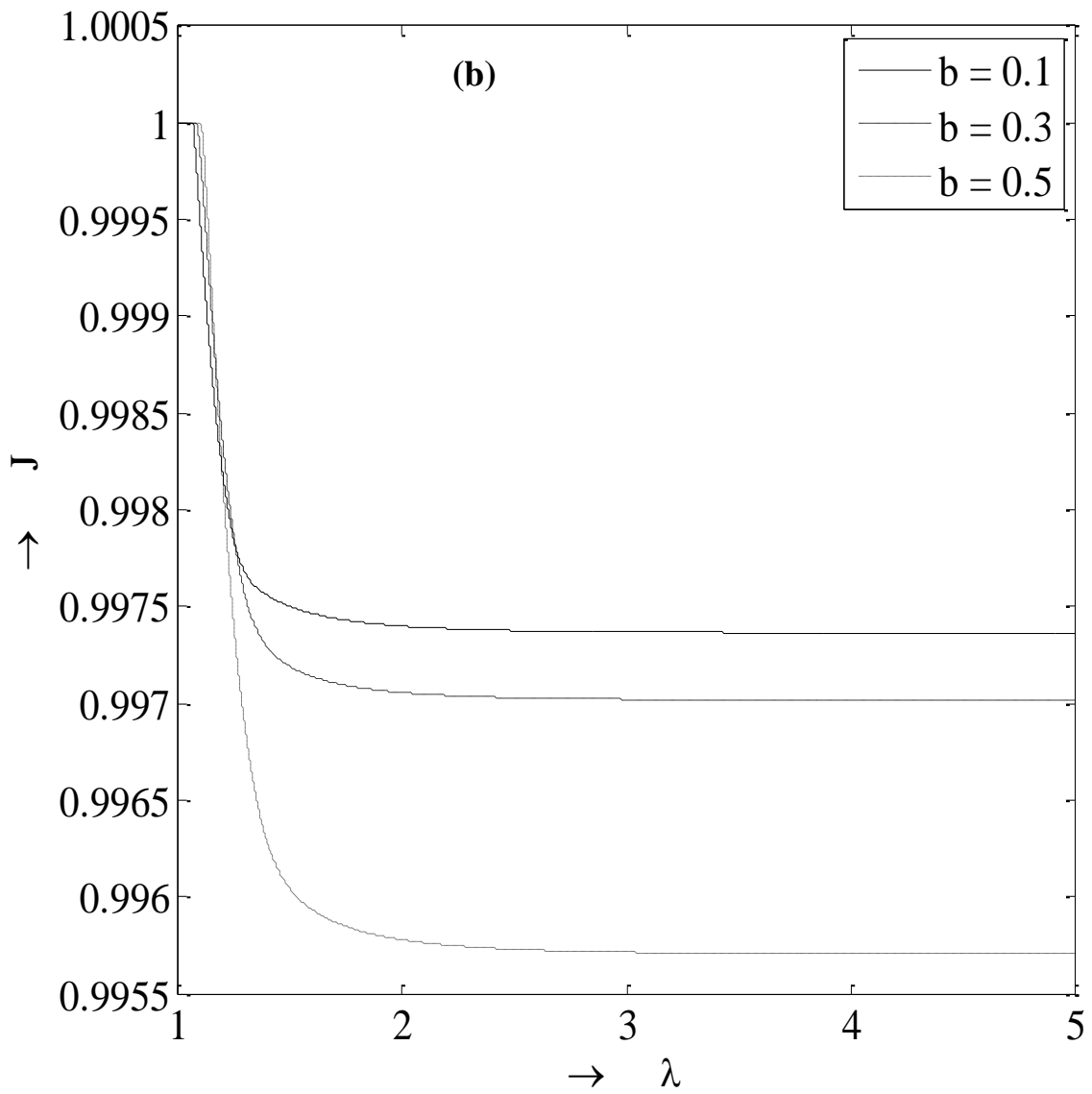


Figure 7.9(b). Radiation profiles for Royce EOS when $\Gamma_0 = 1.4$, $\sigma = 1.42$, and $\Omega = 3$

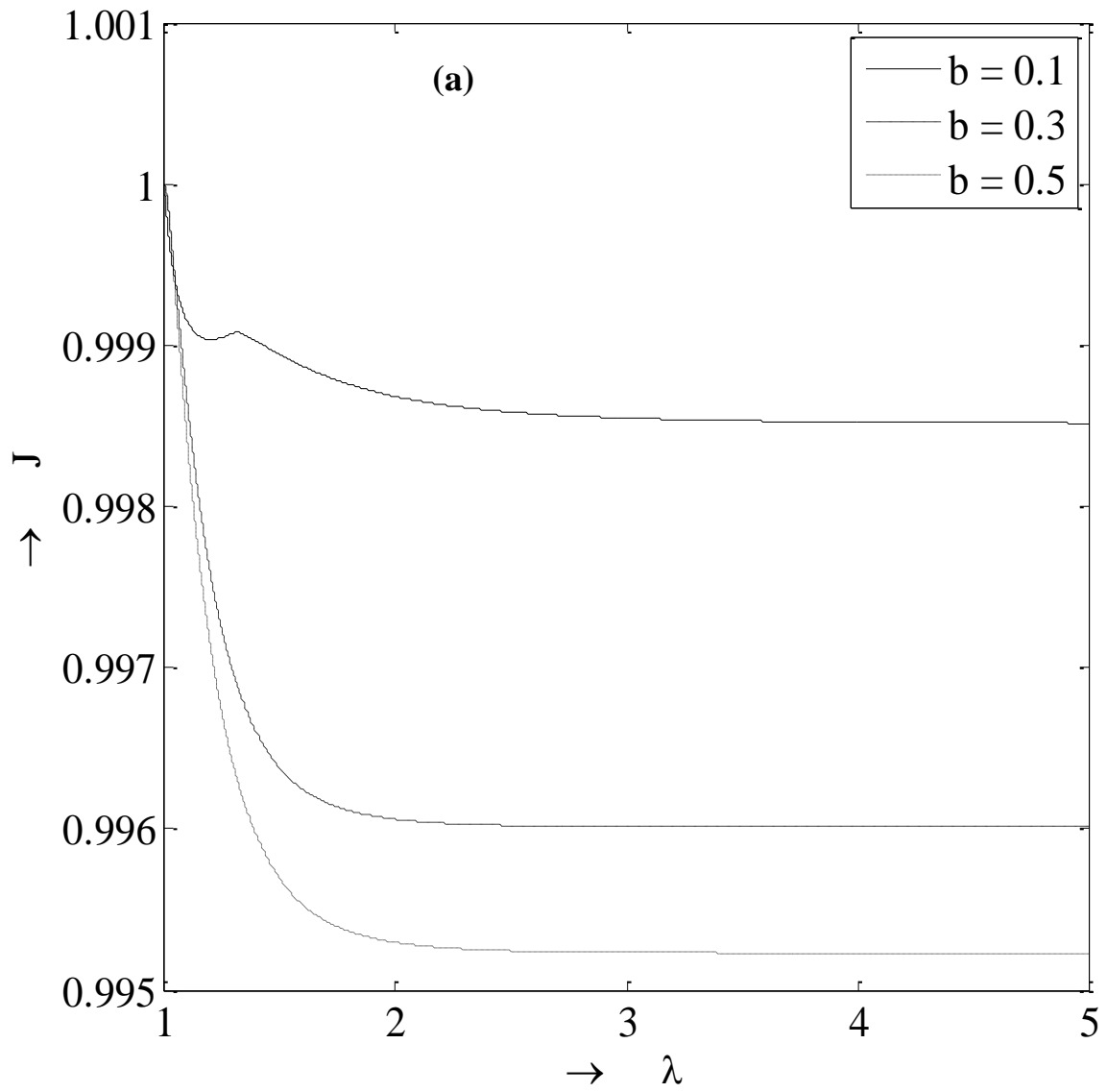


Figure 7.10(a). Radiation profiles for Royce EOS when $\Gamma_0 = 2.0$, $\sigma = 1.42$, and $\Omega = 2$

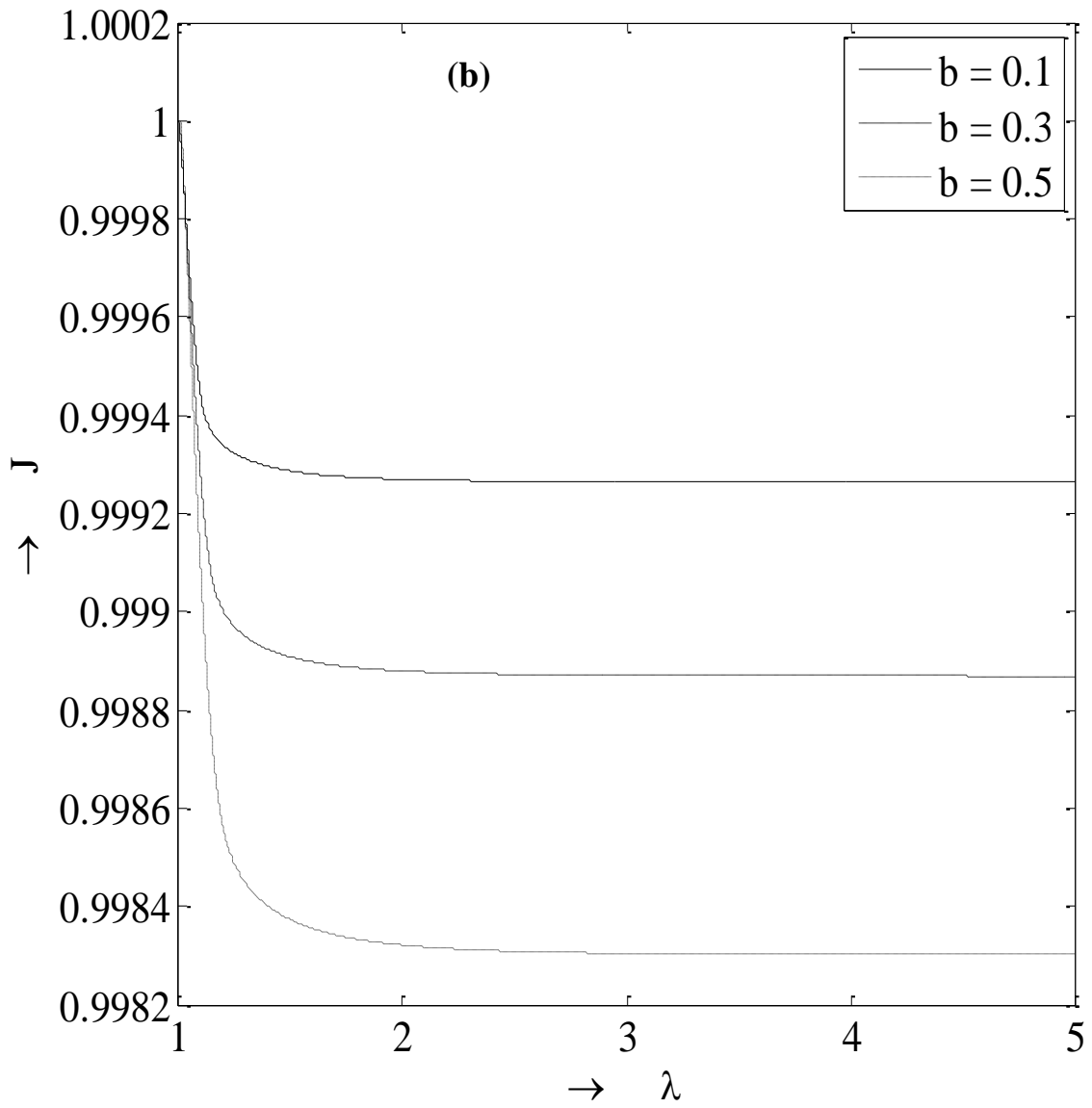


Figure 7.10(b). Radiation profiles for Royce EOS when $\Gamma_0 = 2.0$, $\sigma = 1.42$, and $\Omega = 3$

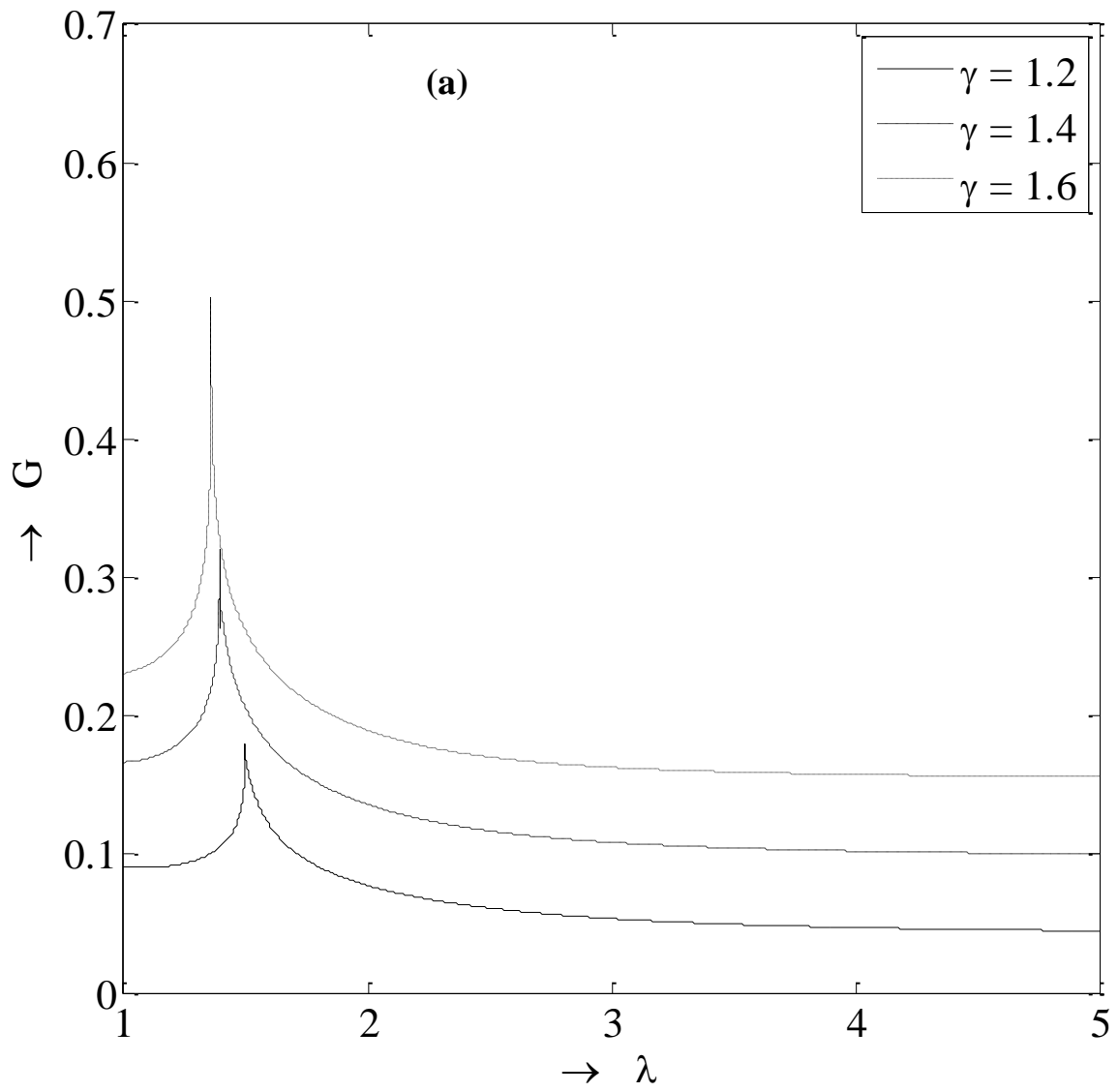


Figure 7.11(a). Density profiles for perfect gas when $\sigma = \gamma, \Omega = 2$

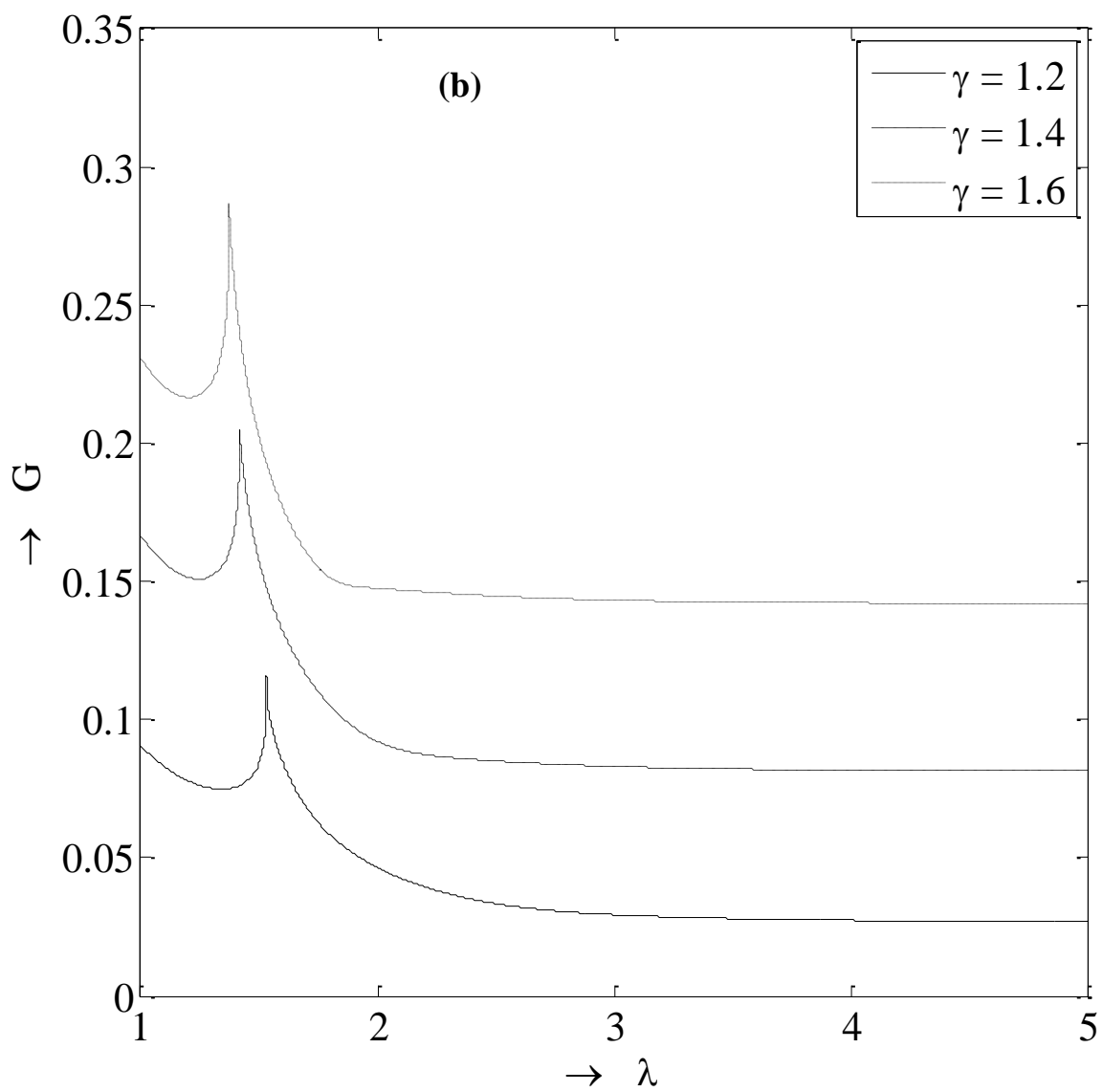


Figure 7.11(b). Density profiles for perfect gas when $\sigma = \gamma, \Omega = 3$

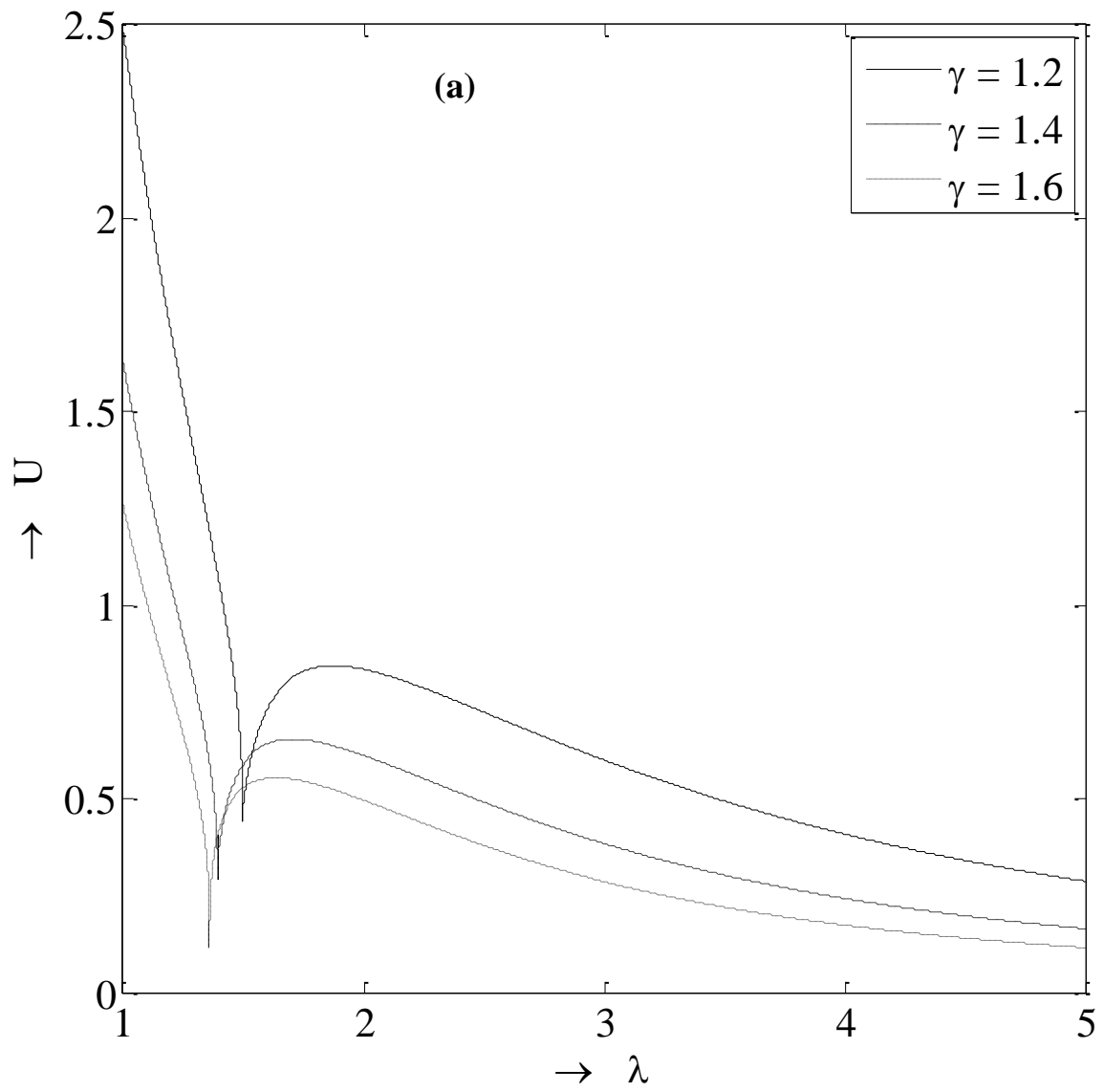


Figure 7.12(a). Velocity profiles for perfect gas when $\sigma = \gamma$, $\Omega = 2$

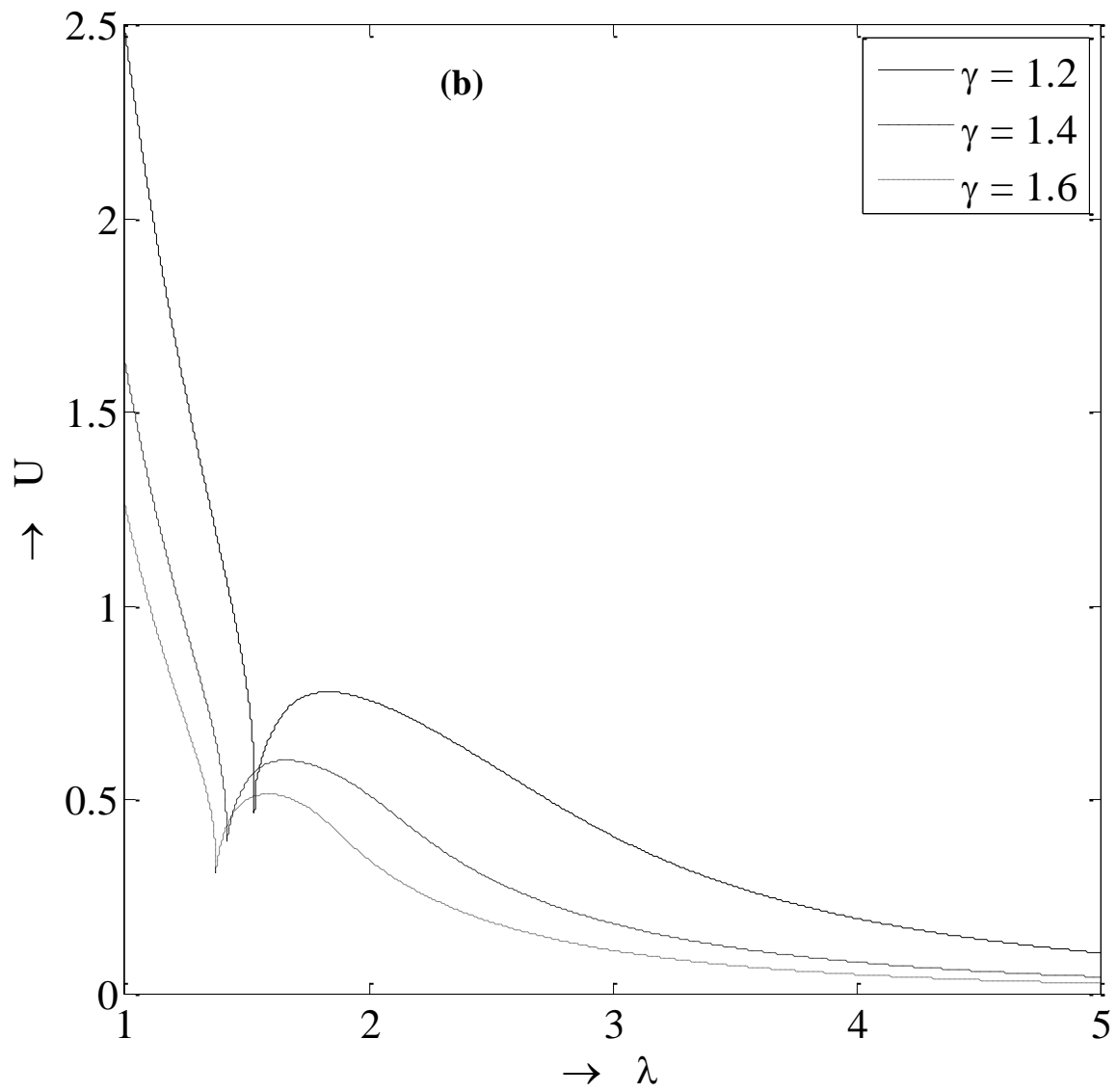


Figure 7.12(b). Velocity profiles for perfect gas when $\sigma = \gamma, \Omega = 3$

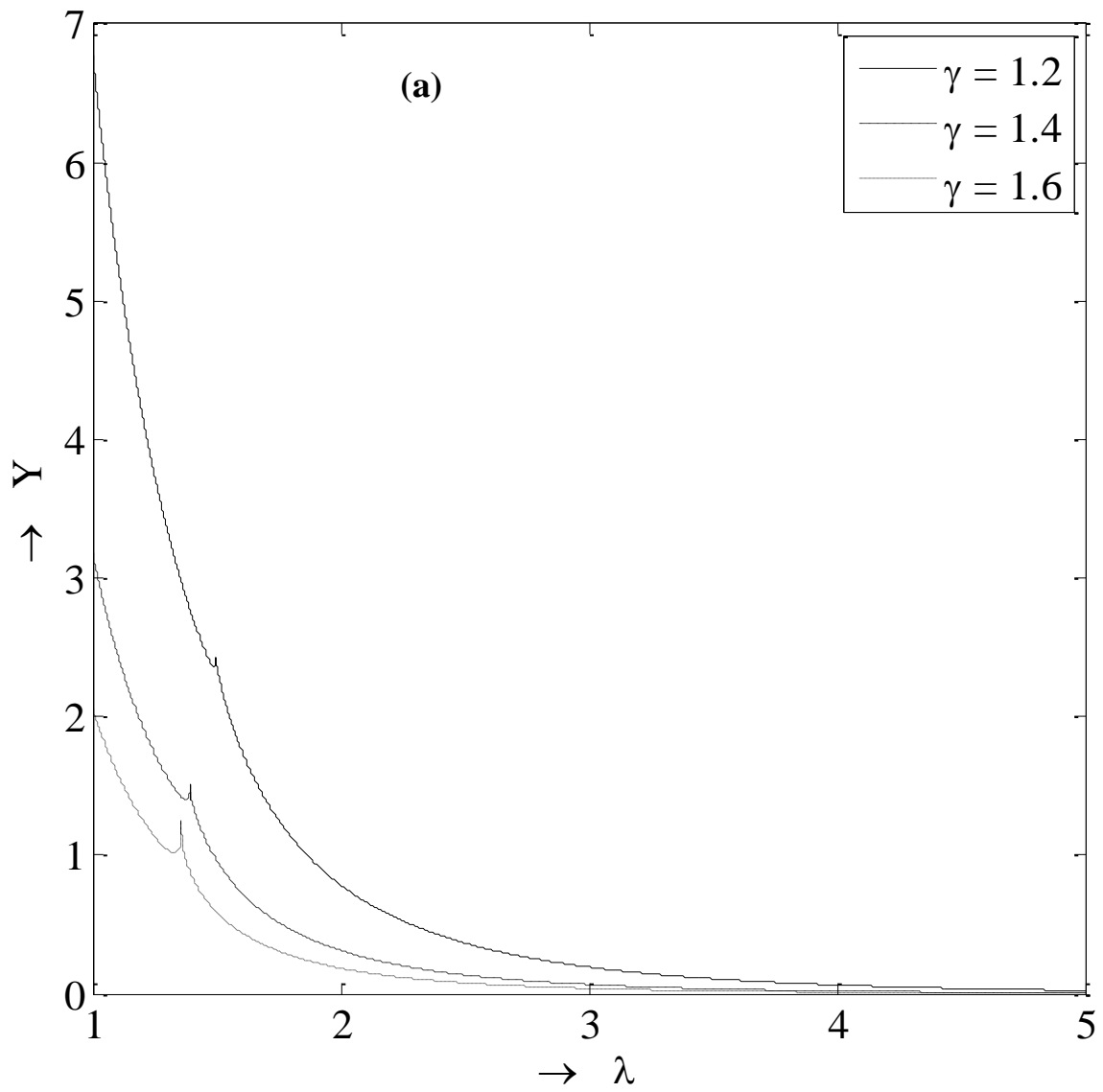


Figure 7.13(a). Pressure profiles for perfect gas when $\sigma = \gamma$, $\Omega = 2$

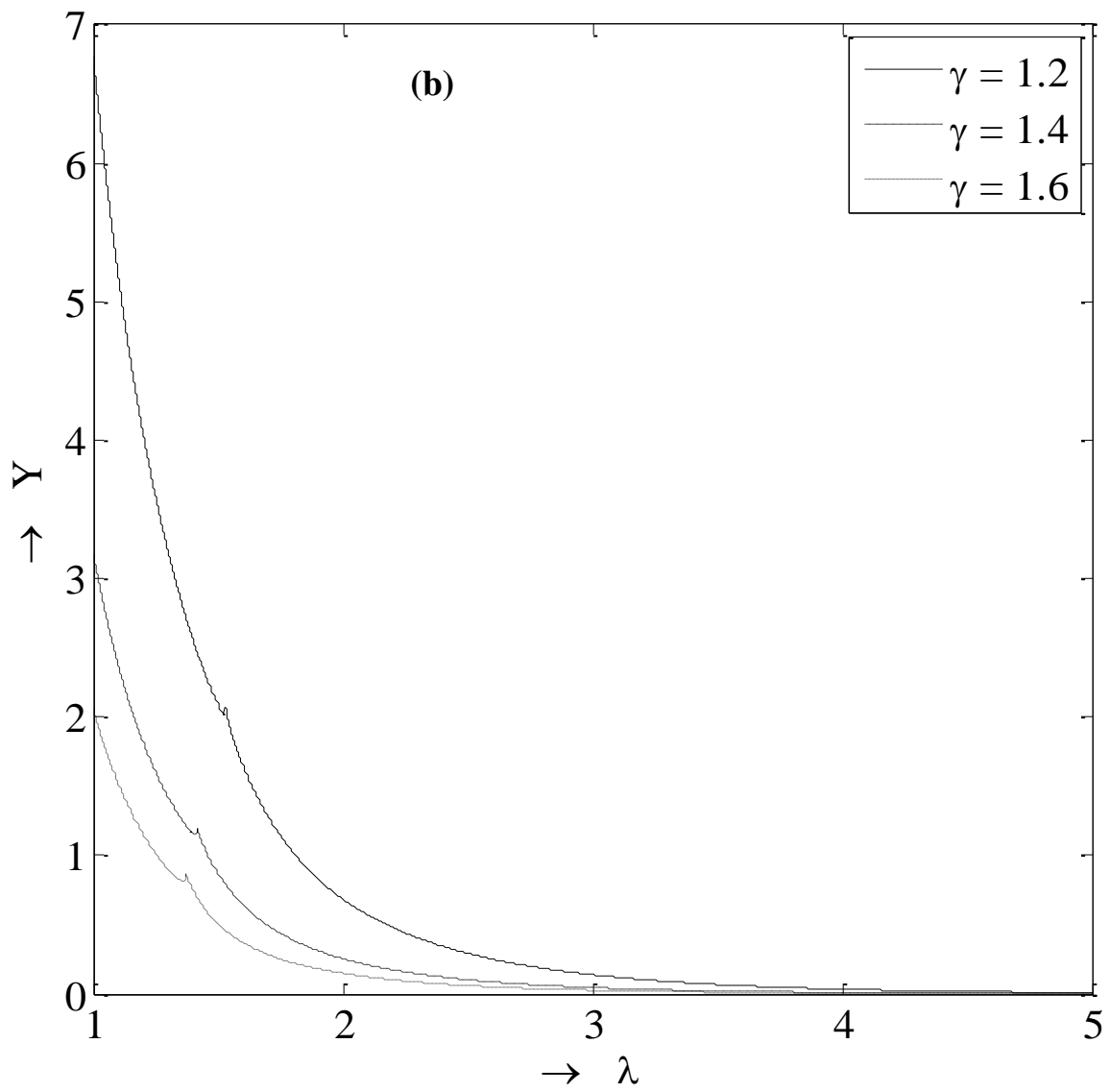


Figure 7.13(b). Pressure profiles for perfect gas when $\sigma = \gamma, \Omega = 3$

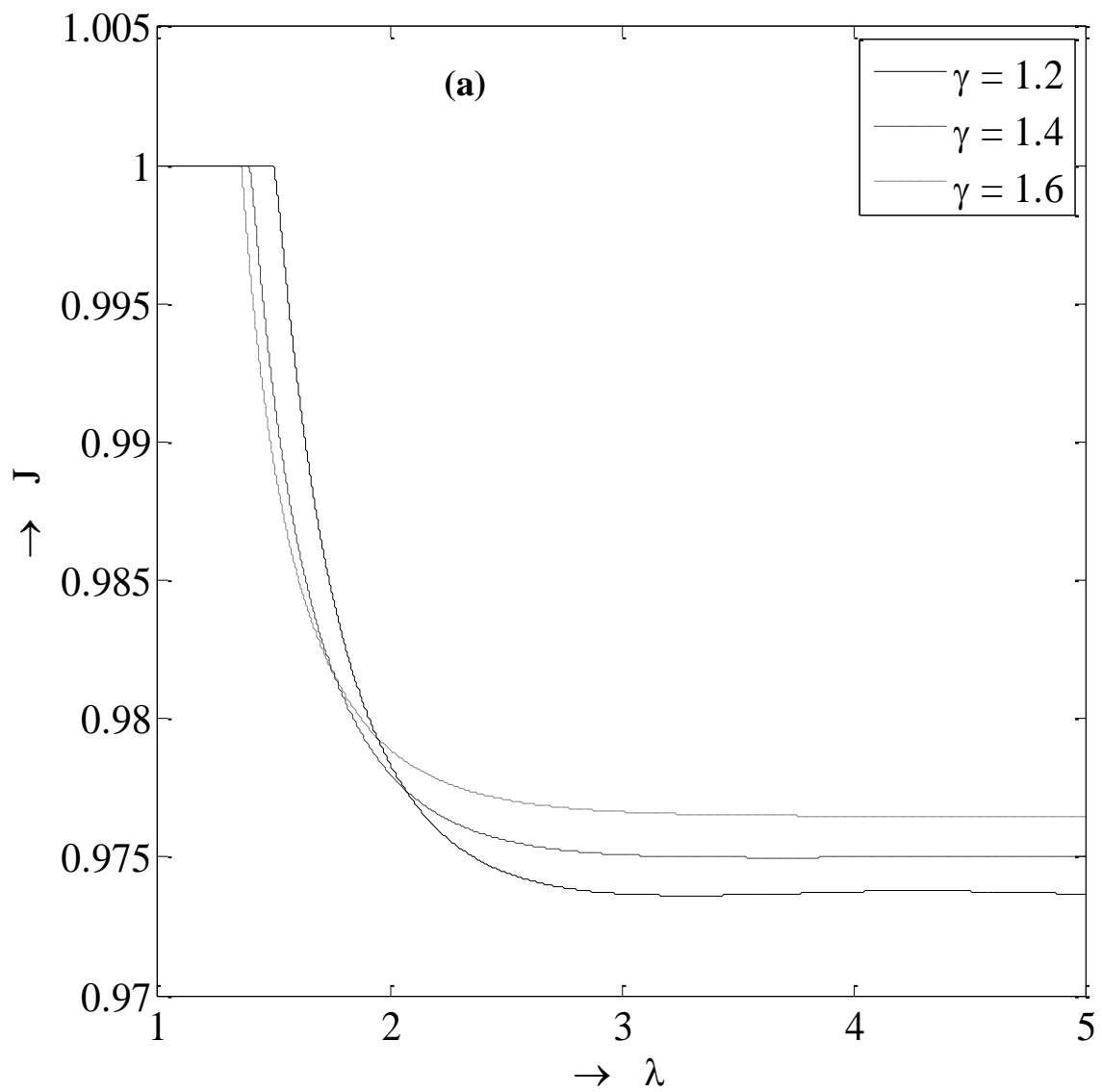


Figure 7.14(a). Radiation profiles for perfect gas when $\sigma = \gamma$, $\Omega = 2$

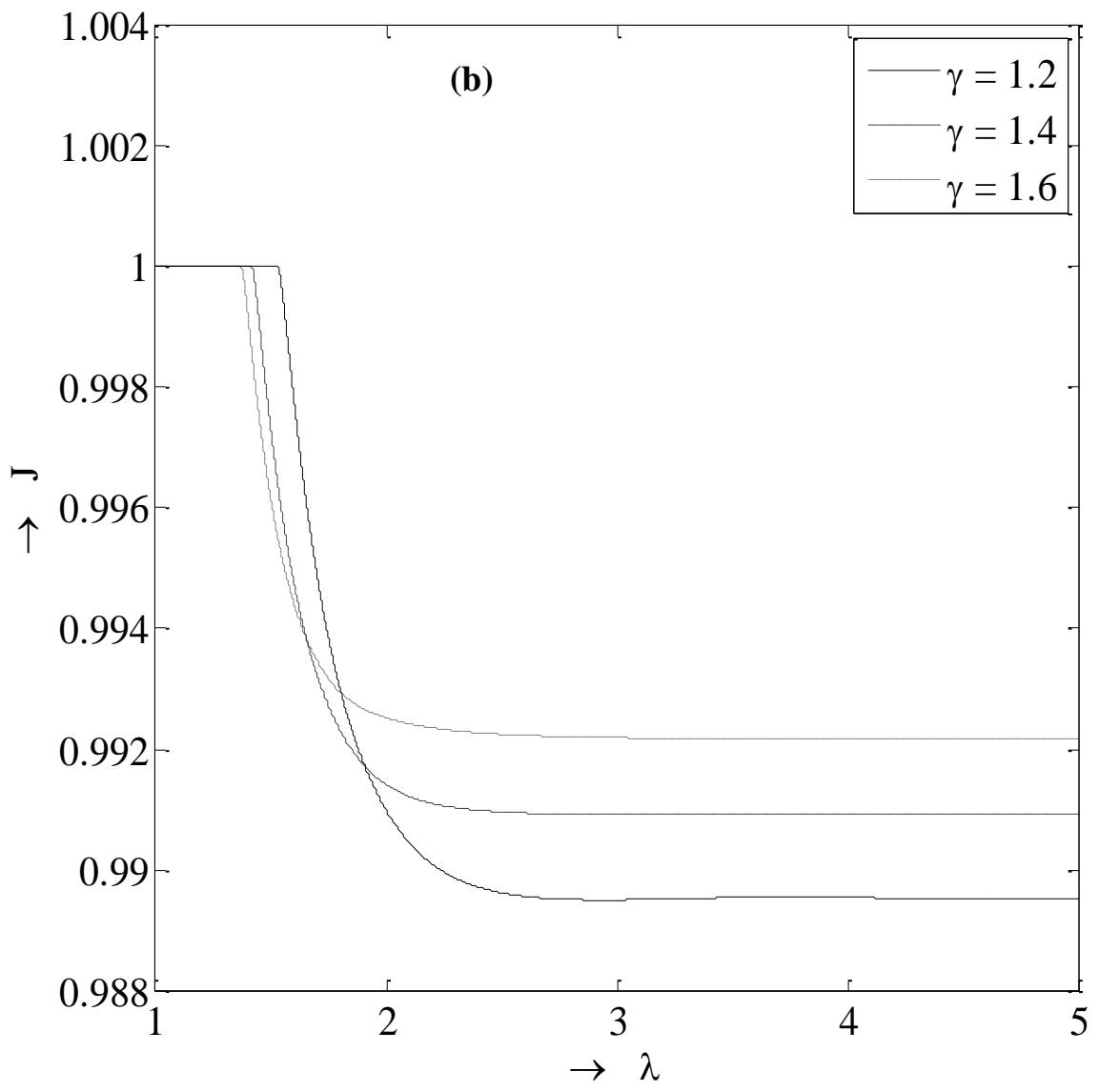


Figure 7.14(b). Radiation profiles for perfect gas when $\sigma = \gamma$, $\Omega = 3$

Chapter-8

Self-Similar Solution of One-dimensional Strong Converging Cylindrical and Spherical Shock Waves in Non-ideal Gas

8.1 Introduction

Shock waves often arise due to balance between wave-breaking nonlinear and wave-damping dissipative forces. Shock waves in condensed matter are generated due to high speed impact of target and projectile. In the case of shock loading of materials in the generation of shock waves, the compression is accompanied by a temperature rise. In general, the material response depends on the nature of pressure loading. Therefore, numerical simulation of high pressure and temperature produced by imploding spherical and cylindrical converging shock waves through condensed media is of theoretical and practical importance because of several applications in the field of astrophysics, astronomy, nuclear engineering, pulsed-power hydrodynamics, cavitation and bubble dynamics, sono-luminescence, impulse technologies, earthquake source dynamics, synthesis of new materials, block ignition, inertial confinement fusion, etc. Imploding shock waves have been a field of research interest over the years as possible methods for generating high-pressure, high-temperature plasmas at the centre of convergence, as well as to understand the basic fluid dynamics is

involved in this process. A theoretical study of the imploding shock wave near the center of convergence in an ideal gas was first studied by Guderely [15]. He exhibited the existence of the self-similar solutions for the shock wave propagating in the vicinity of the centre of the convergence. Later on, many authors [5-7, 32, 38, 50, 53, 54, 85, 96, 97, 121] have presented high-accuracy results adopting alternative approaches.

The problem of contracting spherical or cylindrical shock front propagation into a uniform gas at rest was first studied by Stanyukovich [6]. Fujimoto and Mishkin [85] while analyzing the converging spherical shocks observed a sudden jump in the pressure at the shock front, which continues to increase and reaches a maximum behind the shock front. This concept of single maximum pressure behind the shock front leads to an analytical determination of the shock decay coefficient in closed form. The effects of overtaking disturbances on the motion of converging shock waves were studied by Yousaf [121]. Zeldovich and Raizer [7] studied the problem of implosion of a spherical shock wave in perfect gas and collapse of a spherical bubble in a liquid by using a self-similar solution method [5]. Ponchaut et al. [32] obtained universal solutions for initially infinitesimally weak imploding cylindrical and spherical shock waves in a perfect gas. A power-series solution for the converging strong shock waves in a perfect gas was studied by Hafner [54].

A nonlinear system involving discontinuities such as shocks do not have complete exact solutions, and for analytical work we have to rely on some approximate analytical methods. Hence numerical solutions are used and numerical methods provide useful information to understand the complex physical phenomena completely. Lie group of point transformations is the most powerful method to determine particular solutions to such nonlinear partial differential equations based on the study of their invariance.

In the recent years much attention is focused on the use of group theoretical methods because of their wide applications in determining solutions of non-linear differential equations of physical interest. Lie group symmetry method, is highly algorithmic.

Representation of a Lie group plays an important role in the study of continuous symmetry in mathematics and theoretical physics. Advantages of invariance under Lie group transformation are, (i) reduces the order of an ordinary differential equation, (ii) leads to the superposition of solutions in terms of transforms for a linear partial differential equation and (iii) transforms nonlinear partial differential equation to linear partial differential equation, called determining equations. Moreover, the theory of groups has been applied quite extensively in recent times by several investigators in the field of similarity analysis. These methods received much impetus through the work of [96, 124-127]. Sharma and Radha [96] used the Lie group method described in the works

of [123, 124, 127] to establish the entire class of self-similar solutions for converging shocks in a relaxing gas. The method enables to characterize the medium for which the problem is invariant and admits self-similar solutions. A different approach has been described by Oliveri and Speciale [128] for unsteady equations of perfect gases and ideal magnetogasdynamic equations using substitution principles. Propagation of weak discontinuities in binary mixtures of ideal gas has been discussed by Barbera and Giambo [129]. Jena and Sharma [130] studied the problem of shock wave propagation through a dusty gas mixture obeying the EOS of Mie-Gruneisen type.

Sharma and Radha [131], Pandey et al. [132] using Lie group theory studied symmetry analysis and obtained exact solutions for Euler equations of gasdynamics and magnetogasdynamic equations. Lie group transformations for self-similar shocks in a gas with dust particles have been discussed by Jena [133]. Raja Sekhar and Sharma [134] discussed the evolution of weak discontinuities in classical shallow water equations. Bira and Raja Sekhar [135] have applied to the problem of one dimensional unsteady simple flow of an isentropic, inviscid and perfectly conducting compressible fluid with the effect of transverse magnetic field by employing method of Lie-group analysis.

Self-similar solution of shock wave in condensed matter generated by impulsive load with the medium described by the EOS of Mie-Gruneisen type have been studied by Anisimov and Kravchenko [79]. They found that similarity exponent depends on the EOS parameters. In this chapter, we employed the method of Lie

group invariance under infinitesimal point transformations [123, 124, 127] to study the problem of the self-similar solution of converging spherical and cylindrical imploding shock waves near the centre of implosion. The flow assumes a self-similar character in a non-ideal gas satisfying the EOS of Mie-Gruneisen type. Finite difference method is employed for the numerical solution of the governing equations. The similarity solution remains valid as long as the strong shock approximation is applicable across the shock wave. The one-parameter infinitesimal group of transformations were used with great accuracy to predict the physical behavior of the strong converging spherical and cylindrical shock wave which is normally generated by the rapid release of energy from a centered source and the properties of the ambient gas into which the shock wave is expanding. It is assumed that the limiting motion will be self-similar as the wave converges to the center. The numerical technique employed to study the nature of shock dynamics through a non-ideal medium described by the EOS of Mie-Gruneisen type. In the present study of the problem is to obtain a self-similar solution of converging shock wave near the centre (axis) of implosion and to investigate the behavior of flow parameters immediately behind the shock front in condensed matter EOS for a physically meaningful range of Gruneisen parameters.

8.2 Mathematical Formulation of Problem

8.2.1 Governing equations

We consider the problem of one-dimensional spherical and cylindrical converging strong shock wave propagating into non-ideal medium in the absence of gravity, magnetic field, radiation, and heat transfer. The equations of motion in Euler's form [57, 92, 94]

$$\frac{\partial \rho}{\partial t} + \rho \frac{\partial u}{\partial x} + u \frac{\partial \rho}{\partial x} + (m - 1) \frac{\rho u}{x} = 0 \quad (8.1)$$

$$\frac{\partial u}{\partial t} + u \frac{\partial u}{\partial x} + \frac{1}{\rho} \left(\frac{\partial p}{\partial x} + \frac{\partial q}{\partial x} \right) = 0 \quad (8.2)$$

$$\frac{\partial p}{\partial t} + u \frac{\partial p}{\partial x} - a^2 \left(\frac{\partial \rho}{\partial t} + u \frac{\partial \rho}{\partial x} \right) = 0 \quad (8.3)$$

where $a^2 = \frac{(\Gamma+1)(p+q)}{\rho}$ is the equilibrium speed of sound in viscous medium, Γ is the Gruneisen coefficient, $m = 2$ and 3 denote the cylindrical and spherical geometries of the shock wave. The physical quantities $\rho(x, t)$, $u(x, t)$, $p(x, t)$ and $q(x, t)$ are the density of the gas, gas velocity in the symmetry direction, pressure of the gas, artificial viscosity as functions of radial coordinate x and time coordinate t respectively. These physical quantities are evaluated at a radial distance x from the center of symmetry for all times, t is the time taken by the incident shock front to travel from the point of observation to the centre of the symmetry where it reaches at $t = 0$.

For the present problem, the form of q is taken as [119],

$$q = \frac{1}{2}K^2\rho x^2 \frac{\partial u}{\partial x} \left(\left| \frac{\partial u}{\partial x} \right| - \frac{\partial u}{\partial x} \right) \quad (8.4)$$

where K is a constant parameter, whose value is conveniently adjusted in every numerical evaluation.

The above expression (8.4) may be rewritten as

$$\left. \begin{aligned} q + K^2\rho x^2 \left(\frac{\partial u}{\partial x} \right)^2 &= 0, \quad \text{if } \frac{\partial u}{\partial x} < 0 \\ q &= 0, \quad \text{if } \frac{\partial u}{\partial x} > 0 \end{aligned} \right\} \quad (8.5)$$

where $\frac{\partial u}{\partial x} < 0$ means the viscous effect is present in the flow field comprises of transition flow field between the undisturbed medium and the shock front. The viscosity term is absent for the region $\frac{\partial u}{\partial x} > 0$.

The equations (8.1-8.3, 8.5) represent a set of four non-linear first order partial differential equations of hyperbolic type. Assuming strong shock and shock front radius from the center (axis) to be $R_s(t)$ a power law can be defined as:

$$R_s(t) = \tilde{A}(-t)^\alpha \quad (8.6)$$

where \tilde{A} is a dimensional constant whose dimensions are obtained by the unknown dimensionless number α called as similarity exponent which determines the strength of convergence or equivalently the curvature of the $(x - t)$ trajectory. Similarity exponent α is calculated numerically.

8.2.2 Condensed matter EOS of Mie-Gruneisen model

Equation of state (EOS) describes fundamental thermodynamic properties of matter on its microscopic internal structure. The EOS gives the all the properties of materials in terms of pressure, volume, and energy (or temperature). However, when the gas flow takes place at a high temperature and density is sufficiently low the assumption that the ideal gas is no longer valid. At high temperature, gas is likely to be ionized and non-ideal gas assumption is significant for the present converging shock waves problem. The volumetric fraction of the condensed matter in the mixture at a considered state (ρ, T) is given by

$$Z = Z_0 \frac{\rho}{\rho_0} \quad (8.7)$$

where Z_0 represents the corresponding value at the reference state and it is completely determined by the condensed matter parameters k_c and Γ_0 respectively as follows

$$Z_0 = 1 - k_c \quad (8.8)$$

Assuming, the medium to characterize the equation of state (EOS) of Mie-Gruneisen type [57] under equilibrium condition as

$$p = \rho e \left(\frac{\Gamma-1}{1-Z} \right) \quad (8.9)$$

where e is the specific internal energy of the mixture per unit volume of mass and Γ is the Gruneisen coefficient which is assumed to be dependent on specific

volume only and it is obtained experimentally under normal conditions. Equation (8.9) describes the material behavior during the shock compression. Here, the Gruneisen coefficient for condensed matter can be defined as:

$$\Gamma = \frac{Z_0 \Gamma_0}{(Z_0 + \Gamma_0) V^{Z_0 - \Gamma_0}} \quad (8.10)$$

If we take the values of $k_c = 1.298$, $\Gamma_0 = 1.017$ and $k_c = 1.42$, $\Gamma_0 = 2.12$ (Neal [136]) in the equation (8.10) then we obtain two condensed matter EOS.

The internal energy of the mixture is related to the internal energy of the condensed matter and the internal energy of the perfect gas can be written as

$$e = c_{vm} T = [k_c c_{sc} + (1 - k_c) c_v] T \quad (8.11)$$

where c_{sc} is the specific heat of the materials in condensed matter, c_v is the specific heat of the gas at constant volume, c_{vm} is the specific heat of the mixture at constant volume. For the equilibrium condition, the specific heat of the mixture at constant pressure is

$$c_{pm} = [k_c c_{sc} + (1 - k_c) c_p] \quad (8.12)$$

where k_c is the mass concentration of the condensed material in the mixture taken as a constant in the whole flow field, c_p is the specific heat of the gas at constant pressure.

The incompressibility assumption of the condensed matter implies equality of the specific heat of the materials in condensed matter and specific heats of the gas at constant volume, pressure respectively as follows

$$c_{sc} = c_v = c_p, \quad \text{when } Z_0 = 0 \quad (8.13)$$

The ratio of the specific heat of the mixture is then

$$\Gamma_0 = \frac{c_{pm}}{c_{vm}} \quad (8.14)$$

The Gruneisen coefficient for a perfect gas is a constant and is equal to γ when $Z_0 = 0$, where $\gamma = (c_p/c_v)$ is the ratio of the specific heats of the perfect gas.

8.2.3 Boundary conditions

The boundary conditions due to Rankine-Hugoniot jump conditions connecting the states ahead of and behind the shock front for a strong shock wave are

$$u_1 = \left(1 - \frac{\rho}{\rho_0}\right) \dot{X}_1 \quad (8.15)$$

$$p_1 - p_0 = \rho_0 u_1 \dot{X}_1 \quad (8.16)$$

$$e_1 - e_0 = u_1^2 + \frac{p_0}{\rho_1} \left(1 - \frac{\rho_0}{\rho_1}\right) \quad (8.17)$$

where $\dot{X}_1 = \frac{dR_s(t)}{dt}$ denotes the shock velocity and the subscript 1 and 0 refers the values of flow parameters immediately behind (shocked region) and ahead (unshocked region) of the shock front respectively and dot denotes differentiation

with respect to time. The gas is assumed to be in thermodynamic equilibrium and radiation effects to the energy and pressure are negligible.

The strong shock compression process is characterized by the Rankine-Hugoniot jump relations, then the strong shock conditions for the present problem can be written as

$$u_1 = (1 - \beta)\dot{X}_1 \quad (8.18)$$

$$p_1 = (1 - \beta)\rho_0\dot{X}_1^2 \quad (8.19)$$

$$e_1 = p_1(1 - \beta)/(2\rho_0) \quad (8.20)$$

$$\rho_1 = (\rho_0/\beta) \quad (8.21)$$

$$Z_1 = (Z_0/\beta) \quad (8.22)$$

Equations (8.15-8.17) relate the thermodynamic state variables on each side of the propagating discontinuity but they do not describe the way the material changes from the initial to final state. Using the strong Rankine-Hugoniot jump shock conditions (8.18-8.22), equation (8.9) can be simplified for the shock density ratio across a shock wave as

$$(\beta - 1)\Gamma(\beta) = 2 \quad (8.23)$$

where β is the shock density ratio and it is obtained from the solution of the equation (8.23). This ratio depends on the characteristics of the implosion such

as the shell adiabatic, in general $\beta > 1$. However, the shock efficiency increases if β decreases.

Rankine-Hugoniot conditions are independent of the amount and form of the dissipation, provided that $q \rightarrow 0$ as $x \rightarrow \pm\infty$. Because the R-H equations are direct consequence of the conservation laws. The governing equations of the flow require that in a shock a certain amount of mechanical energy is converted irreversibly into heat. Thus, we have the initial and final values of artificial viscosity term given by

$$u \rightarrow u_0, \quad p \rightarrow p_0, \quad q \rightarrow 0 \quad \text{as } x \rightarrow -\infty \quad (8.24)$$

$$u \rightarrow u_1, \quad p \rightarrow p_1, \quad q \rightarrow 0 \quad \text{as } x \rightarrow +\infty \quad (8.25)$$

8.3 Similarity Analysis by Invariance Groups

The objective of Lie group theory of symmetry analysis of differential equations relies on the invariance of the latter under a transformation of independent and dependent variables. These are called local Lie point symmetries. Since, the system of equations (8.1-8.3, 8.5) contain a set of quasilinear hyperbolic partial differential equations and it is usually difficult to solve, as the equations are highly non-linear, in general, to determine a solution without approximations. Here, we assume that there exists a solution of system of equations (8.1-8.3, 8.5) subject to boundary conditions (8.15-8.17) along a family of curves, called similarity curves, for which system of equations (8.1-8.3, 8.5) of partial

differential equations reduces to a system of ordinary differential equations; this type of solution is called a similarity solution. In order to obtain the similarity solutions of system (8.1-8.3, 8.5), we derive its symmetry group such that the system is invariant under this group of transformations, so that the mathematical problem of solving the equations in certain cases allows to find analytic solutions.

We consider a one-parameter infinitesimal group of transformations with independent variables x, t and dependent variables ρ, u, p, q as [96, 97, 131]

$$\left. \begin{aligned} x^* &= x + \varepsilon\chi(x, t, \rho, u, p, q), & t^* &= t + \varepsilon\psi(x, t, \rho, u, p, q), \\ \rho^* &= \rho + \varepsilon V(x, t, \rho, u, p, q), & u^* &= u + \varepsilon U(x, t, \rho, u, p, q), \\ p^* &= p + \varepsilon P(x, t, \rho, u, p, q), & q^* &= q + \varepsilon G(x, t, \rho, u, p, q) \end{aligned} \right\} \quad (8.26)$$

where the generators χ, ψ, V, U, P and G are functions of t, x, ρ, u, p and q which are to be determined in such a way that system of equations (8.1-8.3, 8.5) of non-linear partial differential equations together with conditions (8.15-8.17) is invariant with respect to transformations (8.26). The group parameter ε is so small such that its square and higher powers may be neglected. The existence of such a group allows the number of independent variables in the problem to be reduced by one, and thereby allowing the system of equations (8.1-8.3, 8.5) to be replaced by a system of ordinary differential equations.

For convenience, we introduce the notation $x_1 = t, x_2 = x, w_1 = \rho, w_2 = u,$

$w_3 = p, w_4 = q$ and $p_l^k = \frac{\partial w_k}{\partial x_l}$, where $k = 1, 2, 3, 4$ and $l = 1, 2$.

Thus the governing equations (8.1-8.3, 8.5) can be written as

$$F_s(x_l, w_k, p_l^k) = 0, \quad s = 1, 2, 3, 4 \quad (8.27)$$

This is said to be constantly conformally invariant under the infinitesimal group (8.26), if there exist constants d_{sr} ($s, r = 1, 2, 3, 4$) such that for all smooth surfaces $w_k = w_k(x_l)$, we have

$$\mathcal{L}F_s = d_{sr}F_r \quad (8.28)$$

where \mathcal{L} is the Lie derivative in the direction of the extended vector field which arise naturally in the context of fluid flow.

$$\mathcal{L} = \xi^l \frac{\partial}{\partial x_l} + \eta^k \frac{\partial}{\partial u_k} + \phi_l^k \frac{\partial}{\partial p_l^k} \quad (8.29)$$

with

$$\xi^1 = \psi, \quad \xi^2 = \chi, \quad \eta^1 = V, \quad \eta^2 = U, \quad \eta^3 = P, \quad \eta^4 = G$$

and

$$\phi_l^k = \frac{\partial \eta^k}{\partial x_l} + \frac{\partial \eta^k}{\partial w_s} p_l^s - \frac{\partial \xi^j}{\partial x_l} p_j^k - \frac{\partial \xi^j}{\partial x_n} p_j^k p_l^n \quad (8.30)$$

where $j = 1, 2, l = 1, 2, k = 1, 2, 3, 4, n = 1, 2, 3, 4$ and $s = 1, 2, 3, 4$. Here, repeated indices imply summation convention and ϕ_l^k are the generators of the derivative transformations.

Along with the equations (8.29) and (8.30), equation (8.28) can be rewritten as follows

$$\xi^l \frac{\partial F_s}{\partial x_l} + \eta^k \frac{\partial F_s}{\partial u_k} + \phi_l^k \frac{\partial F_s}{\partial p_l^k} = d_{sr} F_r, \quad s = 1, 2, 3, 4 \text{ and } r = 1, 2, 3, 4 \quad (8.31)$$

Substituting the equation (8.30) into the equation (8.31) yields a polynomial in terms of p_l^k . Equating the coefficients of partial derivatives p_l^k and $p_l^k p_j^s$ to zero gives an overdetermined system of first order, linear partial differential equations in the generators ψ, V, U, P and G whose integration leads to the infinitesimals of the group. This system is called the system of determining equations and is,

$$\begin{aligned} V_t + uV_x + \rho U_x + \frac{(m-1)}{x} \left[\rho U + uV - \frac{\rho u \chi}{x} \right] &= d_{11} \frac{(m-1)\rho u}{x} + d_{14} q \\ V_\rho - \psi_t - u\psi_x + \frac{(m-1)u\psi}{x} &= d_{11} - a^2 d_{13} \\ V_u - \rho\psi_x + \frac{(m-1)\rho\psi}{x} &= d_{12} \\ V_p &= d_{13} \\ V_q &= 0 \\ U - \chi_t + uV_\rho - u\chi_x + \rho U_\rho + \frac{(m-1)u\chi}{x} &= u(d_{11} - a^2 d_{13}) \\ V + uV_u + \rho U_u - \rho\chi_x + \frac{(m-1)\rho\chi}{x} &= d_{11}\rho + d_{12}u \\ uV_p + \rho U_p &= d_{12}\rho^{-1} + d_{13}u \\ uV_q + \rho U_q &= \rho^{-1}d_{12} \end{aligned} \quad (8.32)$$

$$U_t + uU_x + \rho^{-1}(P_x + G_x) = d_{21} \frac{(m-1)\rho u}{x} + d_{24}q$$

$$U_\rho = d_{21} - a^2 d_{23}$$

$$U_u - \psi_t - u\psi_x = d_{22}$$

$$U_p - \rho^{-1}\psi_x = d_{23}$$

$$U_q - \rho^{-1}\psi_x = 0$$

$$uU_\rho + \rho^{-1}(P_\rho + G_\rho) = u(d_{21} - a^2 d_{23})$$

$$U - \chi_t + u(U_u - \chi_x) + \rho^{-1}(P_u + G_u) = d_{21}\rho + d_{22}u$$

$$uU_p - \rho^{-2}V + \rho^{-1}(P_p + G_p - \chi_x) = d_{22}\rho^{-1} + d_{23}u$$

$$uU_q - \rho^{-2}V + \rho^{-1}(P_q + G_q - \chi_x) = d_{22}\rho^{-1}$$

(8.33)

$$P_t + uP_x - a^2(V_t + uV_x) = d_{31} \frac{(m-1)\rho u}{x} + d_{34}q$$

$$\psi\Gamma_t + \chi\Gamma_x + V\Gamma_\rho - \frac{\rho}{p+q}P_\rho + (\Gamma + 1) \left[V_\rho - \psi_t - u\psi_x - \frac{V}{\rho} + \frac{P}{p+q} \right]$$

$$= (a^2 d_{33} - d_{31}) \frac{\rho}{p+q}$$

$$P_u - a^2 V_u = d_{32}$$

$$P_p - a^2 V_p - \psi_t - u\psi_x = d_{33}$$

$$P_q - a^2 V_q = 0$$

(8.34)

$$\psi\Gamma_t + \chi\Gamma_x + V\Gamma_\rho - \frac{\rho}{p+q}P_\rho + (\Gamma + 1) \left[u^{-1}\chi_t - \chi_x + V_\rho - \frac{V}{\rho} + \frac{U}{u} + \frac{P}{p+q} \right]$$

$$= u(a^2d_{33} - d_{31}) \frac{\rho}{p+q}$$

$$uP_u - a^2uV_u = d_{31}\rho + d_{32}u$$

$$U - \chi_t - a^2uV_p + uP_p - u\chi_x = d_{32}\rho^{-1} + d_{33}u$$

$$uP_q - a^2uV_q = \rho^{-1}d_{32}$$

(8.34)

$$G = d_{44}q + \frac{(m-1)\rho u}{x}d_{41}$$

$$d_{41} - a^2d_{43} = 0$$

$$d_{42} = 0$$

$$d_{43} = 0$$

$$\psi = 0$$

$$u(d_{41} - a^2d_{43}) = 0$$

$$2K^2\rho x^2U_x = \rho d_{41} + ud_{42}$$

$$\rho^{-1}d_{42} + ud_{43} = 0$$

$$\chi = \rho^{-1}d_{42}$$

(8.35)

The solution procedure of the above determining equations (8.32-8.35) is obtained by considering the following two cases:

Case 1: For the region $\frac{\partial u}{\partial x} < 0$, then it means that the viscous effect is present in the flow field comprises of transition flow field between the undisturbed medium and shock front. Then, the system of determining equations (8.35) is solved to obtain the group of transformations as follows:

$$\left. \begin{aligned} G &= d_{44}q \\ \psi &= 0 \\ \chi &= 0 \\ U &= \text{constant} \end{aligned} \right\} (8.36)$$

where d_{44} is an arbitrary constant.

Case 2: For the region $\frac{\partial u}{\partial x} > 0$, then it means that the viscosity effect is absent in the flow field. Then the viscosity term of the system (8.35) is zero (i.e., $G = 0$ when $q = 0$) and the remaining system of determining equations (8.32-8.34) is solved to obtaining the group of transformations as follows

$$\left. \begin{aligned} V &= (d_{11} + b)\rho \\ U &= (d_{22} + b)u, \quad \text{if } m = 2, 3 \\ P &= (2d_{22} + d_{11} + 3b)p \end{aligned} \right\} (8.37)$$

$$\chi = (d_{22} + 2b)x, \text{ if } m = 2, 3$$

$$\psi = bt + c$$

where d_{11} , d_{22} , b and c are arbitrary constants.

We note that the effect of generators ψ and χ is negligible in the presence of viscosity irrespective of the time, space coordinates. The generator G is proportional to the viscosity term q but it is independent of time and space coordinates. Thus, the effect of generators V , U and P on viscosity is considerable so that density, velocity, and pressure vary appreciably over the mean free path in the flow field. Hence, the self-similar solution of present problem in the absence of viscosity by employing Lie-group analysis method is presented in the following section.

8.4 Self-Similar Solutions

The type of motion in which the distribution of flow variables remain similar to themselves with time and vary only as a result of changes in scale is called self-similar. In this type of flow, all the flow variables describing motion i.e., density $\rho(r, t)$, velocity $u(r, t)$, and pressure $p(r, t)$ do not depend on the radial coordinate x and time coordinate t independently but are the functions only of the combination $\frac{x}{t}$. The change of variables from (x, t) to (x^*, t^*) defined as $x^* = x$, $t^* = t + \frac{c}{b}$ does not change the governing equations (8.1-8.3); thus, rewriting

the equations in system (8.37) in terms of the new variables x^* and t^* , and then dropping the asterisk sign, we obtain

$$\begin{aligned}
 V &= (d_{11} + b)\rho \\
 U &= (d_{22} + b)u, \quad \text{if } m = 2, 3 \\
 P &= (2d_{22} + d_{11} + 3b)p \\
 \chi &= (d_{22} + 2b)x, \quad \text{if } m = 2, 3 \\
 \psi &= bt
 \end{aligned}
 \tag{8.38}$$

However, the infinitesimals V , U and P in system (8.38) remain unchanged. To obtain the self-similar solutions, we use the invariant surface conditions, which yield

$$\psi\rho_t + \chi\rho_x = V, \quad \psi u_t + \chi u_x = U, \quad \psi p_t + \chi p_x = P \tag{8.39}$$

The characteristic equations, involving only independent variables x , t to the corresponding set of equations (8.39) are

$$\frac{dt}{d\psi} = \frac{dx}{d\chi} = \frac{d\rho}{dV} = \frac{du}{dU} = \frac{dp}{dP} \tag{8.40}$$

We integrate the above system of characteristic equations associated with transformations (8.38) to obtain the flow variables ρ , u and p in the following form:

$$\begin{aligned}
\rho &= t^{\left(1+\frac{d_{11}}{b}\right)} \hat{V}(\lambda) \\
u &= t^{\alpha-1} \hat{U}(\lambda), \quad \text{if } m = 2, 3 \\
p &= t^{\left(2\alpha-1+\frac{d_{11}}{b}\right)} \hat{P}(\lambda)
\end{aligned}
\tag{8.41}$$

where

$$\alpha = \frac{d_{22}+2b}{b}$$

the functions \hat{V} , \hat{U} and \hat{P} depend only on the dimensionless form of the similarity variable λ , where

$$\lambda = \frac{x}{R_s(t)}, \quad \text{if } m = 2, 3
\tag{8.42}$$

The path of the piston is imposed as a boundary condition. Thereby, an accelerated, a decelerated, or a constant-velocity piston can be specified. The fluid velocities and the pressure in the ambient medium are assumed to be varying and obeying a power law. The density of the ambient medium is assumed to be constant. For shock to be a similarity curve, it may be normalized and $\lambda = 1$. The position of shock wave $R_s(t)$ and the shock velocity \dot{X}_1 are given by

$$\begin{aligned}
R_s(t) &= \tilde{A}(-t)^\alpha, \quad \text{if } m = 2, 3 \\
\dot{X}_1 &= \frac{\alpha R_s(t)}{t}, \quad \text{if } m = 2, 3
\end{aligned}
\tag{8.43}$$

Here t is the time taken negative because the shock converges to the center (axis) of symmetry and time $t = 0$ is taken to be at the instant of shock collapse. At $t =$

0 the shock front reaches the origin and at the immediate next instance, the information about collapse may not reach the far field and hence only the flow at $r = 0$ is immediately affected. This implies that for the solution at $t = 0$ and for the similarity solution for $t > 0$ the exponent α in the similarity variable λ should be same as, before collapse. However, self-similarity requires the velocity of the shock and the velocity of the piston to be proportional to the power law equation (8.6) in time and the strong shock assumption.

At the shock front $\lambda = 1$, we have the following conditions on the functions \hat{V} , \hat{U} and \hat{P}

$$\left. \begin{aligned} \rho &= t^{\left(1+\frac{d_{11}}{b}\right)} \hat{V}(1) \\ u &= t^{\alpha-1} \hat{U}(1), \quad \text{if } m = 2, 3 \\ p &= t^{\left(2\alpha-1+\frac{d_{11}}{b}\right)} \hat{P}(1) \end{aligned} \right\} \quad (8.44)$$

If a one parameter group of transformations leaves invariant an equation and it is accompanying boundary conditions, then the number of variables can be reduced by one. Here, the self-similar motion of flow pattern takes the following form:

$$\rho = \rho_0 \hat{V}(\lambda), \quad u = \dot{X}_1 \hat{U}(\lambda), \quad p = \rho_0 \dot{X}_1^2 \hat{P}(\lambda), \quad q = \rho_0 \dot{X}_1^2 \hat{G}(\lambda) \quad (8.45)$$

where the quantities \hat{V} , \hat{U} , \hat{P} and \hat{G} are the unknown dimensionless functions of the similarity variable λ which can be defined as the ratio between radial distance

x and shock wave position $R_s(t)$ at shock front from the center of axis.

Mathematically, we write it as

$$\lambda = \frac{x}{R_s(t)} \quad (8.46)$$

The dimensionless functions \hat{V} , \hat{U} , \hat{P} and \hat{G} appearing in the equation (8.45) are defined on $t \leq 0$, $0 \leq x \leq R_s(t)$ and $1 \leq \lambda < \infty$ and also may note that spherical or cylindrical converging shock front is positioned at $\lambda = 1$. Further it is for computational convenience we introduce another set of transformations along with above transformations (8.45) as,

$$V^*(\lambda) = \hat{V}(\lambda), \quad U^*(\lambda) = \alpha \frac{\hat{U}(\lambda)}{\lambda}, \quad P^*(\lambda) = \alpha^2 \frac{\hat{P}(\lambda)}{\lambda^2}, \quad G^*(\lambda) = \alpha^2 \frac{\hat{G}(\lambda)}{\lambda^2} \quad (8.47)$$

$$\text{with } Y^*(\lambda) = \frac{P^*(\lambda)}{V^*(\lambda)},$$

where the quantities V^* , U^* , P^* and G^* are new dimensionless functions for density, velocity, pressure, and viscosity respectively. The equations (8.46) and (8.47) are very useful when the shock front moves on a line of a constant λ under certain conditions. In a space-time domain close to the centre and near the instant of collapse this problem admits a similarity solution that describes the asymptotics of the phenomenon [137], which means that the solution depends only on the combination of x and $R_s(t)$.

With the aid of transformations (8.45) and (8.47), the governing Euler equations (8.1-8.3, 8.5) are reduced into a system of the four non-linear ordinary differential

equations in V^* , U^* , P^* and G^* (which on dropping the asterisk sign) for the case of similarity solution:

$$(U - \alpha) \frac{d \ln V}{d \ln \lambda} + \frac{dU}{d \ln \lambda} = -mU \quad (8.48)$$

$$Y \frac{d \ln V}{d \ln \lambda} + (U - \alpha) \frac{dU}{d \ln \lambda} + \frac{dY}{d \ln \lambda} + \frac{1}{V} \frac{dG}{d \ln \lambda} = - \left[2Y + (U - 1)U + \frac{2G}{V} \right] \quad (8.49)$$

$$\frac{dY}{d \ln \lambda} + \Phi \frac{d \ln V}{d \ln \lambda} = -2 \left[\frac{\alpha - 1}{U - \alpha} + 1 \right] Y \quad (8.50)$$

$$\frac{dU}{d \ln \lambda} + U = \frac{(-1)^{1/2}}{K(V/G)^{1/2}} \quad (8.51)$$

where

$$\Phi = Y \left[(1 - \Gamma) - \frac{\Gamma/V}{(\Gamma - 1)} \right] - \frac{(\Gamma - 1)G}{V} \quad (8.52)$$

The transformed boundary conditions for the strong shock with $\lambda = 1$ are

$$V(1) = \frac{1}{\beta}, \quad U(1) = (1 - \beta)\alpha, \quad Y(1) = \beta(1 - \beta)\alpha^2, \quad G(1) = 0 \quad (8.53)$$

8.5 Numerical Solution to Converging Shock Wave

In this section, we present the numerical solution of problem based on finite difference approximations. Numerical calculations are performed to obtain the profiles of flow parameters behind the shock front and total computational work is performed using MATLAB.

8.5.1 Replacing derivatives by finite differences

The derivatives of non-dimensional density, velocity and pressure versus similarity coordinate are approximated with a first order forward difference approximation. The forward difference approximation of the derivatives for the system of equations (8.48-8.51) are defined as

$$\frac{dV}{d\lambda} = \frac{V_{i+1}-V_i}{\Delta\lambda}, \quad \frac{dU}{d\lambda} = \frac{U_{i+1}-U_i}{\Delta\lambda}, \quad \frac{dY}{d\lambda} = \frac{Y_{i+1}-Y_i}{\Delta\lambda}, \quad \frac{dG}{d\lambda} = \frac{G_{i+1}-G_i}{\Delta\lambda} \quad (8.54)$$

Substituting these derivatives in equations (8.48-8.51) and after simplifying result in a system of algebraic equations,

$$(U_i - \alpha)V_{i+1} + V_iU_{i+1} = \left(2 - \frac{mh}{\lambda_i}\right)U_iV_i - \alpha V_i \quad (8.55)$$

$$Y_iV_{i+1} + (U_i - \alpha)V_iU_{i+1} + V_iY_{i+1} + G_{i+1} = 2\left(1 - \frac{h}{\lambda_i}\right)Y_iV_i + \left\{(U_i - \alpha) - \frac{h}{\lambda_i}(U_i - 1)\right\}U_iV_i + \left(1 - \frac{2h}{\lambda_i}\right)G_i \quad (8.56)$$

$$\Phi_iV_{i+1} + V_iY_{i+1} = \left[1 - \frac{2h}{\lambda_i}\left(\frac{U_i-1}{U_i-\alpha}\right)\right]V_iY_i + \Phi_iV_i \quad (8.57)$$

$$U_{i+1} = \left(1 - \frac{h}{\lambda_i}\right)U_i + \frac{(-1)^{1/2}h}{\xi_i K \left(\frac{V_i}{G_i}\right)^{1/2}} \quad (8.58)$$

where

$$\Phi_i = Y_i \left[(1 - \Gamma_i) - \frac{\Gamma_i/V_i}{(\Gamma_i-1)} \right] - \frac{(\Gamma_i-1)G_i}{V_i} \quad (8.59)$$

These equations can be written in the matrix form as follows

$$[A_i][X_{i+1}] = [B_i] \quad (8.60)$$

where $[A_i]$, $[X_{i+1}]$ and $[B_i]$ are 4x4, 4x1 and 4x1 matrices respectively.

$$[A_i] = \begin{bmatrix} (U_i - \alpha) & V_i & 0 & 0 \\ Y_i & (U_i - \alpha)V_i & V_i & 1 \\ \Phi_i & 0 & V_i & 0 \\ 0 & 1 & 0 & 0 \end{bmatrix} \quad (8.61)$$

$$[X_{i+1}] = [V_{i+1} \quad U_{i+1} \quad Y_{i+1} \quad G_{i+1}]^T \quad (8.62)$$

$$[B_i] = \begin{bmatrix} \left(2 - \frac{mh}{\lambda_i}\right) U_i V_i - \alpha V_i \\ 2 \left(1 - \frac{h}{\lambda_i}\right) Y_i V_i + \left\{ (U_i - \alpha) - \frac{h}{\lambda_i} (U_i - 1) \right\} U_i V_i + \left(1 - \frac{2h}{\lambda_i}\right) G_i \\ \left\{ 1 - 2 \frac{h}{\lambda_i} \frac{(U_i - 1)}{(U_i - \alpha)} \right\} V_i Y_i + \Phi_i V_i \\ \left(1 - \frac{h}{\lambda_i}\right) U_i + \frac{(-1)^{1/2} h}{\lambda_i K (V_i / G_i)^{1/2}} \end{bmatrix} \quad (8.63)$$

Employing Crout's reduction method [93] the system of equations (8.60) are solved for flow variables such as density V_{i+1} , velocity U_{i+1} , pressure Y_{i+1} , and viscosity G_{i+1} respectively:

$$V_{i+1} = P_i - \frac{V_i}{(U_i - \alpha)} Q_i + \frac{V_i}{[(U_i - \alpha)^2 - Y_i]} R_i + \frac{1}{[(U_i - \alpha)^2 + \Phi_i - Y_i]} S_i \quad (8.64)$$

$$U_{i+1} = Q_i - \frac{(U_i - \alpha)}{[(U_i - \alpha)^2 - Y_i]} R_i - \frac{(U_i - \alpha)}{[(U_i - \alpha)^2 + \Phi_i - Y_i] V_i} S_i \quad (8.65)$$

$$Y_{i+1} = R_i - \frac{\Phi_i}{[(U_i - \alpha)^2 + \Phi_i - Y_i] V_i} S_i \quad (8.66)$$

$$G_{i+1} = S_i \quad (8.67)$$

where

$$P_i = \frac{(B_{11})^{(i)}}{(U_i - \alpha)} \quad (8.68)$$

$$Q_i = \frac{[(U_i - \alpha)(B_{21})^{(i)} - Y_i(B_{11})^{(i)}]}{[(U_i - \alpha)^2 - Y_i]V_i} \quad (8.69)$$

$$R_i = \frac{[(B_{21})^{(i)} - (U_i - \alpha)(B_{11})^{(i)}]\Phi_i + \{(U_i - \alpha)^2 - Y_i\}(B_{31})^{(i)}}{[(U_i - \alpha)^2 + \Phi_i - Y_i]V_i} \quad (8.70)$$

$$S_i = \left[\frac{(\Phi_i - Y_i)}{(U_i - \alpha)} \right] (B_{11})^{(i)} + (B_{21})^{(i)} - (B_{31})^{(i)} - V_i \frac{[(U_i - \alpha)^2 + \Phi_i - Y_i]}{(U_i - \alpha)} (B_{41})^{(i)} \quad (8.71)$$

where the subscript i represents reduced density, velocity, and pressure at the current reduced distance step, whereas $(i + 1)$ represents the new (future) reduced density, velocity, and pressure and it is a positive integer. Numerical solution of system of equations (8.64-8.67) along with boundary conditions (8.53) are obtained for a step size of $h = 10^{-4}$.

8.6 Analysis for System of Equations (8.48-8.50) without Viscosity

In this section, we described the evaluation of the similarity exponent α appearing in the system of equations (8.48-8.50). It is observed that the similarity variable λ appears in the equations (8.48-8.50) only through the logarithmic derivatives. Similarly, one of the unknown dimensionless function V appears only through the differential $d \ln V$. This property of system of equations (8.48-8.50) which is

characteristic of all self-similar motions, permits the reduction of the system of three differential equations into a single differential equation in U and Y .

The equations (8.48-8.50) are represented in matrix form as:

$$CW = D \quad (8.72)$$

where $W = \left[\frac{dU}{d \ln \lambda}, \frac{d \ln V}{d \ln \lambda}, \frac{dY}{d \ln \lambda} \right]^T$ and the matrix C and the column vector D can be read by inspection from the system of equations (8.48-8.50). It is noted that the unknown parameter i.e., similarity exponent α appearing in system of equations (8.48-8.50) is obtained only by solving as an Eigen value problem but not from dimensional analysis or from energy balance for a system of differential equations (8.48-8.50).

Solving the matrix equation (8.72) for derivatives using phase plane analysis method [7, 15, 57] these derivatives in matrix form (8.60) can be written into the following form:

$$\frac{dU}{d \ln \lambda} = \frac{\Delta_1}{\Delta}, \quad \frac{d \ln V}{d \ln \lambda} = \frac{\Delta_2}{\Delta}, \quad \frac{dY}{d \ln \lambda} = \frac{\Delta_3}{\Delta} \quad (8.73)$$

where Δ , defined as the determinant of the non-singular matrix C and Δ_r ($r = 1, 2, 3$) are the determinants obtained from Δ by replacing the r th column by the column vector D which are given by

$$\Delta = (U - \alpha)^2 - Y[1 - \Phi(V)] \quad (8.74)$$

$$\Delta_1 = mUY[1 - \Phi(V)] - 2Y(1 - \alpha) - U(U - 1)(U - \alpha) \quad (8.75)$$

$$\Delta_2 = U(U - 1) + 2 \frac{(1-\alpha)}{(U-\alpha)} Y - mU(U - \alpha) \quad (8.76)$$

$$\Delta_3 = 2 \frac{Y^2(U-1)}{(U-\alpha)} - \{U(U-1) + 2Y + mU(U-\alpha)\}Y\Phi(V) - 2Y(U-1)(U-\alpha) \quad (8.77)$$

The coefficients of the derivatives of the system of equations (8.48-8.50) depend on V , U and Y . The determinants Δ , Δ_1 , Δ_2 and Δ_3 are functions of V , U and Y . The right-hand side equations (8.48-8.50) depend only on U and Y and do not depend on V and λ . By assuming $[1 - \Phi(V)] = k_c$ where the constant k_c [136]. The system of equations (8.48-8.50) and the determinants Δ , Δ_1 , Δ_2 and Δ_3 are functions of U and Y only. Now, it is possible to reduce the system (8.73) to the autonomous first-order differential equation for Z with respect to U . Dividing the third equation of system (8.73) by the first, we obtain the following first-order ordinary differential equation

$$\frac{dY}{dU} = \frac{\Delta_3(Y,U)}{\Delta_1(Y,U)} \quad (8.78)$$

Evaluation of $Y(U)$ from the equation (8.78) enables to determine $U(\lambda)$ using the first equation in system (8.73). Finally $V(\lambda)$ is obtained by substituting $U(\lambda)$ and $Y(U)$ into the second equation of system (8.73). The plane (Y, U) is called the phase plane. A solution of equation (8.74) is represented by an integral curve in the phase plane. The solution of a given self-similar problem characterized by the boundary conditions is represented in the phase plane by one or more pieces (adequately joined) of the appropriate integral curves which satisfy at their ends the boundary conditions. Any piece represents the solution in a certain domain of the independent variable. In order to determine which integral trajectory

corresponds to a given problem (i.e. to its particular initial and boundary conditions) it is necessary to know the behavior of the solutions near the singular points of equation (8.78). The system of equations (8.48-8.50) are numerically integrated from $\lambda = 1$ (shock surface) to the infinity ($\lambda = \infty$) in the converging phase, under the desired boundary conditions (8.53). The integration is terminated at the singular point such that all the integrated curves for the reduced quantities smoothly pass the singular point. Therefore only an appropriate value of similarity exponent α satisfies this condition as the eigen value. The condition under which the integral curve $Y(U)$ smoothly crosses the parabola, $\Delta = 0$ determines the similarity exponent α , and the curve then monotonically converges to the origin in the (U, Y) plane $Y(\infty) = U(\infty) = 0$.

To evaluate the similarity exponent α with corresponding known values of, Γ_0 , k_c , β and γ , we choose a probable value of α and integrate equations (8.73) from $\lambda = 1$ to $\lambda = \infty$ at which Δ vanishes and then compute the values of V , U , Y and Δ_1 . By successive approximations, the value of α is corrected in such a way that both the determinants Δ and Δ_1 vanish. The correct value of α is determined by employing the one-parameter iterative procedure such that all the determinants Δ , Δ_1 , Δ_2 and Δ_3 become zero simultaneously at the same value of λ (in the domain of interest $1 \leq \lambda < \infty$), which is the singular point of the system. For this correct value of α , we obtain the final non-singular solutions. This method of solution is eigen value problem of the second kind for shock waves.

8.7 Results and Discussion

The numerical computations of similarity exponent α corresponding to the known values of parameters Γ_0 , k_c , β and γ behind the shock front with cylindrical and spherical geometries for perfect gas, condensed matter EOS are summarized in Tables 8.1 and 8.2. The shock front propagates according to the power law equation (8.6) with the various values of similarity exponent α .

In the numerical method, spatial grid of 4000 points and step size of $\Delta\lambda = 10^{-4}$ is employed. The behavior of shock velocity and pressure are shown in Figures 8.1-8.8 for the two different kinds of condensed matter EOS such as aluminum ($\Gamma_0 = 2.12$, $k_c = 1.42$), lithium ($\Gamma_0 = 1.017$, $k_c = 1.298$). The numerical solution gives the rate of approach to the asymptotic solution as well as the dependence of the shock motion and flow profiles.

Table 8.1: Selected results of the similarity exponent α for perfect gas and the condensed matter EOS in the case of cylindrical geometry

Perfect gas				Condensed matter				
γ	α			Γ_0	k_c	β	α	
	FDM	Phase Plane	Lazarus Values				FDM	Phase Plane
1.1	0.88499	0.885249	-					
1.4	0.83483	0.835323	0.8353231919	2.12	1.42	0.4571123	0.8677762652	0.681796988
5/3	0.81555	0.815625	0.8156249014	1.017	1.298	0.2155141	0.9329767828	0.54385697
3	0.77498	0.775667	0.7756666194					

Table 8.2: Selected results of the similarity exponent α for perfect gas and the condensed matter EOS in the case of spherical geometry

Perfect gas				Condensed matter				
γ	α			Γ_0	k_c	β	α	
	FDM	Phase Plane	Lazarus Values				FDM	Phase Plane
1.1	0.78667	0.795969	-					
1.4	0.70908	0.717174	0.717174501	2.12	1.42	0.4571123	0.7664353241	0.70864358
5/3	0.68795	0.688377	0.6883768229	1.017	1.298	0.2155141	0.8743734604	0.71427626
3	0.64286	0.636411	0.6364105940					

From the above Tables 8.1 and 8.2, it may be observed that for condensed matter EOS, the similarity exponent α increases with an increase in any of the parameters Γ_0 , k_c and β for cylindrical geometry whereas in the case of spherical geometry it decreases with an increase in any of the parameters Γ_0 , k_c and β . In the perfect gas EOS, similarity exponent α decreases with an increase in the adiabatic exponent γ for both cylindrical and spherical geometry. This indicates that a decrease/increase of the similarity exponent α is associated with an increase/decrease of measure of the shock strength β and β varies with change in Γ_0 and k_c . The numerical values of similarity exponent α is in close agreement with Lazarus [51, 52] values for perfect gas EOS.

In the absence of viscosity ($K = 0$), the behavior of particle velocity, pressure distributions versus reduced distance λ in both cylindrical, spherical symmetry for lithium, aluminum EOSs are shown in Figures 8.1 and 8.2. The velocity, pressure of fluid changes with reduced distance λ along the shock region in both

the geometries. Lithium gas EOS is presented in Figures 8.1(a) and 8.1(b). It is observed from Figure 8.1(a) that the velocity distribution increases rapidly with an increase in reduced distance λ behind the shock front for cylindrical geometry, whereas in the case of spherical geometry it has similar behavior but velocity distribution has a lower values with an increasing values of reduced distance λ . This means that the acceleration of gas particles (i.e., shock speed) is higher for cylindrical geometry than in case of spherical geometry. Moreover, shock dynamics is non-linear so that the velocity of shock depends on measure of shock strength β . The pressure distribution decreases with an increase in reduced distance λ for both cylindrical, spherical geometries. For the case of cylindrical geometry, in particular, we found that reflected shock appears in the pressure distribution behind the shock front after shock converges to the center, then it increases rapidly and finally decreases slowly as λ increases (Figure 8.1(b)). Moreover, in the case of a cylindrically converging shock wave the implosion effect can be observed with monotonic decrease in pressure profile at the shock front.

The velocity, pressure distributions versus reduced distance λ in the case of aluminum gas EOS are shown in Figure 8.2. The velocity distribution is similar to Figure 8.1(a) (for cylindrical geometry) whereas in the case of spherical geometry it is just reverse effect as shown in Figure 8.2(a). From Figure 8.2(b), we observe that the pressure distribution decreases with increase in reduced distance λ behind the shock front and then decrease constantly as λ increases for

both geometries. Also we found that there is no variation in pressure distribution behind the shock front. This means that decay of shock pressure is significantly lower. Since the mass concentration of the gas particles is finite, the pressure behind the shock front falls off rapidly due to rarefaction waves. These pressure profiles are similar of literature to those of Mitchell and Nellis [138] and Yadav [139].

The velocity, pressure distributions versus reduced distance λ in the presence of viscosity formalism ($K \neq 0$) for lithium gas are shown in Figures 8.5 and 8.6. It is observed that the velocity, pressure distributions (for both cylindrical and spherical geometry) decreases with fixed values of viscosity parameter K . It is observed that flow distributions are high at the shock front, decrease gradually with increase in λ and become constant. It is important to note that the variation in flow distributions is more with an increasing values of viscosity parameter K . In particular, it is seen that velocity profiles are continuous and vary in direction (see Figures 8.1(a), 8.2(a), 8.5(a-b)). This means that artificial viscosity could distinguish between shock wave and adiabatic compression. Moreover, in the case of cylindrical geometry it is observed that pressure damping reduces by adding the value of artificial viscosity ($K = 0.349$) into the flow field during the convergence process. In particular, we observe that the EOS of the medium has effect on the flow variables.

Figures 8.3 and 8.4 compare the particle velocity, pressure distributions versus reduced distance λ in the absence of viscosity ($K = 0$) for two different condensed materials such as lithium, aluminum respectively. From Figure 8.3, we observed that the velocity of gas particles rapidly increases with increase in λ . Also found that the rate of acceleration (i.e., shock speed) is much faster in lithium gas than in aluminum gas for cylindrical geometry whereas in the case of spherical geometry the velocity distribution first falls at the shock front and then increases. This behavior is similar to that as shown in Figure 8.1 for a lithium gas. The velocity distribution decreases with an increasing values of λ in aluminum gas. From these figures, it may be noted that the particle acceleration decreases / increases with the increase/decrease of material density. Figures 8.4(a) and 8.4(b) shown that the pressure distribution decreases as increase in radial distance λ for cylindrical, spherical geometry respectively. However, the rate of decay is much faster in aluminum gas than in lithium gas due to the higher acoustic impedance of aluminum. The results of this investigation indicate that the crossing of the particles through the shock front strongly depends on the charge geometry, the charge size and the material density of the particles. The degree of shock-compressed densities and pressures increases with the geometrical index m .

Figures 8.7 and 8.8 depicts the velocity, pressure distributions (both cylindrical and spherical geometry) versus reduced distance λ in the presence of viscosity formalism ($K \neq 0$) for aluminum gas. We observe a sharp rise in velocity,

pressure distributions behind the shock front, between $\xi = 1$ and $\xi = 2.0$, and then decrease, further, become constant along the axis. It may be observed that variation in these peaks change with decrease in the values of viscosity parameter K . High for the larger values of K but for smaller values of K not significant variation is observed. The variation in flow distributions with increase in λ is more significant for higher values of viscosity parameter K for aluminum gas. The variation in flow distributions is more appreciable in the case of lithium gas than the aluminum gas with introduction of artificial viscosity parameter ($K = 0.000349, 0.00349, 0.0349$ and 0.349).

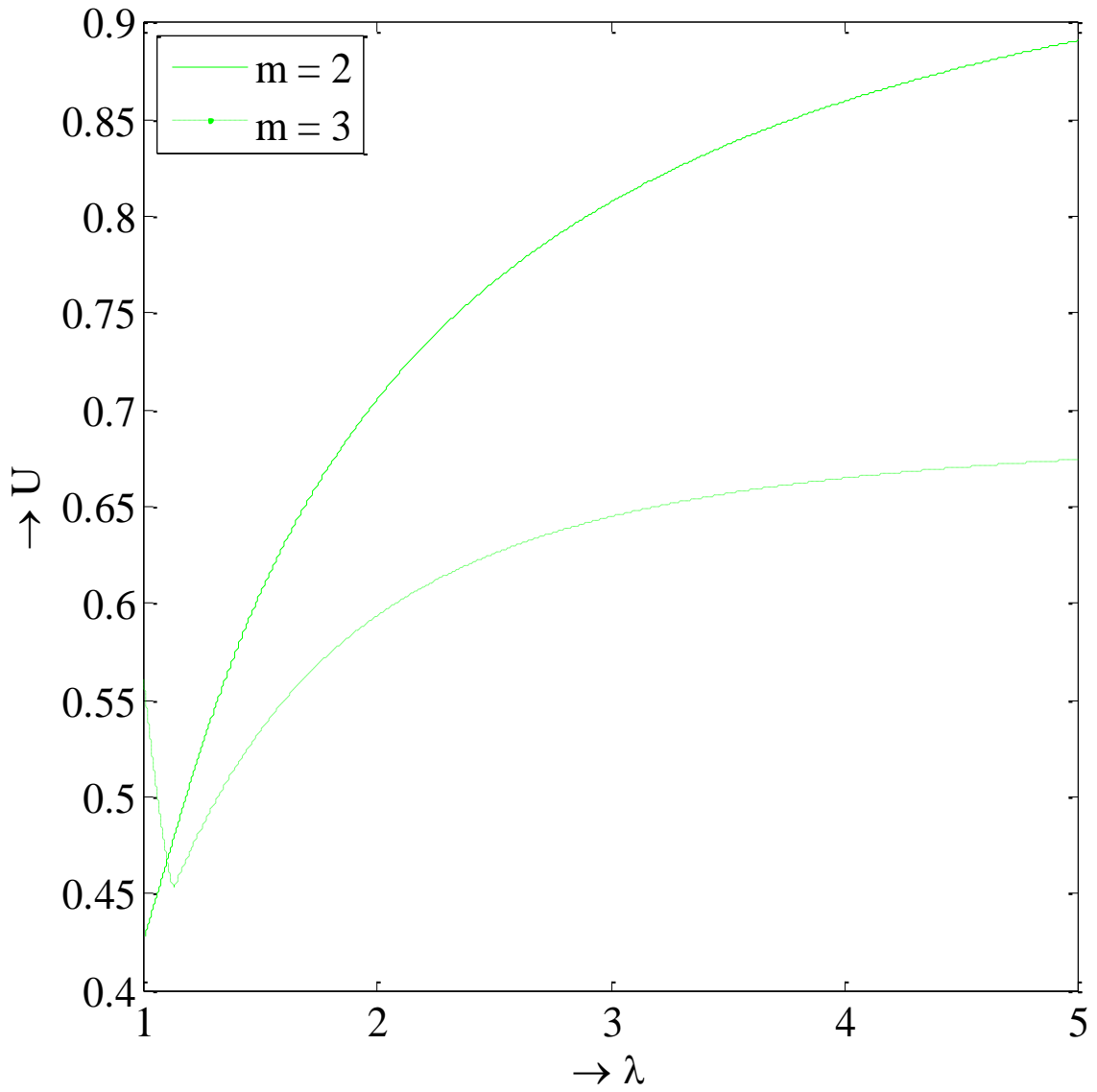


Figure 8.1(a). Velocity profiles for condensed matter when $\Gamma_0 = 1.017$, $m = 2, 3$ and $K = 0$

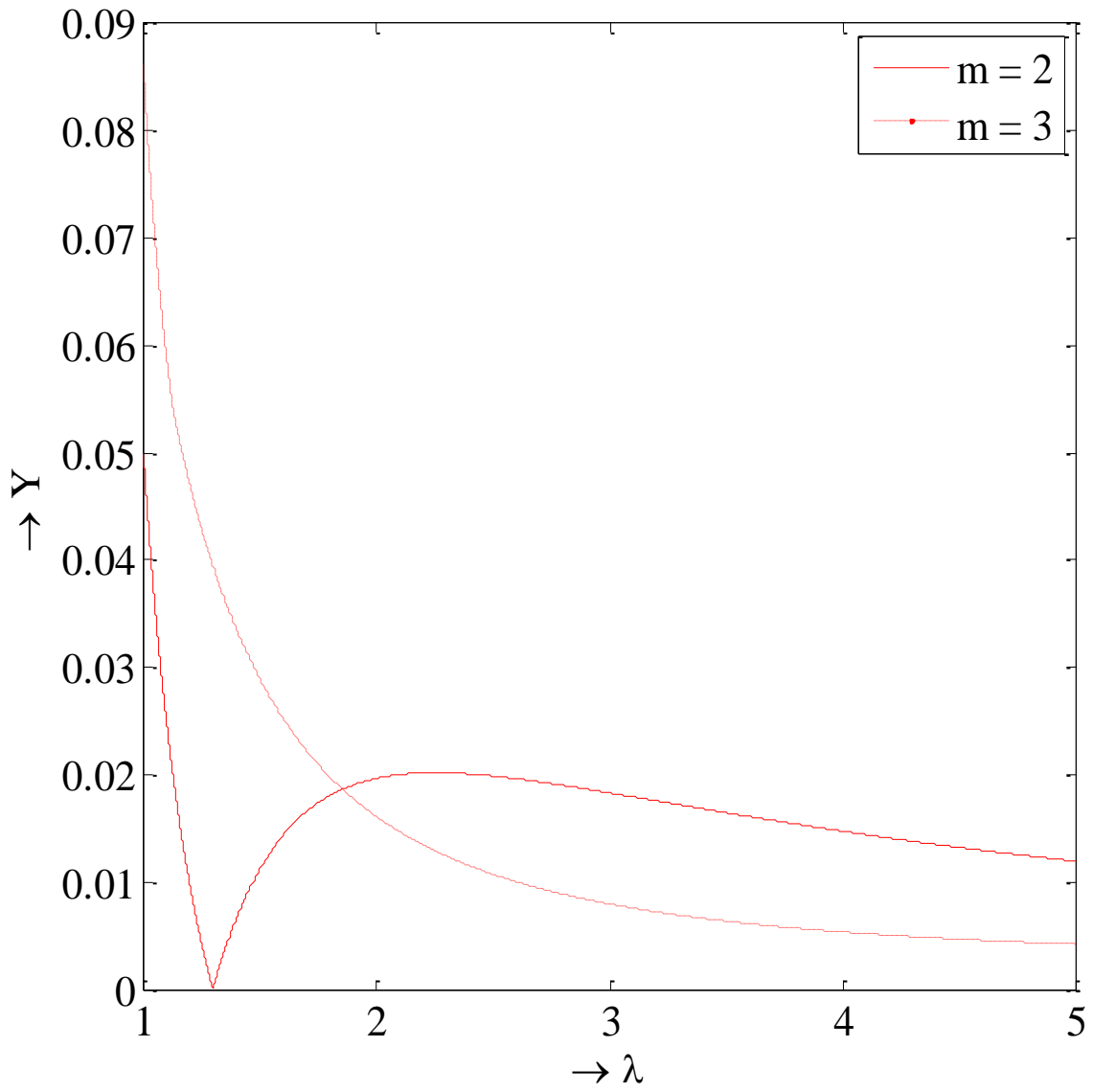


Figure 8.1(b). Pressure profiles for condensed matter when $\Gamma_0 = 1.017$, $m = 2, 3$ and $K = 0$

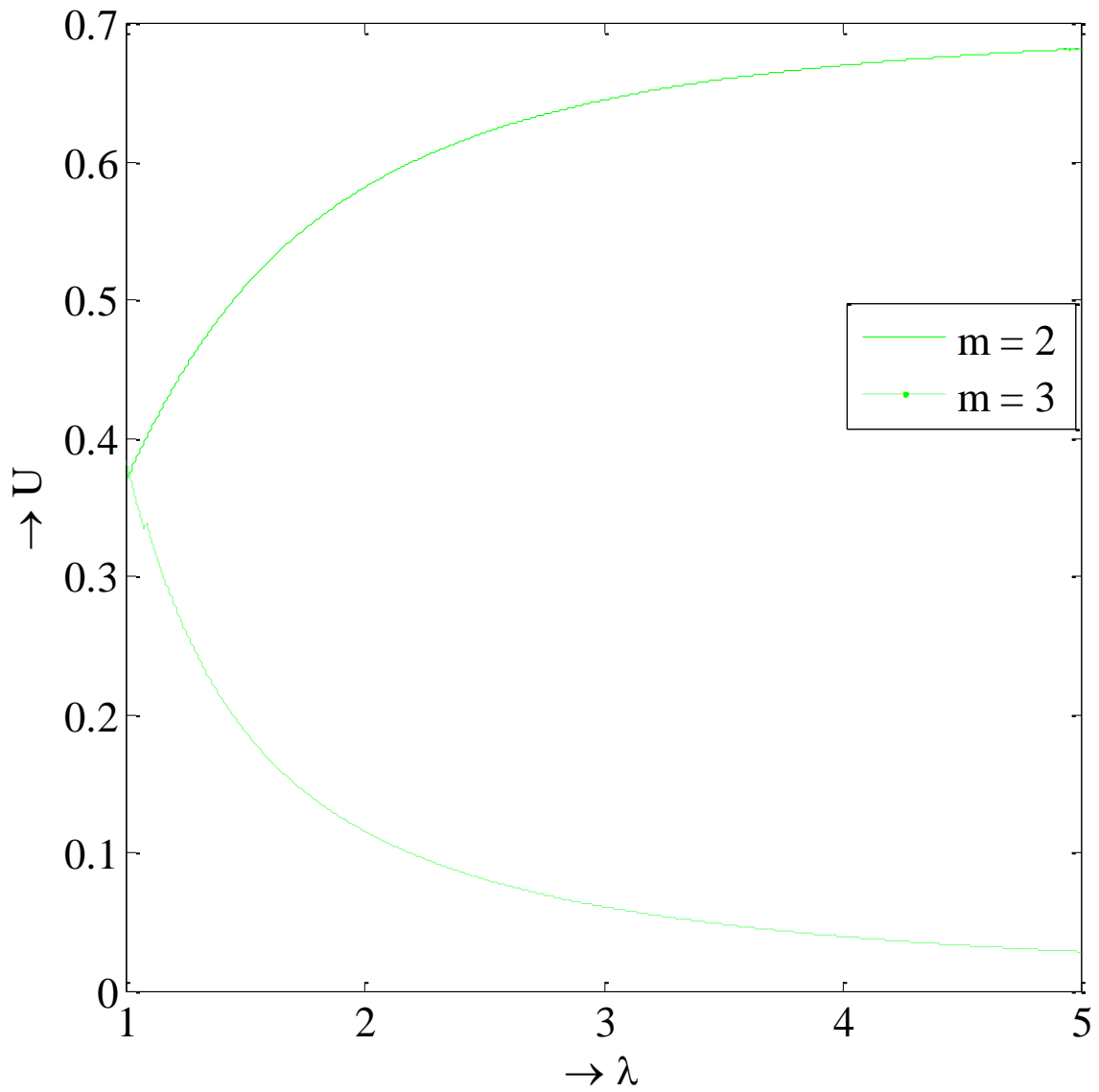


Figure 8.2(a). Velocity profiles for condensed matter when $\Gamma_0 = 2.12$, $m = 2, 3$ and $K = 0$

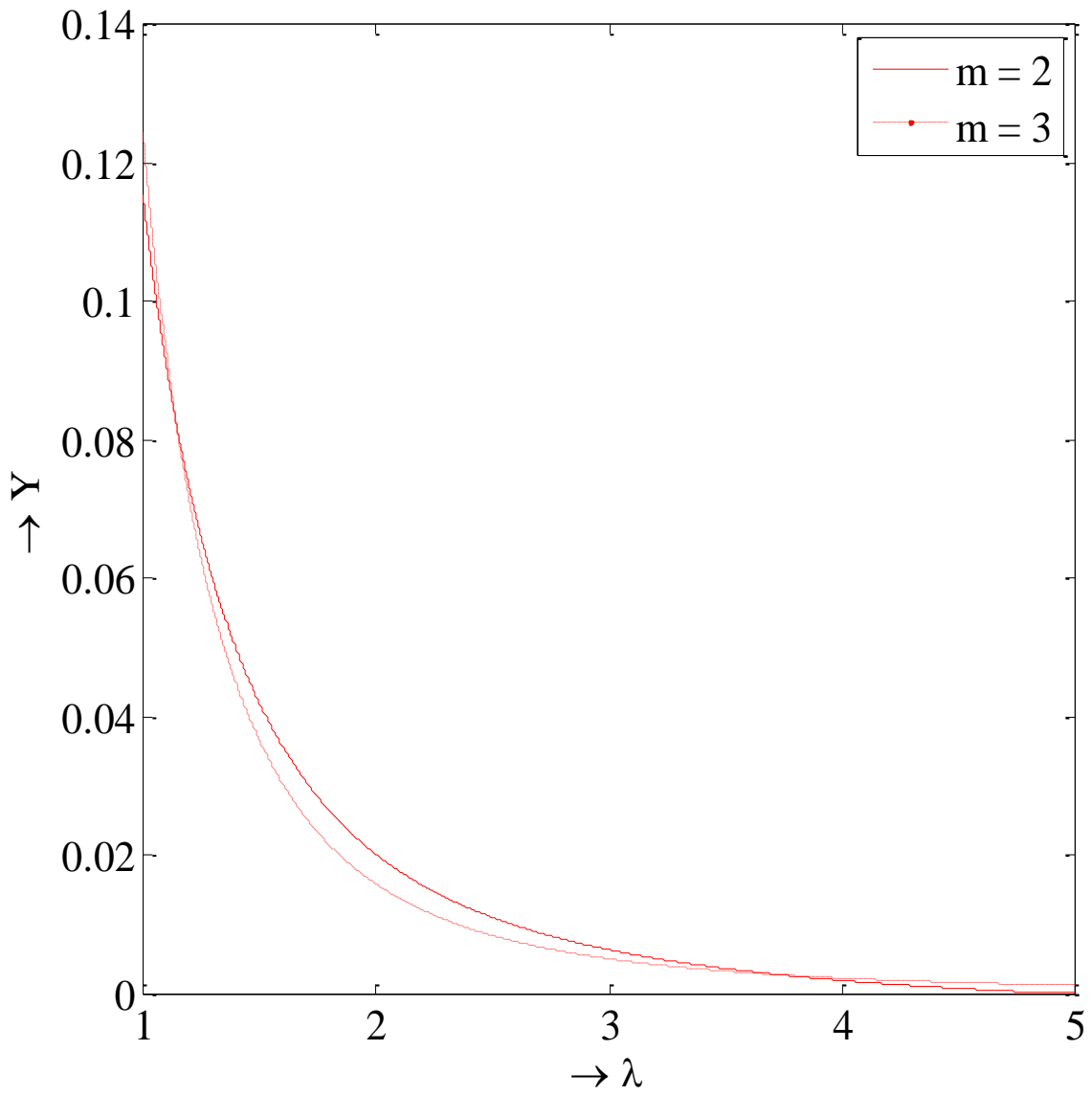


Figure 8.2(b). Pressure profiles for condensed matter when $\Gamma_0 = 2.12$, $m = 2, 3$ and $K = 0$

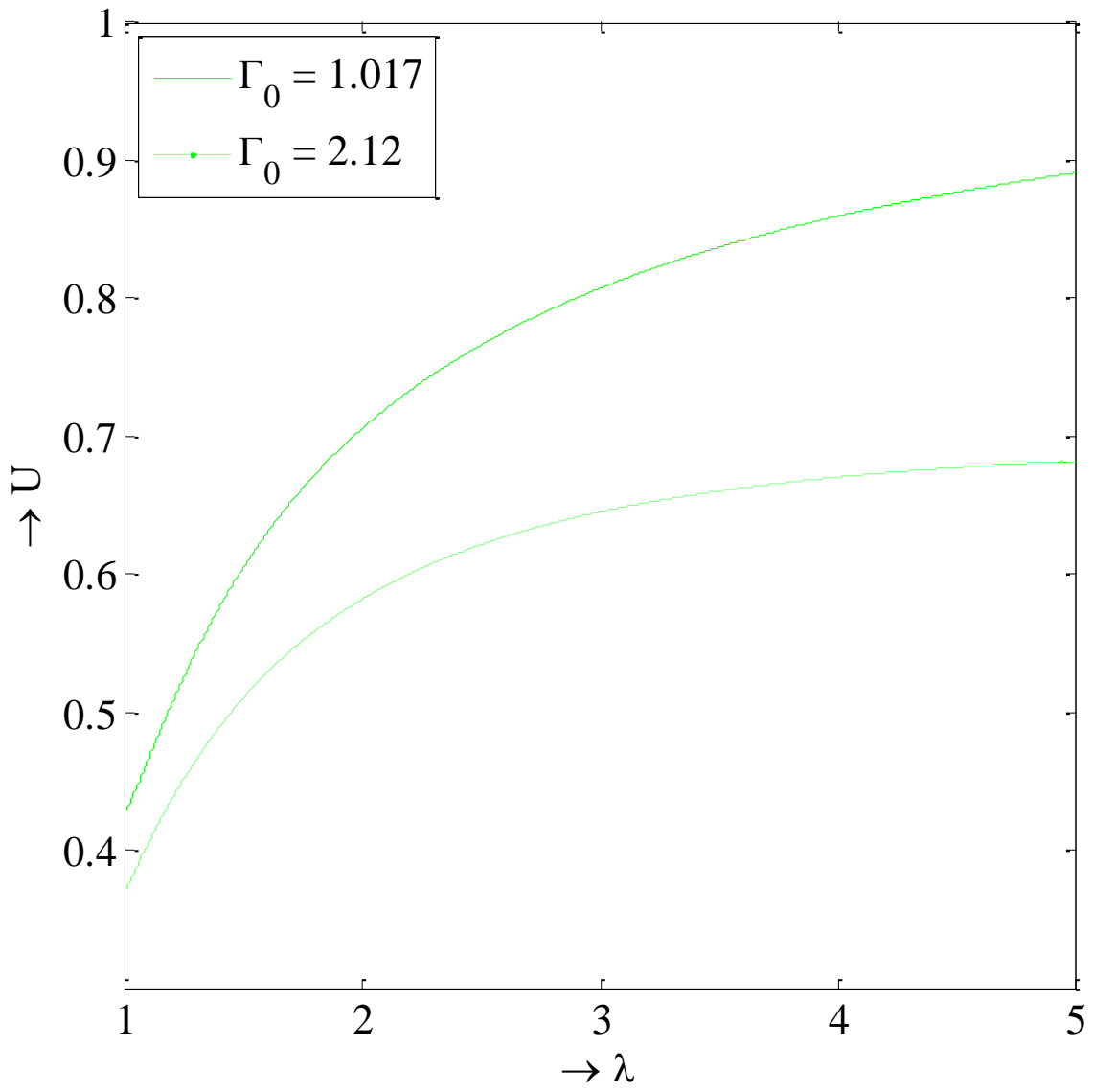


Figure 8.3(a). Velocity profiles for different values of Γ_0 , $m = 2$ and $K = 0$

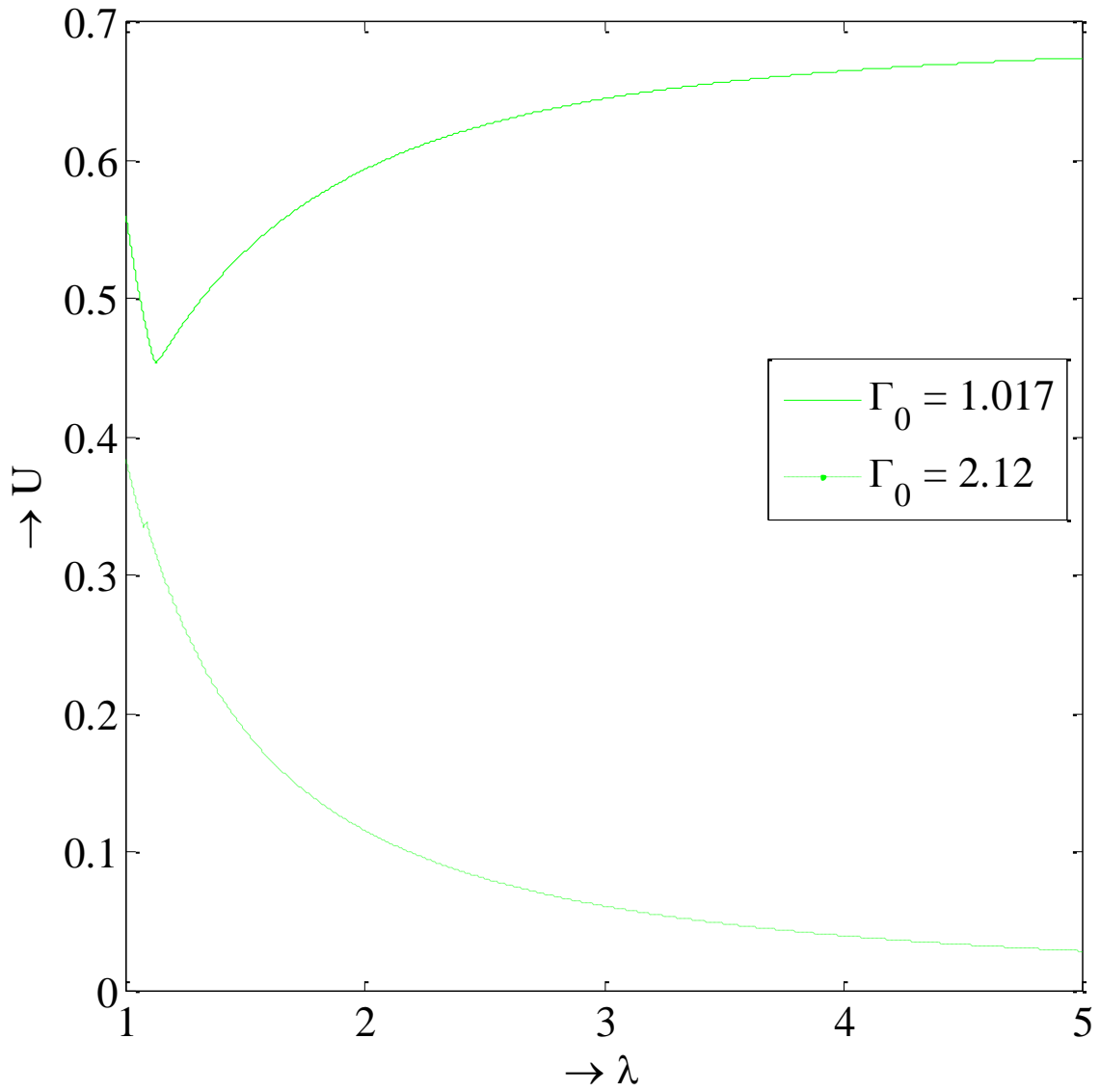


Figure 8.3(b). Velocity profiles for different values of Γ_0 , $m = 3$ and $K = 0$

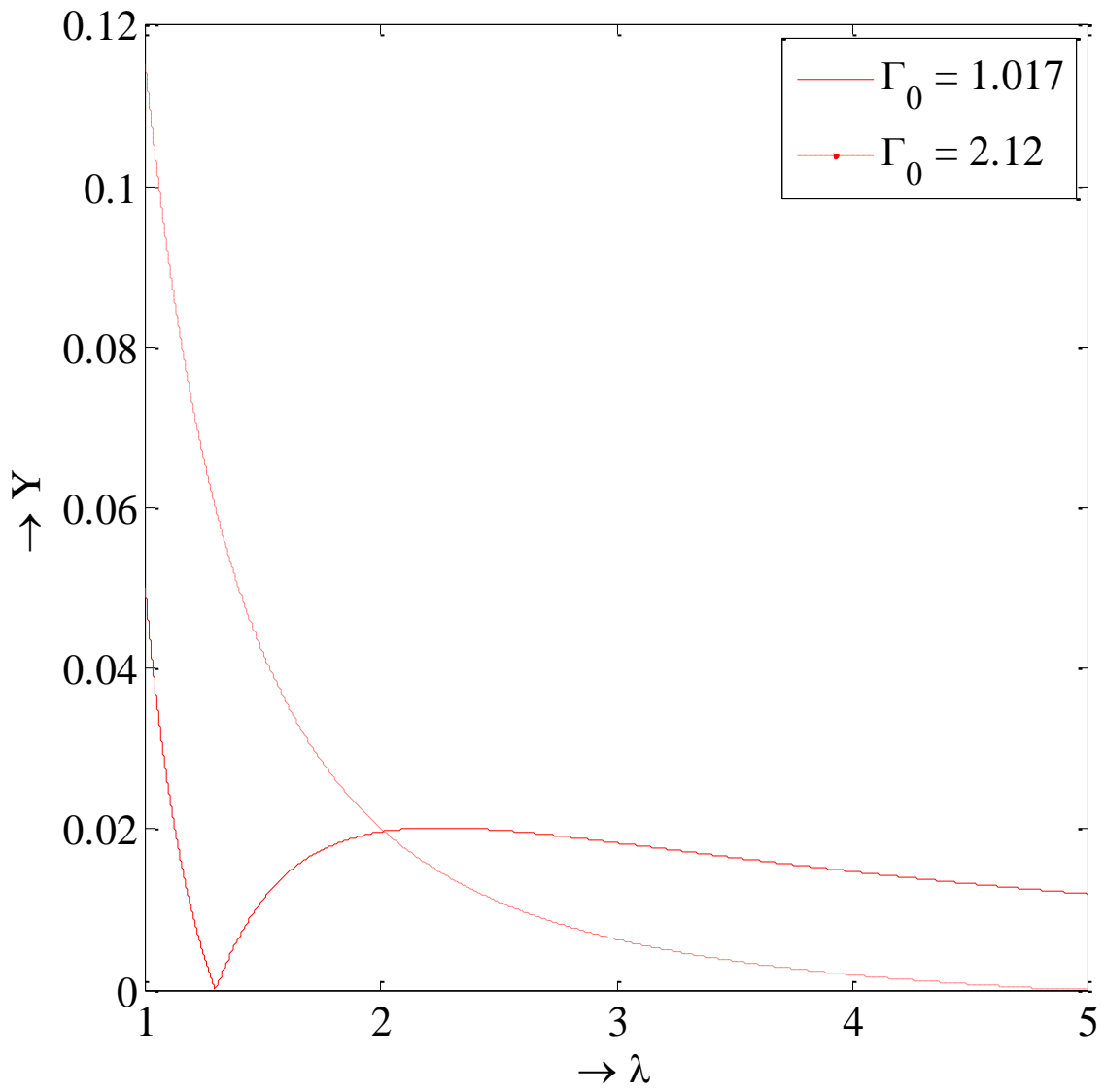


Figure 8.4(a). Pressure profiles for different values of Γ_0 , $m = 2$ and $K = 0$

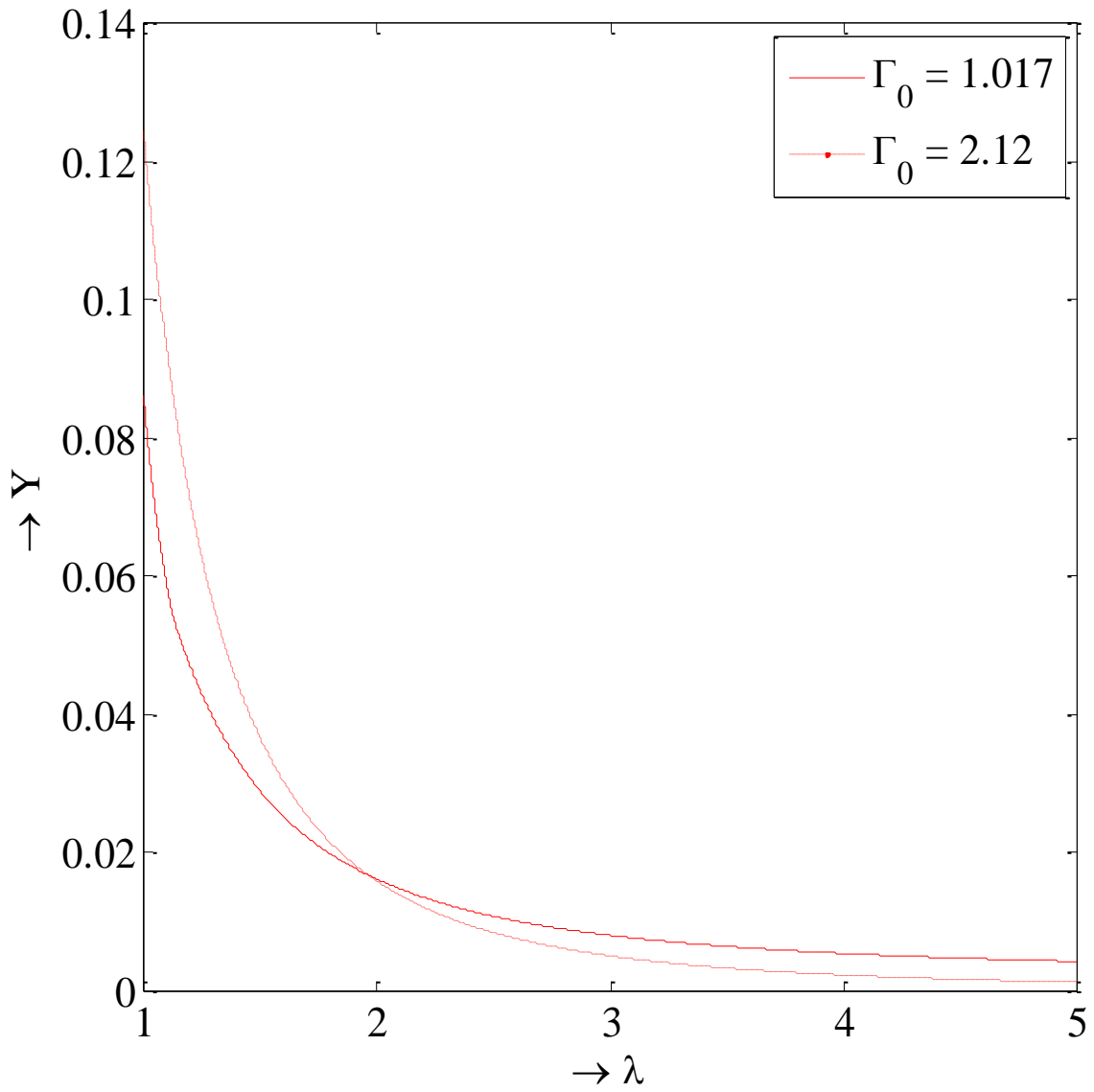


Figure 8.4(b). Pressure profiles for different values of Γ_0 , $m = 3$ and $K = 0$

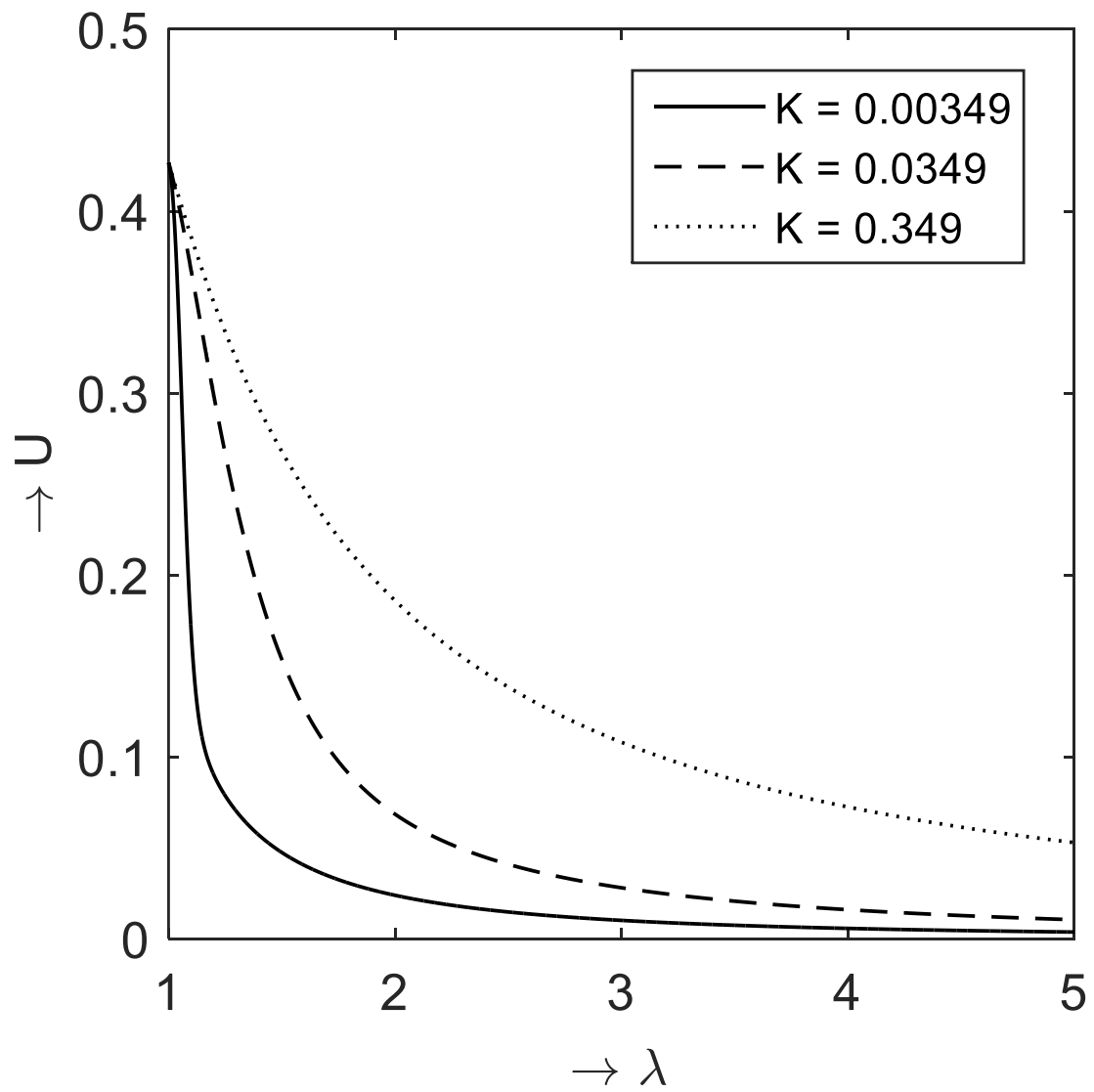


Figure 8.5(a). Velocity profiles for condensed matter when $\Gamma_0 = 1.017$, $m = 2$ and different values of K

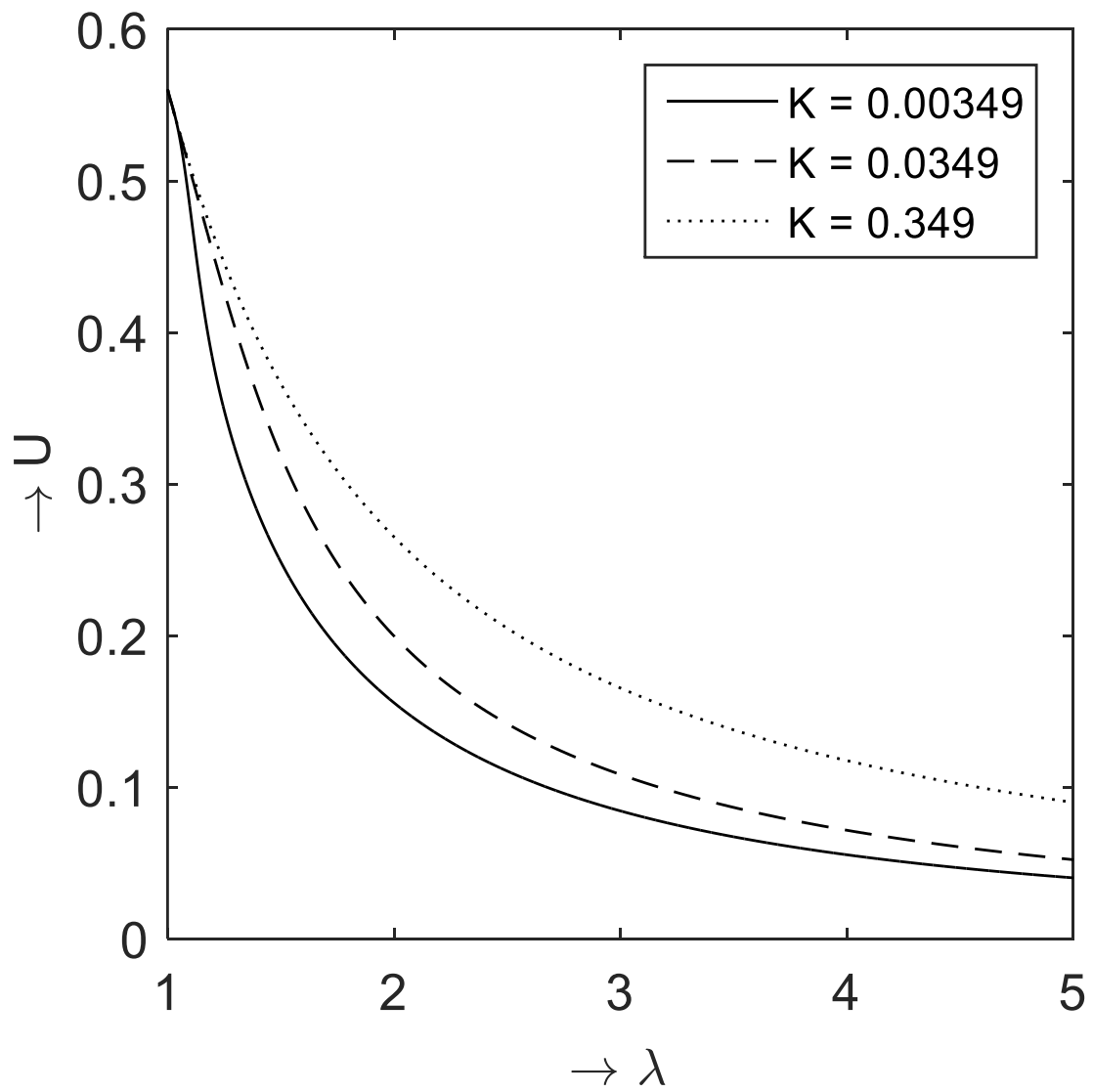


Figure 8.5(b). Velocity profiles for condensed matter when $\Gamma_0 = 1.017$, $m = 3$ and different values of K

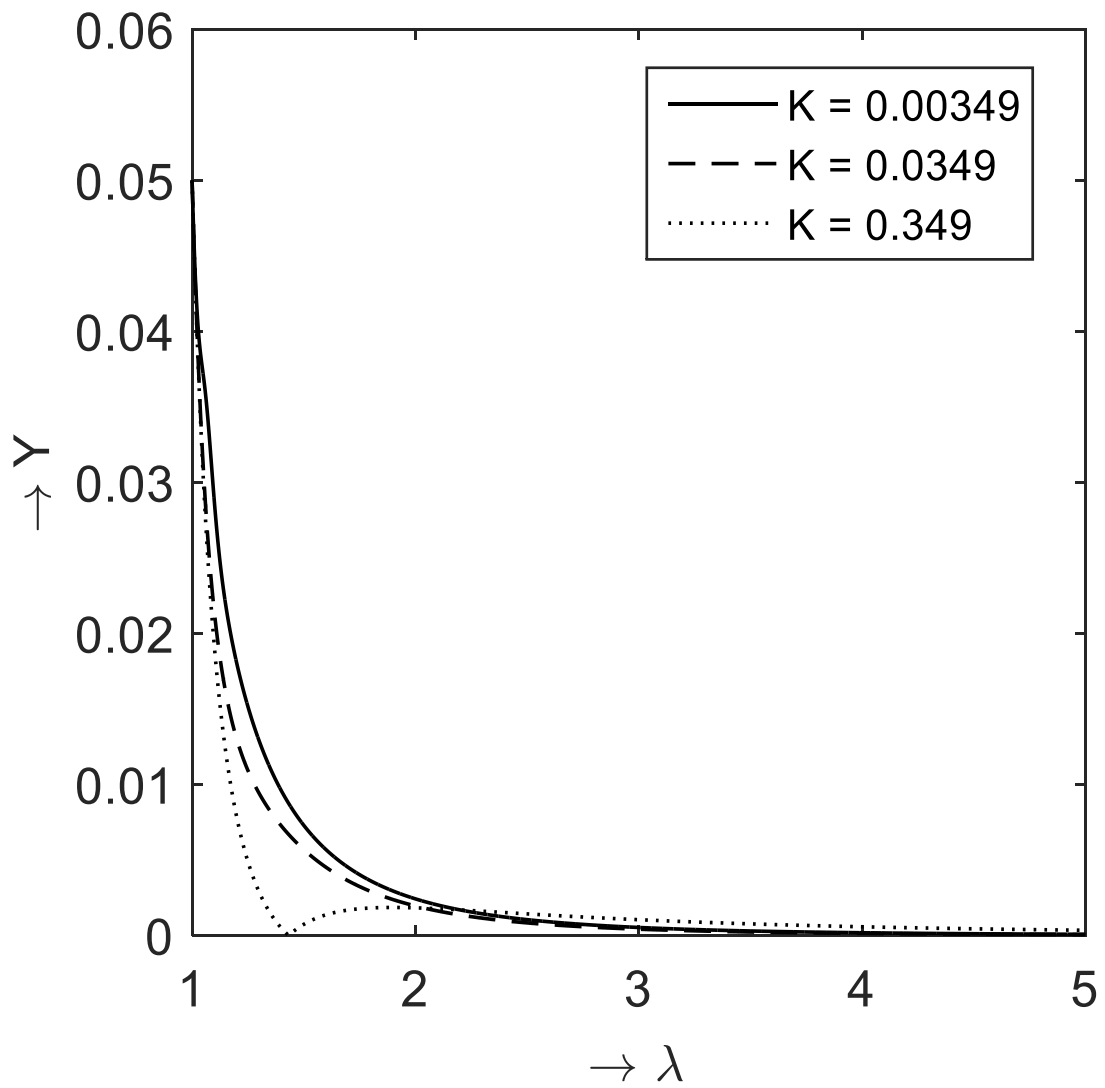


Figure 8.6(a). Pressure profiles for condensed matter when $\Gamma_0 = 1.017$, $m = 2$ and different values of K

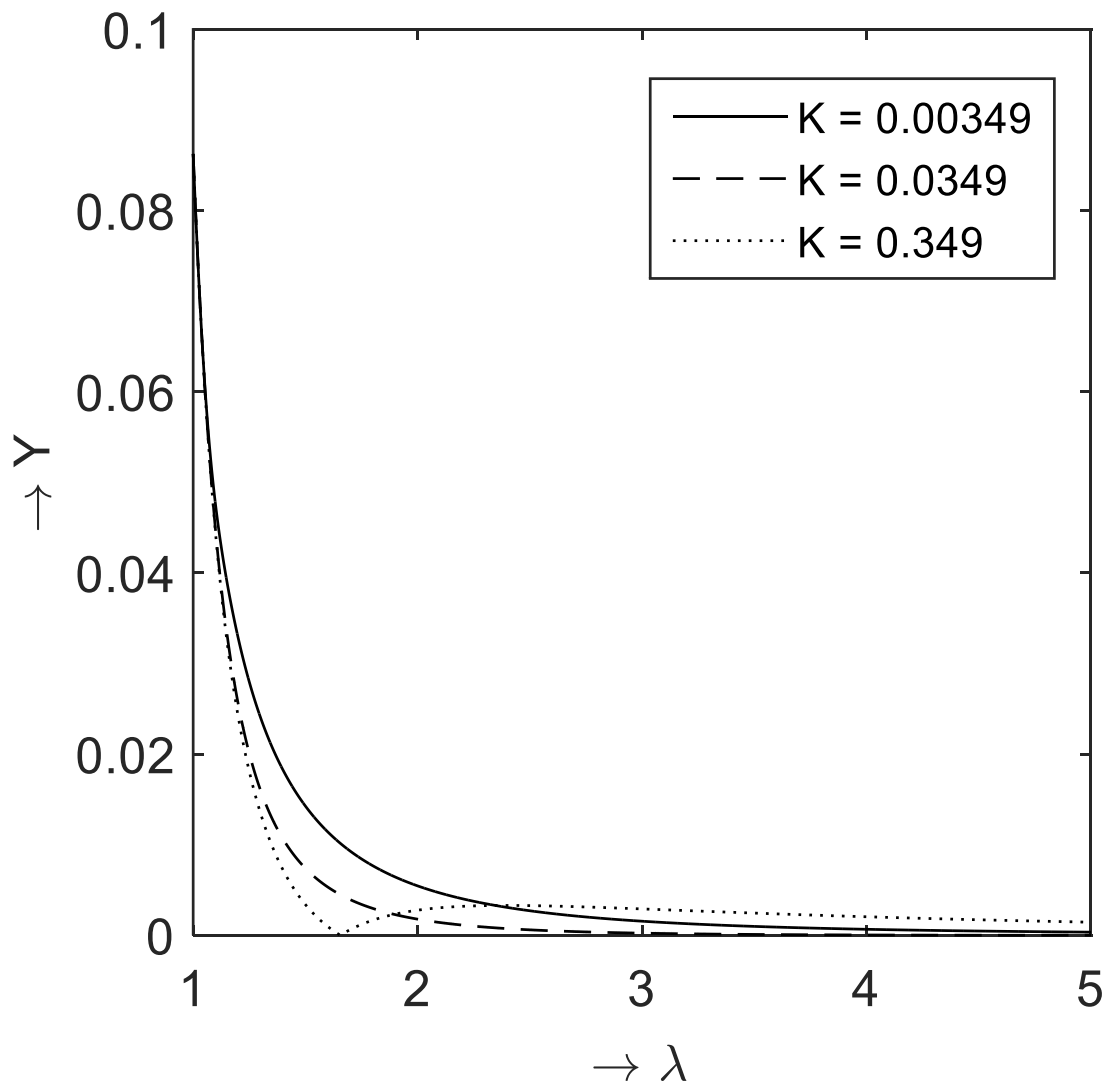


Figure 8.6(b). Pressure profiles for condensed matter when $\Gamma_0 = 1.017$, $m = 3$ and different values of K

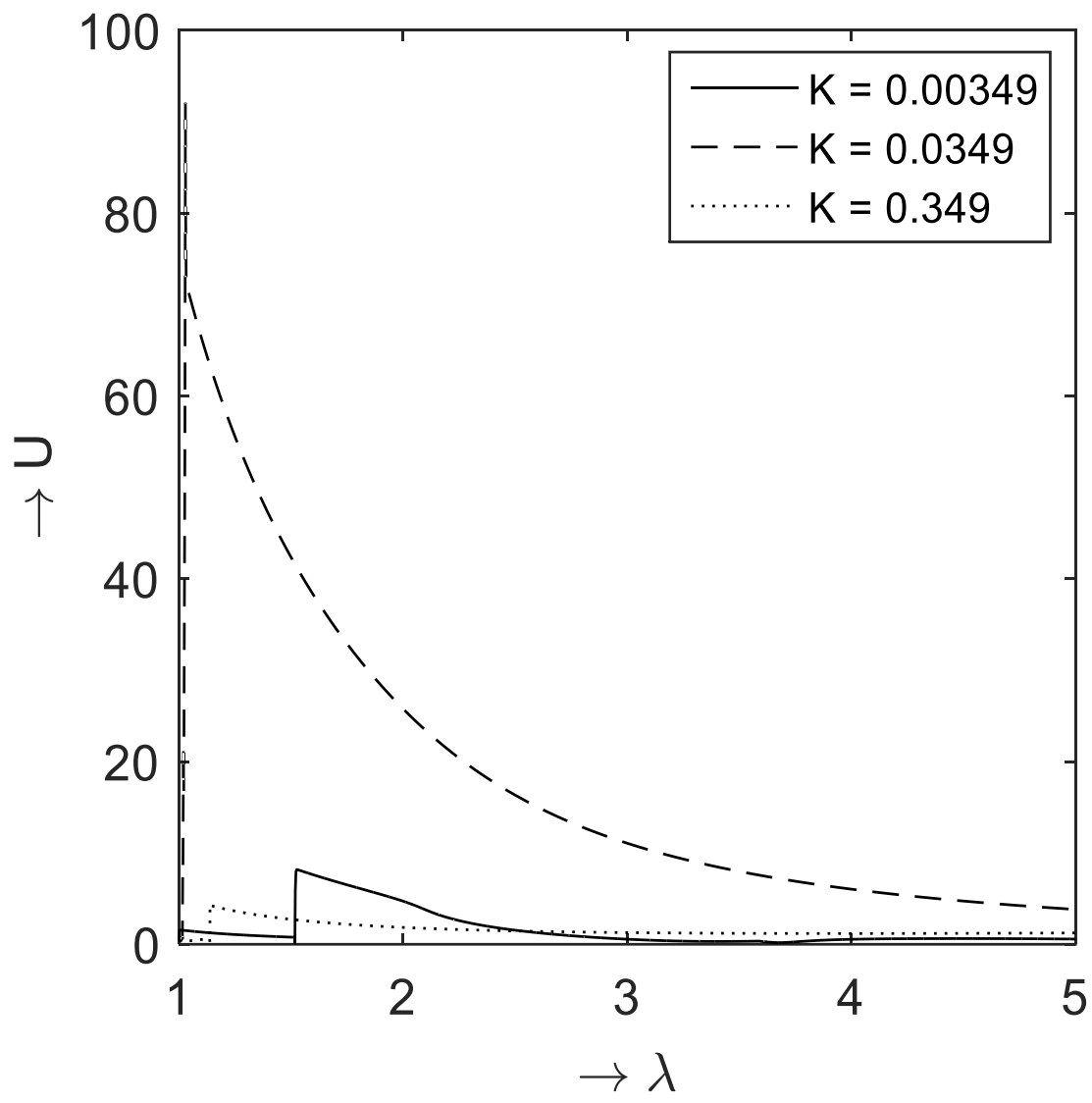


Figure 8.7(a). Velocity profiles for condensed matter when $\Gamma_0 = 2.12$, $m = 2$ and different values of K

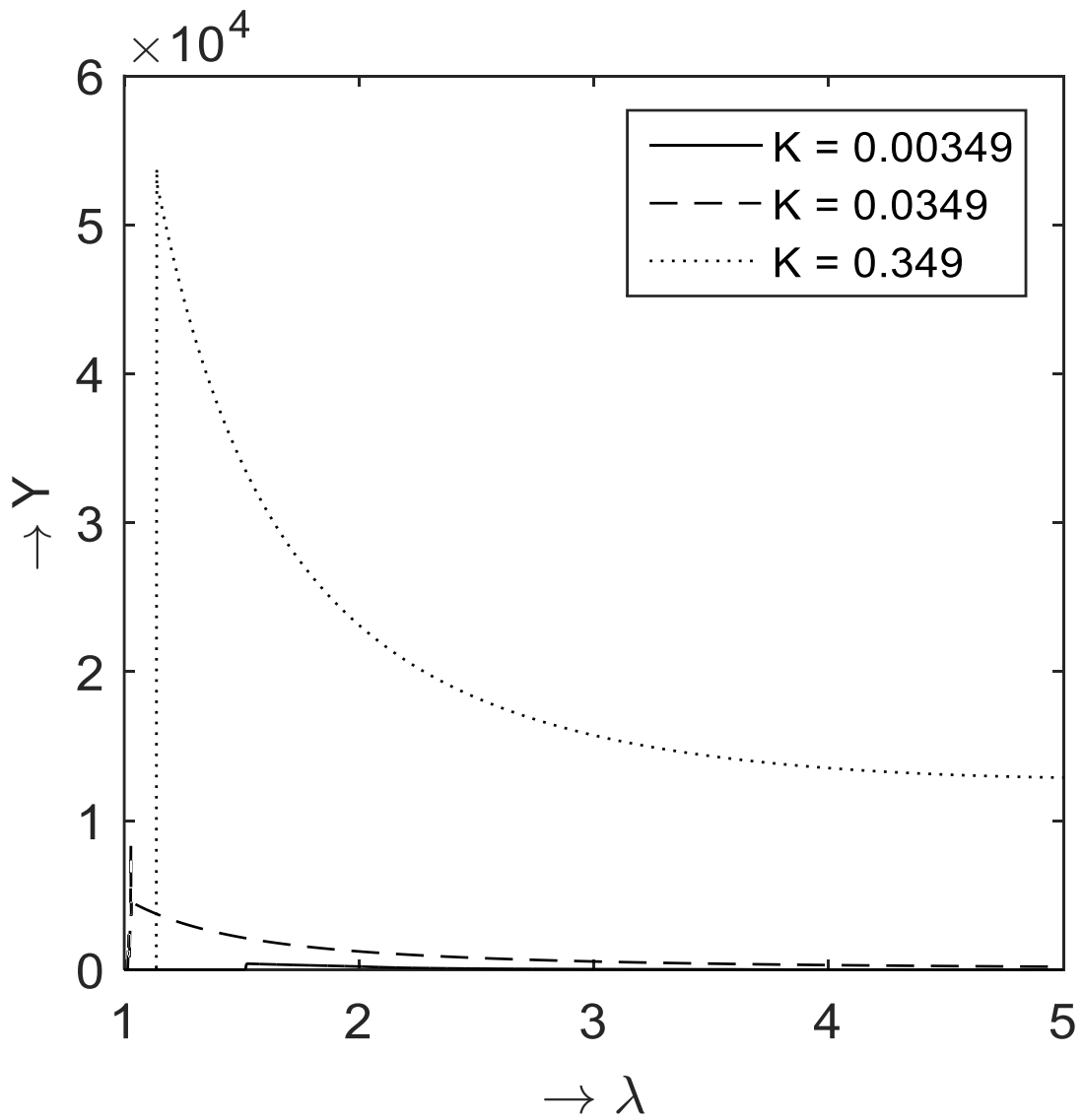


Figure 8.7(b). Pressure profiles for condensed matter when $\Gamma_0 = 2.12$, $m = 2$ and different values of K

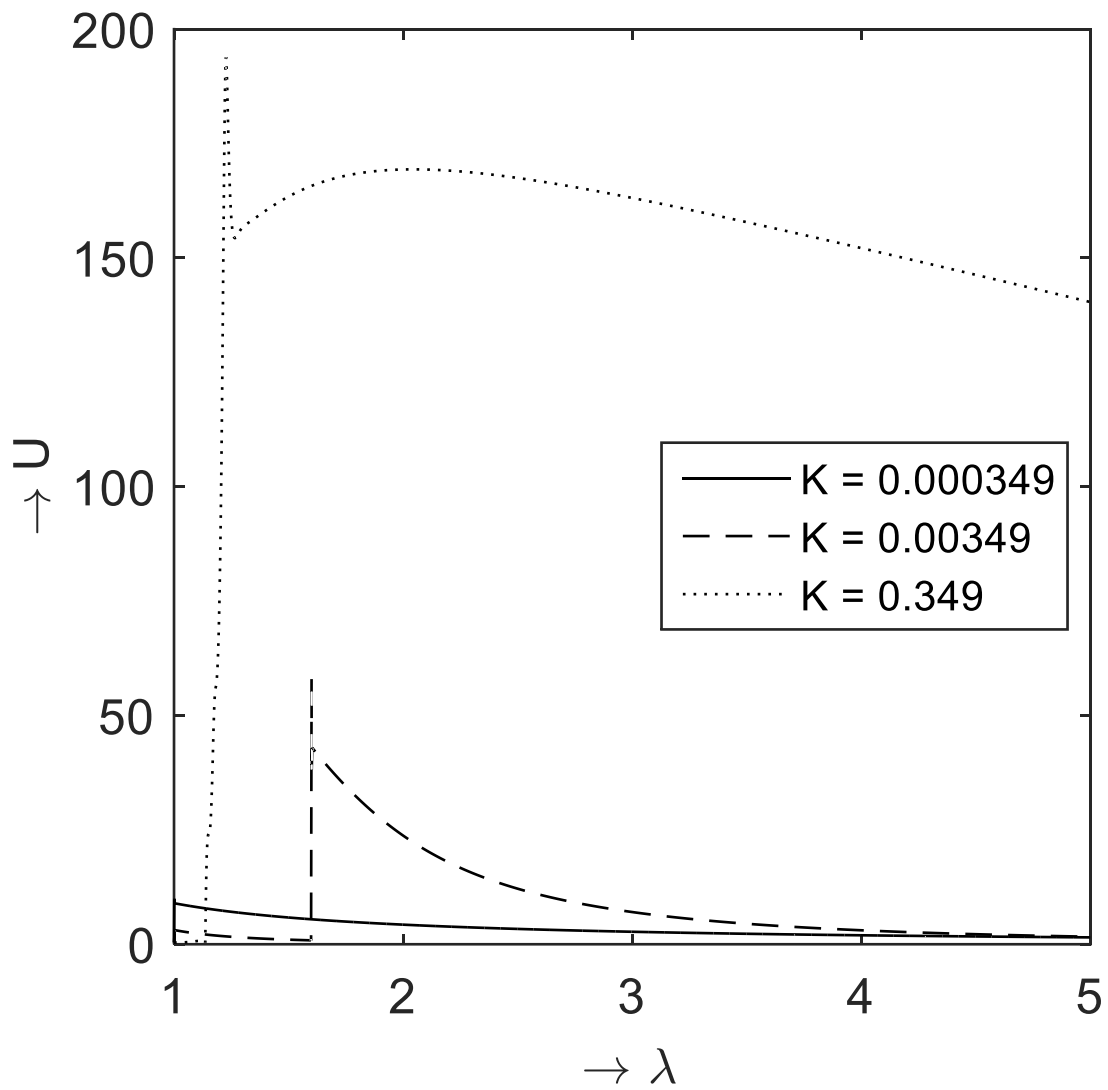


Figure 8.8(a). Velocity profiles for condensed matter when $\Gamma_0 = 2.12$, $m = 3$ and different values of K

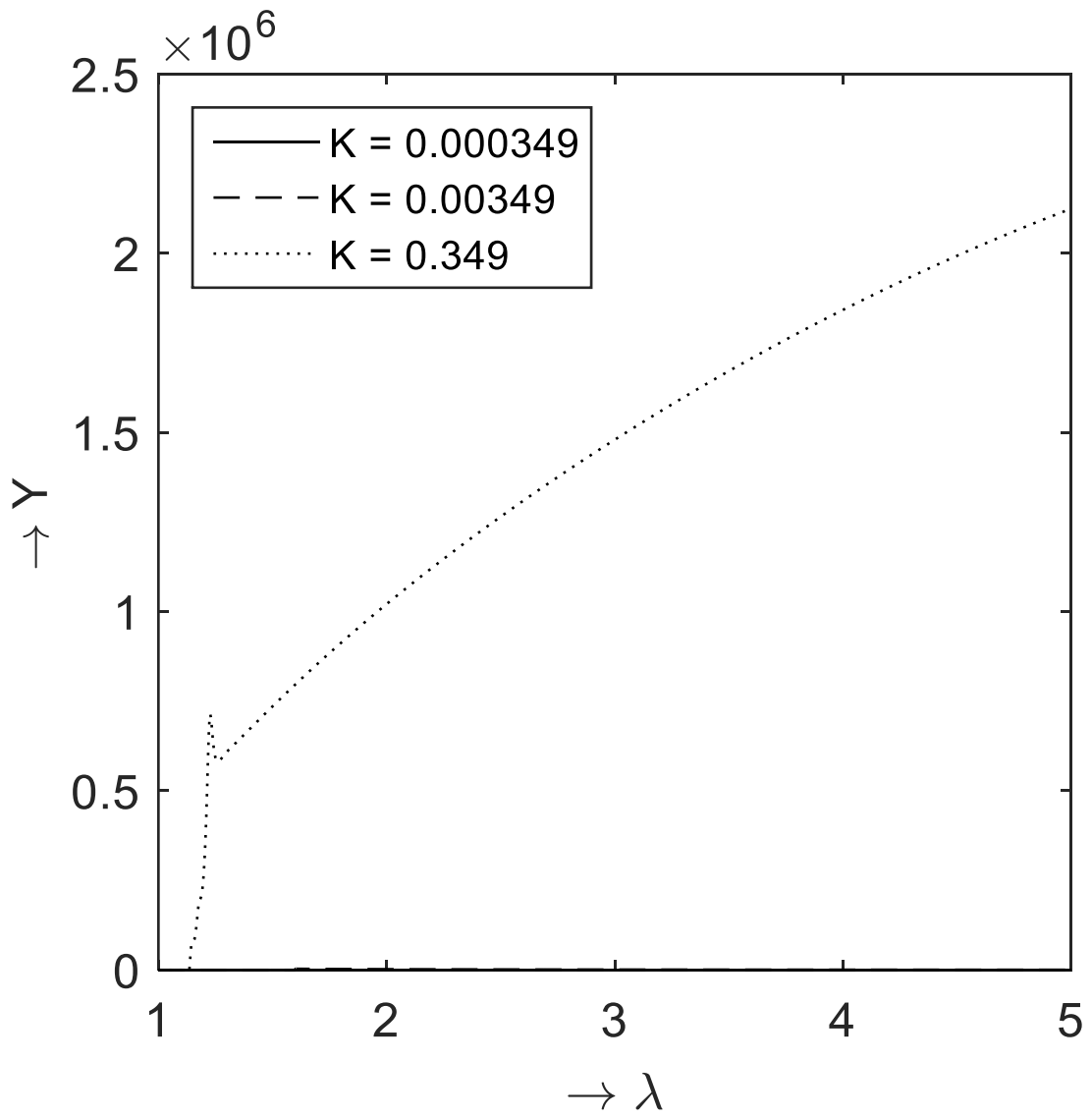


Figure 8.8(b). Pressure profiles for condensed matter when $\Gamma_0 = 2.12$, $m = 3$ and different values of K

CONCLUSIONS

The thesis entitled, “Self-Similar Solutions to Compressible Flow Problems”, comprises of eight chapters. Chapter-1 is introduction and chapter-2 is devoted to literature review. The shock is assumed to be strong and propagating into a non-ideal gas of Mie-Gruneisen EOS. In this thesis work we adopted the following techniques for the solution procedure. The similarity method, group invariance method, CCW method, finite difference method etc., the approximate analytical and numerical solutions for the self-similar flows behind strong shock waves are obtained. All the computational work is carried out using MATLAB. The effect of non-idealness of the equation of state, magnetic pressure, effect of viscosity etc., on the flow variables and the similarity exponent α are discussed in detail.

In chapter-3, similarity solutions to shock waves in non-ideal magnetogasdynamics is studied. In this problem, we used a method of self-similar solutions of second kind to obtain the numerical solution of the system of non-linear ordinary differential equations and determine the similarity exponent. We employed two numerical techniques such as RK method and CCW method to compare the values of similarity exponent in both medium. It is observed that both RK and CCW methods produced a very good approximation for similarity exponents. We provided a description of flow pattern and numerical method employed to ensure the solution when integrating the system of equations passing

through the singular points in the solution. It is observed that the effect of increasing values of magnetic field strength causes to decrease the values of velocity, pressure and magnetic pressure in dusty gas and condensed matter. It is observed that the density decreases with an increase in magnetic field strength for dusty gas flow, whereas in the case of condensed matter density increases with the effect of an increasing values of magnetic field strength. Also, we observed that the values of similarity exponent decreases with increasing values of magnetic field strength. This type of problems have applications in nuclear engineering, fusion research and other physical systems, involving non-linear hyperbolic partial differential equations.

The chapter-4 is the study of numerical solution to strong cylindrical shock wave in the presence of magnetic field. A problem involving a cylindrical converging strong shock wave has been formulated with a gas of varying density obeying a power law and shock propagates through a medium characterized by a Mie-Gruneisen EOS. The governing equations are non-dimensionalized using suitable similarity transformations. A finite difference scheme is employed to solve the system of non-linear differential equations. Crouts reduction technique is used to solve the system of algebraic equations. The nature of flow variables with the effect of magnetic field in the respective models of EOS is investigated.

From the present study, we notice that the similarity exponent α decreases with an increase in the values of M and fixed C_0 causes an increase in β for dusty gas

medium. In perfect gas similarity exponent α decreases with decrease in β with increasing values of γ and fixed C_0 . In case of Royce EOS the similarity exponent α decreases with an increasing values of Γ_0 and fixed constant a and C_0 due to decrease in β . The decay of shock wave is more prominent and slower in the dusty gas EOS. The effect of magnetic field on flow variables is less pronounced for dusty gas particles, because of lower compression between the gas particles. We conclude that the less compressible medium has higher wave propagation speed. As shown in Figures 4.3-4.7, the approximate reduced density, velocity, pressure and magnetic pressure shows largest peaks to the right behind the shock front in Royce EOS, whereas in perfect gas flow variables have small peaks. This is due to fact that the effect of measure of shock strength β , which causes the change in α and also effect of converging geometry or area of contraction of the shock wave.

Considering system of partial differential equations describing a problem involving a cylindrical converging strong shock wave has been formulated with a gas of varying density obeying a power law and shock propagates through a medium characterized by a Mie-Gruneisen EOS. The governing equations are non-dimensionalized using suitable similarity transformations. A finite difference scheme is employed to solve the system of non-linear differential equations. Crouts reduction technique is used to solve the system of algebraic equations. The

nature of flow variables with the effect of magnetic field in the respective models of EOS is investigated.

From the present study, we notice that the similarity exponent α decreases with an increase in the values of M and fixed C_0 causes an increase in β for dusty gas medium. In perfect gas similarity exponent α decreases with decrease in β with increasing values of γ and fixed C_0 . In case of Royce EOS the similarity exponent α decreases with an increasing values of Γ_0 and fixed a and C_0 due to decrease in β . The decay of shock wave is more prominent and slower in the dusty gas EOS. The effect of magnetic field on flow variables is less pronounced for dusty gas particles, because of lower compression between the gas particles. We conclude that the less compressible medium has higher wave propagation speed. As shown in Figures 3 - 7, the approximate reduced density, velocity, pressure and magnetic pressure shows largest peaks to the right behind the shock front in Royce EOS, whereas in perfect gas flow variables have small peaks. This is due to fact that the effect of measure of shock strength β , which causes the change in α and also effect of converging geometry or area of contraction of the shock wave. The one dimensional unsteady cylindrical flow of an inviscid non-ideal gas with dust particles, we studied various aspects of non-linear wave propagation. The medium generated due to implosion is assumed to be of Mie-Gruneisen type with magnetic or non-magnetic in nature. Impulsive motion of the piston produces instantaneous unsteady shock which may grow or decay with time, depending on

the condition of the undisturbed gas and the behaviour of the piston. The forms of these waves are altered by convection which distorts the wave form by causing the compression phase to move forward faster than the expansion phase. This results in the generation of a plasma with an infinite electrical conductivity and permeated by an axial magnetic field orthogonal to the trajectories of gas particles. Similarity solution to this problem is obtained numerically. The numerical solution presented provides a global solution to the implosion problem which is valid for a range of physically meaningful parameters. The computed values of the similarity exponent are in good agreement with those obtained using CCW method and are presented in tabular form. This approximation provides a quick and relatively accurate determination of the similarity exponent and stability of shocks in non-ideal gas. Also the numerical description of the flow field behind the wave front in a non-ideal magnetogasdynamics regime is presented. The effect of magnetic field strength on the flow parameters in a non-ideal medium is presented.

Chapter four is numerical solution to strong cylindrical shock wave in the presence of magnetic field. The medium generated due to implosion is assumed to be of Mie-Gruneisen type with or without magnetic material. In the implosion process plasma is assumed to be generated. The similarity exponent is obtained numerically by an iterative process. In this problem the mechanical properties of shock waves in the presence of strong magnetic field and the behavior of shock

characteristics such as shock strength, shock density, shock speed, shock over pressure, and impulse are presented.

In chapter five a model to determine the similarity solutions to the problem of gas dynamic flow under the influence of strong magnetic field is presented. The problem treated here involves distinct features: the global behavior of the physical parameters is studied; the initial pressure ratio is confined to a moderate value. The path of the piston is imposed as boundary condition. Thus an accelerated, a decelerated or a constant velocity piston can be specified. The numerical values of similarity exponents and profiles of flow variables are obtained. These are presented through the illustrative graphs and tables. The magnetic field effects on the flow variables through a medium and total energy under the influence of strong magnetic field are also presented.

In chapter six, spherically symmetric conservation equations are considered and similarity solution of spherical shock waves and effect of viscosity is studied. This problem is investigated to understand complete mechanism of shock wave which include, viscous terms and study the dissipation effects on the propagation of shock waves including viscosity under the effect of magnetic field. Also the study and confirmed the effect of (i) the non-idealness parameter and the viscosity parameters on the shock strength and the flow variables respectively (ii) effect of discontinuities of the physical parameters due to viscosity and (iii) complete flow field depending on the magnitude of the viscosity. We concluded from the

introduction of artificial viscosity approach, the simplicity, high computational efficiency, dampening of oscillations in the flow profiles and the smoothness in the profiles.

Chapter seven a model to study similarity solutions for the governing partial differential equations (PDEs) of one-dimensional unsteady motion of strong converging spherical and cylindrical shock wave with the effect of radiation. We studied the behavior of flow parameters such as density, velocity, pressure, and radiation flux for flow-field behind a strong converging cylindrical, spherical shock wave propagating through a non-ideal stellar medium in the presence of monochromatic radiation. The finite difference approximation method is employed in the solution process. The effects of various physical parameters such as non-idealness parameter (b), Gruneisen parameter (Γ_0), as well as the specific heat ratio (γ) and material property (σ) on the flow variables are shown graphically. It is observed that increase in measure of shock strength $\beta \left(\frac{\rho}{\rho_0} \right)$ has effect on the shock front i.e., the velocity and pressure behind the shock front increases quickly in the presence of the monochromatic radiation and decreases gradually. We conclude from the above investigation (i) at the shock front discontinuity appeared in density profiles is subject to physical requirement that the radiation flux cannot change across it and the mean collision time of particles is proportional to the gas density and (ii) that effect of radiation from the volume

of a gas becomes important at distances away from the initial point and it modifies the shock structure.

In chapter eight, self-similar solution of shock wave in condensed matter generated by impulsive load with the medium described by the EOS of Mie-Gruneisen type has been studied. The similarity exponent depends on the EOS parameters. In this work we employed the method of Lie group invariance under infinitesimal point transformations to study the problem of the self-similar solution of converging spherical and cylindrical imploding shock waves near the centre of implosion. The flow assumes a self-similar character in a non-ideal gas satisfying the equation of state (EOS) of Mie-Gruneisen type. Finite difference method is employed for the numerical solution of the governing equations. The similarity solution remains valid as long as the strong shock approximation is applicable across the shock wave. The one-parameter infinitesimal group of transformations were used with great accuracy to predict the physical behavior of the strong converging spherical and cylindrical shock wave which is normally generated by the rapid release of energy from a centered source and the properties of the ambient gas into which the shock wave is expanding. It is assumed that the limiting motion will be self-similar as the wave converges to the center. The numerical technique employed to study the nature of shock dynamics through a non-ideal medium described by the equation of state (EOS) of Mie-Gruneisen type. We obtained a self-similar solution of converging shock wave near the

centre (axis) of implosion and investigated the behavior of flow parameters immediately behind the shock front in condensed matter EOS for a physically meaningful range of Gruneisen parameters.

In the present study we have investigated self-similar solutions to the compressible flow problems in the non-ideal medium with and without magnetic effect. The Lie group approach, effect of viscosity and the hypersonic flows for the non-ideal medium for the similarity solutions of EOS of different medium can be explored. The study of relativistic shock waves is another area of interest in the future.

Future Scope of Work

In the present study we have investigated self-similar solutions to the compressible flow problems in the non-ideal medium with and without magnetic effect.

The future scope of work,

The Lie group approach rather than similarity approach,

Incorporating the effect of viscosity in the governing equations and investigating the flow behavior,

Supersonic and hypersonic flows for the non-ideal of Mie-Gruneisen type of EOS of different medium,

MHD fluids with plasma,

Study of relativistic shock waves can be explored.

References

- [1] Taylor, G.I. (1950). The formation of a blast wave by a very intense explosion-I: Theoretical discussion, Proceedings of the Royal Society of London. Series A, Mathematical and Physical Sciences, **201**(1065): 159-174.
- [2] Taylor, G.I. (1946). The air wave surrounding an expanding sphere, Proceedings of the Royal Society of London. Series A, Mathematical and Physical Sciences, **186**(1006): 273-292.
- [3] Sedov, L.I. (1946). Propagation of intense (strong) blast waves, Prikl. Mat. Mek. (PMM), **10**(2): 241.
- [4] Stanyukovich, K.P. (1946). Application of particular solutions for equations of gas dynamics to the study of blast and shock waves, Rep. Acad. Sci. USSR, **52**(7).
- [5] Sedov, L.I. (1959). Similarity and Dimensional Methods in Mechanics, Academic Press, New York.
- [6] Stanyukovich, K.P. (1960). Unsteady Motion of Continuous Media, Pergamon Press, New York.
- [7] Zeldovich, Ya.B. and Raizer, Yu.P. (1966). Physics of Shock Waves and High-Temperature Hydrodynamic Phenomena, Academic Press, New York.

- [8] Barenblatt, G.I. (1979). *Similarity, Self-Similarity, and Intermediate Asymptotics*, Consultants Bureau, Springer, New York and London.
- [9] Maurice, H. (1965). *Basic Developments in Fluid Dynamics. Vol-1*, Academic Press, New York and London.
- [10] Luo, S.N., Swift, D.C., Tierney IV, T.E., Paisley, D.L., Kyrala, G.A., Johnson, R.P., Hauer, A.A., Tschauner, O., and Asimow, P.D. (2004). Laser-induced shock waves in condensed matter: some techniques and applications, *High Pressure Research*, **24**(4): 409-422.
- [11] Lamb, F.K., Callen, B.W., and Sullivan, J.D. (1992). An approximate analytical model of shock waves from underground nuclear explosions, *Journal of Geophysical Research*, **97**(B1): 515-535.
- [12] Trunin, R.F. (1994). Shock compressibility of condensed materials in strong shock waves generated by underground nuclear explosions, *Physics-Uspekhi.*, **37**(11): 1123-1145.
- [13] Fink, M., Hillebrandt, W., and Ropke, F.K. (2007). Double-detonation supernovae of sub-Chandrasekhar mass white dwarfs, *Astronomy and Astrophysics*, **476**(3): 1133-1143.
- [14] Fink, M., Ropke, F.K., Hillebrandt, W., Seitenzahl, I.R., Sim, S.A., and Kromer, M. (2010). Double-detonation sub-Chandrasekhar supernovae: can minimum helium shell masses detonate the core, *Astronomy and Astrophysics*, **514**(A53): 1-10.

- [15] Guderley, G. (1942). Powerful spherical and cylindrical compression shocks in the neighbourhood of the center and of the cylinder axis, *Luftfahrtforschung*, **19**: 302-312.
- [16] Chester, W. (1954). The quasi-cylindrical shock tube, *The London, Edinburgh, and Dublin Philosophical Magazine and Journal of Science*, Series 7, **45**(371): 1293-1301.
- [17] Chisnell, R. F. (1955). The normal motion of a shock wave through a non-uniform one-dimensional medium, *Proceedings of the Royal Society of London. Series A, Mathematical and Physical Sciences*, **232**(1190): 350-370.
- [18] Whitham, G. B. (1958). On the propagation of shock waves through regions of non-uniform area or flow, *Journal of Fluid Mechanics*, **4**(04): 337-360.
- [19] Von Neuman, J. (1941). The point source solution, NDRC, Div. B. Report AM-9.
- [20] Rae, W.J. (1970). Analytical studies of impact-generated shock propagation: survey and new results, Academic Press, New York, 214-286.
- [21] Kinslow, R. (1970). *High-Velocity Impact Phenomena*, Academic Press, New York, London.
- [22] Birman, A., Harel, N.Y., Falcovitz, J., Ben-Artzi, M., and Feldman, U. (1999). Operator-split computation of 3-D symmetric flow, 22nd International Symposium on Shock Waves, Imperial College, London, UK.

- [23] Shyue, K.M. (2001). A fluid-mixture type algorithm for compressible multicomponent flow with Mie-Gruneisen equation of state, *Journal of Computational Physics*, **171**(): 678-707.
- [24] Ali, G., and Hunter, J. K. (1998). Wave interactions in magnetohydrodynamics, *Wave Motion*, **27**(3): 257-277.
- [25] Rosenau, P. and Frankenthal, S. (1976). Equatorial propagation of axisymmetric magnetohydrodynamic shocks, *Physics of Fluids*, **19**(12): 1889-1899.
- [26] Manganaro, N. and Olivieri, F. (1989). Group analysis approach in magneto hydrodynamics: Weak discontinuity propagation in a non-constant state, *Meccanica*, **24**(2): 71-78.
- [27] Deb Ray, G. and Bhowmick, J.B. (1976). Similarity solutions for expansions in stars, *Indian Journal of Pure and Applied Mathematics*, **7**(): 96-103.
- [28] Arora, R. (2007). Similarity solutions for strong shocks in MHD, *Canadian Applied Mathematics Quarterly*, **15**(3): 235-246.
- [29] Pai, S.I. (1977). *Two-Phase Flows*, Vieweg Tracts in Pure and Applied Physics, Springer-Verlag.
- [30] Anisimov, S.I. and Spiner, O.M. (1972). Motion of an almost ideal gas in the presence of a strong point explosion, *Journal of Applied Mathematics and Mechanics*, **36**(5): 883-887.

- [31] Rangarao, M.P. and Ramana, B.V. (1976). Unsteady flow of a gas behind an exponential shock, *Journal of Mathematical and Physical Sciences*, **10**: 465-476.
- [32] Ponchaut, N.F., Hornung, H.G., Pullin, D.I., and Mouton, C.A. (2006). On imploding cylindrical and spherical shock waves in a perfect gas, *Journal of Fluid Mechanics*, **560**(00): 103-122.
- [33] Genot, V. (2009). Analytical solutions for anisotropic MHD shocks, *Astrophysics and Space Sciences Transactions*, **5**(1): 31-34.
- [34] Bazalitski, G., Gurovich, V.Ts., Fedotov-Gefen, A., Efimov, S., and Krasik, Ya.E. (2010). Simulation of converging cylindrical GPa-range shock waves generated by wire array underwater electrical explosions, *Shock waves*.
- [35] Vishwakarma, J.P. and Srivastava, R.K. (2013). Converging cylindrical detonation waves in an ideal gas with an azimuthal magnetic field, *Journal of Pure and Applied Physics*, **1**(4), 23-34.
- [36] Pullin, D.I., Mostert, W., Wheatley, V., and Samtaney, R. (2014). Converging cylindrical shocks in ideal magnetohydrodynamics, *Physics of Fluids*, **26**: 097103(1-18).
- [37] Mostert, W., Wheatley, V., Samtaney, R., and Pullin, D.I. (2015). Effects of magnetic fields on magnetohydrodynamic cylindrical and spherical Richtmyer-Meshkov instability, *Physics of Fluids*, **27**: 104102(1-27).

- [38] Madhumita, G. and Sharma, V.D. (2004). Imploding cylindrical and spherical shockwaves in a non-ideal medium, *Journal of Hyperbolic Differential Equations*, **1**(3): 521-530.
- [39] Hornung, H.G., Pullin, D.I., and Ponchaut, N.F. (2008). On the question of universality of imploding shock waves, *Acta Mechanica*, **201**(1): 31-35.
- [40] Von Neumann, J. and Richtmyer, R.D. (1950). A method for the numerical calculation of hydrodynamic shocks, *Journal of Applied Physics*, **21**(3): 232-237.
- [41] Caramana, E.J., Shashkov, M.J., and Whalen, P.P. (1998). Formulations of artificial viscosity for multi-dimensional shock wave computations, *Journal of Computational Physics*, **144**(1): 70-97.
- [42] Blazek, J. (2001). *Computational Fluid Dynamics: Principles and Applications*, Elsevier, Amsterdam.
- [43] Orta, J.A., Huerta, M.A., and Boynton, G.C. (2003). Magnetohydrodynamic shock heating of the solar corona, *The Astrophysical Journal*, **596**(1):646-655.
- [44] Ballai, I., Forgacs-Dajka, E., and Marcu, A. (2007). Dispersive shock waves in the solar wind, *Astronomische Nachrichten*, **328**(8): 734-737.
- [45] Korzhov, N.P., Mishin, V.V., and Tomozov, V.M. (1985). Viscous interaction of solar wind streams, *Soviet Astronomy*, **29**(2): 215-218.

- [46] Gail, H.P., Cuntz, M., and Ulmschneider, P. (1990). Wave pressure in stellar atmospheres due to shock wave trains, *Astronomy and Astrophysics*, **234**(1-2): 359-365.
- [47] Fleck, B. and Schmitz, F. (1993). On the interactions of hydrodynamic shock waves in stellar atmospheres, *Astronomy and Astrophysics*, **273**: 671-683.
- [48] Barnwal, S.P. and Srivastava, O.S. (1983). Shock waves in dusty gas with radiation effects, *Defence Science Journal*, **33**(1): 59-67.
- [49] NiCastro, J.R.A.J. (1970). Similarity analysis of the radiative gas dynamic equations with spherical symmetry, *Physics of Fluids*, **13**(8): 2000-2006.
- [50] Lazarus, R.B. and Richtmyer, R.D. (1977). Similarity solutions for converging shocks, Technical Report, Los Alamos Scientific Laboratory, Los Alamos, LA-6823-MS.
- [51] Lazarus, R.B. (1980). Comments on 'Analysis of spherical imploding shocks', *Physics of Fluids*, **23**(4): 844-846.
- [52] Lazarus, R.B. (1981). Self-similar solutions for converging shocks and collapsing cavities, *SIAM Journal on Numerical Analysis*, **18**(2): 316-371.
- [53] Van Dyke, M. and Guttman, A.J. (1982). The converging shock wave from a spherical or cylindrical piston, *Journal of Fluid Mechanics*, **120**(1): 451-462.

- [54] Hafner, P. (1988). Strong convergent shock waves near the center of convergence: A power series solution, *SIAM Journal on Applied Mathematics*, **48**(6): 1244-1261.
- [55] Wu, C.C. and Roberts, P.H. (1996). Structure and stability of a spherical shock wave in a Van der Waals gas, *The Quarterly Journal of Mechanics and Applied Mathematics*, **49**(4): 501-543.
- [56] Madhumita, G. and Sharma, V.D. (2003). Propagation of strong converging shockwaves in a gas of variable density, *Journal of Engineering Mathematics*, **46**(1): 55-68.
- [57] Ramu, A. and Rangarao, M.P. (1993). Converging spherical and cylindrical shock waves, *Journal of Engineering Mathematics*, **27**(4): 411-417.
- [58] Patel, N.H. and Rangarao, M.P. (1996). Imploding shocks in a non-ideal medium, *Journal of Engineering Mathematics*, **30**(6): 683-692.
- [59] Meyer-ter-Vehn, J. and Schalk, C. (1982). Self-similar spherical compression waves in gas dynamics, *Zeitschrift fur Naturforschung A*, **37**(8): 954-970.
- [60] Axford, R.A. and Holm, D.D. (1978). Spherical shock collapse in a non-ideal medium, *Symposium on group theoretical methods in mechanics*, Novosibirsk, USSR, 47-56.
- [61] Jena, J. and Sharma, V.D. (1999). Self-similar shocks in a dusty gas, *International Journal of Non-Linear Mechanics*, **34**(2): 313-327.

- [62] Rai, A. (2001). Detonation waves in dusty medium, *Indian Journal of Pure and Applied Mathematics*, **32**(12): 1843-1851.
- [63] Chernous'ko, F.L. (1960). A converging shock-wave in a gas of variable density, *Journal of Applied Mathematics and Mechanics*, **24**(5): 1334-1348.
- [64] Toque, N. (2001). Self-similar implosion of a continuous stratified medium, *Shock Waves*, **11**(3): 157-165.
- [65] Hirschler, T.A. (2002). A parametric study of self-similar collapsing shock waves in radiating gas, *Physics of Fluids*, **14**(4): 1491-1501.
- [66] Hirschler, T. and Steiner, H. (2003). A self-similar solution for the implosion problem in a dusty gas, *Fluid Dynamics Research*, **32**(3): 61-67.
- [67] Ponchaut, N.F. (2005). Part I: 3DPTV: advances and error analysis. Part II: Extension of Guderley's solution for converging shock waves, Ph.D. Thesis, California Institute of Technology.
- [68] Miura, H. and Glass, I.I. (1983). On the passage of a shock wave through a dusty-gas layer. *Proceedings of the Royal Society of London. Series A, Mathematical and Physical Sciences*, **385**(1788): 85-105.
- [69] Miura, H. and Glass, I.I. (1985). Development of the flow induced by piston moving impulsively in a dusty gas, *Proceedings of the Royal Society of London. Series A, Mathematical and Physical Sciences*, **397**(1813): 295-309.

- [70] Korobeinikov, V.P. (1976). Problems in the Theory of Point Explosion in Gases: Proceedings (Proceedings of the Steklov Institute of Mathematics Series No-119), USSR, American Mathematical Society.
- [71] Naidu, G.N., Vekatanandam, K., and Rangarao, M.P. (1985). Approximate analytical solutions for self-similar flows of a dusty gas with variable energy, *International Journal of Engineering Science*, **23**(1): 39-49.
- [72] Suzuki, T., Higashino, F., and Takano, A. (1975). Blast waves in a dusty gas, *Modern development in shock tube research*, Proceedings of the 10th International Shock Tube Symposium, 158-165.
- [73] Higashino, F. and Suzuki, T. (1980). The effect of particles on blast waves in a dusty gas. *Zeitschrift fuer Naturforschung A, A Journal of Physical Science*, **35**(12): 1330-1336.
- [74] Higashino, F. (1983). Characteristic method applied to blast waves in a dusty gas, *Zeitschrift fuer Naturforschung A, A Journal of Physical Science*, **38a**: 399-406.
- [75] Steiner, H. and Hirschler, T. (2002). A self-similar solution propagation in a dusty gas, *European Journal of Mechanics - B/Fluids*, **21**(3): 371-380.
- [76] Gretler, W. and Regenfelder, R. (2001). Similarity solution for laser-driven shock waves in a particle-laden gas, *Fluid Dynamics Research*, **28**(5): 369-382.

- [77] Gretler, W. and Regenfelder, R. (2002). Similarity solution for laser-driven shock waves in a dust-laden gas with internal heat transfer effects, *Fluid Dynamics Research*, **30**(5): 293-313.
- [78] Mamun, A.A. and Shukla, P.K. (2011). Nonplanar shock waves in dusty plasmas, *AIP Conf. Proc.*, **1397**(1): 30-37.
- [79] Anisimov, S.I. and Kravchenko, V.A. (1985). Shock wave in condensed matter generated by impulsive load. *Z. Naturforsch.*, **40a**: 8-13.
- [80] Bushman, A.V. and Fortov, V.E. (1977). Models equations of state of a matter, *Sov. Phys. Usp.*, **26**: 465-496.
- [81] Whitham, G. B. (1974). *Linear and Nonlinear Waves*, Wiley-Interscience Publication, John Wiley and Sons, Inc., New York.
- [82] Singh, J.B. and Pandey, S.K. (1988). Analytical solutions of cylindrical shock waves in magnetogasdynamics-I, *Astrophysics and Space Science*, **148**(1): 85-93.
- [83] Perry, R.W. and Kantrowitz, A. (1951). The production and stability of converging shock waves, *Journal of Applied Physics*, **22**(7): 878-886.
- [84] Chisnell, R. F. (1998). An analytic description of converging shock waves, *Journal of Fluid Mechanics*, **354**: 357-375.
- [85] Fujimoto, Y. and Mishkin, E.A. (1978). Analysis of spherically imploding shocks, *Physics of Fluids*, **21**(11): 1933-1938.

- [86] Nakamura, Y. (1983). Analysis of self-similar problems of imploding shock waves by the method of characteristics, *Physics of Fluids*, **26**(5): 1234-1239.
- [87] Sakurai, A. (1953). On the propagation and structure of the blast wave-I, *Journal of the Physical Society of Japan*, **8**(5): 662-669.
- [88] Sakurai, A. (1954). On the propagation and structure of a blast wave-II, *Journal of the Physical Society of Japan*, **9**(2): 256-266.
- [89] Arora, A. and Sharma, V.D. (2006). Convergence of strong shock in a van der Waals gas, *SIAM Journal on Applied Mathematics*, **66**(5): 1825-1837.
- [90] Roberts, P.H. and Wu, C.C. (2003). The shock wave theory of sonoluminescence: In shock focusing effect in medical science and sonoluminescence (Eds. R. C. Srivastava et al.), Springer-Verlag, Berlin, 1-27.
- [91] Landau, L.D. and Lifshitz, E.M. (1987). *Fluid Mechanics*. Pergamon Press, New York.
- [92] Ramu, A., Narsimhulu, D., and Satpathi, D.K. (2014). Numerical study of shock waves in non-ideal magnetogasdynamics (MHD), *Journal of Egyptian Mathematical Society*, **24**(1):116-124.
- [93] Conte, S.D. and De Boor, C.W. (1980). *Elementary Numerical Analysis: An Algorithmic Approach*, International Series in Pure and Applied Mathematics, 3rd Edition, McGraw-Hill.

- [94] Narsimhulu, D., Ramu, A., and Satpathi, D.K. (2013). Similarity solutions to shockwaves in non-ideal magnetogasdynamics, 11th International conference of Numerical Analysis and Applied Mathematics, AIP Conf. Proc., **1558**:860-864.
- [95] Ramu, A. (1989). Self-Similar Solutions for Some Compressible Flow Problems, Ph.D. Thesis.
- [96] Sharma, V.D. and Radha, Ch. (1995). Similarity solutions for converging shocks in a relaxing gas, International Journal of Engineering Science, **33**(4):535-553.
- [97] Sharma, V.D. and Arora, R. (2005). Similarity solutions for strong shocks in an ideal gas, Studies in Applied Mathematics, **114**(4): 375-394.
- [98] Sen, H.K. (1956). Structure of a magnetohydrodynamic shock wave in a plasma of infinite conductivity, Physical Review, **102**(1): 5-11.
- [99] Hoffmann, F.De. and Teller, E. (1950). Magneto-hydrodynamic shocks, Physical Review, **80**(4): 692-703.
- [100] Bazer, J. and Ericson, W.B. (1959). Hydromagnetic shocks, The Astrophysical Journal, **129**: 758-785.
- [101] Jordan, P.M., Meyer, M.R., and Puri, A. (2000). Causal implications of viscous damping in compressible fluid flows, Physical Review E, **62**(6): 7918-7926.

- [102] Maslov, A.A., Mironov, S.G., Kudryavtsev, A.N., Poplavskaya, T.V., and Tsyryulnikov, I.S. (2010). Wave processes in a viscous shock layer and control of fluctuations, *Journal of Fluid Mechanics*, **650**: 81-118.
- [103] Richard, L. (1955). Similarity solution for a spherical shock wave, *Journal of Applied Physics*, **26**(8): 954-960.
- [104] Zumbun, K. (2010). The refined inviscid stability condition and cellular instability of viscous shock waves, *Physica D: Nonlinear Phenomena*, **239**(13): 1180-1187.
- [105] Khodadad, V. and Khazraiyani, N. (2004). Numerical modelling of ballistic penetration of long rods into ceramic/metal armors, 8th International LS-DYNA Users Conference Drop/Impact Simulations, **14**: 39-50.
- [106] Lee, W.H. and Whalen, P.P. (1984). Calculation of shock problems by using four different schemes, *International Conference on Numerical Methods for Transient and Coupled Problems*, Venice, Italy.
- [107] Chikitkin, A.V., Rogov, B.V., Tirsky, G.A., and Utyuzhnikov, S.V. (2014). Effect of bulk viscosity in supersonic flow past spacecraft, *Applied Numerical Mathematics*, **93**: 47-60.
- [108] Elliott, L.A. (1960). Similarity methods in radiation hydrodynamics. *Proceedings of the Royal Society of London. Series A, Mathematical and Physical Sciences*, **258**(1294): 287-301.
- [109] Helliwell, J.B. (1969). Self-similar piston problems with radiative heat transfer, *Journal of Fluid Mechanics*, **37**(3): 497-512.

- [110] Ghoniem, A.F., Kamel, M.M., Berger, S.A., and Oppenheim, A.K. (1993). Effects of internal heat transfer on the structure of self-similar blast waves, *Journal of Fluid Mechanics*, **117**(1): 473- 491.
- [111] Gretler, W. and Steiner, H. (1993). Blast waves in inhomogeneous atmospheres with counter pressure and heat transfer effects, *Shock Waves*, **3**(2): 83-94.
- [112] Marshak, R.E. (1958). Effect of radiation on shock wave behaviour, *Physics of Fluids*, **1**(1): 24-29.
- [113] Hirschler, T. and Gretler, W. (2002). Similarity analysis of strong converging spherical shock waves in radiating gas, *Acta Mechanica*, **154**(1): 159-177.
- [114] Khudyakov, V.M. (1983). The self-similar problem of the motion of a gas under the action of monochromatic radiation, *Soviet Physics Doklady* (trans. American Institute of Physics), **28**(10): 853-855.
- [115] Zedan, H.A. (2002). Applications of the group of equations of the one-dimensional motion of a gas under the influence of monochromatic radiation, *Applied Mathematics and Computation*, **132**(1): 63-71.
- [116] Leygnac, S., Boireau, L., Michaut, C., Lanz, T., Stehle, C., and Clique, C. and Bouquet, S. (2006). Modelling multidimensional effects in the propagation of radiative shocks, *Physics of Plasmas*, **13**(11):113301(1-10).

- [117] Sampaio, O.P. (2013). Radiation from a D-dimensional collision of shock waves: Numerical methods, *International Journal of Modern Physics A*, **28**(22 & 23): 1340019 (1-37).
- [118] Taylor, K.L. and Ryan, G.M. (2013). New self-similar radiation-hydrodynamics solutions in the high-energy density, equilibrium diffusion limit. *New Journal of Physics*, **15**(9): 095013(1-17).
- [119] Narsimhulu, D., Ramu, A., and Satpathi, D.K. (2016). Similarity solution of spherical shock waves-Effect of Viscosity, *Proyecciones Journal of Mathematics*, **35**(1): 11-31.
- [120] Farnsworth, A.V. and Clarke, J.H. (1971). Radiatively and collisionally structured shock waves exhibiting large emission-convection ratio, *The Physics of Fluids*, **14**(7):1352-1360.
- [121] Yousaf, M. (1986). Imploding spherical and cylindrical shocks, *Physics of Fluids*, **29**(3): 680-684.
- [122] Lie, S. (1880). *Theorie der transformation gruppen*, *Math. Ann.* 16.
- [123] Bluman, G.W. and Cole, J.D. (1974). *Similarity Methods for Differential Equations*, Springer, Vol. 13, New York.
- [124] Logan, J.D. and Perez, J.D.J (1980). Similarity solutions for reactive shock hydrodynamics, *SIAM Journal of Applied Mathematics*, **39**(3):512-527.
- [125] Olver, P.J. (1986). *Applications of Lie Group to Differential Equations*, Springer, Vol. 107, New York.

- [126] Logan, J.D. (1987). *Applied Mathematics: A Contemporary Approach*, John-Wiley.
- [127] Bluman, G. and Kumei, S. (1989). *Symmetries and Differential Equations*, Springer, Vol.81.
- [128] Oliveri, F. and Speciale, M.P. (2002). Exact solutions to the unsteady equations of perfect gases through Lie group analysis and substitution principles, *International Journal of Non-Linear Mechanics*, **37**(2): 257-274.
- [129] Barbera, E. and Giambo, S. (2012). Propagation of weak discontinuities in binary mixtures of ideal gases, *Rendiconti del Circolo Matematico di Palermo*, **61**(2): 167-178.
- [130] Jena, J. and Sharma, V.D. (1999). Self-similar shocks in a dusty gas, *International Journal of Non-Linear Mechanics*, **34**(2): 313-327.
- [131] Sharma, V.D. and Radha, R. (2008). Exact solutions of Euler equations of ideal gasdynamics via Lie group analysis, *Z. Angew. Math. Phys.*, **59**(6): 1029-1038.
- [132] Pandey, M., Radha, R., and Sharma, V.D. (2008). Symmetry analysis and exact solutions of magnetogasdynamic equations, *Quart. J. Mech. Appl. Math.*, **61**(3): 291-310.
- [133] Jena, J. (2009). Lie group transformations for self-similar shocks in a gas with dust particles, *Math. Methods Appl. Sci.*, **32**(16): 2035-2049.

- [134] Raja Sekhar, T. and Sharma, V.D. (2010). Evolution of weak discontinuities in shallow water equations, *Appl. Math. Lett.*, **23**(3): 327-330.
- [135] Bira, B. and Reja Sekhar, T. (2013). Symmetry group analysis and exact solutions of isentropic magnetogasdynamics, *Indian Journal of Pure and Applied Mathematics*, **44**(2): 153-165.
- [136] Neal, T. (1976). Dynamic determination of Gruneisen coefficient in aluminium and aluminium alloys for density up to 6 Mg/ m³, *Phy. Rev-B* **14**: 5172-5181.
- [137] Gratton, J. and Minotti, F. (1990). Self-similar viscous gravity currents: phase-plane formalism, *Journal of Fluid Mechanics*, **210**: 155-182.
- [138] Mitchell, A.C. and Nellis, W.J. (1981). Shock compression of aluminum, copper, and tantalum, *Journal of Applied Physics*, **52**(5): 3363-3374.
- [139] Yadav, H.S. (1980). Attenuation of non-uniform shock wave, *Indian Journal of Pure and Applied Mathematics*, **11**(8): 1085-1094.

List of Publications and Presentations

In Peer-Reviewed Journals:

1. Narsimhulu, D., Ramu, A., Satpathi, D.K., and Sudha, G. (2013). Phase-plane analysis application to Guderley's problem, published in Journal of Emerging Trends in Engineering and Applied Sciences (JETEAS), Vol. 4(3): 406-411.
2. Narsimhulu, D., Ramu, A., and Satpathi, D.K. (2013). Similarity solutions to shock waves in non-ideal magnetogas dynamics (*Chapter-3*), published in American Institute of Physics (AIP) conference proceedings, AIP Conf. Proc., **1558**: 860-864.
3. Ramu, A., Narsimhulu, D., and Satpathi, D.K. (2014). Numerical study of shock waves in non-ideal magnetogas dynamics (MHD), published in Journal of Egyptian Mathematical Society (JOEMS), **24**(1): 116-124 (*Chapter-5*).
4. Narsimhulu, D., Ramu, A., and Satpathi, D.K. (2016). Similarity solution of spherical shock waves - Effect of viscosity, published in Proyecciones Journal of Mathematics (PJM), **35**(1): 11-31 (*Chapter-6*).
5. Narsimhulu D., Ramu, A., and Satpathi, D.K. (2017). Self-similar motion of strong converging cylindrical and spherical shock waves in non-ideal

stellar medium (*Chapter-7*). This paper is accepted for publication in Journal of Applied Fluid Mechanics (JAFM).

6. Narsimhulu D., Ramu, A., and Satpathi, D.K. (2017). Numerical solution to strong cylindrical shock wave in the presence of magnetic field (*Chapter-4*). This work will appear in the proceedings of IAENG World Congress on Engineering (WCE).
7. Narsimhulu D., Ramu, A., and Satpathi, D.K. (2018). Self-similar solution of one-dimensional strong converging cylindrical and spherical shock waves in non-ideal gas (*Chapter-8*). This paper has been communicated to International Journal of Non-Linear Mechanics.

Papers presented in National / International Conferences:

1. Narsimhulu, D. and Ramu, A. “Similarity solutions of shock waves in non-ideal magnetogasdynamics”, presented in the International Conference on Mathematical Sciences (ICMS), SSES Amt’s Science College, Nagpur, India, December 28-31, **2012**.
2. Narsimhulu, D., Ramu, A., and Satpathi, D.K., part of the work of “Similarity solutions to shock waves in non-ideal magnetogasdynamics”, presented in the 11th International Conference of Numerical Analysis and Applied Mathematics (ICNAAM), Rhodes, Greece, September 21-27, **2013**.

3. Narsimhulu, D. and Ramu, A. “Self-similar motion of strong converging cylindrical and spherical shock waves in non-ideal medium”, presented in International Conference on Current Trends in PDEs: Theory and Computations (**ICCT-PDEs: TC**), South Asian University, New Delhi, India, December 28-30, **2015**.
4. Narsimhulu, D. and Ramu, A. “An explicit forward scheme to one-dimensional strong converging cylindrical and spherical shock waves in non-ideal gas”, presented in International Conference on Applicable Mathematics (**ICAM**), Stella Maris College, Chennai, India, Nov 30-Dec 1, **2016**.
5. Narsimhulu D., Ramu, A., and Satpathi, D.K. Numerical solution to strong cylindrical shock wave in the presence of magnetic field, presented in IAENG World Congress on Engineering (**WCE**), London, U.K., 5-7 July, **2017**.

BIOGRAPHY OF THE CANDIDATE

Name of the Candidate: NARSIMHULU DUNNA

Date of Birth: 12th June 1987

E-mail: narsimha.maths@gmail.com

Education Qualifications:

- **Ph. D (Applied Mathematics)**
Thesis is submitted in 2018
Department of Mathematics
Birla Institute of Technology and Science, Pilani
Hyderabad Campus, Telangana, India.
- **M. Sc (Mathematics)**
University topper in Mathematics
University: Pondicherry Central University, Pondicherry
Subject: Mathematics
Year: 2009
Percentage: 8.39 (CGPA).
- **Bachelor of Science (B.Sc.)**
University: Andhra University, Visakhapatnam, A.P
Subject: Maths, Physics, Chemistry
Year: 2007
Percentage: 77 (86.5% in Mathematics)

Awards / Scholarships:

- Innovation in Science Pursuit for Inspired Research (INSPIRE) Fellow (IF 110071), Department of Science and Technology (2011 - Present). This fellowship is given by Department of Science and Technology, India for pursuing science carrier with outstanding scholastic record.
- Gold medal in Postgraduate level.

Academic achievements:

- Secured **6th** rank, Pondicherry Central University MSc Mathematics Entrance Exam 2007.
- Secured **6th** rank, Andhra University MA-Education (Mathematics) Entrance Exam 2007.
- Secured **25th** rank, Acharya Nagarjuna University MSc Mathematics Entrance Exam 2007.
- Secured **113th** rank, Andhra University MSc Mathematics Entrance Exam 2007.

BIOGRAPHY OF THE SUPERVISOR

Name of the Candidate: Dr. ADDEPALLI RAMU

Address: Department of Mathematics,
BITS-PILANI, Hyderabad Campus
Shameerpet (Mandel), Jawahar Nagar
Telangana – 500078.

E-mail: addepallir@gmail.com

Education Qualifications:

- **Ph. D (Applied Mathematics)**
Area of Research: Compressible Fluids (CFD)
Institute: IIT Bombay
- **M. Sc (Applied Mathematics)**
University: Osmania University, Hyderabad

Experience:

- Teaching: BITS-PILANI, Hyderabad Campus, D.O.J: November, 2001.
- Research: Industrial research experience at Tata Steel R & D division and DRDL, Hyderabad.

Publications: More than 25 publications in peer reviewed National and International Journals and Conferences

Research Activity: Supervising 2 students for Ph.D.